Ricard Cònsul Serracanta

DOCTORAL THESIS

UPC – September 2002

UPC **CTTC**

Development of Numerical Codes for the Evaluation of Combustion Processes. Detailed Numerical Simulations of Laminar Flames

Centre Tecnològic de Transferència de Calor
Departament de Màquines i Motors Tèrmics
Universitat Politècnica de Catalunya

Ricard Cònsul Serracanta
Doctoral Thesis

Development of Numerical Codes for the Evaluation of Combustion Processes. Detailed Numerical Simulations of Laminar Flames

Ricard Cònsul Serracanta

TESI DOCTORAL

presentada al

Departament de Màquines i Motors Tèrmics
E.T.S.E.I.T.
Universitat Politècnica de Catalunya

per a l'obtenció del grau de

Doctor Enginyer Industrial

Terrassa, September 2002

Development of Numerical Codes for the Evaluation of Combustion Processes. Detailed Numerical Simulations of Laminar Flames

Ricard Cònsul Serracanta

Directors de la Tesi

Dr. Carlos David Pérez-Segarra

Dr. Assensi Oliva Llena

Tribunal Qualificador

Dr. Ramon Carreres Planells
Universitat Politècnica de Catalunya

Dr. Miquel Costa Pérez
Universitat Politècnica de Catalunya

Dr. Eduard Egusquiza Estévez
Universitat Politècnica de Catalunya

Dr. Valeriano Ruiz Hernández
Universidad de Sevilla

Dr. Antonio Pascau Benito
Universidad de Zaragoza

Acknowledgements

Aprofitant les poques paraules que puc escriure en català en aquesta tesi, m'estimo més utilitzar un llenguatge més amè i personal, per agrair a totes aquelles persones que d'una manera o altra m'han donat suport durant aquests darrers anys. Anys que si ens posem a fer números, ja podrien ben bé ser un 10% de la meva vida si algun dia deixo de fumar.

En primer lloc, i complint amb el protocol, vull agrair als meus directors de la tesi, l'Assensi Oliva i el Carles i/o David Pérez-Segarra, el seu recolzament. A l'Assensi, li agraeixo, entre moltes altres coses, haver-me transmès la passió amb la qual viu la recerca i el seu suport al llarg de la tesi. Al David, haver intentat transmetre'm el seu rigor científic i la seva gran capacitat, virtuts de les quals sempre he intentat, en la mesura del que he estat capaç, encomenar-me'n una mica.

Em veig forçat també a agrair als companys Jordi Cadafalch i Joaquim Rigola el mateix que ells comenten de mi a les seves tesis. No voldria afegir cap més comentari que pogués suposar la ruptura de l'amistat que sempre ens ha unit.

Abans d'agrair en general a tota la fauna de la termosecta el seu suport i temps d'enriquidora convivència, voldria felicitar-me per haver conegut a una persona com el Kilian Claramunt. Agraint-li la facilitat amb la qual hem treballat plegats aquests darrers anys i l'ajut que en qualsevol moment sempre m'ha donat.

Voldria també, fer menció del suport que el Campus de Terrassa m'ha donat durant el transcurs de la realització de la tesi, especialment pel fet d'haver-me inculcat una virtut tant preuada a tota persona com és la puntualitat.

Abans de concloure, faltaria més, voldria agrair especialment a la meva àvia i a la meva mare tot el han fet per la meva germana i per mi. M'és impossible trobar les paraules per agrair-los haver regalat la seva vida per nosaltres.

Contents

Chapter 1

Introduction

1.1 Prologue

Many text books and scientific literature start magnifying the role that combustion phenomena has played in human history. In fact, the discovery of fire supposed the beginning of a new age, and the ability of employing fire at their own benefit has been considered by many historians as the first human success, and the first steps to a more advanced technology.

Ancients employed fire basically for lighting, heating and cooking, or even for bellical purposes. As science evolved, for combustion technology as well, and combustion applications started to grow. Nowadays, it is quite difficult to imagine our lives without combustion systems or equipment: power production by coal and oil burning is the main energy power supply; gas and oil equipment are the most predominant ways for heating and cooking at home; pyrometallurgy is the base of the industry development; most transports use internal combustion engines; the employment of modern jet engines by the aircraft industry; and rockets for aerospace technology.

Currently, about 80 % of the worldwide energy support is provided by combustion of liquid, solid and gaseous fossil fuels. Other energy sources as nuclear energy or renewable energies still account for less than 20% of the total energy consumption [1]. These trends are not expected to change much in a near future due to both political and economical interests.

In spite of the considerable advantages that combustion has given to our quality of live, combustion also has its dark face. Thousands of forests are destroyed every year. Large amounts of pollutants are formed, and their emission to the atmosphere effects seriously the environment and the planet's health. Oxides of carbon, oxides of nitrogen, sulfur oxides, soot, and unburnt hydrocarbons are generated together with the harmful effects that they are causing.

In this way, and far from moving away combustion of our lives, that can be considered extremely unprobably in the next decades, the necessity of improving the

efficiency of combustion equipment is a common and challenging objective. Pollutant emissions can be reduced by improving the efficiency of the combustion process, thereby increasing fuel economy.

Multidisciplinary characteristics of combustion phenomena

The main attribute of combustion processes that attracted human interest is the generation of heat. From a chemical point of view, combustion is associated with fast chemical reactions that proceed with a large conversion of chemical energy to sensible heat. This process, rarely involve a single reaction, usually in combustion processes the oxidation of a given fuel is composed by thousands of elementary consecutive, competitive, and opposing steps, the so-called chain-reactions. Thus, fundamentals of reactive system are described by *chemical kinetics* together with *thermodynamics*.

Before 1850, wood was the primary combustion fuel. Nowadays, energy provided by combustion is obtained mostly from coal, petroleum and natural gas. The wide range of physical states that fuels present, together with the fact that combustion products are usually in gaseous state, makes *phase change* phenomena play also an important role in these processes.

The heat release by the chemical reactions raises the temperature of the medium. This temperature increment is transferred to the surroundings by conduction, convection and radiation. Fundamentals of *heat transfer* are thereby involved both affecting the evolution of the reactions and the properties of the medium. Together with molecular transport, heat transfer by convection has a predominant contribution. Gas motion is generated either by the flow supplying the flame, or is due to buoyancy effects (i.e. gravitational field). Therefore, fundamental aspects of *fluid mechanics* governs combustion phenomena, existing a strong feedback between the flow and the chemistry.

As a consequence of the chemical reactions, a wide range of chemical species are produced. The combustion of hydrocarbon fuels produces mainly water and carbon dioxide, but also other species like hydrogen and carbon monoxide, soot, and pollutants like nitrogen oxides, sulfur oxides, etc. Moreover, in the chemical mechanisms (i.e. the path description followed by the reactants on its conversion to products) hundreds of chemical species are involved, the so-called intermediate species. Although these species are consumed as soon as they are produced, due to the fast reactions where are they involved, their presence is clue on the combustion description. Obviously, *mass transfer* is also an involved discipline.

As an example of combustion phenomena, we just have to analyze the complex physical processes involved in a simple candle. Due to the heat release by the candle itself, heat mainly transferred by radiation heats and liquefies the top of the candle. The liquid vax raises into the wick where it is vaporized to gaseous fuel that reacts within the flame. Then, a complex system of reactions take place, producing hot

gases that together with the surrounding air raises over the flame. The presence of intermediate species of the chemical mechanism can be noted by observing a slightly blue color at the base of the flame produced by the emission of visible light by the CH radicals. In certain flames, like in candle's flame, there is also an important emission of yellow light. This light is emitted by soot, which are particles of slightly hydrogenated carbon [2]. Commonly, it is said that the 90% of the physical phenomena involved in combustion equipment can be observed in a candle's flame.

Candle's flame is also a good example to introduce the first classification that is usually employed to describe combustion systems. In the candle, we can distinguish two main regions, an inner one containing reducing gases, and an outer containing oxidizer gases. Both regions are separated by a thin zone where chemical reactions mostly take place. This flame structure, typical of several flames, is defined as *non-premixed* or *diffusion* flames. Chemical reactions appear as soon as fuel and oxidizer get in contact, in this sense, is said that combustion is controlled by the rate of mixing. Other, typical examples of non-premixed flames are Diesel engines or H_2/O_2 rocket motors. On the other hand, when fuel and oxidizer are mixed before they react, we talk about *premixed* flames. For instance, spark-ignited gasoline engines and gas turbines [3].

The second classification refers to the flow structure of the flames. Nearly always, combustion takes place within a turbulence flow field just to increase the mixing process and thereby enhance combustion [1]. For instance, industrial furnaces and burners. Nevertheless, there are also situations where the flow regime is laminar as in radiant burners for heating, wood fire, etc.

Combustion systems can be therefore classified into: premixed or non-premixed combustion, and laminar or turbulent flames. Research carried out on combustion topics usually differentiates these four main categories in order to help the understanding of their main features.

History of combustion science

Although combustion is considered as the oldest technology and has had an enormous impact on history, earlier thoughts associated combustion to mysterious and philosophical beliefs. Until the 18th century, it was supposed that fuels were phlogisticated bodies that decompose liberating energy. Combustion was understood as a decomposition rather than the union or combination as it is [2].

The scientific revolution starts with the reflections of Lavoisier who ended the Phlogiston Theory. During the 19th century, there was a considerable science evolution owing to remarkable studies on thermochemistry and chemical thermodynamics (Benjamin Thompson (1800), Joule (1842), Robert Bunsen (1855), ...). But it was not until 1883, when Le Chatelier, who was recommended to optimize the lighting system of Paris, posed the first flame theory.

In the late nineteenth and at the beginnings of the twentieth century, theoretical treatments of combustion processes evolved, and combustion was recognized as an area of study. For instance, in this period Arrhenius (1889) posed his empirical expression for the temperature dependence of chemical reactions velocities, and Burke-Schumann (1928) presented their theoretical studies about the height and shape of diffusion flames. The first Combustion Institute meeting (1928) supposed the beginning of a new age.

During the World War II, there was a rapid advance in combustion field motivated by the interest of increasing the efficiency and performance of bellical equipment. The development of gas turbines, rockets and weapons, gave special emphasis to the research of high-temperature kinetics, spray combustion, and detonations respectively. New instrumentation and computational resources emerged opening a new hopeful future for combustion research.

Since then, theoretical basis at least for gaseous-phase processes have been posed [4][5][6]. Combustion modeling grew every year in importance and sophisticated experimental techniques such laser diagnostics, improve the accuracy of the measurements.

Nowadays, and in part motivated by fuel crisis of mid-1970 and by the environmental policies of pollutant control, combustion research focuses the attention on the improvement of equipment efficiency and reduction of contaminant emissions. These new necessities have emphasized the studies of chemical kinetics and microscopic details of combustion.

Environmental effects of combustion

The main disadvantage inherent to combustion systems and equipment, is the considerable harmful environmental effects that they produce. These evident effects, that can be easily observed in our daily lives, are damaging the health of the planet, and thereby the quality of live of the people worldwide. Main environmental effects are: acid rain, climate change, and smog [7].

Acid rain is a term employed to define a serious environmental problem caused by the falling out of acids of the atmosphere. Technically speaking, this effect is known as acid deposition, which have a wet and a dry contribution. Wet deposition is associated with rain, fog and snow, while dry deposition refers to acid gases and particles. Acid deposition has a wide range of harmful consequences, specially on lakes and rivers, trees, and thereby on human health. Acid rain causes lakes and rivers to become acidic. The increase of acid levels kill lots of fish, but also in long-term stops the fish reproduction. The acid damages specially trees. Acid reacts with many of their nutrients starving them, and making trees more susceptible to other forms of damage (i.e. as being blown down, or breaking under the weight of snow). The ingestion of food or water with a great level of toxic metals produced by the consequences of acid

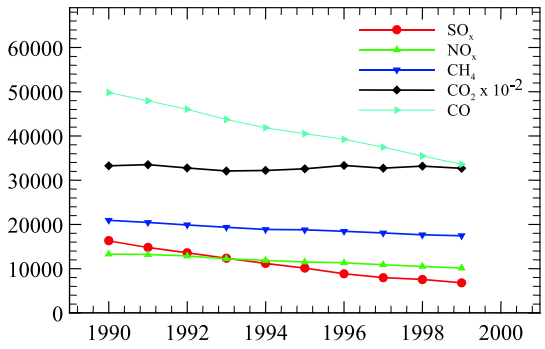

Figure 1.1: Anthropogenic annual EU emission data for the period 1990-1999 (1000 tones per year). Environmental European Agency [8].

deposition, can produce diseases and even damage seriously our organs.

Acid rain is mainly produced by the emission of sulfur oxides (SO_x) and nitrogen oxides (NO_x) from the burning of fossil fuels in transport vehicle, energy and manufacturating industries [1]. In the atmosphere, and in the presence of ultraviolet light, reactions involving sulfur and nitrogen oxides, oxygen and ozone are established. As a consequence, nitric and sulfuric acids are formed, which are transported to the earth's surface.

Another harmful effect of pollutant emissions is the climate change due to a *global earth warming*. Greenhouse gases, primarily water vapor, carbon dioxide, methane and nitrous oxide, trap some of the infrared radiation emitted by the earth, retaining heat like the glass panels of a greenhouse. Consequently, earth's surface temperature has risen about one degree in the past century. Although these changes could be attributed to climate cycles, the fact that the amount of greenhouse gases in atmosphere has increased notably since the beginning of the industrial revolution, is an evidence. Climate models predict that the global temperature will rise by about 1.45.8 K by the year 2100. This change would be much larger that any climate change experienced over at least the last 10.000 years. Stabilizing atmospheric concentrations of greenhouse gases will demand a major effort. It is in this context that the Kyoto Protocol signed in 1997 required a binding commitment to reduce the emission six greenhouse gases by at least 5% compared to 1990 levels by the period 2008-2012 [9].

Smog, that comes of the coupling of the words smoke and fog, is another conse-

[1] European Environmental Agency emission inventory (1990-1999) [8]. Anthropogenic annual emission in 1000 tones per year in 1999: SO_x, 6803; NO_x, 10136; CO: 33602, CO_2: 3271000. By sectors: Energy industries (17% NO_x, 63% SO_x, 1% CO, 30% CO_2), manufacturating industries and construction (14% NO_x, 17% SO_x, 88% CO, 9% CO_2), transport (54% NO_x, 5% SO_x, 60% CO, 25% CO_2).

quence of air-pollution. Specially in summertime, cities seem to be covered by a cloud of pollution due to mostly the emission of vehicles exhaust gases. The consequences of smog are the visibility reduction and health diseases: eye irritation, irritation of the respiratory tract, chest pains, cough, shortness of breath, nausea and headache. Again, sulfur and nitrogen oxides are the main responsible of smog formation.

During the last decades, the harmful effects pollutant emission have acquired an international awareness, and the social environmental consciousness has notably increased. Governmental policies have been developed and are being applied, forcing industries to control and reduce their emissions. Research in this topic has increased in importance and many works are given especial emphasis to the understanding of the kinetics of pollutant formation and its reduction. Figure 1.1 shows the evolution of main pollutant emissions in EU. From 1990 to 1999 the amount of carbon dioxide produced has been maintained. However, there is a positive tendency on the reduction of other main contaminants. Specially carbon monoxide and sulfur oxides.

1.2 Outline

Emersion of computers and its evolution during the second half of the twentieth century has supposed a considerable advance both for the scientific and industrial communities. Numerical methods on heat transfer and fluid flow have been consolidated as an indispensable tool for the resolution of thermal and mechanical engineering problems, being nowadays an essential complement to the experimental studies. Computational Fluid Dynamics (CFD) computations have reduced the production costs and time to market of industrial products, decreasing notably the high number of traditional experimental studies based on trial-and-error analysis which were needed on the optimization of thermal equipment.

However, the research on the improvement of the performance of the numerical methods and the accuracy of the numerical models, still constitute an essential task for the successful application of CFD computations in industrial interests. The necessity of improving numerical strategies become more relevant when we are talking about combustion phenomena. The considerable complexity inherent to combustion problems (i.e. turbulence, chemical reactions, radiation in participating media, phase change, huge local effects, ...) emphasizes the necessity of developing enhanced numerical methods to reduce the computational effort that their simulation supposes. At the same time and together with a deep knowledge of combustion characteristics, provided by both detailed numerical and experimental studies, the development of improved models to be applied in industrial applications becomes a promising challenge on the production of more efficient and cleaner combustion equipment.

The main objective of the research presented in this thesis, is the development of a numerical infrastructure for the multidimensional numerical simulations of combus-

tion processes. The work here presented starts from the know-how of the Laboratori de Termotècnia i Energètica, Centre Tecnològic de Transferència de Calor (CTTC), in the mathematical formulation and numerical resolution of heat and mass transfer phenomena. The know-how of the Group has been the basis from which the numerical resolution of combustion phenomena has been hold.

The work developed in this thesis has been mainly focussed to solve numerically combustion phenomena with the maximum level of accuracy. Rather than assuming lower mathematical approaches and consider their application to engineering problems, the main intention of our Group has been centered to the development of numerical tools that enable the feasible resolution of combustion problems with the highest level of detail.

Within the wide range of combustion fields, laminar flames are an illustrative example of combustion phenomena. The detailed numerical simulation of these kind of flames has supposed and still represents a challenging problem. Detailed numerical simulations of laminar flames have been used on the design and optimization of industrial equipment (e.g. domestic gas burners), and for the understanding of pollutant formation and more complex flows, being a basic ingredient on their modelization. The detailed numerical simulation of laminar flames has supposed for the author, directors, and in general, the people who forms our center, the acquisition of a know-how for the mathematical formulation and numerical treatment of combustion problems.

The thesis has been organized in four main chapters. In chapter two, theoretical analysis of multicomponent reactive flows is introduced and the mathematical formulation adopted for the numerical simulation of laminar flames is discussed. A continuum mechanics derivation has been considered to obtain the set of governing equations. An approximation to a rigorous kinetic theory formulation has been followed to model molecular transport fluxes. Continuum and kinetic-theory formulations are compared to find a relationship among them and to adjust the definition of molecular fluxes. Radiant heat transfer fundamentals are introduced, assuming optically thin approximation on its mathematical modelization.

Next, in chapter three special emphasis is given to the modelization of chemical reactions. Combustion mechanisms are introduced, and the evaluation of the production/consumption rates is described in detail. The different levels of chemical models employed in this thesis and the actual tendencies on the reduction of the complexity of the chemical approaches are commented.

Chapter four accounts for the numerical methodology employed. When detailed models are used, special attention has to be paid to the numerical method and on the discretization. The numerical method has to be able to treat the resulting set of stiff governing equations, while the discretization has to be fine enough to treat adequately the flame fronts. As a consequence, the computational effort in terms

of CPU and in terms of memory requirements, becomes considerable and at some times prohibitive. The chapter references main numerical strategies employed in the literature to solve this kind of problems and the strategy adopted in this thesis to do so. The main goal achieved is the development of a parallel multiblock algorithm able to perform efficiently with loosely coupled computers, the so-called *Beowulf clusters*. The main features of the algorithm, and its ability to overcome numerical difficulties of combustion related problems are pointed out. Computational savings obtained by the optimization of the discretization and the parallelization of the code are described.

The methodology employed for the analysis of the numerical solutions is also described in this chapter. Numerical results are submitted to a verification process by means of a post-processing procedure based on the Generalized Richardson extrapolation for h-refinement studies and on the Grid Convergence Index (GCI) proposed by Roache. Estimates of the uncertainty due to discretization are evaluated in order to assess the accuracy of the numerical solutions.

The application of the developed numerical infrastructure to the analysis of laminar flames is presented in chapter five. Partially premixed co-flow methane-air flames are simulated taken into account different levels of premixing: from infinite (completely non-premixed) to 2.464. Available experimental and numerical studies are reproduced and sensitive studies to validate the appropriateness of the adopted mathematical formulation are presented. Chemical approaches, transport and radiation models are compared giving special emphasis to the influence of their numerical treatment to main flame properties and contaminant formation.

Finally, conclusions and future actuations are described. Some of the work already done and work in progress is commented. Our main short-time objectives on the higher level of modelization of radiant heat exchange and on the numerical simulation of turbulent flames are discussed.

Acknowledgments

This thesis has been financially supported by the Comisión Interministerial de Ciencia y Tecnología, Spain (project TIC1999-0770), and by the Comissionat per Universitats i Recerca de la Generalitat de Catalunya.

References

[1] N. Peters. *Turbulent combustion*. Cambridge University Press, 2000.

[2] G.L. Borman and Ragland K.W. *Combustion engineering*. McGraw-Hill, 1998.

[3] J. Warnatz, U. Maas, and Dibble R.W. *Combustion*. Springer-Berlag, 1996.

[4] J.O. Hirschfelder, C.F. Curtiss, and R.B. Bird. *Molecular theory of gases and liquids*. John Wiley and Sons Inc., 1954.

[5] R.B. Bird, E.E. Stewart, and E.N. Lightfoot. *Transport phenomena*. John Wiley and Sons Inc., 1960.

[6] F.A. Williams. *Combustion theory*. The Benjamin/Cummings Publishing Company, Inc., 1985.

[7] United States Environmental Protection Agency (EPA). Unknown title 9.

[8] B. Gugele, M. Ritter, and A. Barkman. Annual european community clrtap emission inventory 1990-99. Technical report, European Environment Agency, 1989.

[9] United Nations. Framework convention on climate change.

Chapter 2

Mathematical formulation

In this chapter a theoretical analysis of multicomponent reactive flows is introduced. The conservation laws are posed from a continuum derivation. On the definition of molecular transport fluxes, and due to the absence of a mathematical formulation from a continuum mechanics point of view, we resort to molecular kinetic theory treatment. Main concepts together with the equations of change are introduced looking for its equivalence to continuum mechanics. Assessed both derivations, molecular transport fluxes are rigorously defined and approximations are considered on the evaluation of transport coefficients. The formulation finishes with the modelization of radiant heat transfer.

Finally, the mathematical formulation presented for chemically reactive flows is simplified for the treatment of low-Mach number laminar combustion problems. Main approximations related basically to low velocity flows, transport fluxes, and radiant heat exchange are discussed.

2.1 Basic transport equations for multicomponent reactive flows

2.1.1 Mass conservation laws

The mass conservation equation for a component of a reactive mixture reads,

$$\frac{\partial \rho_i}{\partial t} + \nabla \cdot (\rho_i \vec{v}_i) = \dot{w}_i \tag{2.1}$$

where, the left-hand side indicates the change of mass of ith species for a given control volume by either the change of density with time and by the mass flow rate balances. The right-hand side, expresses the rate of production or consumption of mass of ith species due to chemical reactions. This term, that will be treated in detail in the next chapter, indicates a source of mass m_i, if positive, or a sink of mass, if negative.

The mass conservation equation of the mixture, can be obtained by summing up the N species conservation equations,

$$\sum_{i=1}^{N}\left(\frac{\partial \rho_i}{\partial t}+\nabla\cdot(\rho_i\vec{v}_i)\right)=\sum_{i=1}^{N}\dot{w}_i \tag{2.2}$$

taking into account that for chemically reactive mixtures, no generation or destruction of total mass occurs,

$$\sum_{i=1}^{N}\dot{w}_i=0 \tag{2.3}$$

and the definition of the *mixture's mass-averaged velocity* $\vec{v}$,

$$\vec{v}=\frac{1}{\rho}\sum_{i=1}^{N}\rho_i\vec{v}_i \tag{2.4}$$

the mixture's mass conservation law is written as is known for a single-component formulation,

$$\frac{\partial \rho}{\partial t}+\nabla\cdot(\rho\vec{v})=0 \tag{2.5}$$

Species mass conservation equations are usually written considering mass fluxes of species relative to mixture's mass-average velocity. These so-called *mass diffusion fluxes*, are evaluated considering the following relationship:

$$\vec{j_i}=\rho_i\left(\vec{v}_i-\vec{v}\right)=\rho_i\vec{V}_i \tag{2.6}$$

where $\vec{V}_i$ are the *diffusion velocities*. From the definition of the mixture's mass-averaged velocity, the sum of mass diffusion fluxes of the N species forming part of the mixture satisfy:

$$\sum_{i=1}^{N}\vec{j_i}=\sum_{i=1}^{N}\rho_i\vec{V}_i=0 \tag{2.7}$$

Substituting equation 2.6 into equation 2.1, species mass conservation reads:

$$\frac{\partial \rho_i}{\partial t}+\nabla\cdot(\rho_i\vec{v})=-\nabla\cdot\vec{j_i}+\dot{w}_i \tag{2.8}$$

or in terms of the species mass fraction ($Y_i=\rho_i/\rho$):

$$\frac{\partial \rho Y_i}{\partial t}+\nabla\cdot(\rho Y_i\vec{v})=-\nabla\cdot\vec{j_i}+\dot{w}_i \tag{2.9}$$

2.1.2 Momentum

The conservation of momentum for a given species i of the mixture reads,

$$\frac{\partial\left(\rho_i\vec{v}_i\right)}{\partial t}+\nabla\cdot\left(\rho_i\vec{v}_i\vec{v}_i\right)=\nabla\cdot\vec{\sigma}_i+\rho_i\vec{b}_i+\dot{w}_i\vec{v}_i \tag{2.10}$$

where, $\vec{b_i}$ is the body force per unit of mass affecting the ith species, $\dot{w}_i\vec{v}_i$ is the rate of generation of momentum per unit volume of ith species, and $\vec{\sigma}_i$ is the ith species stress tensor, that can be split into an isotropic part due to partial pressure and a deviatoric part due to the shear of viscous stresses:

$$\vec{\sigma}_i=-p_i\vec{\delta}+\vec{\tau}_i \tag{2.11}$$

An overall mixture's momentum conservation equation can be derived by summing the contribution of each species, and postulating that overall momentum is neither created nor destroyed by chemical reactions [1], i.e. $\sum\dot{w}_i\vec{v}_i=0$, then:

$$\sum_{i=1}^{N}\left(\frac{\partial\left(\rho_i\vec{v}_i\right)}{\partial t}+\nabla\cdot\left(\rho_i\vec{v}_i\vec{v}_i\right)\right)=\nabla\cdot\sum_{i=1}^{N}\vec{\sigma}_i+\sum_{i=1}^{N}\rho_i\vec{b}_i \tag{2.12}$$

The total rate of change of linear momentum can be arranged considering the definition of the species velocities as the sum of the species diffusion velocities plus mixture's averaged velocity. Thus, momentum fluxes are composed by an averaged mixture's momentum flux and the sum of species *diffusional momentum fluxes*:

$$\begin{aligned}\sum_{i=1}^{N}\rho_i\vec{v}_i\vec{v}_i &= \sum_{i=1}^{N}\rho_i\left(\vec{V}_i-\vec{v}\right)\left(\vec{V}_i-\vec{v}\right)\\ &= \rho\vec{v}\vec{v}+\sum_{i=1}^{N}\rho_i\vec{V}_i\vec{V}_i+2\vec{v}\sum_{i=1}^{N}\rho_i\vec{V}_i\\ &= \rho\vec{v}\vec{v}+\sum_{i=1}^{N}\rho_i\vec{V}_i\vec{V}_i\end{aligned}$$

Rewriting equation 2.12 we have:

$$\frac{\partial}{\partial t}\left(\rho\vec{v}\right)+\nabla\cdot\left(\rho\vec{v}\vec{v}\right)=\nabla\cdot\sum_{i=1}^{N}\vec{\sigma}_i-\nabla\cdot\left(\sum_{i=1}^{N}\rho_i\vec{V}_i\vec{V}_i\right)+\sum_{i=1}^{N}\rho_i\vec{b}_i \tag{2.13}$$

Considering Dalton's law, which defines static pressure as the sum of species partial pressures, the sum of the stresses of individual species gives the overall mixture's

stress tensor:

$$\vec{\sigma} = \sum_{i=1}^{N} \vec{\sigma}_i = -p\vec{\delta} + \sum_{i=1}^{N} \vec{\tau}_i \tag{2.14}$$

Therefore, the total rate of change of linear momentum can be written as:

$$\frac{\partial}{\partial t}(\rho\vec{v}) + \nabla \cdot (\rho\vec{v}\vec{v}) = -\nabla p + \nabla \cdot \sum_{i=1}^{N} \vec{\tau}_i - \nabla \cdot \sum_{i=1}^{N} \left(\rho_i \vec{V}_i \vec{V}_i\right) + \sum_{i=1}^{N} \rho_i \vec{b}_i \tag{2.15}$$

2.1.3 Kinetic energy

No additional principles are needed to formulate a conservation equation of kinetic energy for a given species of the mixture ($e_{c_i} = \vec{v}_i \cdot \vec{v}_i \,/2$). It can be easily derived by means of the dot product of $\vec{v_i}$ with the species momentum equation (equation 2.10).

$$\frac{\partial}{\partial t}(\rho_i e_{c_i}) + \nabla \cdot (\rho_i \vec{v}_i e_{c_i}) = \vec{v}_i \cdot \nabla \cdot \vec{\sigma}_i + \vec{v}_i \cdot \rho_i \vec{b_i} + \vec{v}_i \cdot \dot{w}_i \vec{v}_i \tag{2.16}$$

Postulating that overall kinetic energy is neither created nor destroyed by chemical reactions, and summing the individual species kinetic energy conservation equations we obtain:

$$\sum_{i=1}^{N} \left(\frac{\partial}{\partial t}(\rho_i e_{c_i}) + \nabla \cdot (\rho_i \vec{v}_i e_{c_i}) \right) = \sum_{i=1}^{N} \left(\vec{v}_i \cdot \nabla \cdot \vec{\sigma}_i + \rho_i \vec{v}_i \cdot \vec{b}_i \right) \tag{2.17}$$

Defining the mixture's averaged kinetic energy as:

$$e_c = \frac{1}{\rho} \sum_{i=1}^{N} \rho_i e_{c_i} \tag{2.18}$$

the overall kinetic energy conservation equation reads:

$$\frac{\partial}{\partial t}(\rho e_c) + \nabla \cdot (\rho \vec{v} e_c) = \sum_{i=1}^{N} \left(\vec{v}_i \cdot \nabla \cdot \vec{\tau}_i - \vec{v}_i \cdot \nabla p - \nabla \cdot \vec{j}_i e_{c_i} + \rho_i \vec{v}_i \cdot \vec{b}_i \right) \tag{2.19}$$

2.1.4 Energy

The first thermodynamic law is applied to the fluid contained in a control volume to derive the total energy conservation equation. The total energy is expressed as the sum of the thermal and mechanical energies.

The variation of the total energy stored in the control volume, plus the energy transported with the fluid motion, must be equal to the heat fluxes balance across its boundaries and the energy transferred as work to the CV.

$$\begin{aligned}\sum_{i=1}^{N}\frac{\partial\left(\rho_i\left(u_i+e_{c_i}\right)\right)}{\partial t} &+ \sum_{i=1}^{N}\nabla\cdot\left(\rho_i\vec{v}_i\left(u_i+e_{c_i}\right)\right)=-\sum_{i=1}^{N}\nabla\cdot\vec{q}_i-\nabla\cdot\vec{q}^{\,R}\\ &- \sum_{i=1}^{N}\nabla\cdot p_i\vec{v}_i+\sum_{i=1}^{N}\nabla\cdot\vec{v}_i\cdot\vec{\tau}_i+\sum_{i=1}^{N}\rho_i\vec{v}_i\cdot\vec{b}_i \qquad (2.20)\end{aligned}$$

On the right-hand side of eq. 2.20, $\vec{q}_i$ is the molecular heat flux of ith species, $\vec{q}^{\,R}$ is the radiant heat flux, and the other terms account for the work transferred to the control volume due to pressure, viscous and body forces respectively. By the definition of the mixture's internal energy,

$$u=\frac{1}{\rho}\sum_{i=1}^{N}\rho_i u_i \qquad (2.21)$$

we can arrange the left-hand side divergence terms,

$$\begin{aligned}\sum_{i=1}^{N}\nabla\cdot\left(\rho_i\vec{v}_i\left(u_i+e_{c_i}\right)\right) &= \sum_{i=1}^{N}\nabla\cdot\left(\left(\vec{j}_i+\rho_i\vec{v}\right)\left(u_i+e_{c_i}\right)\right)\\ &= \nabla\cdot\left(\rho\vec{v}\left(u+e_c\right)\right)+\nabla\cdot\left(\sum_{i=1}^{N}\vec{j}_i\left(u_i+e_{c_i}\right)\right)\end{aligned}$$

obtaining the conservation equation in terms of the mixture's internal energy and averaged kinetic energy:

$$\begin{aligned}\frac{\partial\left(\rho\left(u+e_c\right)\right)}{\partial t} &+ \nabla\cdot\left(\rho\vec{v}\left(u+e_c\right)\right)=-\nabla\cdot\sum_{i=1}^{N}\vec{q}_i-\nabla\cdot\vec{q}^{\,R}\\ &+ \nabla\cdot\left(\sum_{i=1}^{N}\vec{v}_i\cdot\vec{\sigma}_i\right)-\nabla\cdot\left(\sum_{i=1}^{N}\vec{j}_i\left(u_i+e_{c_i}\right)\right)\\ &+ \sum_{i=1}^{N}\rho_i\vec{v}_i\cdot\vec{b}_i \qquad (2.22)\end{aligned}$$

2.1.5 Thermal energy

Thermal energy equation can be obtained subtracting the kinetic energy equation (2.19) to total energy equation (2.22):

$$\frac{\partial(\rho u)}{\partial t} + \nabla \cdot (\rho \vec{v} u) = -\nabla \cdot \sum_{i=1}^{N} \vec{q}_i - \nabla \cdot \vec{q}^{\,R} + \sum_{i=1}^{N} \vec{\sigma}_i : \nabla \vec{v}_i - \nabla \cdot \sum_{i=1}^{N} \vec{j}_i u_i \tag{2.23}$$

In thermal energy equation, it is interesting to point out the terms that involve the the dyadic product of the stress tensor and the species velocity gradient, $\sum \vec{\sigma}_i : \nabla \vec{v}_i$. In the total energy conservation equation (2.22), we defined the work done on the fluid by pressure and viscous forces as:

$$\nabla \cdot \left(\sum_{i=1}^{N} \vec{v}_i \cdot \vec{\sigma}_i \right) = -\sum_{i=1}^{N} \nabla \cdot p_i \vec{v}_i + \sum_{i=1}^{N} \nabla \cdot \vec{v}_i \cdot \vec{\tau}_i \tag{2.24}$$

These works can be split into two terms:

$$\begin{aligned} -\nabla \cdot \textstyle\sum p_i \vec{v}_i \quad &= \underset{(Ia)}{-\textstyle\sum \vec{v}_i \cdot \nabla p_i} \quad \underset{(IIa)}{-\textstyle\sum p_i \nabla \vec{v}_i} \\ \nabla \cdot (\textstyle\sum \vec{v}_i \cdot \vec{\tau}_i) \quad &= \underset{(Ib)}{\textstyle\sum \vec{v}_i \cdot \nabla \cdot \vec{\tau}_i} \quad \underset{(IIb)}{+\textstyle\sum \vec{\tau}_i : \nabla \vec{v}_i} \end{aligned}$$

The first terms (Ia/Ib), represent the useful (or mechanical) work performed due to pressure/viscous forces. These terms are the responsible of the increment or decrement of kinetic energy e_c (see equation 2.19).

The IIa term, represents the (reversible) work done on the fluid due to compressibility effects. For example, for an expansion process this term is positive, the kinetic energy increases in the same quantity as internal energy decreases (reversible exchange between both quantities). On the other hand, when a reversible compression process is given, this exchange is done in the opposite direction.

The last term (IIb), represents the irreversible part of the transferred work due to viscous forces, being a irreversible transfer from kinetic energy to internal energy.

Internal energy of ith species u_i, is given by,

$$u_i = h_i - \frac{p_i}{\rho_i} \tag{2.25}$$

where h_i , is the specific enthalpy of ith species. Defining the mixture's internal energy in a similar way as (2.21) it is easy to obtain,

$$u = h - \frac{p}{\rho} \tag{2.26}$$

and substituting both definitions into equation 2.23, we obtain:

$$\begin{aligned}\frac{\partial(\rho h)}{\partial t}+\nabla\cdot(\rho\vec{v}h) &- \frac{\partial p}{\partial t}-\nabla\cdot(\vec{v}p)=-\nabla\cdot\sum_{i=1}^{N}\vec{q}_i-\nabla\cdot\vec{q}^{\,R}\\ &+ \sum_{i=1}^{N}\vec{\tau}_i:\nabla\vec{v}_i-\sum_{i=1}^{N}p_i\nabla\cdot\vec{v}_i\\ &- \sum_{i=1}^{N}\nabla\cdot\vec{j}_i h_i+\sum_{i=1}^{N}\nabla\cdot\frac{\vec{j}_i}{\rho_i}p_i \end{aligned} \tag{2.27}$$

Replacing mass diffusive fluxes $\vec{j}_i$, by its definition, and writing the last term on the left-hand side as,

$$\begin{aligned}\sum_{i=1}^{N}\nabla\cdot\frac{\vec{j}_i}{\rho_i}p_i &= \sum_{i=1}^{N}\nabla\cdot(\vec{v}_i-\vec{v})\,p_i=\sum_{i=1}^{N}\nabla\cdot(\vec{v}_i p_i)-\nabla\cdot(\vec{v}p)\\ &= \sum_{i=1}^{N}\vec{v}_i\nabla p_i+\sum_{i=1}^{N}p_i\nabla\cdot\vec{v}_i-\nabla\cdot(\vec{v}p)\end{aligned}$$

thermal energy conservation equation yields:

$$\begin{aligned}\frac{\partial(\rho h)}{\partial t} &+ \nabla\cdot(\rho\vec{v}h)=-\nabla\cdot\sum_{i=1}^{N}\vec{q}_i-\nabla\cdot\vec{q}^{\,R}-\nabla\cdot\sum_{i=1}^{N}\vec{j}_i h_i\\ &+ \sum_{i=1}^{N}\vec{\tau}_i:\nabla\vec{v}_i+\frac{\partial p}{\partial t}+\sum_{i=1}^{N}\vec{v}_i\nabla p_i\end{aligned} \tag{2.28}$$

2.2 Modelization of the molecular transport terms

Once the conservation laws have been applied in order to obtain the governing equations for multicomponent reactive flows, the molecular fluxes of mass $\vec{j}_i$, momentum $\vec{\sigma}_i$, and heat $\vec{q}_i$, have to be modeled.

The modelization that relates the molecular transport fluxes to the primitive variables appearing in the governing equations requires the introduction of transport coefficients. These coefficients are defined by means of a development based on the molecular kinetic theory. Mathematical models for calculating individual momentum $\vec{\sigma}_i$, and energy fluxes $\vec{q}_i$ are extremely complex.

To overcome these modelization difficulties, we will look at the conservation laws derived from the kinetic theory. Its comparison with the present derivation using continuum mechanics, will allow to assume criteria for the modelization of the above mentioned fluxes.

2.2.1 Conservation laws from a kinetic theory point of view. Comparison to the continuum mechanics derivation

Introduction to the molecular kinetic-theory

The kinetic theory focuses the analysis of the fluid-dynamical conservation laws from a microscopic point of view. A gas is seen as a system of particles moving in all directions and interacting each other in a highly complex manner.

The properties of these systems can be completely described by specifying the *velocity distribution function* $f(\vec{x}, \vec{v}, t)$, that denotes the probable number of molecules at the position $\vec{x}$ moving with a velocity $\vec{v}$ at time t. As it is extremely difficult to give such detailed description of macroscopic systems, gases are usually described as an ensemble of a large replicas of a single system [2]. In this way, the kinetic theory describes the non-equilibrium systems by the definition of a velocity distribution function for each chemical species that forms the gas mixture, $f_i(\vec{x}, \vec{v}, t)$ for $i = 1, ..., N$.

The rigorous evaluation of the system of velocity distribution functions can be done via the solution of *Lioville equation*. The considerable complexity of this evaluation can be reduced by assuming the gas densities sufficiently low to consider that molecular collisions involving more than two molecules are negligible (i.e. dilute gases). Under this assumption, simpler velocity distribution functions can be evaluated by the resolution of an integro-differential equation known as *Boltzmann equation*.

The macroscopic behavior of a dilute gas, conservation equations of mass, momentum and energy, can be obtained by means of *Enskog's general equation of change*, derived directly from Boltzmann equation. In these equations of change, the fluxes of mass, momentum and energy, are related to the diffusion velocities, the stress tensor and the heat flux. The definition of these quantities differs from the definition given in the derivation of the conservative equations from the point of view of continuum mechanics (section 2.1), since the kinetic-theory derivation do not need the introduction of diffusion terms. For instance, diffusional momentum fluxes are not defined, because the evaluation of individual stress tensors $\vec{\sigma}_i$ is not necessary [2][3].

Definitions of kinetic theory

In a microscopic point of view, the average linear velocity of species of type i is defined by the kinetic theory as,

$$\vec{v}_i = \langle \vec{v}_{i,m} \rangle = \frac{1}{n_i} \int \vec{v}_{i,m} \, f_i(\vec{x}, \vec{v}, t) \, d\vec{v}_i \tag{2.29}$$

where, $\vec{v}_{i,m}$ is the velocity of a given molecule m of type i, n_i is the number density of molecules of type i, and $f_i(\vec{x}, \vec{v}, t)$ is the distribution function associated to these molecules.

Mass-averaged velocity of the mixture is defined as,

$$\vec{v} = \frac{1}{\rho} \sum_{i=1}^{N} n_i m_i \vec{v}_i \tag{2.30}$$

where m_i, is the mass of the molecules of type i and ρ the gas density.

$$\rho = \sum_{i=1}^{N} n_i m_i \tag{2.31}$$

Diffusion effects are introduced via the definition of the diffusion velocities,

$$\vec{V}_i = \vec{v}_i - \vec{v} \tag{2.32}$$

and the peculiar velocities,

$$\vec{V}_{i,m} = \vec{v}_{i,m} - \vec{v} \tag{2.33}$$

$$\vec{V}'_{i,m} = \vec{v}_{i,m} - \vec{v}_i \tag{2.34}$$

related by the following equation:

$$\vec{V}_{i,m} = \vec{V}'_{i,m} + \vec{V}_i \tag{2.35}$$

Equations of change

From the kinetic theory, gradients of the macroscopic physical properties (mass, average velocity and temperature) of a gas under non-equilibrium conditions are caused by the molecular transport of mass m_i, momentum $m_i \vec{V}_{i,m}$ and internal energy $m_i u_{i,m}$. Internal energy of molecules of type i is expressed as the sum of the translatory kinetic energy plus additional internal energy terms (rotational, vibrational, etc). Averaged total internal energy of the ith species is given by [1],

$$u_i = \langle u_{i,m} \rangle = \langle \frac{1}{2} \vec{V}'_{i,m} \cdot \vec{V}'_{i,m} + i_{i,m} \rangle = \frac{1}{2} \langle \vec{V}'_{i,m} \cdot \vec{V}'_{i,m} \rangle + i_i \tag{2.36}$$

and the averaged internal energy of the mixture per unit volume is defined as:

$$\rho u^T = \sum_{i=1}^{N} \left(\rho_i \langle \frac{1}{2} \vec{V}_{i,m} \cdot \vec{V}_{i,m} \rangle + \rho_i i_i \right) \tag{2.37}$$

Notice that in equation 2.36, and in order to evaluate the averaged species internal energies, the translatory kinetic energy has been defined by means of the relative

molecular velocities of species $\vec{V}'_{i,m}$. That is, the molecular velocity of species $\vec{v}_{i,m}$, related to the mean species velocity $\vec{v}_i$. In fact, this translatory kinetic energy represents the flux of energy of molecules of type i due to molecular transport. In contrast, when averaged mixture internal energy is defined (equation 2.37), the relative molecular velocities of the species $\vec{V}_{i,m}$, have been considered respect the averaged mixture's velocity $\vec{v}$. Taking into account both definitions, averaged mixture internal energy can be related to species internal energies employing equation 2.35 and assuming by definition $\langle \vec{V}'_{i,m} \rangle = 0$:

$$\begin{aligned} \rho u^T &= \sum_{i=1}^{N} \left(\rho_i \langle \frac{1}{2} (\vec{V}'_{i,m} + \vec{V}_i) \cdot (\vec{V}'_{i,m} + \vec{V}_i) \rangle + \rho_i i_i \right) \\ &= \sum_{i=1}^{N} \left(\rho_i \langle \frac{1}{2} \vec{V}'_{i,m} \cdot \vec{V}'_{i,m} \rangle + \rho_i \frac{1}{2} \vec{V}_i \cdot \vec{V}_i + \rho_i i_i \right) \\ &= \sum_{i=1}^{N} \left(\rho_i u_i + \rho_i \frac{1}{2} \vec{V}_i \cdot \vec{V}_i \right) \end{aligned} \tag{2.38}$$

The application of the mentioned physical quantities to the *Enskog's general equation of change*, leads the conservations equations of mass, momentum, and internal energy [2]:

$$\frac{\partial \rho}{\partial t} + \nabla \cdot (\rho \vec{v}) = 0 \tag{2.39}$$

$$\frac{\partial \rho_i}{\partial t} + \nabla \cdot (\rho_i \vec{v}) = -\nabla \cdot \rho_i \vec{V}_i + \dot{w}_i \tag{2.40}$$

$$\frac{\partial}{\partial t} (\rho \vec{v}) + \nabla \cdot (\rho \vec{v} \vec{v}) = \nabla \cdot \vec{\sigma}^{\,T} + \sum_{i=1}^{N} \rho_i \vec{b}_i \tag{2.41}$$

$$\frac{\partial}{\partial t} \left(\rho u^T \right) + \nabla \cdot \left(\rho \vec{v} u^T \right) = -\nabla \cdot \vec{q}^{\,T} - \nabla \cdot q^{\vec{R}} + \vec{\sigma}^{\,T} : \nabla \vec{v} + \sum_{i=1}^{N} \rho_i \vec{V}_i \cdot \vec{b}_i \tag{2.42}$$

where mixture momentum and heat fluxes are expressed respectively as [1]:

$$\vec{\sigma}^{\,T} = -\sum_{i=1}^{N} \rho_i < \vec{V}_{i,m} \vec{V}_{i,m} > \tag{2.43}$$

$$\vec{q}^{\,T} = \sum_{i=1}^{N} \rho_i < (\frac{1}{2} \vec{V}_{i,m} \cdot \vec{V}_{i,m} + i_{i,m}) \vec{V}_{i,m} > \tag{2.44}$$

Notice again, that mixtures fluxes are defined by means of peculiar species velocities defined respect mean mass-averaged mixtures velocities. On the other hand, and as

in the definition of species internal energy, individual species momentum and heat fluxes are written as:

$$\vec{\sigma}_i = -\rho_i < \vec{V}'_{i,m}\vec{V}'_{i,m} > \tag{2.45}$$

$$\vec{q}_i = \rho_i < (\frac{1}{2}\vec{V}'_{i,m} \cdot \vec{V}'_{i,m} + i_{i,m})\vec{V}'_{i,m} > \tag{2.46}$$

Employing the relationship given by the equation 2.35, mixture momentum and heat fluxes can be related to the species individual fluxes [1]:

$$\vec{\sigma}^{\,T} = \sum_{i=1}^{N} \vec{\sigma}_i - \sum_{i=1}^{N} \rho_i \vec{V}_i \vec{V}_i \tag{2.47}$$

$$\vec{q}^{\,T} = \sum_{i=1}^{N} \vec{q}_i - \sum_{i=1}^{N} \vec{V}_i \cdot \vec{\sigma}_i + \sum_{i=1}^{N} \rho_i u_i \vec{V}_i + \sum_{i=1}^{N} \frac{1}{2}\rho_i (\vec{V}_i \cdot \vec{V}_i)\vec{V}_i \tag{2.48}$$

Kinetic theory vs continuum mechanics

Comparing the conservation equations from the continuum mechanics derivation (equations 2.5, 2.8, 2.15 and 2.23) to those given by the kinetic-theory derivation (equations 2.39, 2.40, 2.41 and 2.42), can be observed that for both derivations overall mass and species conservations equations coincide. However, some differences exist between the equations of overall conservation of momentum and conservation of energy.

In kinetic theory, the stress tensor includes in its definition the stresses due to diffusional momentum transport (equation 2.47) [1], aspect that continuum mechanics clearly differentiates (see equation 2.15). Once this difference is considered, both derivations are identical.

More apparent discrepancies appear when thermal energy conservation equations are compared. Nevertheless, considering the kinetic-theory definition of the internal energy (equation 2.38) and treating the total energy conservation equation from the continuum mechanics derivation (2.20), we can find similarities about both derivations.

Let's write again the total energy conservation equation from a continuum mechanics formulation:

$$\begin{aligned} \frac{\partial}{\partial t}\left(\sum_{i=1}^{N} \rho_i \left(u_i + e_{c_i}\right)\right) &+ \nabla \cdot \left(\sum_{i=1}^{N} \rho_i \vec{v}_i \left(u_i + e_{c_i}\right)\right) = -\nabla \cdot \sum_{i=1}^{N} \vec{q}_i - \nabla \cdot \vec{q}^{\,R} \\ &+ \nabla \cdot \left(\sum_{i=1}^{N} \vec{v}_i \cdot \vec{\sigma}_i\right) + \sum_{i=1}^{N} \rho_i \vec{v}_i \cdot \vec{b}_i \end{aligned} \tag{2.49}$$

we can start taking into account the mixture total energy defined in continuum mechanics and introducing the definition of species diffusion velocities. Thus, we deal with a relationship between the total energy with its kinetic-theory definition:

$$\begin{aligned}
\sum_{i=1}^{N} \rho_i (u_i + e_{c_i}) &= \rho \sum_{i=1}^{N} \left(Y_i u_i + Y_i \left(\frac{1}{2} \vec{v}_i \cdot \vec{v}_i \right) \right) \\
&= \rho \sum_{i=1}^{N} \left(Y_i u_i + Y_i \left(\frac{1}{2} (\vec{V}_i + \vec{v}) \cdot (\vec{V}_i + \vec{v}) \right) \right) \\
&= \rho \frac{1}{2} \vec{v} \cdot \vec{v} + \rho \sum_{i=1}^{N} \left(Y_i u_i + Y_i \frac{1}{2} \left(\vec{V}_i \cdot \vec{V}_i \right) \right) \\
&= \rho \frac{1}{2} \vec{v} \cdot \vec{v} + \rho u^T
\end{aligned}$$

On the left-hand side, total energy divergence can be also arranged introducing the definition of species diffusion velocities:

$$\begin{aligned}
\sum_{i=1}^{N} \rho_i \vec{v}_i \left(u_i + e_{c_i} \right) &= \sum_{i=1}^{N} \rho_i \left(\vec{V}_i + \vec{v} \right) \left(u_i + e_{c_i} \right) \\
&= \sum_{i=1}^{N} \rho_i \vec{v} \left(u_i + e_{c_i} \right) + \sum_{i=1}^{N} \rho_i \vec{V}_i \left(u_i + e_{c_i} \right) \\
&= \rho \vec{v} \, \frac{1}{2} \vec{v} \cdot \vec{v} + \rho \vec{v} u^T \\
&+ \sum_{i=1}^{N} \rho_i \vec{V}_i \left(u_i + \frac{1}{2} (\vec{V}_i + \vec{v}) \cdot (\vec{V}_i + \vec{v}) \right) \\
&= \rho \vec{v} \, \frac{1}{2} \vec{v} \cdot \vec{v} + \rho \vec{v} u^T + \sum_{i=1}^{N} \rho_i \vec{V}_i \, \frac{1}{2} \left(\vec{V}_i \cdot \vec{V}_i \right) \\
&+ \sum_{i=1}^{N} \rho_i \vec{V}_i u_i + \sum_{i=1}^{N} \rho_i \vec{V}_i \left(\vec{V}_i \cdot \vec{v} \right)
\end{aligned}$$

On the other hand, analyzing the right-hand side terms, the work done by pressure

and viscous forces can be decomposed in the following way:

$$\begin{aligned}\nabla \cdot \left(\sum_{i=1}^{N} \vec{v}_i \cdot \vec{\sigma}_i \right) &= \sum_{i=1}^{N} \vec{v}_i \cdot \nabla \cdot \vec{\sigma}_i + \sum_{i=1}^{N} \vec{\sigma}_i : \nabla \vec{v}_i \\ &= \sum_{i=1}^{N} (\vec{V}_i + \vec{v}) \cdot \nabla \cdot \vec{\sigma}_i + \sum_{i=1}^{N} \vec{\sigma}_i : \nabla (\vec{V}_i + \vec{v}) \\ &= \nabla \cdot \left(\sum_{i=1}^{N} \vec{V}_i \cdot \vec{\sigma}_i \right) + \vec{v} \cdot \nabla \cdot \sum_{i=1}^{N} \vec{\sigma}_i + \sum_{i=1}^{N} \vec{\sigma}_i : \nabla \vec{v}\end{aligned}$$

and the work performed by the body forces, can be also split into:

$$\sum_{i=1}^{N} \rho_i \vec{v}_i \cdot \vec{b}_i = \sum_{i=1}^{N} \rho_i \vec{V}_i \cdot \vec{b}_i + \sum_{i=1}^{N} \rho_i \vec{v} \cdot \vec{b}_i \tag{2.50}$$

Replacing the analyzed terms into the total energy conservation equation (2.49), we obtain:

$$\begin{aligned}\frac{\partial}{\partial t} \left(\rho u^T + \rho \frac{1}{2} \vec{v} \cdot \vec{v} \right) &+ \nabla \cdot \left(\rho \vec{v} u^T + \rho \vec{v} \frac{1}{2} \vec{v} \cdot \vec{v} \right) = -\nabla \cdot \left(\sum_{i=1}^{N} \rho_i \vec{V}_i u_i \right) \\ &- \nabla \cdot \left(\sum_{i=1}^{N} \rho_i \vec{V}_i \frac{1}{2} \left(\vec{V}_i \cdot \vec{V}_i \right) \right) - \nabla \cdot \left(\sum_{i=1}^{N} \rho_i \vec{V}_i \left(\vec{V}_i \cdot \vec{v} \right) \right) \\ &- \nabla \cdot \sum_{i=1}^{N} \vec{q}_i - \nabla \cdot \vec{q}^{\,R} \\ &+ \nabla \cdot \left(\sum_{i=1}^{N} \vec{V}_i \cdot \vec{\sigma}_i \right) + \vec{v} \cdot \nabla \cdot \sum_{i=1}^{N} \vec{\sigma}_i + \sum_{i=1}^{N} \vec{\sigma}_i : \nabla \vec{v} \\ &+ \sum_{i=1}^{N} \rho_i \vec{V}_i \cdot \vec{b}_i + \sum_{i=1}^{N} \rho_i \vec{v} \cdot \vec{b}_i\end{aligned} \tag{2.51}$$

In this equation, the left-hand side terms account for rate of change of an "averaged" mixture's total energy. To obtain the thermal energy conservation equation, we can subtract from 2.51 an "averaged" mixture's kinetic energy equation obtained by means of the dot product of $\vec{v}$ with the momentum equation. Treating the diffu-

sional momentum terms, this scalar equation can be written as:

$$\begin{aligned}\frac{\partial}{\partial t}\left(\rho\frac{1}{2}\vec{v}\cdot\vec{v}\right) &+ \nabla\cdot\left(\rho\vec{v}\frac{1}{2}\vec{v}\cdot\vec{v}\right) = \vec{v}\cdot\nabla\cdot\sum_{i=1}^{N}\vec{\sigma}_i + \vec{v}\cdot\sum_{i=1}^{N}\rho_i\vec{b}_i \\ &- \nabla\cdot\left(\vec{v}\cdot\sum_{i=1}^{N}\rho_i\vec{V}_i\vec{V}_i\right) + \sum_{i=1}^{N}\rho_i\vec{V}_i\vec{V}_i : \nabla\vec{v} \end{aligned} \tag{2.52}$$

Subtracting the obtained scalar equation to equation 2.51, and being,

$$\sum_{i=1}^{N}\rho_i\vec{V}_i\left(\vec{V}_i\cdot\vec{v}\right) = \vec{v}\cdot\sum_{i=1}^{N}\rho_i\vec{V}_i\vec{V}_i \tag{2.53}$$

thermal energy conservation equation reads:

$$\begin{aligned}\frac{\partial\left(\rho u^T\right)}{\partial t} &+ \nabla\cdot\left(\rho\vec{v}u^T\right) = \left(\sum_{i=1}^{N}\vec{\sigma}_i - \sum_{i=1}^{N}\rho_i\vec{V}_i\vec{V}_i\right) : \nabla\vec{v} \\ &- \nabla\cdot\left(\sum_{i=1}^{N}\vec{\sigma}_i + \rho_i\vec{V}_i u_i + \rho_i\vec{V}_i\,\frac{1}{2}\left(\vec{V}_i\cdot\vec{V}_i\right) + \sum_{i=1}^{N}\vec{V}_i\cdot\vec{\sigma}_i\right) \\ &- \nabla\cdot\vec{q}^{\,R} + \sum_{i=1}^{N}\rho_i\vec{V}_i\cdot\vec{b}_i \end{aligned} \tag{2.54}$$

Finally, taking into account the momentum and heat fluxes definitions given by the kinetic-theory (equations 2.47 and 2.48), we obtain the usual thermal energy conservation equation given by its kinetic-theory derivation.

$$\frac{\partial}{\partial t}\left(\rho u^T\right) + \nabla\cdot\left(\rho\vec{v}u^T\right) = -\nabla\cdot\vec{q}^{\,R} - \nabla\cdot\vec{q}^{\,T} + \vec{\sigma}^{\,T} : \nabla\vec{v} + \sum_{i=1}^{N}\rho_i\vec{V}_i\cdot\vec{b}_i, \tag{2.55}$$

Conclusions

Mathematical models to relate the individual pressure tensors $\vec{\sigma}_i$, and heat fluxes $\vec{q}_i$, to primitive variables by means of the introduction of transport coefficients, if exists, are extremely complex. In its default, and based on a molecular kinetic-theory development, mathematical models exist for the global momentum $\vec{\sigma}^{\,T}$, and heat fluxes $\vec{q}^{\,T}$.

In this section, the conservation equations of mass, momentum and energy, derived from the continuum mechanics or from the kinetic theory, have been compared in order to get deeper insight of the physical meaning of the different terms.

In the next section, the mathematical formulation of global momentum and heat fluxes given by the kinetic-theory are introduced. Based on continuum mechanics point of view, the mathematical models will be used to model a group of physical quantities instead of just the individual stress tensors and heat fluxes.

2.2.2 Flux vectors

Mass transport

In a multicomponent dilute gas, species mass diffusion fluxes $\vec{j}_i$, from a rigorous kinetic theory formulation, are associated to three mechanical forces and to one thermal force. Mass fluxes are caused by: i) concentration gradients $\vec{j}_{X,i}$; ii) pressure forces $\vec{j}_{p,i}$, for example in a rotating gas formed by heavy and light species; iii) body force $\vec{j}_{b,i}$, for instance, in a mixture submitted to an electrical field and where the mixture contains some species with magnetic properties; iv) temperature gradients $\vec{j}_{T,i}$. These contributions are usually called *ordinary*, *pressure*, *forced* and *thermal* diffusion. The last one is also known as *Soret effect*, who was one of the first scientist analyzing this phenomena (1879).

$$\vec{j}_i = \vec{j}_{X,i} + \vec{j}_{p,i} + \vec{j}_{b,i} + \vec{j}_{T,i} \tag{2.56}$$

For ideal gas low-density mixtures, these contributions can be formulated with the following expressions [3]:

$$\vec{j}_{X,i} = \frac{\rho M_i}{M^2} \sum_{j=1}^{N} M_j D_{ij} \nabla X_j \tag{2.57}$$

$$\vec{j}_{p,i} = \frac{\rho M_i}{M^2} \sum_{j=1}^{N} M_j D_{ij} \left(X_j - Y_j\right) \frac{1}{p} \nabla p \tag{2.58}$$

$$\vec{j}_{b,i} = -\frac{\rho M_i}{M^2} \sum_{j=1}^{N} M_j D_{ij} \left(X_j M_j \left(\vec{b}_j - \sum_{k=1}^{N} \frac{\rho_k}{\rho} \vec{b}_k \right) \right) \tag{2.59}$$

$$\vec{j}_{T,i} = -D_i^T \nabla \left(\ln T\right) \tag{2.60}$$

where, D_{ij} and D_i^T are the multicomponent diffusion coefficients and the multicomponent thermal diffusion coefficients respectively. It is worth to highlight that D_{ij} are the diffusion coefficients of species i to species j both forming part of a multicomponent mixture.

Species mass diffusion fluxes are related to species diffusion velocities, that in a compact manner, are written as [3]:

$$\vec{V_i} = \frac{1}{X_i M} \sum_{j=1}^{N} M_j D_{ij} \vec{d_j} - \frac{D_i^T}{\rho Y_i} \nabla \ln T \tag{2.61}$$

where, the term $\vec{d_j}$ accounts for ordinary, pressure and external forces diffusion effects.

$$\vec{d_j} = \nabla X_j + (X_j - Y_j) \frac{1}{p} \nabla p - X_j M_j \left(\vec{b_j} - \sum_{k=1}^{N} Y_k \vec{b_k} \right) \tag{2.62}$$

On the other hand, and from a rigorous kinetic theory derivation, a relationship among species diffusion velocities can be found (equation 2.63). The main aspect that can be pointed out, is the employment of binary diffusion coefficients $\mathcal{D}_{ij}$, instead of the multicomponent ones. This property allows to simplify notably the evaluation of mass diffusion fluxes under some restrictive hypothesis that will be analyzed in the next section [4].

$$\sum_{j=1}^{N} \left(\frac{X_i X_j}{\mathcal{D}_{ij}} \right) \left(\vec{V_j} - \vec{V_i} \right) = \vec{d_i} - \sum_{j=1}^{N} \left(\frac{X_i X_j}{\mathcal{D}_{ij}} \right) \left(\frac{D_j^T}{Y_j} - \frac{D_i^T}{Y_i} \right) \nabla \left(\ln T \right) \tag{2.63}$$

Momentum transport

In the kinetic theory development, mixture stress tensor includes the individual contribution of species stress tensors and diffusional momentum fluxes. Considering this kinetic-theory development, and assuming a Newtonian fluid, the mixture stress tensor can be formulated in a similar manner as for a single-component formulation [2]:

$$\vec{\sigma}^{\,T} = \sum_{i=1}^{N} \vec{\sigma}_i - \sum_{i=1}^{N} \rho_i \vec{V_i} \vec{V_i} = -p\vec{\delta} + \vec{\tau}^{\,T} \tag{2.64}$$

where the total shear viscous stresses are formulated considering a multicomponent mixture transport coefficient [2].

$$\vec{\tau}^{\,T} = \mu \left(\nabla \vec{v} + \nabla \vec{v}^{\,t} \right) - \left(\frac{2}{3} \mu \nabla \cdot \vec{v} \right) \vec{\delta} \tag{2.65}$$

[2] In equation 2.65, $\vec{v}^{\,t}$ means transpost of velocity vector

Energy transport

Molecular transport of energy (equation 2.46) is associated to three main contributions: the energy flux due to temperature gradients, the flux of energy related to mass transport, and an additional effect based on *Onsager*'s reciprocal relations of irreversible thermodynamics, which implies a reciprocal process between mass and heat fluxes. The flux of energy produced by concentration gradients is known as *Duffour* effect.

The usual expression to formulate the energy flux is given below [2],

$$\vec{q}^{\,T} = -\lambda^{'}\nabla T + \sum_{i=1}^{N} \vec{j}_i h_i + RT \sum_{i=1}^{N} \left(\frac{D_i^T}{X_i M_i} \right) \vec{d}_i \tag{2.66}$$

in this equation, the contribution of concentration gradients is given in terms of diffusion velocities. Thus, $\lambda^{'}$ is not thermal conductivity as it is usually defined. This coefficient includes some contribution due to thermal diffusion that should be taken into account on its modelization.

2.2.3 Mixture averaged transport coefficients

In order to close the mathematical formulation of mass, momentum and energy fluxes, a mathematical model to formulate multicomponent transport coefficients has to be derived. From a kinetic-theory development, and assuming a dilute gas, these coefficients can be defined in terms of intermolecular forces and the dynamics of binary collisions.

The rigorous formulation of transport multicomponent coefficients will not be considered in this work. Although multicomponent formulations are available in the literature, their evaluation supposes a considerable computational cost. For multidimensional numerical simulations of reactive flows, that is the main interest of this work, the computational time to evaluate detailed multicomponent properties could be excessive. An alternative, and simpler formulation of these coefficients is considered hereafter. Their derivation is based on a kinetic theory formulation assuming first approximations assessed with experimental measurements. Usually, they are referred as semi-empirical formulations, and in general they are not problem independent. The resultant coefficients are expressions that relates mixture's transport coefficients to species coefficients and species concentrations. These transport coefficients are known as mixture-averaged properties.

Diffusion coefficients

On the evaluation of multicomponent diffusion D_{ij}, instead of looking to their multicomponent complex formulation, it is very common to take advantage of equation

2.63, where binary diffusion coefficients are employed $\mathcal{D}_{ij}$. The formulation of these coefficients is considerable simpler than the first ones, and they are independent to species concentrations. This property allows the employment of temperature-pressure dependent functions that can be defined in a pre-processing task.

Looking to equation 2.63, and considering the ordinary diffusion contribution to mass fluxes, we can write what are called *Stefan-Maxwell* equations:

$$\sum_{j=1}^{N} \left(\frac{X_i X_j}{\mathcal{D}_{ij}} \right) \left(\vec{V}_j - \vec{V}_i \right) = \nabla X_i \tag{2.67}$$

that for a binary mixture gets the Fick-like formula [5]:

$$\vec{V}_i = -\frac{\mathcal{D}_{im}}{X_i} \nabla X_i \tag{2.68}$$

Here $\mathcal{D}_{im}$ is in fact $\mathcal{D}_{12} = \mathcal{D}_{21}$, and accounts strictly for a binary mixture. Due to its attractive simple formulation, this formula is usually employed in multicomponent mass diffusion problems. Nevertheless, it is not possible to derive an exact formulation of these diffusion coefficients of species in the mixture, and further restrictive hypothesis must be considered.

One of the most used hypothesis to formulate mixture diffusion coefficients is the *trace-species* approximation. The equivalent Fickian diffusion coefficient is obtained by assuming that a given species see the rest moving with the same averaged velocity. Rearranging equation 2.67, multicomponent coefficient $\mathcal{D}_{im}$ reads [6]:

$$\mathcal{D}_{im} = \frac{1 - Y_i}{\sum_{\substack{j=1 \\ j \neq i}}^{N} X_j / \mathcal{D}_{ij}} \tag{2.69}$$

This approximation gives sufficiently good accuracy when the mixture is composed mostly by one species.

Considering again the hypothesis that the mixture is composed mostly for one species, and therefore neglecting the gradients of the mixture mass weight, rearranging equation 2.68 we can yield with the well-known Fick's Law.

$$\vec{j}_{x,i} = -\rho \mathcal{D}_{im} \nabla Y_i \tag{2.70}$$

In general the employment of such mixture-averaged coefficients do not satisfy the identity $\sum \vec{j}_i = 0$. To overcome this inconvenient, mass diffusion fluxes have to be corrected. The imbalance, is usually assigned proportionally to each species in function of its concentration.

Thermal diffusion ratios

Thermal diffusion coefficients are usually formulated assuming *trace-species* approximation from the definition of species diffusion coefficients. In this way, and assuming also light component limit, the contribution of temperature gradients to species diffusion fluxes reads [3],

$$\vec{j}_{T,i} = -\rho_i \frac{\mathcal{D}_{im}\Theta_i}{X_i} \nabla \left(\ln T\right) \tag{2.71}$$

where Θ_i is the thermal diffusion ratio of ith species and is given by [6]:

$$\Theta_i = \sum_{j=1}^{N} \theta_{ij} X_i X_j \tag{2.72}$$

Here, θ_{ij} are the pairs of thermal diffusion ratios for light species into all other components of the mixture. These ratios are only given for chemical species with mass weights lower that 5 g/mol, that are those where thermal diffusion effects becomes more important. As θ_{ij} are no concentration dependent, these ratios are usually defined in a pre-processing task in terms of temperature dependent polynomials.

Viscosity coefficient

On the evaluation of the mixture viscosity coefficient, and from an approximation of the rigorous kinetic formulation, Buddenberg and Wilke [6] suggested the following expression:

$$\mu = \sum_{i=1}^{N} X_i \left(\frac{X_i}{\mu_i} + 1.385 X_j \sum_{\substack{j=1 \\ j\neq i}}^{N} p M_i \mathcal{D}_{ij} \right)^{-1} \tag{2.73}$$

As can be seen, the mixture viscosity can be easily evaluated in terms of species viscosities, pressure, and binary diffusion coefficients. Although, this formula is derived from the most rigorous formulation, it is interesting to point out that originally in the formula appeared a 2 instead of the factor 1.385. Experimental studies carried out by the authors motivated them to make such change [2]. For this reason, it is usually referred as a semi-empirical formulation.

Based on this formulation, Bird et al. [3] proposed the following expression, that is used in most standard transport properties software packages [6]:

$$\mu = \sum_{i=1}^{N} \frac{X_i \mu_i}{\sum_{j=1}^{N} X_j \Phi_{ij}} \tag{2.74}$$

where in this case, the binary diffusion coefficients are not directly included, and in their default the quantity Φ_{ij} is defined as:

$$\Phi_{ij} = \frac{1}{\sqrt{8}} \left(1 + \frac{M_i}{M_j}\right)^{-\frac{1}{2}} \left(1 + \left(\frac{\mu_i}{\mu_j}\right)^{\frac{1}{2}} \left(\frac{M_j}{M_i}\right)^{\frac{1}{4}}\right)^2 \tag{2.75}$$

Thermal conductivity coefficient

On the definition of energy fluxes (equation 2.66), the transport coefficient that we have employed is $\lambda^{'}$, that includes the contribution due to thermal diffusion. This coefficient can be formulated rigorously as [6]:

$$\lambda^{'} = \lambda + \frac{1}{2} R \sum_{i=1}^{N} \sum_{\substack{j=1 \\ j \neq i}}^{N} \frac{RT X_i X_j}{p \mathcal{D}_{ij}} \left(\frac{D_i^T}{X_i M_i} - \frac{D_j^T}{X_i M_j}\right)^2 \tag{2.76}$$

and can be obtained by means of a kinetic-theory formulation. Due to its complexity, its evaluation could be excessively time-consuming in a CFD simulation, in this way and when appropriate, simplified formulations are recommended. One of the most employed models is based on the evaluation of mixture's averaged viscosity formulation proposed by Wilke [6]:

$$\lambda^{'} = \sum_{i=1}^{N} \frac{\lambda_i}{1 + \left(\sum_{\substack{j=1 \\ j \neq i}}^{N} 1.065 X_j \Phi_{ij}\right)^{-1}} \tag{2.77}$$

As can be seen, this formulation forces the evaluation of individual species due to the presence of the Φ_{ij} variable. In many situations, where momentum equations are not needed to be solved (i.e. if constant pressure is assumed or no convection processes occurs), more simpler semi-empirical formulations can be adopted. For instance, among them we can find the following expression, that according to some experience gives results with discrepancies in the range of a few percent [5]:

$$\lambda^{'} = \frac{1}{2} \left(\sum_{i=1}^{N} X_i \lambda_i + \left(\sum_{i=1}^{N} \frac{X_i}{\lambda_i}\right)^{-1}\right) \tag{2.78}$$

Non-dimensional numbers

When possible, heat transfer and fluid flow problems are given in a non-dimensional form and physical properties are given in terms of non-dimensional numbers. Among

them, in heat and mass transfer problems we point out: *Prandtl* number Pr, which is a global measure of the relative importance of momentum transfer respect to heat transfer; *Schmidt* number Sc, which gives a ratio between momentum transfer and mass transfer; and *Lewis* number Le, which accounts for the relative importance of heat transfer against mass transfer. These non-dimensional numbers are written in terms of the transport coefficients as:

$$Pr = \mu c_p/\lambda \qquad Sc_i = \mu/\rho D_{im} \qquad Le_i = \lambda/\rho D_{im} c_{p_i}$$

The definition of an averaged *Lewis* number for a given chemical species is commonly used in heat and mass transfer problems in order to minimize the computational effort due to the evaluation of diffusion coefficients. One can obtain species diffusion coefficients in the mixture from the *Lewis* number, density, thermal conductivity and species specific heat. We have to keep in mind that the evaluation of these coefficients, even with a simplified formulation, involves the evaluation of $N^2/2$ binary diffusion coefficients, aspect that in some problems could suppose a considerable task. On the definition of species *Lewis* number, it is probed that in many gases its value is very near to the unity or slightly less than unity in some of them. Several studies have been carried out to define *Lewis* species numbers for different chemical species, and comparative studies analyzing the influence of their values to application problems are available [7].

2.2.4 Pure-species transport coefficients

Based on kinetic-theory formulations, single species transport coefficients of dilute gases are defined in terms of intermolecular forces and the dynamics of binary collisions. In a first approximation, tabulated Lennard-Jones potential data is employed to determine temperature and/or pressure dependence [8].

As an example, single species viscosities reads,

$$\mu_i = \frac{5}{16} \frac{\sqrt{\pi M_i k_B T}}{\pi \phi_i^2 \Omega^{(2,2)*}} \tag{2.79}$$

where, ϕ_i is the Lennard-Jones collision diameter, $\Omega^{(2,2)*}$ are the species non-dependent collision integrals, and k_B is the Boltzmann constant. Species non-dependent collision integrals, available in a tabulated form, are given in function of two parameters, the reduced temperature T_i^* and the reduced dipole moment δ_i^*. These parameters can be evaluated by means of the species Lennard-Jones potential ϵ_i, and the species dipole moment γ_i.

$$T_i^* = k_B T/\epsilon_i \quad ; \quad \delta_i^* = (1/2)\gamma_i^2/(\epsilon_i \phi_k^3)$$

Similar expressions are defined for species thermal conductivities and binary diffusion coefficients. Fitting procedures are adopted to formulate temperature and/or pressure dependence of the transport properties with polynomial functions [9].

2.3 Thermal radiation

In the formulation of the energy conservation equation one of the physical contributions involved is the radiant heat flux $\vec{q}^{\,R}$, actually the net input rate of heat transfer by radiation expressed in terms of the divergence of radiant heat flux.

Two theories have been developed to study the propagation and interaction of electromagnetic radiation with matter: the classical electromagnetic wave theory and the radiative (photon) transfer theory. Both theories describe the same phenomena although they are conceptually very different. In short, the electromagnetic wave theory study the propagation and interaction of electromagnetic radiation with matter from a microscopic point of view, and the radiative transfer theory from a macroscopic or phenomenological point of view. The first approach predicts the macroscopic properties of the medium which are the coefficients of the second approach. The radiation transfer theory ignores the wave nature of radiation and treats it as light rays of photons. The radiation transfer equation (RTE) describes the transfer of radiant energy in a participating medium. RTE can be derived from a simplification of the Maxwell equations in which , for example, polarization effects are not considered. RTE accounts for the rate of change of radiation intensity along a path in terms of the physical processes of absorption, emission and scattering [10][11]. From the resolution of RTE, radiative fluxes involved in energy equation can be evaluated.

2.3.1 Radiation transfer equation

Photon transport conservation law is considered to pose RTE equation. A conservation equation for the density number of photons having wavelengths in the range λ to $\lambda+d\lambda$ and whose flight paths lie within a solid angle $d\omega$ about the direction $\vec{s}$ is posed. These amount of photons are defined in terms of radiant energy intensity I, that is given per unit time, surface, solid angle and wavelength. For every point of the space $\vec{x}$ at time t, we have a directional distribution of the radiant energy density for each wavelength of the spectra, $I_{\lambda\omega}(\vec{x},\vec{s})$. Considering radiation as a quasi-steady phenomena, and assuming an isotropic behavior of the optical properties, radiation transfer equation in terms of this radiant energy intensity can be written in a differential form as:

$$\nabla \cdot I_{\lambda\omega}\vec{s} = \kappa_\lambda I_{b\lambda} - \kappa_\lambda I_{\lambda\omega} - \sigma_{s\lambda} I_{\lambda\omega} + \frac{\sigma_{s\lambda}}{4\pi}\int_{4\pi} I(\vec{x},\vec{s}\,',\lambda)\Phi(\vec{s}\,',\vec{s},\lambda)\,d\omega' \qquad (2.80)$$

Radiant energy intensity variation in a angular direction responds to the emitted and absorbed energy, the energy diverted to other directions and regions of the space (out-scattering), and the energy coming from other directions and regions of the space (in-scattering). These contributions are considered in the right-hand side of equation 2.80. Emission and in-scattering effects (first and fourth terms), contribute to increase

the radiant energy intensity in a given direction. In an opposite way, absorption and out-scattering effects, reduce it.

In equation 2.80, κ_λ and $\sigma_{s\lambda}$ are the absorption and scattering coefficients, $I_{b\lambda}$ is the black-body radiant intensity, and Φ is the phase function, namely, the percentage of energy coming from the direction $\vec{s}'$ that is diverted to $\vec{s}$.

2.3.2 Radiant heat fluxes

Radiant heat flux vector through a given direction, can be obtained by means of the integration of the radiant energy intensity field obtained by means of the solution of the RTE for the whole wavelength and solid angle.

$$\vec{q}^{\,R} = \int_0^\infty \int_{4\pi} I_{\lambda\omega}\vec{s}\, d\omega d\lambda \tag{2.81}$$

Radiant contributions in the energy conservation equation, appear as the divergence of the radiant heat flux vector. Thus, the net input rate of heat transfer by radiation along the whole wavelengths and directions in a finite volume Ω bounded by a closed surface S can be obtained directly by the integration of this divergence as:

$$\begin{aligned} \int_\Omega \nabla \cdot \vec{q}^{\,R} d\Omega &= \int_0^\infty \int_{4\pi} \int_\Omega \nabla \cdot \left(I_{\lambda\omega}\vec{s}\right) d\Omega d\omega d\lambda \\ &= \int_0^\infty \int_{4\pi} \int_\Omega \left(\kappa_\lambda I_{b\lambda} - \kappa_\lambda I_{\lambda\omega}\right) d\Omega d\omega d\lambda \end{aligned} \tag{2.82}$$

The integrated contribution of the scattering terms is zero because it only implies a redistribution of energy.

2.3.3 Optical coefficients

The accuracy of radiative transfer predictions is limited by the accuracy of the radiative properties of the medium. This accuracy is specially critical in combustion problems. Combustion products are formed by particles (basically soot) and specially gases (typically water vapor and carbon dioxide). Combustion gases do not scatter radiation significantly, but they are strong selective absorbers and emitters of radiant energy [12]. According to quantum mechanics, when an electromagnetic wave interacts with a gas cloud it is absorbed only if the amount of energy of the wave is exactly (neither higher nor lower) the quantity to raise the molecular energy state from lower to higher levels. Since the energy of the wave is in discrete amounts in inverse proportional to the wavelength, hc/λ, where h is the Planck constant and c is the speed of the wave, only a corresponding wavelength λ is affected. Most gas molecules have several hundreds even thousands of possible energy states so the gas absorption present

thousands of absorption lines. The typically combustion gases (CO_2, H_2O and CO) have a number of lines roughly between 10^5 and 10^6. The problem gets more difficult because these lines present a mountain-like shape, the so-called broadening process, with a exponential shape peaked at the center and with a rapid decay. The shape and width of these lines are function of the temperature and pressure of the medium. The Lorentz profile is normally used at moderate temperatures to characterize such lines. The typical line width is of the order of 10^{-3} μm.

Given the strong wavelength variation of the absorption coefficient (equal to the emission coefficient according to Kirchoff's law) a fully spectral study of the RTE equation, the so-called line by line radiation, is presently beyond the possibilities for most of the engineering studies. It would represent to solve as many RTE as line number. One model developed is to joint all the lines that due to the broadening process actually overlap between them. This is the so-called narrow band model with a typical band width of 0.05 mm which is considered quite narrow for most applications. Other models, less precise, define a bandwidth for the absorption coefficient of about 0.5 mm (wideband model) which coincide with a vibration-rotation band. A strong criticism of these methods is that the coefficient of absorption obtained which is an average over an spectral band has no physical meaning. It has been shown that the errors introduce can be quite large [13]. For thin optical thickness (less than unity) the Planck coefficient can be applied. It is a spectrally mean coefficient where the spectral details are lost. This approach is considered to be the state-of-the-art in the combustion community [14] for its simplicity and for the lack of accuracy of more sophisticated methods.

2.4 Mathematical formulation for low-Mach number laminar flames

Hereafter, the mathematical formulation considered in this thesis for the numerical simulation of laminar flames is presented. Governing equations, molecular transport fluxes and radiant energy transfer, are approximated in order to develop a computational suitable model for the multidimensional simulation of laminar flames. The appropriateness of the considered mathematical formulation is assessed in chapter 5, where the influence of some hypothesis is analyzed comparing numerical results with available experimental data.

2.4.1 Governing equations

The governing equations derived from continuum mechanics introduced in section 2.1, and their kinetic-theory equivalent form presented in section 2.2.1, are slightly simplified to the situations of interest of this work: low-Mach number laminar flames.

In the problems that are analyzed in the next chapters, gravitational forces are the only body forces acting to the fluid flow, and flow velocities are sub-sonic. Taking into account these assumptions the resulting set of governing equations can be rewritten as:

$$\frac{\partial \rho}{\partial t} + \nabla \cdot (\rho \vec{v}) = 0 \tag{2.83}$$

$$\frac{\partial \rho_i}{\partial t} + \nabla \cdot (\rho_i \vec{v}) = -\nabla \cdot \vec{j}_i + \dot{w}_i \tag{2.84}$$

$$\frac{\partial}{\partial t}(\rho \vec{v}) + \nabla \cdot (\rho \vec{v}\vec{v}) = -\nabla p + \nabla \cdot \vec{\tau}^{\,T} + \rho \vec{g} \tag{2.85}$$

$$\frac{\partial}{\partial t}(\rho u) + \nabla \cdot (\rho \vec{v} u) = -\nabla \cdot \vec{q}^{\,T} - \nabla \cdot \vec{q}^{\,R} + \vec{\tau}^{\,T} : \nabla \vec{v} - \nabla \cdot (p \vec{v}) \tag{2.86}$$

$$\rho = \frac{pM}{RT} \tag{2.87}$$

In energy conservation equation, total thermal energy u^T approximates to total internal energy u since, due to the low-Mach number hypothesis, diffusional species kinetic energy can be neglected. Considering these hypothesis, equation 2.86 can be written in terms of enthalpy as:

$$\frac{\partial}{\partial t}(\rho h) + \nabla \cdot (\rho \vec{v} h) = -\nabla \cdot \vec{q}^{\,T} - \nabla \cdot \vec{q}^{\,R} + \vec{\tau}^{\,T} : \nabla \vec{v} + \frac{\partial p}{\partial t} + \vec{v} \cdot \nabla p \tag{2.88}$$

In low-Mach number flames, pressure may be treated as spatially constant [15], and viscous dissipation can also be neglected. Thus, energy conservation equation reduces to:

$$\frac{\partial}{\partial t}(\rho h) + \nabla \cdot (\rho \vec{v} h) = -\nabla \cdot \left(\vec{q}^{\,T} + \vec{q^{R}} \right) \tag{2.89}$$

2.4.2 Molecular transport

Species mass diffusion fluxes $\vec{j}_i$, are evaluated considering *ordinary* and *thermal* contributions. *Pressure* diffusion is neglected due to the spatially constant hypothesis introduced above, while there is no contribution to body forces since gravity affects equally all species.

In methane/air laminar flames, *trace-species* approximation defined in section 2.2.3, can be suitable since the mixture is formed mostly by nitrogen. Thus, species diffusion fluxes can be evaluated considering the Fick-like formula as:

$$\vec{j}_i = -\rho \mathcal{D}_{im} \nabla Y_i - D_i^T \nabla (\ln T) \tag{2.90}$$

For the evaluation of molecular heat fluxes, the contribution due to concentration gradients is commonly neglected in laminar flame modeling. *Duffour* effect is negligible small in combustion processes, although it may not be in other reacting flows [16]. In this way, molecular heat fluxes are formulated in the following way:

$$\vec{q}^{\,T} = -\lambda^{'}\nabla T + \sum_{i=1}^{N} \vec{j}_i h_i \tag{2.91}$$

Shear-stress tensor for Newtonian fluids together with the mixture-averaged properties described in section 2.2.3 are considered.

Pure-species transport coefficients are evaluated from fitting coefficients provided by the CHEMKIN-package [9]. Fitting procedures are adopted to formulate temperature and/or pressure dependence of the transport properties with polynomial functions. In many heat and mass transfer problems, and in order to reduce the level of discrepancies among the solutions obtained from different researchers, it is very common to use the same criteria to define species transport coefficients. In this way, CHEMKIN-package [9], is one of the most commonly employed. This code uses polynomial fits of the logarithm of the property versus the logarithm of the temperature. Thus, species viscosities, thermal conductivities and binary diffusion coefficients are fitted as:

$$\ln \mu_i = \sum_{n=1}^{P} a_{n,i} \left(\ln T\right)^{(n-1)} \tag{2.92}$$

$$\ln \lambda_i = \sum_{n=1}^{P} b_{n,i} \left(\ln T\right)^{(n-1)} \tag{2.93}$$

$$\ln \mathcal{D}_{ij} = \sum_{n=1}^{P} d_{n,ij} \left(\ln T\right)^{(n-1)} \tag{2.94}$$

In these expressions binary diffusion coefficients have been evaluated at atmospheric pressure. To correct these values, we have to consider their linear pressure dependence. Since thermal diffusion ratios depend weakly on temperature, polynomials in temperature, rather than logarithm of temperature, are defined.

$$\theta_{ij} = \sum_{n=1}^{P} e_{n,i} T^{(n-1)} \tag{2.95}$$

2.4.3 Radiation submodel

Radiant heat transfer in flames can be modeled, in a first approximation, assuming non-participating media. With this approximation the medium is defined as trans-

parent and RTE (equation 2.80) reduces to:

$$\nabla \cdot I_{\lambda\omega}\vec{s} = 0 \tag{2.96}$$

This means that the radiant energy density neither increase nor decrease through a given direction due to the presence of the transport media. Radiant energy transfer reduces to the exchange of radiation among opaque elements. Specially at elevated temperatures, this approximation is not very suitable, all kind of substances emit and absorb energy in form of radiation.

A less rough model is based on the assumption that the amount of energy emitted is considerable larger than the absorbed [17]. No-scattering occurs. *Emission approximation*, do not need to solve RTE equation to evaluate the net rate of heat transfer by radiation, since they only depend on the black-body radiant intensity $I_{b\lambda}$, not to the local values of radiant energy intensity $I_{\lambda\omega}$. However, to avoid the resolution of RTE equation, further approximations have to be considered to take into account the exchange of radiation among opaque elements.

A variant to *emission approximation* is the assumption of *optically thin model*. This model, typically employed in combustion flames modeling, assumes optically thin radiation transfer between the combustion gases and the cold surroundings. Each radiation point has an unimpeded isotropic view of the cold surroundings. The radiative loss term per unit volume (W/m^3) is expressed as:

$$\nabla \cdot \vec{q}^{\,R} = 4\sigma(\kappa_P T^4 - \kappa_I T_s^4) \tag{2.97}$$

where σ is the Stefan-Boltzmann constant, T_s is the surroundings temperature, κ_P is the Planck mean absorption coefficient, and κ_I is the incident (Planck) mean absorption coefficient. These two mean coefficients are defined below.

If $T_s << T$, equation can be replaced by equation:

$$\nabla \cdot \vec{q}^{\,R} = 4\sigma\kappa_P(T^4 - T_s^4) \tag{2.98}$$

since the term involving T_s is considered to avoid the unphysical solution of a gas at a temperature below the surroundings, having no effect around the flame region. But if T_s similar to T, then equation 2.4.3 should be used. This situation may occur when the flame is confined in an adiabatic enclousure, or when the walls of the chamber are not cooled.

For a mixture of gases, the Plank mean absorption and incident mean absorption coefficients, are linearly proportional to the partial pressure and individual species pressure-based absorption coefficients:

$$\kappa_P = \sum_{i=1}^{N} p_i \kappa_{P_i} \qquad \kappa_I = \sum_{i=1}^{N} p_i \kappa_{I_i} \tag{2.99}$$

Individual Plank mean absorption coefficients are defined as:

$$\kappa_P(T,P) = \frac{\int_0^\infty \kappa_\lambda(\lambda,T,P) I_{b\lambda}(T) d\lambda}{\int_0^\infty I_{b\lambda}(T) d\lambda} \tag{2.100}$$

where $I_{b\lambda}(T)$ is Planck's function. On the other hand, individual incident mean absorption coefficients can be written as:

$$\kappa_I(T,T_s,P) = \frac{\int_0^\infty \kappa_\lambda(\lambda,T,P) I_{I\lambda}(T_s,\lambda) d\lambda}{\int_0^\infty I_{I\lambda}(T_s,\lambda) d\lambda} \tag{2.101}$$

where $I_{I\lambda}(T_s,\lambda)$ is the intensity of radiation originated from the source at temperature T_s and incident on the flame.

For methane/air flames, the most important radiation species are CO_2 and H_2O, and in less extension CH_4 and CO. For these species, Planck mean and incident mean pressure-based absorption coefficients are evaluated from species spectral absorption coefficients κ_λ. These coefficients can be predicted using a narrow-band model and a combination of tabulated properties and theoretical approximations. Like in molecular transport coefficients, it is very common the employment of software packages. For optical properties, the commonly used package is RADCAL [18]. Running RADCAL, κ_{P_i} and κ_{I_i} are tabulated at different temperatures.

Optically thin radiation model together with the commented RADCAL absorption coefficients will be used in this work. The expected accuracy of this assumption has been shown to be quite reasonable [19][17], although according to Mazumber and Modest [14] an over-prediction of both absorption in colder regions and emission in hotter regions is produced.

References

[1] F.A. Williams. *Combustion theory.* The Benjamin/Cummings Publishing Company, Inc., 1985.

[2] J.O. Hirschfelder, C.F. Curtiss, and R.B. Bird. *Molecular theory of gases and liquids.* John Wiley and Sons Inc., 1954.

[3] R.B. Bird, E.E. Stewart, and E.N. Lightfoot. *Transport phenomena.* John Wiley and Sons Inc., 1960.

[4] L.M.T. Sommers and L.P.H. De Goey. A numerical study of a premixed flame on a slit burner. *Combustion Science and Technology*, 108:121–132, 1995.

[5] L.M.T. Somers. *The simulation of flat flames with detailed and reduced chemical models.* PhD thesis, Technical University of Eindhoven, 1994.

[6] R.J. Kee, J.A. Miller, and T.H. Jefferson. Chemkin: a general-purpose, problem-independent, transient, fortran chemical kinetics code package. Technical report, Sandia National Laboratories, 1989.

[7] K. Prasad and E.W Price. A numerical study of the leading edge of laminar diffusion flames. *Combustion and Flame*, 901:155–173, 1992.

[8] R.A Svehla. Estimated viscosities and thermal conductivities of gases at high temperatures. Technical Report R-132, National Aeronautics and Space Administration.

[9] R.J. Kee, G. Dixon-Lewis, J. Warnatz, M.E. Coltrin, and J.A Miller. A fortran computer code package for the evaluation of gas-phase multi-component transport properties. Technical report, Sandia National Laboratories, 1986.

[10] M.F. Modest. *Radiative heat transfer*. McGraw-Hill, 1993.

[11] R. Siegel and J.R. Howell. *Thermal radiation heat transfer*. Taylor and Francis, 2001.

[12] R. Viskanta and M.P. Mengüç. Radiation heat transfer in combustion systems. *Progress in Energy and Combustion Science*, 13:97–160, 1987.

[13] J. Taine and J.P Petit. *Heat transfer*. Prentice Hall, 1993.

[14] S. Mazumder and M.F. Modest. Advanced nongray radiation model coupled with a CFD code for large-scale fire and combustion applications. Technical report, National Sciencie Foundation, 2001.

[15] J.D. Buckmaster and G.S.S. Ludford. *Theory of laminar flames*. Cambridge University Press, 1982.

[16] J. Warnatz, U. Maas, and Dibble R.W. *Combustion*. Springer-Berlag, 1996.

[17] X.L. Zhu, J.P. Gore, A.N. Karpetis, and Barlow A.N. The effects pf self-absorption of radiation on an opposed flow partially premixed flame. *Combustion and Flame*, 129:342–345, 1980.

[18] W.L. Grosshandler. Unknown title 3. *International Journal of Heat and Mass Transfer*, 23:0–0, 1980.

[19] R.S. Barlow, A.N. Karpetis, and J.Y. Frank, J.H. Chen. Scalar profiles and NO formation in laminar opposed-flow partially premixed methane/air flames. *Combustion and Flame*, 127:2102–2118, 2001.

Chapter 3

Combustion kinetics

In the previous chapter, the governing equations for a reactive gas (continuity, momentum, energy, species conservation and state equation) together with the modelization of molecular and radiant fluxes have been posed. In the species conservation equation, we pointed out the species production rates. The evaluation of these rates, that are the responsible of the production/consumption of chemical species due to the chemical reactions that take place in reactive processes, such as combustion, is discussed in detail in this chapter.

3.1 Introduction

Although thermodynamics can predict the equilibrium composition of a reactive mixture, it can not give the rate at which the reaction proceeds and its influence to the changes in composition, pressure and temperature. Chemical kinetics together with thermodynamics are needed to predict the reaction rates of reactive systems.

In this chapter, the basic laws of chemical reactions based on a macroscopic observation are reviewed. A detailed evaluation of the reaction rates for different kind of reactions present in a chemical model is mathematically formulated.

Then, we continue with the analysis of the physical-chemical phenomena that takes place in a combustion process, the so-called *combustion mechanisms*. The path followed by the fuel in the process of oxidation is analyzed. The different type of consecutive steps (i.e. chain reactions) and their interaction are described. The evaluation of the production/consumption rates for each species involved in the reaction mechanism is given.

The large number of chemical species and chemical reactions involved in these mechanisms, together with a wide range of physical time-scales, makes difficult the task of employing them in a detailed numerical simulation. Nevertheless, and due to the improvement of the numerical methods and the increase of the computing power, nowadays these complex mechanisms are being used in some basic numerical

simulations, but are still far to be considered in the numerical modelization of practical systems of industrial interest.

During the last decades the scientific community has been working on the development of simplified chemical models in order to treat the commented above complexity inherent to the combustion mechanism, and to formulate feasible chemical models to be employed in practical systems. In this chapter, different levels of chemical approaches, together with the hypothesis assumed on their modelization, are introduced.

Being natural gas one of the most employed fuels for industrial applications, in this thesis we focus our attention on its combustion process. This gas can be considered as a mixture of mostly methane CH_4, together with ethane C_2H_6 and some traces of higher hydrocarbons like propane C_3H_8 diluted in nitrogen N_2. The actual composition of natural gas depends on the exploitation (i.e. industrial processes and geo-physical properties). Nevertheless, and in an average way, can be said that gas natural is composed by $80 \div 90\%$ of methane.

In this way, and rather than considering the actual composition of natural gas that increases notably the complexity of the chemical models, we consider pure methane-air combustion, for which kinetic data is relatively well-known. Chemical approaches given throughout this chapter are centered on this kind of flames.

3.2 Reaction kinetics

3.2.1 Rate of reactions

Chemical processes are composed by a number of reversible (or irreversible) reactions that involve N chemical species. Each one of these reactions can be represented in the general form:

$$\sum_{i=1}^{N} \nu_i^{'} m_i \Leftrightarrow \sum_{i=1}^{N} \nu_i^{''} m_i \tag{3.1}$$

Here, m_i represents the chemical symbol of the ith species, and ν_i its stoichiometric coefficients. The subscripts $'$ and $''$ indicate its definition as reactant and product respectively.

All chemical reactions proceed at a defined rate that depends on different parameters such as the concentration of the different species, the temperature and the pressure. For a given reaction, the rate of reaction is the quantitative measure of its evolution, namely, the number of moles of products produced (or reactants consumed) per unit of time and volume. The *rate law* describes an empirical formulation of these reaction rates.

In order to introduce the formulation of the reaction rates, let us consider an irreversible reaction:

$$\sum_{i=1}^{N} \nu_i^{'} m_i \rightarrow \sum_{i=1}^{N} \nu_i^{''} m_i \tag{3.2}$$

The molar consumption/production rate of species reads,

$$\frac{d[X_i]}{dt} = \left(\nu_i^{''} - \nu_i^{'}\right) q \tag{3.3}$$

where, $[X_i]$ is the molar concentration of the ith species, and q is the rate-of-progress variable defined as:

$$q = k \prod_{i=1}^{N} [X_i]^{n_{r_i}} \tag{3.4}$$

In this expression, n_{r_i} is the *reaction order* of the ith reactive species and k the *rate constant*. The sum of all n_{r_i} is the *overall reaction order*.

Considering a reversible reaction (3.1), analogous rate law can be formulated to evaluate the ratio at which the products react to form reactants,

$$q^b = k^b \prod_{i=1}^{N} [X_i]^{n_{p_i}} \tag{3.5}$$

In this case, n_{p_i} is the *reaction order* of the ith product species, and k^b the backward *rate constant*.

Joining both forward and backward rates, the net rate-of-progress variable q, at which the concentration of a given species varies can be written as:

$$q = k^f \prod_{i=1}^{N} [X_i]^{n_{r_i}} - k^b \prod_{i=1}^{N} [X_i]^{n_{p_i}} \tag{3.6}$$

When the reactive process finishes, species concentrations do not change in a macroscopic level (i.e. $q = 0$). Chemical equilibrium is established and forward and backward rates are equal. At this moment, we can say that the reaction is at chemical equilibrium and the following relation is established:

$$\frac{k^f}{k^b} = \frac{\prod [X_i]^{n_{p_i}}}{\prod [X_i]^{n_{r_i}}} \tag{3.7}$$

Being the left-hand side of equation 3.7 the equilibrium constant of the reaction, forward and backward rate constants are related as:

$$K_c = \frac{k^f}{k^b} \tag{3.8}$$

This relationship is of special interest, since usually only forward rate constants are given in the literature. Backward rate constants are evaluated from forward ones and the equilibrium constants, which are calculated with thermodynamic properties [1].

3.2.2 Reaction orders

In a chemical process, we may distinguish two main types of reactions: *elementary* reactions and *overall* reactions.

Elementary reactions are those that take place as a result of a collision process and occur on a molecular level in the same manner as they are written. These reactions depend on the intermolecular potential forces existing during the collision encounter, the quantum states of the molecules, and the transfer of energy.

On the other hand, *overall* reactions are those that are the consequence of several elementary reactions. The most illustrative example is the overall stoichiometric reaction for methane combustion:

$$CH_4 + 2O_2 \rightarrow CO_2 + 2H_2O$$

Considering an irreversible process and assuming considerable restrictive hypothesis, methane combustion could be written assuming the above reaction. Being this overall reaction, the consequence of the combination of a large number of reactions that actually take place.

The distinction between elementary and overall reactions let us introduce the evaluation of the reaction orders. For an elementary reaction, generally the reaction order coincides with the *molecularity of the reaction*. We can distinguish three main types of elementary reactions: *unimolecular*, *bimolecular* and *trimolecular* reactions. In unimolecular reactions, a given reactive molecule dissociates to form products. The reaction rate is first-order. That means that the rate of reaction doubles when the concentration of the reactive species doubles too. Bimolecular reactions proceed by the collision of two molecules (of the same or different chemical species). These are the most frequent type of reactions and their reaction rates are second-order (when the species concentrations are doubled, reaction rates quadruple). In a similar manner trimolecular reactions are defined.

Taking into account these definitions, the reaction orders of species for elementary reactions can be directly related to their stoichiometric coefficients. Thus, the net

rate-of-progress variable of the reaction reads:

$$q = k^f \prod_{i=1}^{N} [X_i]^{\nu_i^{'}} - k^b \prod_{i=1}^{N} [X_i]^{\nu_i^{''}} \tag{3.9}$$

This straightforward evaluation is not possible when overall reactions are considered. In fact, as they are a consequence of such complex processes, one must go to experimental studies or mathematical models to evaluate the reaction orders. It is pointless to mention that these ordersare not universal, and depend on the problem to be analyzed. Supposing that the difficulties associated to the evaluation of the reaction orders could be overcome, reaction orders can adopt real values, and even negative values.

3.2.3 Rate constants

Arrhenius in 1889, analyzing experimentally the characteristics of rate coefficients, posed the well-known *Arrhenius Law*. This law, that pointed out the extremely temperature dependence of these coefficients, was written as follows:

$$k = A^{'} exp\left(-\frac{E}{RT}\right) \tag{3.10}$$

where $A^{'}$, is a constant which units depends on the molecularity of the reaction and accounts for the number of collisions between molecules in a reaction system, while $exp\,(-E/RT)$ is related to the fraction of molecules that are energetically capable of participating in the reaction. Generally, both quantities are positive and an increase of temperature also represents an increase of the rate constants.

Further experimental studies, Kooij (1893) [2], found a temperature dependence of $A^{'}$, that was described with the following expression:

$$A^{'} = A\,T^{\beta} \tag{3.11}$$

In this equation, β is the temperature exponent which values round about -1 and 2. Although, for some reactions the temperature dependence of $A^{'}$ is very important, normally this temperature dependence is very weak.

Harcourt (1895), consider higher approximations to fit rate constants temperature dependence:

$$k = \frac{a}{T} + b\,\ln(T) + c\,T + d \tag{3.12}$$

However, the limitations of accuracy of experimental data, and the fact that slow differences among rate coefficients could cause considerable changes on the rate constants, motivated the common acceptance of a modified Arrhenius equation:

$$k = AT^{\beta} exp\left(-\frac{E}{RT}\right) \tag{3.13}$$

It is important to highlight that equations 3.10 and 3.13 are empirical expressions based on fitted experimental data and not on elemental reaction analysis [2]. Rate coefficients are usually calculated for a finite range of temperature.

A rigorous analysis of rate constants dependence to the temperature is given by the kinetic theory. From a rigorous development, it is found that Arrhenius expression can be considered a good approximation from a detailed mathematical formulation. Examining resemblances, E can be related to the *activation energy* (i.e. E_a), while $A^{'}$ is defined as the *pre-exponential factor*.

Activation energy is defined as the energy required to bring the reactants to a energetic state, such that the chemical bonds can be broken to form products. A reaction will proceed if the different molecules of chemical species collide with an appropriate orientation and with enough velocity. In a rigorous theoretical analysis, collision processes are governed by the Schrödinger equation of quantum mechanics, from which resolution, activation energies can be calculated [3]. However, the calculation of activation energies is extremely difficult, and only recently has been possible to calculate, with certain accuracy, the activation energy of stable molecules and atoms [4]. The extremely difficulties arising from the detailed evaluation, forces the employment of semi-empirical procedures to obtain reaction rate constants.

Rate coefficients can be experimentally evaluated only for elementary reactions, which are those that really physically exist. *Overall activation energies* can be estimated but without such level of problem independent properties and accuracy. Experimental setups are formed by reactor chambers where temperature dependence of the rate constants is analyzed. Reactants, usually reactive atoms or radicals, are generated artificially with microwaves or laser beams from the decomposition of stable molecules. Product concentrations are measured by means of mass spectrometry, electron spin resonance, optical spectrometry or gas chromatography [5]. E_a is found evaluating the best-fit straight line of the $ln(k)$ against $1/T$ measured distribution. *Pre-exponential* factor is obtained from the measured values of k and the estimation of E_a.

A summary table of evaluated kinetic data for combustion modeling is given in [6]. As an example, figure 3.1 plots the rate coefficients of some elementary reactions. The usual behavior of rate constant temperature dependence can be observed in figure 3.1a. Here pre-exponential factor is zero, and the negative slope of $ln(k)$ vs. $1/T$ represents the value E_a/R that fits experimental data. On the other hand, figure

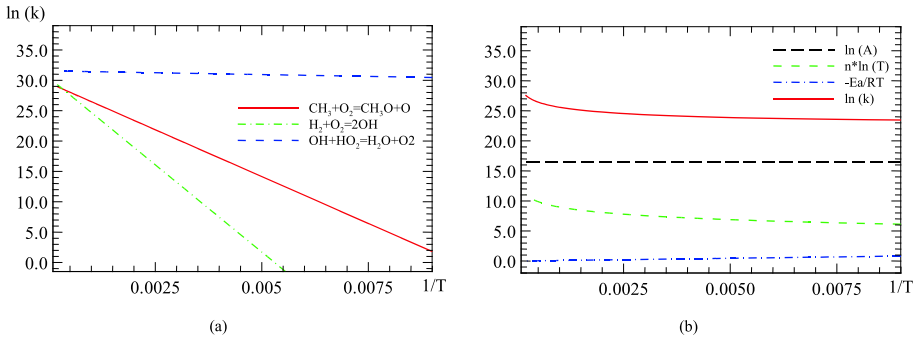

Figure 3.1: Reaction rates constants. $k = AT^{\beta}exp(-E_a/RT)$. Units=$mol$, cm, s, cal, K. a) Usual rate constants behavior; b) High dependence of pre-exponential factor with temperature.

3.1b show the temperature dependence of the reaction $CO + OH \rightarrow CO_2 + H$. In this case, the temperature dependence of the pre-exponential factor is clear, and even E_a is negative.

3.2.4 Three-body reactions

Elementary dissociation reactions describe the decomposition of a given molecule forming two molecules. These dissociation or recombination processes usually need the presence of a third component to proceed, commonly called "third body". A typical example of a three-body reaction is one of the initiation reactions of methane combustion,

$$CH_4 + M \Leftrightarrow CH_3 + H + M$$

The reaction rate depends on the concentration of the third body,

$$q = [M]\left(k^f \prod_{i=1}^{N} [X_i]^{\nu_i^{'}} - k^b \prod_{i=1}^{N} [X_i]^{\nu_i^{''}}\right) \tag{3.14}$$

which is evaluated weighting all species concentrations with a certain species efficiency, α_i:

$$[M] = \sum_{i=1}^{N} \alpha_i [X_i] \tag{3.15}$$

If all species contribute equally on the composition of the third body (default situation), all efficiencies are set to 1, and the third body concentration is the total concentration of the mixture. In some reactions, all species do not contribute in the same manner, and species efficiencies may be given. An example is the hydrogen dissociation reaction given by,

$$H_2 + M \Leftrightarrow H + H + M$$

where $\alpha_H = 2.0$, $\alpha_{H_2} = 3.0$, $\alpha_{H_2O} = 6.0$, and it is considered that other species do not contribute [7].

3.2.5 Pressure-dependent reactions

For some dissociation/recombination reactions and bimolecular reactions, has been observed that under certain situations, reaction rates depend strongly on the pressure as well on the temperature. These reactions are commonly called dissociation/recombination *fall-off* reactions and *chemically activated* bimolecular reactions. In a general manner, in the first ones the rate of reaction increases with the pressure, while for the second type decreases when the pressure increases.

The pressure dependence of the rates of these reactions are described by two limiting situations, *low-pressure* and *high-pressure* limits. An example is the methyl recombination to form ethane. At low pressures, a third-body concentration is needed to provide enough energy to the collisions to make possible the reaction:

$$CH_3 + CH_3 + M \Leftrightarrow C_2H_6 + M$$

On the other hand, at high-pressures, this contribution is not necessary, and the appropriate description of the reaction is:

$$CH_3 + CH_3 \Leftrightarrow C_2H_6$$

The evaluation of the reaction rates for these limiting situations should be done as has been commented previously. However, between these extreme circumstances, exist and intermediate case, the so called "fall-off" region, where pressure and temperature dependence is not so clearly differentiated, and the reactions are usually written as:

$$CH_3 + CH_3(+M) \Leftrightarrow C_2H_6(+M)$$

The behavior of the reaction rates in these regions are described by several methodologies [8][9][10], from which and due to its usual employment, the first and simplest method proposed by Lindenmann [8] is hereafter described. Variants to this method are also considered.

The net rate of progress variable for these reactions are evaluated without the contribution of third body 3.14. Its contribution is directly given on the evaluation of the rate constants, k. Two different reaction rates are defined: the high-pressure limit k_∞, and the low-pressure limit k_0. Rate coefficients for both constants are defined:

$$k_0 = A_0 T^{\beta_0} exp\left(-E_0/R_c T\right) \tag{3.16}$$

$$k_\infty = A_\infty T^{\beta_\infty} exp\left(-E_\infty/R_c T\right) \tag{3.17}$$

The reaction rate constant is expressed as,

$$k = k_\infty \left(\frac{P_r}{1+P_r}\right) F \tag{3.18}$$

where F is the blending function, and P_r is the reduced pressure given by,

$$P_r = \frac{k_0[M]}{k_\infty} \tag{3.19}$$

In the Lindenmann form, F is the unity. Variants to this method involves more complex expressions to determine the value of F.

Troe et al [9], estimates F with the following equation:

$$F = exp\left(\left(1+\left(\frac{lnP_r + c}{n - d(lnP_r + c)}\right]^2\right]^{-1} ln(F_{cent})\right) \tag{3.20}$$

where,

$$\begin{aligned} c &= -0.4 - 0.67\, ln(F_{cent}) \\ n &= 0.75 - 1.27\, ln(F_{cent}) \\ d &= 0.14 \end{aligned}$$

and F_{cent} is evaluated employing the following equation and defining specific a_i parameters for each reaction:

$$F_{cent} = (1-a_0)\, exp\left(-\frac{T}{a_1}\right) + a_0\, exp\left(\frac{T}{a_2}\right) + exp\left(-\frac{a_3}{T}\right) \tag{3.21}$$

The third description, is the one considered at SRI International by Steward et al [10]. Here F, is evaluated as:

$$F = a_3 \left(a_0 + exp\left(-\frac{a_1}{T}\right) + exp\left(-\frac{T}{a_2}\right)\right]^X T^{a_4} \tag{3.22}$$

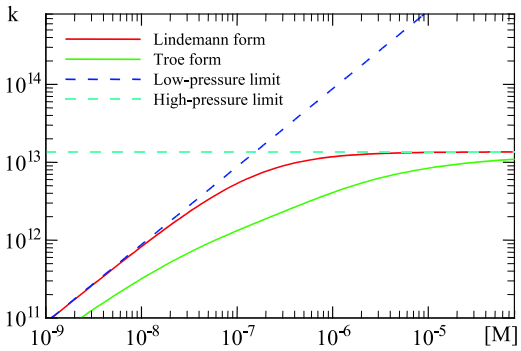

Figure 3.2: Pressure-dependent rate constant versus third-body concentration for the unimolecular fall-off reaction $CH3 + CH3(+M) \Leftrightarrow CH_6(+M)$ at $T = 1000$ K. Data taken from Wagner and Wardlow [11]. Low- and high-pressure constants: $A_0 = 1.135e36$, $\beta_0 = -5.246$, $E_0 = 1704.8$, $A_\infty = 6.22e16$, $\beta_\infty = -1.174$, $E_\infty = 635.8$. Troe parameters: $a_0 = 0.405$, $a_1 = 1120$, $a_2 = 69.6$.

specifying again a_i parameters for each reaction and defining X as:

$$X = \frac{1}{1 + ln^2 P_r} \tag{3.23}$$

In order to illustrate the pressure dependence on the evaluation of the rate-of-progress variable for such reactions, we refer to the example given in [1]. In figure 3.2, methyl recombination rate constant versus third-body concentrations at 1000 K is plotted. The kinetic data is given by Wagner and Wardlow [11]. Lindemann and Troe forms are shown together with the low and high pressure limits.

3.2.6 Consecutive/competitive reactions

Until now, we have been talking about kinetic properties of simple reactions. When several reactions are involved in a reactive process, the contribution of each one has to be considered in order to evaluate the molar consumption/production rates of species. These rates are obtained by summing up the individual contribution of the N_R reactions involved:

$$\dot{\omega}_i = \sum_{j=1}^{N_R} \left(\nu_{i,j}^{''} - \nu_{i,j}^{'} \right) q_j \tag{3.24}$$

where, $\nu_{i,j}^{'}$, $\nu_{i,j}^{''}$ are the stoichiometric coefficients of the ith species appearing as a reactant and as a product in the reaction j respectively, and q_j is the rate-of-progress

variable for the jth reaction.

If chemical process are formed by elementary steps, molar consumption/production rates read:

$$\dot{\omega}_i = \sum_{j=1}^{N_R} \left(\nu_{i,j}^{''} - \nu_{i,j}^{'} \right) \left(k_j^f \prod_{i=1}^{N} [X_i]^{\nu_{i,j}^{'}} - k_j^b \prod_{i=1}^{N} [X_i]^{\nu_{i,j}^{''}} \right] \tag{3.25}$$

Mass production/consumption rates are obtained from the molar ones just multiplying by the species mass weights.

$$\dot{w}_i = M_i \dot{\omega}_i \tag{3.26}$$

3.3 Combustion mechanisms

In combustion processes the oxidation of a given fuel is composed by several elementary steps, the so-called *chain-reactions*. These steps consist of a series of consecutive, competitive, and opposing elementary reactions, that describe the path of how the fuel is oxidized. The complete set of elementary reactions together with their rates constants is known as *combustion mechanism*.

In this section, combustion mechanisms for methane/air combustion are introduced. Their elementary steps are analyzed distinguishing their relative function and importance in the combustion scheme. From this analysis, and in order to reduce the complexity of combustion mechanisms, problem dependent simpler descriptions of the combustion process are presented.

3.3.1 Chain reactions

Among the different reactions involved in a combustion process, we distinguish four main types: *initiating*, *chain propagating*, *chain branching* and *terminating* reactions.

Initiating reactions are those which are responsible of the ignition of the reaction chain. Stable species (S) reacts forming radicals (R•), molecules with an unpaired electron such CH_3, H, O, etc. An Illustrative example in methane-air combustion is the attack of methane molecules by oxygen:

$$CH_4 + O_2 \Leftrightarrow CH_3 + HO_2$$

Chain branching reactions, are those where stable species are broken by radicals, and where the number of radicals increases as a result of the reaction. These reactions are very important to emphasize the oxidation process, since they represent a source of radicals that will be involved in the most relevant reactions of the mechanism. An example is:

$$CH_4 + O \Leftrightarrow CH_3 + OH$$

In *chain propagating* reactions, stable species are broken by radicals, but the number of radicals does not change. In addition stable or chemically excited molecules (S*) are formed:

$$OH + H_2 \Leftrightarrow H_2O + H$$

Finally the oxidation process ends because of the so-called *chain terminating* or *chain breaking* reactions. In these reactions, radicals react to form stable products or disappear due to molecular collisions with surrounding walls. The latter ones are specially important in determining explosion limits at low pressure conditions [12]. A typical example of such reactions is:

$$OH + H + M \rightarrow H_2O + M$$

Summarizing, hydrocarbon combustion path can be written considering the following generic set:

- Initiation $S \rightarrow R\bullet$
- Branching ($\alpha > 1$) $S + R\bullet \rightarrow \alpha R\bullet + S*$
- Propagating $S + R\bullet \rightarrow R\bullet + S*$
- Terminating $S + R\bullet \rightarrow S$

The good understanding of complex combustion mechanisms and chain reactions set, is a key aspect on the developing of more feasible mechanisms.

3.3.2 Full kinetic mechanisms

The complete set of chain reactions that are involved in a combustion process form the so-called "full" kinetic or combustion mechanisms. These mechanisms are composed by a large number of chemical species involved in elementary reactions. Detailed mechanisms for only few fuels, such as hydrogen, methane, methanol and ethane, are nowadays available. Several scientists work to improve such mechanisms and to provide further mechanisms for more complex hydrocarbons. Full mechanisms, are considered to be problem independent. They are tested under a wide range of combustion situations, and their authors ask the combustion community for testing them in their problems of interest.

An example of full mechanism is the GRI-Mech mechanism for methane-air combustion developed at the University of California at Berkeley, Stanford University, the University of Texas at Auston and SRI International, and sponsored by the Gas Research Institute [13]. The last release (3.0) considers 53 chemical species and 325 elementary reactions. Full chemical mechanisms are obtained from a comprehensive numerical and experimental studies, and provide a list of reactions together with their

rate coefficients. Special care is recommended to not change any rate constant neither subtract any reaction, since they are extremely related and have been selected to perform an accurate behavior.

Usually, these mechanisms account for the carbon reaction path in a very detailed manner. Reactions involving C_2- and C_3-hydrocarbons are considered. From a rigorous point of view, methane can follow a reaction path where higher hydrocarbons can be involved and its consideration, can be in some situations, a key aspect to describe properly the combustion properties. In addition, full combustion mechanisms also consider the formation of contaminant species like NO, the so-called NO_x, that are of special interest for environmental reasons (see Appendix).

3.3.3 Skeletal mechanisms

The enormous complexity of "full" combustion mechanisms makes prohibitive their employment for the multidimensional numerical simulation of combustion processes in problems of industrial interest. Even under laminar flow regimes, the available computational resources are nowadays insufficient to consider such mechanisms in systematic parametric studies of industrial equipment optimization.

In order to overcome these numerical difficulties, *skeletal* mechanisms are developed. These simplified chemical approaches analyze the relative importance of all set of elementary reactions that form the full mechanism.

For a given problem of interest, experimental and numerical studies are carried out. Solving the combustion problem with full mechanisms, sensitive analysis of the relatively weight of each reaction are done [14][15]. As a consequence of these studies, some elementary steps are subtracted or combined to formulate "elemental" assumed reactions. It is worth to point out that *skeletal* mechanisms are not problem independent, and special attention has to be paid on its adequacy when it is employed in a given problem.

On the other hand, skeletal mechanisms usually do not provide information about NO_x since it is commonly assumed that these species and their inherent reactions do not affect considerably the main combustion properties of flames (i.e. burning velocity, temperature, main species concentrations, etc). Further discussion about how contaminants production can be modeled is given in next sections.

Skeletal mechanisms are the easiest way to eliminate faster reactions and to reduce the number of chemical species involved (to about 15 species or to about 27 species if NO_x are considered). Both properties help the numerical resolution of the combustion problems where they are applied, decreasing the level of stiffness of the governing equations and the computational costs.

To introduce these simplified kind of mechanisms, a *skeletal* mechanism commonly used for methane-air atmospheric combustion is analyzed [7]. The selected skeletal

mechanism consider only the group of reactions involving C-hydrocarbons. Specifically, 15 species and 42 reactions are involved. The list of reactions together with the proposed rate coefficients are given in table 3.1.

Oxidation of methane starts when the methane's carbon-hydrogen bond is broken to form radicals (reaction $r1$ and $r2$). Initiating reactions are of minor importance in the general features of laminar steady state flames (i.e. concentrations, temperature and burning velocity). However, these reactions are essential in ignition processes, where other initiating reactions may be taken into account.

Once the hydrocarbon radicals are produced, they react rapidly with oxygen molecules ($r6$ and $r7$) to produce methyloxide CH_3O, and formaldehyde CH_2O. Parallely, methane is also broken by H, O and OH radicals, by means of chain branching and chain propagating reactions ($r3$, $r4$, $r5$, $r8$ and $r9$), increasing in this way the number of radicals.

No.	Reaction	A	β	E_a
$r1$.	$CH_4 + M \Leftrightarrow CH_3 + H + M$	$1.000e+17$	0.00	$8.600e+04$
$r2$.	$CH_4 + O_2 \Leftrightarrow CH_3 + HO_2$	$7.900e+13$	0.00	$5.600e+04$
$r3$.	$CH_4 + H \Leftrightarrow CH_3 + H_2$	$2.200e+04$	3.00	$8.750e+03$
$r4$.	$CH_4 + O \Leftrightarrow CH_3 + OH$	$1.600e+06$	2.36	$7.400e+03$
$r5$.	$CH_4 + OH \Leftrightarrow CH_3 + H_2O$	$1.600e+06$	2.10	$2.460e+03$
$r6$.	$CH_3 + O_2 \Leftrightarrow O + CH_3O$	$7.000e+12$	0.00	$2.565e+04$
$r7$.	$CH_3 + O_2 \Leftrightarrow OH + CH_2O$	$5.200e+13$	0.00	$3.457e+04$
$r8$.	$CH_3 + O \Leftrightarrow H + CH_2O$	$6.800e+13$	0.00	$0.000e+00$
$r9$.	$CH_3 + OH \Leftrightarrow H_2 + CH_2O$	$7.500e+12$	0.00	$0.000e+00$
$r10$.	$CH_3O + M \Leftrightarrow CH_2O + H + M$	$2.400e+13$	0.00	$2.881e+04$
$r11$.	$CH_3O + H \Leftrightarrow CH_2O + H_2$	$2.000e+13$	0.00	$0.000e+00$
$r12$.	$CH_3O + OH \Leftrightarrow CH_2O + H_2O$	$1.000e+13$	0.00	$0.000e+00$
$r13$.	$CH_3O + O \Leftrightarrow CH_2O + OH$	$1.000e+13$	0.00	$0.000e+00$
$r14$.	$CH_3O + O_2 + \Leftrightarrow CH_2O + HO_2$	$6.300e+10$	0.00	$2.600e+03$
$r15$.	$CH_2O + OH \Leftrightarrow HCO + H_2O$	$7.530e+12$	0.00	$1.670e+02$
$r16$.	$CH_2O + H \Leftrightarrow HCO + H_2$	$3.310e+14$	0.00	$1.050e+04$
$r17$.	$CH_2O + M \Leftrightarrow HCO + H + M$	$3.310e+16$	0.00	$8.100e+04$
$r18$.	$CH_2O + O \Leftrightarrow HCO + OH$	$1.810e+13$	0.00	$3.082e+03$
$r19$.	$HCO + OH \Leftrightarrow CO + H_2O$	$5.000e+12$	0.00	$0.000e+00$
$r20$.	$HCO + M \Leftrightarrow CO + H + M$	$1.600e+14$	0.00	$1.470e+04$
$r21$.	$HCO + H \Leftrightarrow CO + H_2$	$4.000e+13$	0.00	$0.000e+00$
$r22$.	$HCO + O \Leftrightarrow CO + OH$	$1.000e+13$	0.00	$0.000e+00$
$r23$.	$HCO + O_2 \Leftrightarrow CO + HO_2$	$3.000e+12$	0.00	$0.000e+00$
$r24$.	$CO + O + M \Leftrightarrow CO_2 + M$	$3.200e+13$	0.00	$-4.200e+03$
$r25$.	$CO + OH \Leftrightarrow CO_2 + H$	$1.510e+07$	1.30	$-7.580e+02$
$r26$.	$CO + O_2 \Leftrightarrow CO_2 + O$	$1.600e+13$	0.00	$4.100e+04$
$r27$.	$CO + HO_2 \Leftrightarrow CO_2 + OH$	$5.800e+13$	0.00	$2.293e+04$

continued on next page

continued from previous page

$r28.$	$O_2 + H_2 \Leftrightarrow 2OH$	$1.700e+13$	0.00	$4.778e+04$
$r29.$	$H_2 + OH \Leftrightarrow H + H_2O$	$1.170e+09$	1.30	$3.626e+03$
$r30.$	$H + O_2 \Leftrightarrow O + OH$	$2.000e+14$	0.00	$1.680e+04$
$r31.$	$H_2 + O \Leftrightarrow H + OH$	$1.800e+10$	1.00	$8.826e+03$
$r32.$	$HO_2 + O \Leftrightarrow O_2 + OH$	$4.800e+13$	0.00	$1.000e+03$
$r33.$	$2OH \Leftrightarrow O + H_2O$	$6.000e+08$	1.30	$0.000e+00$
$r34.$	$O_2 + M \Leftrightarrow 2O + M$	$1.850e+11$	0.50	$9.556e+04$
$r35.$	$H + O_2 + M \Leftrightarrow HO_2 + M^a$	$2.100e+18$	-1.00	$0.000e+00$
$r36.$	$H + 2O_2 \Leftrightarrow O_2 + HO_2$	$6.700e+19$	-1.42	$0.000e+00$
$r37.$	$H + O_2 + N_2 \Leftrightarrow HO_2 + N_2$	$6.700e+19$	-1.42	$0.000e+00$
$r38.$	$HO_2 + OH \Leftrightarrow O_2 + H_2O$	$5.000e+13$	0.00	$1.000e+03$
$r39.$	$H + HO_2 \Leftrightarrow 2OH$	$2.500e+14$	0.00	$1.900e+03$
$r40.$	$H_2 + M \Leftrightarrow 2H + M^b$	$2.230e+12$	0.50	$9.260e+04$
$r41.$	$H + OH + M \Leftrightarrow H_2O + M^c$	$7.500e+23$	-2.60	$0.000e+00$
$r42.$	$H + HO_2 \Leftrightarrow O_2 + H_2$	$2.500e+13$	0.00	$7.000e+02$

Third Body efficiencies:

M^a H_2 : 3.3; H_2O : 21.0

M^b H : 2.0; H_2 : 3.0; H_2O : 6.0

M^c H_2O : 20.0

Table 3.1: Skeletal mechanism for atmospheric methane-air combustion [7]. $k = A\,T^{\beta}\,exp(-E_a/RT)$, A in moles, cm, s, E_a in cal/mole.

The amount of methyloxide produced, reacts rapidly to generate formaldehyde (from $r10$ to $r14$), which also reacts very quickly (from $r15$ to $r18$) to create formyl HCO. After that, formyl is converted to carbon monoxyde (from $r19$ to $r23$). The process of consecutive/competitive reactions is extremely fast, and each intermediate species (CH_3, CH_3O, CH_2O and HCO) are rapidly produced and consumed.

Oxidation of methane finishes with the oxidation of CO to CO_2, that is common for all organic fuels oxidation (from $r24$ to $r27$), being the most relevant one the reaction of CO with OH radical ($r25$). This recation is relatively slow, and controls globally the combustion process.

Radicals, that contribute notably in the carbon oxidation path, are also produced by chain branching and propagating reactions (from $r28$ to $r34$), involving both reactants (O_2) products (H_2), and intermediate species (H, OH, O). Finally, the reactions ends with the considered chain-terminating reactions (from $r28$ to $r34$).

As has been commented, skeletal mechanisms depend strongly on the combustion conditions (equivalence ratio, pressure, etc). As an example, reaction flow analysis in a premixed stoichiometric methane-air flame and for a nonpremixed flame at atmospheric pressures are shown in figures 3.3 and 3.4 respectively. The relative importance of each reactions are plotted increasing the the wideness of the arrows, and are printed with solid red lines.

As can be seen, basically the main reaction path is that explained for the commented above skeletal mechanism. Nevertheless, for an accurate resolution of the

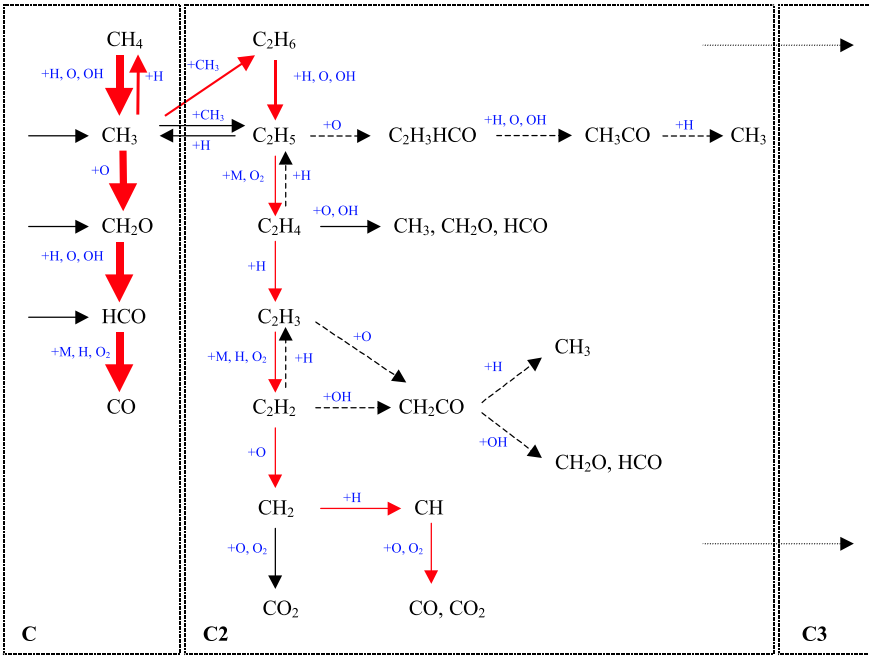

Figure 3.3: Path reaction flow analysis in a premixed stoichimetric CH_4-air flame at $p = 1$ bar, $T_u = 298\ K$ [5].

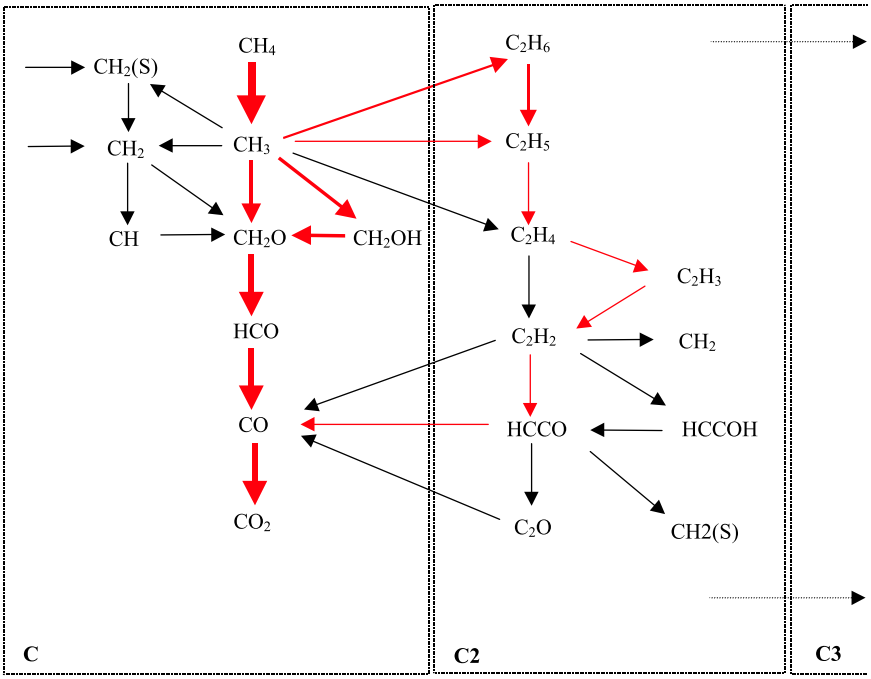

Figure 3.4: Path reaction flow analysis in a coflow non-premixed CH_4-air laminar flame at $p = 1$ bar [15].

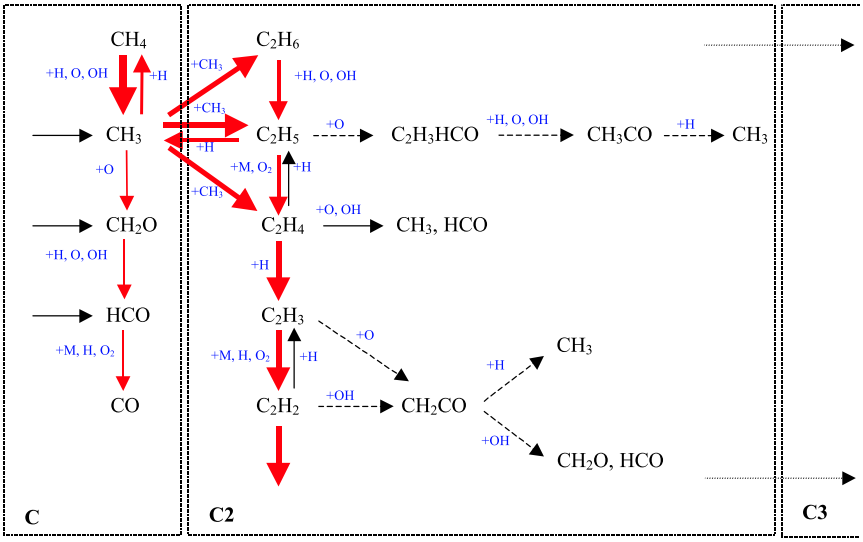

Figure 3.5: Path reaction flow analysis in a premixed rich CH_4-air flame at $p = 1$ bar, $T_u = 298\ K$ [5].

combustion problem, $C2$-chain initiated with the methyl recombination to produce ethane C_2H_6, should also be considered. Illustrative differences appear for premixed and nonpremixed conditions. Different species and reaction processes are involved in both reaction paths.

$C2$-chain becomes more important in rich mixtures. Reaction flow analysis in a premixed rich methane-air flame at $p = 1$ bar is shown in figure 3.5. Here the no consideration of ethane formation and higher hydrocarbons chain, should provoque considerable inaccuracies on the modelization of the combustion phenomena . In these conditions, the exposed skeletal mechanism do not estimate correctly the reaction path.

3.4 Reduction Techniques

Even though *skeletal* mechanisms represent a reduction of the complexity of combustion mechanisms, these simplifications could still be insufficient and further simplifications, so-called reductions of the mechanism complexity, should be needed to model situations of industrial interest. Chemical reduction techniques have been developed for years, and still represent one of the most important areas in combustion research.

We can point out, that first chemical approaches were developed even before detailed reaction mechanisms were available.

In this section a brief description of the most relevant chemical approaches is introduced. Among the different methods, three main groups can be differentiated: *Conventional Reduction Methods (CRM)*, *Mathematical Reduction Methods (MRM)* and *Global reaction schemes*.

CRM have a considerable background on the analysis of detailed mechanisms. Knowledge about combustion mechanisms and kinetics of elemental reactions are needed to succeed with an accurate modelization. As global schemes, reduced models are particularized to a specific combustion process (i.e. pressure conditions, inlet temperatures, equivalence ratios). On the other hand, MRM methods are based on a higher mathematical development and they are independent to the combustion problem to be applied. Global reaction schemes are the less accurate. They were the first approaches to model combustion kinetics and are based on semi-empirical formulations.

3.4.1 Conventional Reduction Methods (CRM)

This reduction technique is based on a systematic numerical and/or experimental analysis of a combustion problem, determining the relative importance of each reaction and the particular behavior of chemical species [16][17]. During the last decade, considerable effort was given to such reduction methods, and models for premixed and non-premixed methane-air flames at atmospheric pressure [18][19] were developed. Also, reduced mechanisms for other fuels (e.g. methanol, propane) were formulated to describe the asymptotic structure of combustion flames [19].

Complex mechanisms are simplified by means of the selection of the most relevant reactions. Starting points can be both available full or skeletal mechanisms. The reactions with lower contribution are eliminated. After that, *steady-state* and *partial-equilibrium* approximations are introduced.

Steady-state approximation is applied to species conservation equations for intermediate species. These species are those that even participate actively in the reaction path, they are consumed as soon as they are produced. Considering this process fast enough, we should consider that species production/consumption rates for these species are null.

Partial-equilibrium approximation affects particular reactions instead of particular species. Partial-equilibrium can be considered if for the jth reaction involved in the combustion mechanism, the rate-of-progress variable is approximately zero (i.e. $q_j = 0$). Being forward and backward rates almost equal, they are need also to be considerable large. Small changes in forward/backward rates may not suppose a considerable change on $q_j = 0$, that could contribute notably on species molar concentrations [3].

Partial-equilibrium approximation helps to decrease the stiffness of the conservation equations since faster reactions can be eliminated. On the other hand, this hypothesis also allow the formulation of algebraic expressions for species molar concentrations employed on the evaluation of non-intermediate species consumption rates.

Joining both approximations, and combining species conservation equations, a set of global reactions can be posed. Production/consumption rates for the species involved in this reduced mechanisms can be obtained from the original mechanism and from the algebraic equations obtained with both steady-state and partial equilibrium approximations.

The selection of the species to be considered in steady-state and reactions to which partial-equilibrium can be applied, is done by means of a sensitive analysis of the solutions obtained under the consideration of more complex mechanisms [20][14][21]. The achievement of the global reactions and their reaction rates is usually done via numerical codes that makes this task easier.

The reduced mechanisms obtained, usually guarantee that the resulting system of governing equations becomes less stiff. Nevertheless, special attention may be given to their implementation in a CFD code. Some guides about this aspect, are given in [22]. Among others, inner iterations in the evaluation of the reaction rates, relaxation parameters, and initial species concentrations are recommended.

Example: Systematically reduced reaction scheme for lean CH_4-air premixed flames

A skeletal mechanism involving 40 reactions (Miller et al [23]) is the starting point for the achievement of the systematically reduced mechanism proposed by Peters [18]. The mechanism was developed to model lean methane-air flames at sufficiently high temperatures. The author considered suitable the application of this scheme for the modelization of automotive engines and gas turbine combustion chambers.

The skeletal mechanism is simplified by the analysis of the relative importance of each reaction in the combustion process. Reactions of this reduced mechanism are listed in table 3.2. The scheme is considered to be complete in the sense that there is a path from reactants CH_4 and O_2 to main products CO_2 and H_2O.

Steady state assumption is applied for intermediate species (CH_3, CH_2O, HCO, O, OH and HO_2), being six reaction rates for the system eliminated. Trying to eliminate the faster reactions combining species weighted conservations equations (referred

with $L(Y_i)$ operator), the following expressions are found:

$$\begin{aligned} L(Y_{CH_4}) &= -q_1 - q_2 \\ L(Y_{O_2}) &= -q_{10} - q_{16} \\ L(Y_{CO_2}) &= q_9 \\ L(Y_{H_2O}) &= -q_1 - q_2 - q_9 + 2q_{10} + 2q_{16} \\ L(Y_{CO}) &= q_1 + q_2 - q_9 \\ L(Y_{H_2}) &= 4q_1 + 4q_2 + q_6 + q_8 + q_9 - 3q_{10} + q_{14} + q_{15} - 3q_{16} \end{aligned}$$

Only 9 reactions are maintained from the simplified list (table 3.2). In this way, the author only provides rate coefficients for the resting of the reactions. Looking at the molar production rates, one can formulate a global set of reactions which production rates satisfy analogous expressions.

$$\begin{array}{ll} \text{I} & CH_4 + 2H + H_2O \Leftrightarrow CO + 4H_2 \\ \text{II} & CO + H_2O \Leftrightarrow CO_2 + H_2 \\ \text{III} & H + H + M \Leftrightarrow H_2 + M \\ \text{IV} & O_2 + 3H_2 \Leftrightarrow 2H + 2H_2O \end{array}$$

Rates-of-progress for these global reactions are written in terms of rates of elementary steps:

$$\begin{aligned} q_I &= q_1 + q_2 \\ q_{II} &= q_9 \\ q_{III} &= q_6 + q_8 + q_{14} + q_{15} \\ q_{IV} &= q_{10} + q_{16} \end{aligned}$$

With these assumptions, the combustion scheme is composed by 6 reactant species and four global reactions. Only species conservation equations for the species involved in the mechanism and for the inert species may be solved in the application problem.

No.	Reaction	A	β	E_a
$r1$.	$CH_4 + H \Leftrightarrow CH_3 + H_2$	$2.200e+04$	3.00	$8.760e+03$
$r2$.	$CH_4 + OH \Leftrightarrow CH_3 + H_2O$	$1.600e+06$	2.10	$2.450e+03$
$r3$.	$CH_3 + O \Leftrightarrow H + CH_2O$			
$r4$.	$CH_2O + OH \Leftrightarrow HCO + H_2O$			
$r5$.	$CH_2O + H \Leftrightarrow HCO + H_2$			
$r6$.	$HCO + H \Leftrightarrow CO + H_2$	$2.000e+14$	0.00	$0.000e+00$
$r7$.	$HCO + M \Leftrightarrow CO + H + M$	$7.140e+14$	0.00	$1.680e+04$
$r8$.	$HCO + O_2 \Leftrightarrow CO + HO_2$	$3.000e+12$	0.00	$0.000e+00$

continued on next page

continued from previous page

$r9.$	$CO + OH \Leftrightarrow CO_2 + H$	$4.400e+06$	1.50	$-7.400e+02$
$r10.$	$H + O_2 \Leftrightarrow O + OH$	$1.200e+17$	-0.91	$1.652e+04$
$r11.$	$O + H_2 \Leftrightarrow OH + H$			
$r12.$	$H_2 + OH \Leftrightarrow H_2O + H$			
$r13.$	$2OH \Leftrightarrow O + H_2O$			
$r14.$	$H + O_2 + M \Leftrightarrow HO_2 + M$	$2.000e+18$	-0.80	$0.000e+00$
$r15.$	$H + OH + M \Leftrightarrow H_2O + M^c$	$2.150e+22$	-2.00	$0.000e+00$
$r16.$	$H + HO_2 \Leftrightarrow 2OH$	$1.500e+14$	0.00	$1.000e+03$
$r17.$	$H + HO_2 \Leftrightarrow H_2 + O_2$	$2.500e+13$	0.00	$6.900e+02$
$r18.$	$OH + HO_2 \Leftrightarrow H_2O + O_2$	$2.000e+14$	0.00	$0.000e+00$

Table 3.2: Most important reactions suggested by Peters in lean methane-air combustion [18] from the skeletal mechanism proposed by Miller et al. [23]. $k = A\,T^{\beta}\,exp(-E_a/RT)$, A in moles, cm, s, E_a in cal/mole. Rates constants not defined are not necessary on the formulation of the production/consumption rates for the proposed systematically reduced model.

However, on the evaluation of production rates we still have a difficulty to overcome. Elementary reactions involved in the global scheme need on its evaluation some intermediate species. HCO and HO_2 molar concentrations are obtained combining assumed steady-state conservation equations for $CH3$ and CH_2O,

$$
\begin{aligned}
[X_{HCO}] &= \frac{k_1[X_{CH_4}][X_H] + k_2[X_{CH_4}][X_{OH}]}{k_6[X_H] + k_7[M] + k_8[X_{O_2}]} \\
[X_{HO_2}] &= \frac{k_8[X_{HCO}][X_{O_2}] + k_{14}[X_H][X_{O_2}]}{k_6 + k_{17}[X_H] + k_{18}[X_{OH}]}
\end{aligned}
$$

while OH, O molar concentrations are obtained assuming partial equilibrium for reactions 11 and 12:

$$
\begin{aligned}
[X_{OH}] &= \frac{[X_H][X_{H_2O}]}{[X_{H_2}]K_{c,12}} \\
[X_O] &= \frac{[X_H][X_{OH}]}{[X_{H_2}]K_{c,11}}
\end{aligned}
$$

Replacing intermediate molar concentrations in the rate-of-progress of elementary steps, the following expressions are obtained:

$$
\begin{aligned}
q_1 &= k_1[X_{CH_4}][X_H] \\
q_2 &= \left(\frac{k_2}{K_{c,12}}\right)\left(\frac{[X_{CH_4}][X_H][X_{H_2O}]}{[X_{H_2}]}\right) \\
q_6 &= \left(\frac{k_1+(k_2[X_{H_2O}])/(K_{c,12}[X_{H_2}])}{k_6[X_H]+k_7[M]+k_8[X_{O_2}]}\right) k_6[X_{CH_4}][X_H]^2 \\
q_8 &= \left(\frac{k_1+(k_2[X_{H_2O}])/(K_{c,12}[X_{H_2}])}{k_6[X_H]+k_7[M]+k_8[X_{O_2}]}\right) k_8[X_{O_2}][X_{CH_4}][X_H] \\
q_9 &= \left(\frac{k_9}{K_{c,12}}\right)\left(\frac{[X_{CO}][X_{H_2O}]}{[X_{H_2}]}-\frac{[X_{CO_2}]K_{c,12}}{K_{c,9}}\right)[X_H] \\
q_{10} &= k_{10}[X_H]\left([X_{O_2}]-\frac{[X_H]^2[X_{H_2O}]^2}{[X_{H_2}]^3K_{c,10}K_{c,11}K_{c,12}^2}\right) \\
q_{14} &= k_{14}[X_H][X_{O_2}][M] \\
q_{15} &= \left(\frac{k_{15}}{K_{c,12}}\right)\left(\frac{[X_{H_2O}][X_H]^2[M]}{[X_{H_2}]}\right) \\
q_{16} &= k_{16}\left(\frac{q_8+q_{14}}{(k_{16}+k_{17}+(k_{18}[X_{H_2O}])/([X_{H_2}]K_{c,12})}\right)
\end{aligned}
$$

where, third body concentration is defined by species efficiencies ($\alpha_{CH_4} = 6.54$, $\alpha_{O_2} = 0.4$, $\alpha_{CO_4} = 1.5$, $\alpha_{H_2O} = 6.5$, $\alpha_{CO} = 0.75$, $\alpha_H = 1.0$, $\alpha_{H_2} = 1.0$, $\alpha_{N_2} = 0.4$), and equilibrium constants are approximated as:

$$
\begin{aligned}
K_{c,12} &= 0.2657\,T^{-0.0247}\,exp(7618.33/T) \\
K_{c,9}/K_{c,12} &= 3.828\,10^{-5}\,T^{0.8139}\,exp(4954.18/T) \\
K_{c,10}K_{c,11}K_{c,12}^2 &= 11.687\,T^{-0.2467}\,exp(5738.17/T)
\end{aligned}
$$

The exposed reduced mechanism has therefore two main attributes:

- The original number of species conservations equations to be solved for skeletal mechanism suggested by Miller et al has been reduced notably (i.e. from 15 to 7 considering only N_2 as inert species).
- The faster reactions have been subtracted. In this way the resulting set of governing equations becomes less stiff, and the inherent difficulties for their resolution are smoothed.

3.4.2 Mathematical Reduction Method (MRM)

This method, introduced by Mass and Pope [24][25][26], focuses the attention on the mathematical treatment of kinetic mechanisms. Analyzing their characteristics, tries

to find out the way of how the resulting set of consumption/production rates reach their steady-state values rapidly. Differences to conventional reduced mechanism appear since they are not limited to any combustion problem.

The way of how reaction rates tend to their steady-state values are described by means of directions that are obtained by the chemical reaction mechanism itself. Varying species concentrations in all possible directions, chemical reaction rates are examined. A Jacobian matrix for $d\dot{w}_i/d\phi$ ($\phi = Y_i, T, ...$) is evaluated, and the eigenvalues of the Jacobian are associated with the chemical time scales [27]. Slow and fast reaction groups are estimated (Jacobian eigenvalues).

The method introduces what are called *Intrinsic Low-Dimensional Manifolds (ILDM)* in the reaction space. The manifolds are subspaces in the composition space where only slow processes take place, steady-state assumptions are considered for the faster group of reactions.

As a result of the elimination of the faster group of reactions (i.e. large Jacobian eigenvalues) species concentrations are related to a number of control or progress variables, that are in fact the concentrations of some species (e.g suitable variables could be H_2O and CO_2 mass fractions). Jacobian eigenvalues are computed in a preprocessing task. For discrete values of the progress variables, manifolds composition are computed and stored in a data base. Look-up tables are developed.

On the solution of the application problem, conservation equations are solved for the progress variables, while mixture composition is given by the manifold composition stored in the database.

The attractive features of this method has motivated a considerable research on its improvement. ILDM reduces both stiffness of the governing equations, the number of conservation equations to be solved, and thereby the computational costs. Furthermore, they can also be applied to model turbulent flows, considering progress variables time-averaged (or Favre-averaged) quantities.

Nevertheless, still exist considerable difficulties to overcome. Steady-state assumptions are not well defined for low temperatures, aspect that may cause some computational problems. Some species concentrations (mostly radicals) could adopt huge or negative values [27]. Look-up tables could become very large and its quality (in terms of discrete values) and its interpolation strategies, are also needed to be improved.

3.4.3 Global reaction schemes

Simplest chemical approaches assume that fuel and oxygen are converted to products in one irreversible step. Stoichiometric reactions define the chemical process. Arrhenius parameters for the rate constant and reaction orders are obtained to fit experimental or detailed numerical results. Both experimental and numerical simulations are carried out with laboratory flames, characterized by their geometrical

simplicity. Flat-flame burners for premixed combustion [14] and Bunsen burners for non-premixed or partially premixed flames [28] are suitable for this purpose.

One-step global reactions are found to be reasonably adequate to model flame-shape stability or flashback behavior [27]. However, they do not provide information about essential aspects of the combustion process such contaminants production.

Even though the limitations of these chemical approaches, irreversible single-step reactions still receive interest of the combustion community. An illustrative example is the global reaction for premixed methane-air flames suggested by Lange et al [29].

$$q = A\,[X_{CH_4}]^a [X_{O_2}]^b\, exp\left(-\frac{E_a}{RT}\right) \tag{3.27}$$

Reaction parameters that fits experimental data are respectively: $a = 2.8$, $b = 1.2$, $A = 3.9712\,10^{28}\ (mol/cm\,s)^{-3}$, $E_a = 33583.94\ cal/mol\,K$.

This interest increases when more complex hydrocarbons are taken into account. Global reaction schemes for several hydrocarbons provided by Westbrook and Dryer [30] are summarized in table 3.3.

Fuel	A (one-step)	A (two-step)	E_a	a	b
CH_4	$1.3\,10^9$	$2.8\,10^9$	48400	−0.30	1.30
CH_4	$8.3\,10^9$	$1.5\,10^7$	30000	−0.30	1.30
C_2H_6	$1.1\,10^{11}$	$1.3\,10^{12}$	30000	0.10	1.65
C_3H_8	$8.6\,10^{11}$	$1.0\,10^{12}$	30000	0.10	1.60
C_4H_{10}	$7.4\,10^{11}$	$8.8\,10^{11}$	30000	0.25	1.50
C_5H_{12}	$6.4\,10^{11}$	$7.8\,10^{11}$	30000	0.25	1.50
C_6H_{14}	$5.7\,10^{11}$	$7.0\,10^{11}$	30000	0.25	1.50
C_7H_{16}	$5.1\,10^{11}$	$6.3\,10^{11}$	30000	0.25	1.50
C_8H_{18}	$4.6\,10^{11}$	$5.7\,10^{11}$	30000	0.25	1.50
C_8H_{18}	$7.2\,10^{11}$	$9.6\,10^{12}$	40000	0.25	1.50
C_9H_{20}	$4.2\,10^{11}$	$5.2\,10^{11}$	30000	0.25	1.50
$C_{10}H_{22}$	$3.8\,10^{11}$	$4.7\,10^{11}$	30000	0.25	1.50
CH_3OH	$3.2\,10^{11}$	$3.7\,10^{12}$	30000	0.25	1.60
C_2H_5OH	$1.5\,10^{12}$	$1.8\,10^{12}$	30000	0.15	1.60
C_6H_6	$2.0\,10^{11}$	$2.4\,10^{11}$	30000	−0.05	1.85
C_7H_8	$1.6\,10^{11}$	$1.9\,10^{11}$	30000	−0.10	1.85

Table 3.3: Chemical kinetic data for modeling hydrocarbon combustion using global single and two-steps reaction schemes [30]. Units: cm, g, mol, s, cal and K.

One-step approaches tend to overestimate the heat release rate and in consequence the combustion temperatures. To improve the chemical modelization, reduced global reaction schemes consider more than a single step to reproduce more accurately main

combustion features. The common two steps approach reads:

$$Fuel + a\, O_2 \rightarrow b\, CO_2 + c\, H2_O$$
$$CO + \frac{1}{2} O_2 \rightarrow CO_2$$

The kinetic coefficients employed for the first step are listed in table 3.3. The pre-exponential factor differs if one or two steps are considered. For the second step, carbon monoxide oxidation, the rate coefficients are: $A = 8\ 10^8\ (mol/cms)^{-0.5}$ and $E_a = 40000\ cal/mol\ K$.

Although, two-steps schemes are optimized to describe main combustion characteristics (e.g. burning velocity, thermal profile, particular experiment configuration, etc.) still are deficient in a number of important aspects [31]. In fact, the main limitation of these schemes is the omission of hydrogen, H_2.

In order to improve the commented above limitations, Jones and Lindsted suggested a four-step scheme for premixed and non-premixed flames [32]. The main attributes pointed out by the authors were the acceptable mathematical tractability with good agreement for flame speeds, flame thickness and species profiles for both kind of flames.

I	$C_nH_{2n+2} + \frac{n}{2}O_2 \rightarrow nCO + (n+1)H_2$
I	$C_nH_{2n+2} + nH_2O \rightarrow nCO + (2n+1)H_2$
III	$H_2 + \frac{n}{2}O_2 \Leftrightarrow H_2O$
IV	$CO + H_2O \Leftrightarrow CO_2 + H_2$

Net rate of progress variable for each reaction, are defined by the following expressions:

$$\begin{aligned}
q_I &= k_I^f [X_{C_nH_{2n+2}}]^{0.5} [X_{O_2}]^{1.25} \\
q_{II} &= k_{II}^f [X_{C_nH_{2n+2}}][X_{H_2O}] \\
q_{III} &= k_{III}^f [X_{H_2}]^{0.5} [X_{O_2}]^{2.25} [X_{H_2O}]^{-1.0} - k_{III}^b [X_{O_2}]^{1.75} [X_{H_2}]^{0.75} \\
q_{IV} &= k_{IV}^f [X_{CO}][X_{H_2O}] - k_{IV}^b [X_{CO_2}]^{-1.0} [X_{H_2}]
\end{aligned}$$

where, forward rate constants are listed in table 3.4, and backward ones are obtained as usual from equilibrium constants.

As can be seen, third step involves a negative water concentration dependence, which can produce convergence problems. Jones and Lindsted comment this aspect in their work [32]. When numerical problems occur, they provide an alternative expression:

$$q_{III}^{'} = k_{III}^{f,'} [X_{H_2}]^{0.25} [X_{O_2}]^{1.5} - k_{III}^{b,'} [X_{O_2}]^{1.0} [X_{H_2}]^{-0.75} [X_{H_2O}]$$

Step	n	A	β	E_a
I	1	$6.8\,10^{15}$	-1.0	40000
	2	$9.0\,10^{15}$	-1.0	40000
	3	$8.5\,10^{15}$	-1.0	40000
	4	$7.5\,10^{15}$	-1.0	40000
II	1	$3.0\,10^{8}$	0.0	30000
III	1	$2.5\,10^{16}$	-1.0	40000
	2	$3.5\,10^{16}$	-1.0	40000
	3	$3.0\,10^{16}$	-1.0	40000
	4	$2.8\,10^{16}$	-1.0	40000
$III^{'}$	1	$6.8\,10^{15}$	-1.0	40000
	2	$9.0\,10^{15}$	-1.0	40000
	3	$8.5\,10^{15}$	-1.0	40000
	4	$7.5\,10^{15}$	-1.0	40000
IV	1	$2.7\,10^{9}$	0.0	20000

Table 3.4: Chemical kinetic data for modeling hydrocarbon combustion using global four-steps reaction schemes [32]. Units: m, kg, s, kmol, cal and K.

However, this expression can be considered less accurate, specially in fuel-lean regions. Thus, if possible, original formulation is recomended.

3.5 Nitrogen oxide kinetics

The interest of developing cleaner combustion devices has motivated special attention to the modeling of pollutant formation in flames. One of the most important pollutant products are nitrogen oxides, the so-called NO_x. This nitrogen oxides are basically NO and NO_2. Since, the latter is considerable lower, usually most studies concern to the formation of NO.

The main sources of nitrogen oxide emissions that take place in combustion devices are due to the nitrogen oxidation in the post-flame zones (*thermal NO*), and in the flame zone (*prompt NO*). Together with the contribution related to the oxidation of nitrogen-containing compounds in the fuel (*fuel-bond NO*) [12]. The relative importance of these contributions depends on the operation conditions of the devices. For instance, at high temperatures an excess of oxygen in the post-flame zone can suppose an important source of thermal NO.

Last releases of full combustion mechanisms account for the formation of nitrogen oxides [13]. However, the discussed numerical difficulties for the employment of detailed mechanisms for engineering purposes, has motivated recently an important research on the development of reduced chemical models that include NO_x formation [27][33][34].

In problems of industrial interest, and being computationally prohibitive the employment of more detailed modelizations, the evaluation of NO is done via simplified

approaches. For high temperature applications, such as internal combustion engines, NO concentration can be feasibly evaluated assuming thermodynamic equilibrium. However, for moderate temperature applications, such as furnaces, the assumption of thermodynamic equilibrium can not be considered very suitable, but assuming steady-state hypothesis for nitrogen atom N is assumed.

Another common practice, in this case when modeling laminar flames with accurate enough mechanisms, is the assumption that species and reactions involved in NO chemistry has a minor influence on main properties of the combustion phenomena (i.e. burning velocities, temperature profile and main combustion species). Thus, the evaluation of nitrogen oxides is done via a *post-processing* procedure. In this way, the computational effort can be notably reduced.

The basic mechanism for *thermal* NO formation is described by the well-known Zeldovich reactions:

$$\begin{array}{ll} 1 & O + N_2 \Leftrightarrow NO + N \\ 2 & N + O_2 \Leftrightarrow NO + O \\ 3 & N + OH \Leftrightarrow NO + H \end{array}$$

being the molar rate of NO production:

$$\begin{aligned} \dot{\omega}_{NO} &= k_1^f [X_O][X_{N_2}] - k_1^b [X_{NO}][X_N] \\ &- k_2^f [X_N][X_{O_2}] - k_2^b [X_{NO}][X_O] \\ &- k_3^f [X_N][X_{OH}] - k_3^b [X_{NO}][X_H] \end{aligned}$$

and N atom molar concentration:

$$[X_N] = \frac{k_1^f [X_O][X_{N_2}] + k_2^b [X_{NO}][X_O] + k_3^b [X_{NO}][X_H]}{k_1^b [X_{NO}] + k_2^f [X_{O_2}] + k_3^f [X_{OH}]}$$

where kinetic rate constants suggested by Flagan and Seinfeld [35] and listed in table 3.5 are usually used.

3.6 Conclusions

In this chapter, and in order to evaluate species production/consumption rates that take place in reactive processes, the basic laws of chemical kinetics based on a macroscopic observation have been introduced. A detailed evaluation of the reaction rates for different kind of reactions present in a chemical model has been mathematically formulated.

Combustion processes have been described as a set of consecutive, competitive, and opposing elementary reactions (i.e. chain reactions) that forms what are known as

	k^f		k^b	
Reaction	A	T_o	A	T_o
1	$1.8\ 10^{14}$	38370	$3.8\ 10^{13}$	38370
2	$1.8\ 10^{10}$	4680	$3.8\ 10^{09}$	20820
3	$7.1\ 10^{13}$	450	$1.7\ 10^{14}$	24560

Table 3.5: Chemical kinetic data for modeling thermal NO formation [35]. $k = Aexp(-T_o/T)$. Units: cm, g, mol, s, cal and K.

full kinetic mechanisms. It has been highlighted the problem independence properties of these mechanisms and the considerable effort that the scientific community is given to their improvement.

The enormous complexity of full mechanisms, due to the considerable amount of chemical species and reactions that they involved, has forced the development of chemical approaches able to describe properly the combustion processes with lower computational costs, and able to be used on the numerical modeling of problems of industrial interest. In this sense, skeletal mechanisms and reduction methodologies have been discussed, exposing the most relevant properties of each approach.

It has not been the purpose of this thesis to develop any chemical mechanism. Actually, our main interest have been focused to the analysis of the most relevant features of different chemical approaches. In the next chapters, the numerical performance of several selected models is compared.

References

[1] R.J. Kee, F.M Rupley, E. Meeks, and J.A Miller. Chemkin-III: a fortran chemical kinetic package for the analysis of gas-phase chemical and plasma kinetics. Technical report, Sandia National Laboratories, 1996.

[2] K.J. Leider. *Chemical kinetics*. Harper Collins Publishers, Inc., 1987.

[3] F.A. Williams. *Combustion theory*. The Benjamin/Cummings Publishing Company, Inc., 1985.

[4] M.J. Pilling and P.W. Seakins. *Reaction kinetics*. Oxford Science Publications, 1995.

[5] J. Warnatz, U. Maas, and Dibble R.W. *Combustion*. Springer-Berlag, 1996.

[6] D.L. Baulch, C.J. Cobos, R.A. Cox, P. Frank, G. Hayman, TH. Just, J.A. Kerr, T. Murrels, Pilling M.J., Troe J., Walker R.W., and Warnatz J. Summary table of evaluated kinetic data for combsution modelling: supplement i. *Combustion and Flame*, 98:59–79, 1994.

[7] M.D. Smooke, R.E. Mitchell, and D.E. Keyes. Numerical solution of two-dimensional axisymmetric laminar diffusion flames. *Combustion Science and Technology*, 67:85–122, 1989.

[8] F. Lindemann. Unknown title 5. *Oxidation Comm.*, 17:0–0, 1922.

[9] R.G. Gilbert, K. Luther, and J. Troe. Unknown title 2. *Ber. Busenges Phys. Chem.*, 87:0–0, 1983.

[10] P.H. Stewart, C.W. Larson, and D.M. Golden. Unknown title 6. *Combustion and Flame*, 75:0–0, 1989.

[11] A.F. Wagner and S.B. Wardlow. Unknown title 7. *Journal of Physical Chemistry*, 92:0–0, 1988.

[12] G.L. Borman and Ragland K.W. *Combustion engineering*. McGraw-Hill, 1998.

[13] G.P. Smith, D.M. Golden, M. Frenklach, N.W. Moriarty, B. Eiteneer, M. Goldenberg, C.T. Bowman, R.K. Hanson, S. Song, W.C. Gardiner, V.V. Lissianski, and Z. Qin. Gri-Mech 3.0, http://www.me.berkeley.edu/gri_mech/.

[14] L.M.T. Somers. *The simulation of flat flames with detailed and reduced chemical models*. PhD thesis, Technical University of Eindhoven, 1994.

[15] J.B. Bell, M.S. Day, J.F. Grcar, and M.J Lijewski. Stochastic algorithms for the analysis of numerical flame situations. Technical report, Computing Science of Lawrence Berkeley National Laboratory, 2002.

[16] K. Seshadri and N. Peters. The inner structure of methane-air flames. *Combustion and Flame*, 81:96–118, 1990.

[17] G. Chesshire and W.D. Henshaw. Composite overlapping meshes for the solution of partial differential equations. *Journal of Computational Physics*, 90(1):0–0, 1990.

[18] N. Peters. Numerical and assymptotic analysis of sistematically reduced schemes for hydrocarbon flames. *Lecture Notes in Physics*, 241:90–109, 1985.

[19] N. Peters and F.A. Williams. Asymptotic structure and extinction of methane-air diffusion flames. *Combustion and Flame*, 68:185–207, 1989.

[20] M.D. Smooke, P. Lin, J.K. Lam, and M.B. Long. Computational and experimental study of a laminar axissymmetric methane-air diffusion flame. In *Proceedings of the Twenty-Third Symposium (International) on Combustion*, pages 575–582, 1990.

[21] L.M.T. Somers and L.P.H De Goey. Analysis of a systematical reduction technique. In *Proceedings of the Twenty-Fifth Symposium (International) on Combustion*, pages 957–963, 1994.

[22] W. Wang and B. Rogg. Reduced kinetic mechanisms and their numerical treatment i: wet co flames. *Combustion and Flame*, 81:271–292, 1993.

[23] J.A. Miller, R.J. Kee, M.D. Smooke, and J.F Grcar. The computation of the structure and extinction limit of methane-air stagnation point diffusion flame, paper wss/ci 84-10. In *Western States Section of the Combustion Institute, Spring Meeting*, pages 0–0, 1984.

[24] U. Mass and S.B. Pope. Simplifying chemical kinetics: intrinsic low-dimensional manifolds in composition space. *Combustion and Flame*, 88:0–0, 1989.

[25] U. Mass and S.B. Pope. Implementation of simplified chemical kinetics based on low-dimensional manifolds. In *Proceedings of the Twenty-Fourth Symposium (International) on Combustion*, pages 0–0, 1992.

[26] U. Mass and S.B. Pope. Laminar flame calculations using simplified chemical kinetics based on intrinsic low-dimensional manifolds. In *Proceedings of the Twenty-Fifth Symposium (International) on Combustion*, pages 0–0, 1994.

[27] R.L.G.M. Eggels. *Modelling of Combustion Processes and NO Formation with Reduced Reaction Mechanisms*. PhD thesis, Technical University of Eindhoven, 1996.

[28] R.E. Mitchell, Sarofim, and L.A. Clomburg. Experimental and numerical investigation of confined laminar diffusion flames. *Combustion and Flame*, 37:227–244, 1980.

[29] H.C. Lange and L.P.H. De Goey. Two-dimensional methane/air flames. *Combustion Science and Technology*, 92:423–427, 1993.

[30] Westbrook and Dryer. Chemical kinetic modeling of hydrocarbon combustion. *Progress in Energy and Combustion Science*, 108:1–57, 1984.

[31] A.Y. Abdalla, D. Chin S.B. Bradley, and C. Lam. Unknown title 1. *Oxidation Comm.*, pages 4–113, 1983.

[32] W.P. Jones and R.P. Lindstedt. Global reaction schemes for hydrocarbon combustion. *Combustion and Flame*, 73:233–249, 1988.

[33] C.P. Chou, J.Y. Chen, C.G Yam, and K.D. Marx. Numerical modeling of NO formation in laminar Bunsen flames - A flamelet approach. *Combustion and Flame*, 114:420–435, 1998.

[34] D.D. Thomsen, Kuligowski F.F., and N.M Laurendau. Modelling of no formation in premixed, high-pressure methane flames. *Combustion and Flame*, 114:307–318, 1999.

[35] R.C. Flagan and J.H Seinfeld. *Fundamentals of air pollution engineering*. Prentice Hall, 1988.

Chapter 4

Detailed numerical simulation of laminar flames by a parallel multiblock algorithm using loosely coupled computers.

A parallel algorithm for detailed multidimensional numerical simulations of laminar flames able to work efficiently with loosely coupled computers is described. The governing equations have been discretized using the finite volume technique over staggered grids. A SIMPLE-like method has been employed to solve the velocity-pressure fields while the species equations have been calculated in a segregated manner with the possibility of an operator-splitting technique. The domain decomposition method is used to optimize the domain's discretization and to parallelize the code. The main attributes and limitations, together with the computational features (computational effort, parallel performance, memory requirements, etc.), are shown considering different degrees of chemical modeling and two benchmark problems: a premixed methane/air laminar flat flame, and a confined co-flow non-premixed methane/air laminar flame. In order to asses the validity of the numerical solutions, a post-processing procedure based on the generalized Richardson extrapolation for h-refinement studies and on the Grid Convergence Index has been used.

4.1 Introduction

4.1.1 Preamble

Due to the increase of the computing power and the improvement of the numerical methods that has occurred during the last decades, CFD computations are being employed by many technologists and engineers in the resolution of thermal and me-

chanical engineering problems. Nevertheless, the research on the improvement of the performance of the numerical algorithms and the accuracy of the mathematical models, still constitutes an essential task for the successful application of CFD computations of industrial interests. An illustrative example is the numerical simulation of combustion processes for industrial equipment, where the complex phenomena involved, often three-dimensional turbulent flames with radiatively participating media, do not allow the resolution of a detailed modeling, and considerable restrictive hypothesis have to be considered in order to develop computationally capable models.

Within the wide range of combustion fields, laminar flames are an illustrative example of combustion phenomena. The detailed numerical simulation of these kind of flames has supposed, and still represents, a challenging problem. Detailed numerical simulations of laminar flames are being used for the design and optimization of industrial equipment (e.g. domestic gas burners), and for the understanding and modeling of more complex flows (e.g. turbulent flames).

The main feature of a mathematical model for laminar flames is the complex phenomena involved. This complexity remains basically on the chemical mechanisms (e.g. the last release of GRI-Mech 3.0 for methane combustion, involves 53 species and 325 reactions) and on the flames characteristics (i.e. presence of high gradients regions, flame fronts).

When detailed models are used, special attention has to be paid to the numerical method and on the domain discretization. The numerical method has to be able to treat the resulting set of stiff governing equations, while, the discretization has to be fine enough to treat adequately the flame fronts. As a consequence, the computational effort in terms of CPU and in terms of memory requirements, becomes considerable and some times prohibitive.

4.1.2 Computational resources

Since few years ago, and due to the mentioned above computational requirements, detailed numerical simulations of laminar flames were performed on workstations [1] [2], and when possible, on supercomputers [3]. Recently, and due to the increase of computing power available on the average desktop computers (in terms of flops, RAM memory and disk space), the CFD community has started to use PCs on their simulations [4][5]. Nowadays, a typical PC has performance exceeding that of a supercomputer of a decade ago.

This tendency in the increase of the PCs computing power is not clear that can be sustained for many years in single processor systems, due to both technical and economical reasons. Taking into account this limitation, and the exceptionally cost of fast sequential computers (need of special hardware with a reduced market), parallel computing systems seem to be the most attractive option in a near future, specially owing to the irruption of a new class of parallel computers: the so-called *Beowulf*

clusters (http://www.beowulf.org/) of personal computers running Linux [6].

The most attractive aspect that *Beowulf clusters* have in comparison to conventional parallel computers is their considerable lower cost, being the computing power and RAM memory similar. Nevertheless, while parallel computers can have either shared or distributed memory, *Beowulf clusters* have distributed memory (access to other processors' data must be done through a network). These clusters are called *loosely coupled* parallel computers because of their poor communication performance (low bandwidth and high latency). In order to take advantage of these "low cost" parallel computers, parallel algorithms tolerant to slow networks must be developed in order to use them efficiently for the simulation of problems such combustion.

The main attribute that may have an algorithm to be used efficiently on loosely coupled parallel computers, remains basically on the reduction of the communication work among the several processors. Due to the fact that the network performance is very low in comparison to the CPU's computing power, the work to be done by a given processor has to be large enough before it could need data from the others.

4.1.3 Numerical Strategies Overview

The stiffness and high non-linearity that characterize the system of governing equations, make that conventional CFD methods based on segregated algorithms have serious difficulties on their resolution. Time-marching algorithms can be used to aid the convergence to steady state solutions. The choice of an adequate time-step have to be based on the physical time-scales of the problem. This means that when finite rate kinetics is considered ("full" or "skeletal" mechanisms), the shortest time scales have to be chosen and therefore, the convergence process is so slow that becomes computationally prohibitive [7]. In order to overcome these numerical difficulties, coupled methods appear to be an attractive alternative. Thus, among others, two main numerical methods have been used on the resolution of stiff system of equations: i) damped Newton's methods [2][4][8][9]; ii) segregated algorithms based on operator-splitting methods [10][11][12][13][14][15].

Concerning the discretization, and due to the presence of high gradients, the use of fine control volumes is highly recommendable. As a consequence, when orthogonal structured meshes are employed, fine levels of discretization in zones with smooth gradients are forced, increasing the computational effort notably. To avoid these disadvantages, locally refined rectangular gridding is the most commonly method used in laminar flames simulations [2][4][16]. An alternative to these locally refined unstructured meshes is the employment of domain decomposition methods on structured meshes [17]. The main advantages of this strategy are: i) the structured properties of the grid allow an easier arrays indexation and a more consistent and easier evaluation of physical quantities at the edges of the node cells; ii) the use of more efficient solvers for the resolution of the linear systems of equations; iii) the possibility of choosing

different levels of discretization for the different blocks, allowing a higher level of refinement where necessary and reducing the number of grid nodes where not [15].

Another important topic in laminar flames simulations is the assessment of the credibility of the numerical solutions. The common methodology employed is based on the analysis of the evolution of some simulation values with the level of discretization. In laminar flames simulations these are for example, the maximum temperature and the flame height. A criteria involving weighted gradients and higher derivatives of physical quantities are usually used in order to choose what cells have to be refined. Due to the high coupling among the flow field, energy and species, and the error transport phenomena, this methodology could lead to inappropriate level of refinement in some places, and could affect the accuracy of the numerical solution. To improve the computational error analysis and the refinement criteria, considerable work is being carried out in combustion problems [4][18].

4.1.4 Proposal of this work

The main objective of this chapter is to describe the methodology employed in the numerical simulation of laminar flames, and to present the competitive features of a parallel multiblock algorithm able to perform efficiently with loosely coupled computers.

The governing equations have been discretized using the finite volume technique with fully implicit temporal differentiation, using structured Cartesian or cylindrical staggered grids. The discretized equations have been solved in a segregated manner, employing a pressure-based SIMPLE-like method to couple the velocity-pressure fields. The chemical terms are coupled by means of operator-splitting techniques. The domain decomposition technique is used to optimize the discretization and to parallelize the code, assigning one or several subdomains to different CPUs. The main attributes of this approach are: i) little communication work, one per outer iteration, in comparison to the computational work; ii) an easier code parallelization, allowing the use of pre-existent sequential algorithms.

The work gives emphasis to two main aspects: i) the treatment of the governing equations, specially to the operator-splitting procedure; ii) and the appropriateness of the parallel multiblock algorithm to solve these kind of problems, both in terms of the domain discretization and of the computational efficiency.

Concerning to the parallel multiblock algorithm, single block (S) versus multiblock (M) discretizations are analyzed. In these studies, the grid nodes distribution coincides for all discretizations. Multiblock discretizations are obtained simply dividing the domain in a defined number of blocks or subdomains. Three main aspects are pointed out: i) the influence of the multiblock discretization to the iterative procedure; ii) the parallel performance in terms of computational time savings; iii) and the uncertainty of the numerical solutions.

In order to analyze the first and second aspects, the numerical performance of single block discretizations, in terms of outer iterations and CPU time, are compared to those obtained with multiblock technique analyzing the influence of the number of blocks considered.

To analyze the third, all numerical solutions are submitted to a verification process by means of a post-processing procedure developed at CTTC [18], based on the Generalized Richardson extrapolation for h-refinement studies and on the Grid Convergence Index (GCI) proposed by Roache [19]. Estimates of the uncertainty due to discretization are evaluated in order to assess that the employment of the multiblock technique does not decrease the accuracy of the numerical solutions, and in order to find the appropriate discretization parameters.

Once the good performance of the parallel multiblock algorithm has been shown, multiblock discretizations are optimized reducing the number of grid nodes in regions with smooth gradients. In this optimization, again, verification studies are used to select the appropriate grid nodes distribution. In the work, these kind of discretizations are referred as optimized multiblock discretizations (OM).

A *Beowulf cluster* composed by 48 standard PCs (AMD K7 CPU at 900 MHz and 512 Mbytes of RAM) with a conventional network (100 Mbits/s 3COM network card and a 3COM switch) and running with Debian Linux 2.1 (kernel version 2.7.2.3), has been used to perform the numerical simulations.

Results are presented considering different chemical models and two benchmark problems. Full mechanisms (GRI-Mech 1.2, GRI-Mech 2.11 and GRI-Mech 3.0), a skeletal mechanism [9], a global reduced mechanism [20], and irreversible single-step models [21] [22], are taken into account. The two benchmark problems selected are: a premixed methane/air laminar flat flame [16], and a confined co-flow non-premixed methane/air laminar flame [23].

4.2 Mathematical model

4.2.1 Governing equations

The governing equations for a reactive gas (continuity, momentum, energy, species and state equation) can be written as follows [3]:

$$\frac{\partial \rho}{\partial t} + \nabla \cdot (\rho \vec{v}) = 0 \tag{4.1}$$

$$\frac{\partial (\rho Y_i)}{\partial t} + \nabla \cdot (\rho Y_i \vec{v}) = -\nabla \cdot \vec{j}_i + \dot{w}_i \tag{4.2}$$

[3] Even though the mathematical formulation has been presented in detail in chapter 2, a short review of the main aspects here considered have been included for clarity.

$$\frac{\partial(\rho\vec{v})}{\partial t} + \nabla\cdot(\rho\vec{v}\vec{v}) = \nabla\cdot\vec{\tau}^{\,T} - \nabla p + \rho\vec{g} \tag{4.3}$$

$$\frac{\partial(\rho h)}{\partial t} + \nabla\cdot(\rho\vec{v}h) = -\nabla\cdot\vec{q}^{\,T} \tag{4.4}$$

$$\rho = \frac{pM}{RT} \tag{4.5}$$

where t is time; ρ mass density; $\vec{v}$ average velocity of the mixture; $\vec{\tau}^{\,T}$ stress tensor; p pressure; $\vec{g}$ gravity; N total number of chemical species; h specific enthalpy of the mixture; Y_i mass fraction of ith species; $\vec{j}_i$ diffusion mass fluxes of ith species; $\dot{w}_i$ net rate of production of the ith species; h_i specific enthalpy of the ith species; T temperature; $\vec{q}^{\,T}$ heat flux; M molecular weight of the mixture; R the universal gas constant.

The stress tensor is evaluated taking into account Stokes' law for Newtonian fluids, while the heat flux is defined by Fourier's law.

Enthalpy and temperature are related as,

$$h = \sum_{i=1}^{N} h_i Y_i = \sum_{i=1}^{N} \left(h_i^o + \int_{T^o}^{T} c_{p_i} dT \right) Y_i \tag{4.6}$$

where h_i^o is standard heat of formation of the ith species; c_{p_i} is specific heat of the ith species; and T^o is standard state temperature.

Mass fluxes of species relative to mass-average velocity, diffusion fluxes, are evaluated considering ordinary diffusion by means of a Fick's law formulation for multicomponent mixtures:

$$\vec{j}_i = \rho_i(\vec{v}_i - \vec{v}) = -\rho D_{im}\nabla Y_i \tag{4.7}$$

where D_{im} is effective diffusivity of the ith species in the mixture. Transport and thermophysic properties have been evaluated using CHEMKIN's database [24].

4.2.2 Chemical models

Four different levels of modeling have been considered for the treatment of the chemical reactions: i) "full" GRI-Mech mechanisms (version 1.2, comprising 177 reactions and 32 species; version 2.11, with 279 reactions and 49 species [25]; and version 3.0 with 325 reactions and 53 species [26]); ii) an skeletal mechanism comprising 42 reactions and 15 species [9]; iii) a four-step global reduced mechanism [20]; iv) an irreversible single-step model for premixed flames [22], and the flame-sheet hypothesis for non-premixed flames [21].

In the most general situation, finite-rate chemistry, the evaluation of the net rate of production of each species due to N_R reactions, is obtained by summing up the

individual contribution of each reaction:

$$\dot{w}_i = M_i \sum_{j=1}^{N_R} \left(\nu_{i,j}^{''} - \nu_{i,j}^{'} \right) \left[k_j^f \prod_{i=1}^{N} [X_i]^{\nu_{i,j}^{'}} - k_j^b \prod_{i=1}^{N} [X_i]^{\nu_{i,j}^{''}} \right] \tag{4.8}$$

Here, $[X_i]$ represents the molar concentration and M_i the molecular weight of ith species; $\nu_{i,j}$, $\nu_{i,j}^{''}$ the stoichiometric coefficients of the ith species appearing as a reactant and as a product in the reaction j respectively; and k_j^f, k_j^b the forward and backward rate constants.

4.3 Methodology

4.3.1 Numerical Method

The governing equations have been discretized using finite volume techniques with fully implicit temporal differentiation for calculating steady or transitory compressible or incompressible flows, using cartesian or cylindrical staggered grids. Third order schemes have been used for the evaluation of convection terms [27]. A SIMPLE-like algorithm has been considered to solve in a segregated manner the velocity-pressure fields coupling [28]. A multigrid solver has been employed on the resolution of the system of algebraic equations [29].

Resolution of species equations.

Two approaches have been explored. The first one uses a standard implicit procedure in the same way as the other conservation equations: momentum and energy. Very small time steps should be used due to the stiffness of the species equations. The second approach uses the pseudo-time splitting technique. This technique is based on the split of each species equations into two steps: the convective-diffusion step, and the chemical step [13].

Related to this second approach, several possibilities can be found in the literature considering different kind of operator-splitting strategies [10][11][12][13][14][15][30]. Depending on how the convection-diffusion equation for species mass conservations are split, and how the chemical source terms are integrated, the method represents a numerical approximation to the original non-split discretized equations. The operator-splitting method used in this work is based on a pseudo-time splitting procedure. A brief explanation of the method is given below.

The discretized species mass conservation equations with a fully implicit formula-

tion in two dimensions take the form:

$$\rho_P^o \frac{Y_{i,P} - Y_{i,P}^o}{\Delta t} V_P \qquad +(J_e - F_e Y_{i,P}) - (J_w - F_w Y_{i,P}) \\ +(J_n - F_n Y_{i,P}) - (J_s - F_s Y_{i,P}) = \dot{w}_{i,P} V_P \tag{4.9}$$

where F and J represent the mass fluxes and the convection-diffusion terms at the faces of the control volume, for example, for the east face:

$$J_e = \left(\rho u Y_i - \rho D_{im} \frac{\partial Y_i}{\partial x} \right)_e S_e \tag{4.10}$$

Defining an intermediate species mass fractions (Y_i^*), the discretized equation (4.9) can be split forcing a second-step with the chemical source terms to be solved in an implicit manner (key aspect in these kind of stiff system of equations). The consistency of each species equation is maintained when the evaluation of the intermediate species (i.e. first step) is treated explicitly:

- First step, convection-diffusion terms:

$$\rho_P^o \frac{(Y_{i,P}^* - Y_{i,P}^o)}{\Delta t} V_P \qquad +(J_e - F_e Y_{i,P}) - (J_w - F_w Y_{i,P}) \\ +(J_n - F_n Y_{i,P}) - (J_s - F_s Y_{i,P}) = 0 \tag{4.11}$$

- Second step, chemistry term:

$$\rho_P^o \frac{Y_{i,P} - Y_{i,P}^*}{\Delta t} V_P = \dot{w}_{i,P} V_P \tag{4.12}$$

To increase the robustness of the method in the first step, an implicit treatment has been enforced via a deferred correction [31]:

$$\rho_P^o \frac{(Y_{i,P}^* - Y_{i,P}^o)}{\Delta t} V_P \qquad +(J_e^* - F_e Y_{i,P}^*) - (J_w^* - F_w Y_{i,P}^*) \\ +(J_n^* - F_n Y_{i,P}^*) - (J_s^* - F_s Y_{i,P}^*) = b_{spl} \tag{4.13}$$

where the deferred term (b_{spl}), is evaluated subtracting both the actual mass fluxes and the convection-diffusion terms as:

$$b_{spl} \quad = (J_e^* - J_e) - (J_w^* - J_w) + (J_n^* - J_n) - (J_s^* - J_s) \\ +(F_e - F_w + F_n - F_s)(Y_{i,P}^* - Y_{i,P}) \tag{4.14}$$

For each outer iteration, the split convection-diffusion equations (4.13) are solved in a segregated manner, while the chemical step (4.12) is solved in a coupled manner

for all species and for each control volume using the Modified Damped Newton's method for stiff ordinary differential equations [16].

It is interesting to point out that the intermediate species mass fractions (Y_i^*) loss its physical concept in this approach. The intermediate values are those that, for each time-step, the discretized species diffusion equations (4.9) are fully satisfied. Thus, and depending on the considered species, Y_i^* can take even negative values. Thus, source terms linearizations, usually recommended in finite volume discretizations for always-positive variables, are not employed [28].

Treatment of the energy equation.

As can be observed in equation 5.4, the store of energy in the control volume and the flux of energy due to the fluid motion are written in terms of enthalpy, while the heat fluxes are evaluated considering the Fourier's law in terms of temperature gradients. Usually, on the formulation of a discretized energy equation two main approaches are followed: i) writing the energy equation with temperature as dependent variable, introducing a numerical approach for the convective fluxes (4.15); ii) or writing it in terms of enthalpy, expressing the Fourier's law in terms of enthalpy and species mass fractions gradients (4.16).

$$c_p \frac{\partial (\rho T)}{\partial t} + c_p \nabla \cdot (\rho \vec{v} T) = \nabla \cdot (\lambda \nabla T) - \sum_{i=1}^{N} \left(\nabla \cdot \left(h_i \vec{j_i} \right) + h_i^o \dot{w}_i \right) \tag{4.15}$$

$$\frac{\partial (\rho h)}{\partial t} + \nabla \cdot (\rho \vec{v} h) = \nabla \cdot \left(\frac{\lambda}{c_p} \nabla h \right) - \sum_{i=1}^{N} \nabla \cdot \left(h_i \vec{j_i} + \frac{\lambda}{c_p} \nabla Y_i \right) \tag{4.16}$$

When the second approach is considered, temperature is usually evaluated from the enthalpy-temperature relationship (5.8), using for example, a Newton's method [30].

In this paper, a different methodology has been followed. The energy equation has been considered in its original form (5.4). An energy convection-diffusion equation with temperature as dependent variable has been formulated, introducing the full energy equation in the source term by means of a deferred correction. Thus, the solved temperature field are directly that which satisfies the original energy equation.

With this formulation, energy fluxes are directly evaluated with temperature and enthalpy nodal values by means of the employed numerical schemes and without any further numerical approach. Furthermore, no extra computing time is needed to evaluate temperatures from the enthalpies values.

4.3.2 Domain Decomposition Method. Parallel algorithm

The domain decomposition method has been used as a strategy to reduce the number of grid nodes far from the flame fronts and as a parallelization technique. The whole

domain is divided into several overlapped *subdomains* joined by the interpolation boundaries.

The discretized governing equations are solved in each block (subdomain) with the appropriate boundary conditions and the required grid (inner iteration). Once all blocks have been calculated, information of the interpolation boundaries is transferred among the different blocks in an explicit manner (outer iteration). This strategy allows to solve several blocks simultaneously by different CPUs. The processors communicate only once per outer iteration. Thus, the communication work is notably lower than the calculation work. This property benefits the employment of the proposed algorithm in *Beowulf clusters*.

This approach may not be efficient as parallelization strategy for elliptic problems. Due to the explicit information transfer, the number of outer iterations needed increases with the number of subdomains. Nevertheless, for parabolic flows such those involved in laminar flames, the number of outer iterations remains almost constant, see results section, and the large-grain approach of the algorithm allows good efficiencies even on loosely-coupled parallel computers [32].

Concerning to boundary conditions at the interpolation boundaries, which are responsible for the information transfer among subdomains, they are calculated using appropriate *interpolation schemes*. For the Navier-Stokes equations, the normal boundary velocity is calculated via local mass balances, and the tangential velocity using local balances of the tangential-momentum fluxes [17]. This procedure has been proved to be suitable on laminar simply connected incompressible flows. For the scalar fields (Y_i and T) an asymptotically conservative scheme based on bi-quadratic Lagrangian interpolations has been employed [15][33]. When operator-splitting techniques are used for the species equations, the interpolated boundary conditions are only needed for the intermediate species mass fractions (Y_i^*), while species mass fractions (Y_i) are directly evaluated decoupled at each CV from the chemistry step (equation 4.12).

The parallel implementation of the code has two main goals: allow maximum portability between different computing platforms, and keep the code as similar as possible to the sequential version. To achieve the first, MPI library has been used as message passing protocol (LAM 6.1). To achieve the second, all the calls to low-level message passing functions have been grouped on a program module and a set of input-output functions has been implemented. The code for the solution of a single-domain problem remains virtually identical to the previous sequential code. In fact, it can still be compiled without MPI library and invoked as a sequential code [32].

4.3.3 Verification of the numerical solutions

All numerical solutions here presented have been submitted to a verification process by means of a post-processing procedure [18] based on the Generalized Richardson

extrapolation for h-refinement studies and on the Grid Convergence Index (GCI) proposed by Roache [19]. With this procedure, global and local estimates are calculated giving criteria about the sensitivity of the numerical solutions to the computational model parameters that account for the discretization (the mesh spacing and the order of accuracy), and about the credibility of the estimates themselves.

The first step in this procedure is to chose a grid where the post-process will be performed. The procedure processes three consecutive numerical solutions of the h-refinement studies. These solutions are interpolated at the post-processing grid. The most relevant parameters arisen from the verification process are the GCI, the observed order of accuracy of the numerical solution, p, and the percentage of nodes of the post-processing grid where it has been possible to apply the post-processing procedure, which are called as Richardson nodes. These estimates are obtained for the finer mesh and for each one of the dependent variables of the problem. Typically, the post-processing grid will be the coarsest of the three meshes employed in the post-processing procedure. However, provided that the post-processing grid is coarse enough so as to assure that extrapolations from the numerical solutions are not made, other meshes can also be used. This aspect allows to limit the domain where the post-processing will be performed to those zones of particular interest.

Both global and local estimators of the GCI and p are calculated. The global GCI is an estimate of the uncertainty due to discretization. This estimation is credible when the global observed order of accuracy p approaches the theoretical value (e.g. 2 in second differencing schemes), and when the number of Richardson nodes is high enough. These global estimates permit a uniform reporting of the results of the verification procedure in a compact manner. On the other hand, the local estimates make it possible to find out local source of error such as zones with inadequate mesh concentration or problems with an inadequate formulation of the boundary conditions or of the interpolation schemes used for the multiblock method.

Numerical results presented in this work are given together with the global GCIs. The corresponding percentages of Richardson nodes were always beyond 80% and the observed order of accuracy had usually an average value of 2. This agree with the theoretical order of accuracy of the numerical schemes used. That is: 2 for the diffusive terms (Central differences) and 1 to 3 for the convective ones (SMART).

It is worth to highlight that meshes and numerical schemes used in the solutions here presented have been chosen according to the results of the verification process. Other computations here not presented using different discretization parameters were also performed. Some of them had numerical solutions similar to that here presented but their global GCIs were not credible because the low number of Richardson nodes observed and/or because the observed order of accuracy did not approach the theoretical value. In this process of finding the appropriate discretization parameters, the local estimates obtained from the post-processing tool help to take decisions such as

where the discretization mesh requires further refinement. Local estimates of p and GCI of one of the cases under study are given as example in section 4.5.3.

4.4 Test cases

4.4.1 Case A: Premixed methane/air flat flame on a perforated burner

A methane-air homogeneous mixture flows through a drilled burner plate to an open domain. The burner plate forms a regular pattern of small drilled holes. This plate may be viewed as an ensemble of tiny premixed Bunsen-like burners of a diameter d ordered in a regular honeycomb structure with pitch p (see figure 4.2). Choosing a small enough diameter and a small enough pitch, the three-dimensional behavior of the flame is reduced notably adopting a global flat structure disturbed only at the edges of the burner rim and in the vicinity of the drilled holes. Neglecting the effects of the burner rim, the combustion phenomena can be modeled adopting a two-dimensional computational domain enclosed within two symmetry planes, as shown in figure 4.2a, accounting for a half burner hole and the corresponding part of the open domain above the burner [16].

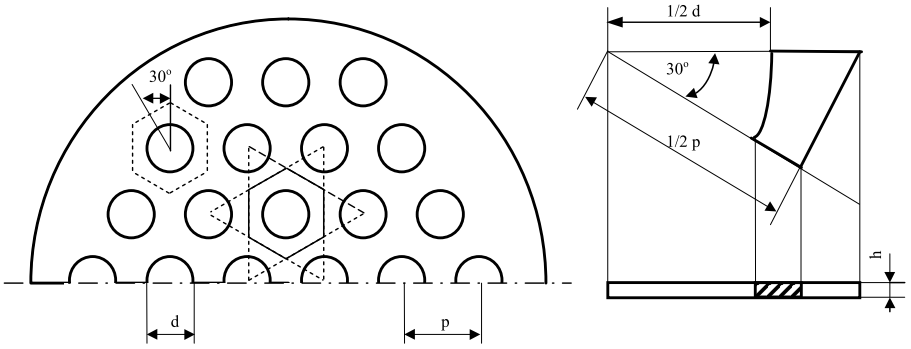

Figure 4.1: Case A: Premixed methane/air laminar flat flame on a perforated burner. Burner geometry.

Two geometrical configurations are considered, $d = 0.03$ cm (narrow flame) and $d = 0.10$ cm (wide flame). The porosity of the drilled surface is maintained to $d/p = 2/3$. A computational domain length of $L = 0.4$ cm has been chosen.

The boundary conditions that close the test are as follows. At the inlet, the mass flow rate, the temperature and the mixture's equivalence ratio are imposed.

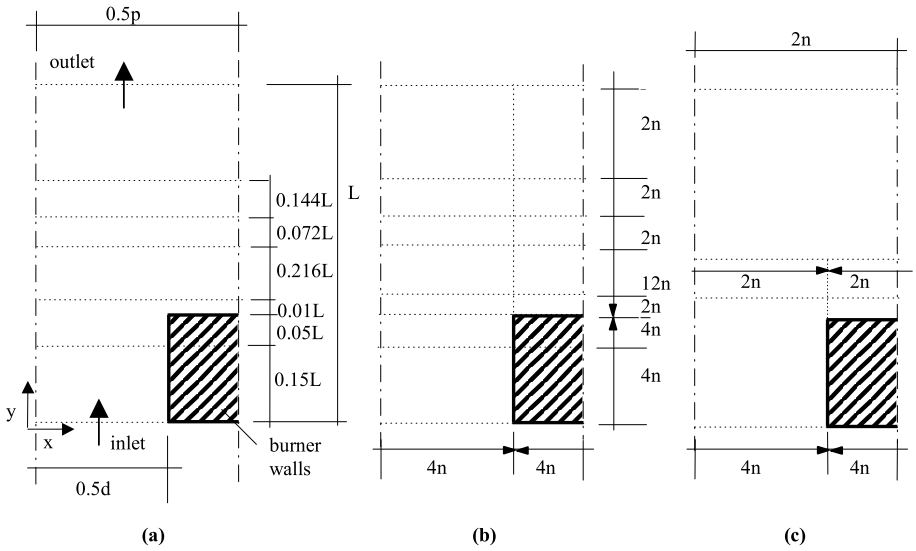

Figure 4.2: Case A: Premixed methane/air laminar flat flame on a perforated burner. (a) Burner geometry and definition of the different zones for the nonequispaced cartesian grid. (b) Computational domain and mesh nodes distribution. (c) x-direction grid nodes distribution for optimized multiblock discretization.

A parabolic velocity profile is assumed. At the outlet, pressure is imposed. The results are presented for the particular case of mass flow rate, inlet temperature and equivalence ratio of 0.05929 g/cm^2s, 298.2 K, and 1.0 respectively.

Concerning to discretization, the domain is divided into several zones with different regular nodes distribution (see figure 4.2b). For the zones closer to the burner walls, the nodes distribution has been intensified by means of a tanh-like function [34]. The number of nodes corresponding to each zone are indicated in terms of the grid parameter n, and the direction of the intensified distribution is indicated by a solid triangle. Concentration factors of 1 and 2 have been employed. The h-refinement study is performed with five levels of refinement, $n = 1$, 2, 4, 8 and 16. For example, $n = 16$ corresponds to a discretization of 57.344 control volumes.

When multiblock discretization is employed, the computational domain is divided into several subdomains along the direction of the fluid motion (i.e. y-direction). For the optimized multiblock discretization, the nodes distribution has been maintained along the y-direction, while along the x-direction, the number of grid nodes and the tanh-like function's factor have been reduced above the flame front. The optimized discretization is schematically described in figure 4.2c. Three zones with different

nodes distributions are shown.

The verification processes have been carried out in a post-processing domain enclosed in the space region limited by $0.15L \leq y \leq 0.25L$.

4.4.2 Case B: Confined co-flow non-premixed methane/air flame

As a second test case, the confined co-flow axisymmetric non-premixed methane/air flame has been selected. The burner is formed by two concentric tubes. A stream of methane is injected through the inner tube, while a stream of air injected through the outer tube surrounds it. A cylindrical chimney confines the flame.

Many computational and experimental studies have been carried out for these flames in different physical configurations [2][9][14][21]. In this work, we have taken into account the burner defined in [35].

The following geometrical parameters are used: inner tube's inner radius $r_i = 0.555\ cm$, inner tube thickness $W_i = 0.08\ cm$, outer tube's inner radius $r_o = 4.76\ cm$, outer tube thickness $W_o = 0.34\ cm$. The cylindrical chimney that confines the flame has therefore a radius of 5.10 cm. It extends to different heights upon the vertical position of the burner. A height of the chimney of $L = 20$ cm has been considered. The inner and outer tubes, and the chimney are made of brass. The inner tube contains glass beds to smooth the flow. Nevertheless, at its exit the velocity profile is fully-developed. A perforated brass plate, glass beds, and finally a ceramic honeycomb straighten the air flow (see [35] for details).

The computational domain is only defined in the cylindrical chimney where the flame is confined ($z \geq 0$). The methane and air flow within the inner and outer tubes have not been numerically simulated. Thus, special attention should be paid to the boundary conditions at the inner flow section of the computational domain ($z = 0$). The boundary conditions have been chosen in order to relate their values with the known values at the bottom of the burner (section B in figure 4.3a). For instance, species mass fractions are evaluated fixing the species mass flow rates and considering that no reactions occur in this region:

$$(\rho v_z Y_i)_B = \left(\rho v_z Y_i - \rho D_{im} \frac{\partial Y_i}{\partial z} \right)_{z=0} \tag{4.17}$$

Following a similar treatment, an enthalpy flux is evaluated at section B and then the temperature is estimated as:

$$(\rho v_z h)_B = \left(\rho v_z h - \lambda \frac{\partial T}{\partial z} - \sum_{i=1}^{N} h_i \rho D_{im} \frac{\partial Y_i}{\partial z} \right)_{z=0} \tag{4.18}$$

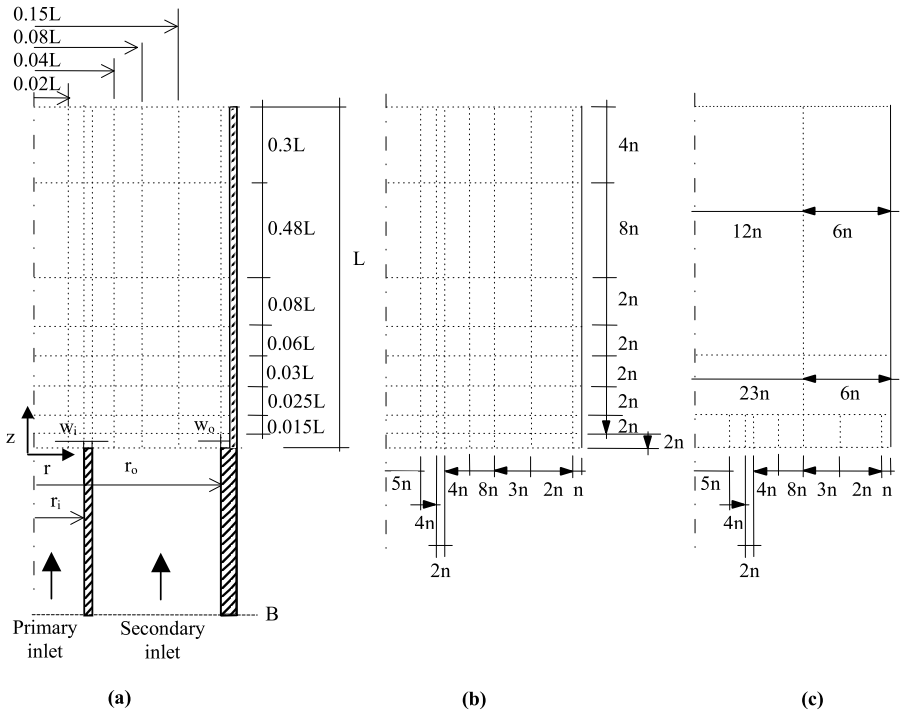

Figure 4.3: Case B: Confined co-flow non-premixed methane/air laminar flame. (a) Burner geometry and definition of the different zones for the nonequispaced cylindrical grid. (b) Computational domain and mesh nodes distribution. (c) r-direction grid nodes distribution for optimized multiblock discretization.

Due to the burner's configuration commented above, the radial component of the velocity has been neglected at the exit of both primary and secondary inlets. A plug-flow profile has been considered for axial component at the secondary inlet, while for the primary one, a parabolic mass flow rate profile has been assumed. The velocity profile is calculated from the assumed mass flow rate and the local density value. In this way, the considerable temperature gradients involved in this regions are taken into account.

Results are presented for mass flow rates of $Q_{CH_4} = 0.2165\ g/min$ and $Q_{air} = 51.88\ g/min$ respectively. The burner's inlet temperature has been fixed to $T_B = 298K$.

The computational domain has been divided into different zones increasing the

nodes distribution density at the vicinity of the inner's tube outlet, where the gradients of methane are higher (figure 4.3b). The h-refinement study is performed with five levels of refinement, $n = 1$, 2, 4, 8 and 16. For example, $n = 16$ corresponds to a discretization of 178.176 control volumes.

The same procedure used in case A has been followed when multiblock discretization is employed. The computational domain is divided into several subdomains along the direction of the fluid motion (i.e. in this case z-direction). The number of grid nodes considered in the r-direction when optimized multiblock discretization is employed, is schematically described in figure 4.3c. The number of grid nodes is reduced as we move away from the entrance.

For this flame, the verification processes have been done in a post-processing domain enclosed in the space region limited by $0 \leq r \leq 0.0795L$ and $0 \leq z \leq L$.

4.5 Results

The good efficiency of a parallel multiblock algorithm is conditioned, basically, on the following aspects: i) the explicit treatment of the interpolated boundaries should have minor impact on the number of global outer iterations to converge a steady-state solution; ii) the amount of work carried out for each processor involved in the resolution should be similar (good load balances); iii) when loosely coupled computers are used, the communication work between the involved processors should be small enough in comparison to their calculation work; iv) the employment of a multiblock discretization should not decrease the accuracy of the numerical solutions.

These desirable properties are analyzed in the following sections. Results are given for both selected benchmark problems using the skeletal mechanism on the chemistry modeling. The narrow geometrical configuration has been selected for the premixed flame test (case A).

The appropriateness of the parallel multiblock algorithm in terms of the domain discretization and in terms of computational efficiency, is analyzed in sections 4.5.1 and 4.5.2 respectively. Single block (S) versus multiblock (M) discretizations are compared. In section 4.5.3 and by means of the commented verification process, the estimates of the uncertainty of the numerical solutions are analyzed.

Optimized multiblock discretizations (OM) are presented in section 4.5.4. The optimum grid nodes distributions are chosen from the previous verification studies. Improved computational features are shown.

Finally, in section 4.5.5, results are given for all chemical models, pointing out the numerical possibilities of the presented algorithm, and giving a reference about both uncertainty of the solutions and computational effort.

4.5.1 Multiblock algorithm

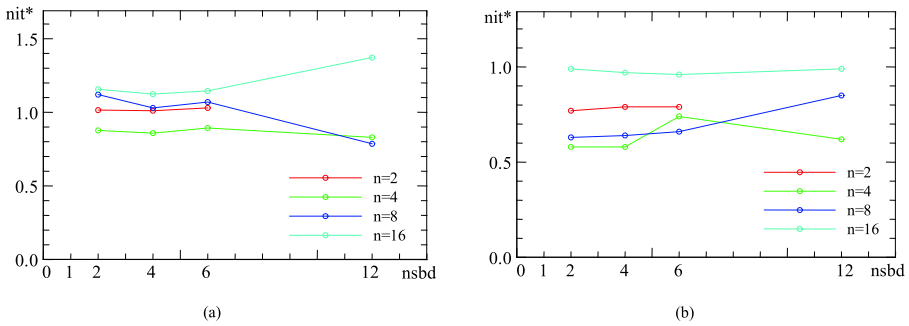

Figure 4.4: Multiblock algorithm. Influence of the number of subdomains ($nsbd$) to the number of outer iterations (nit^*) for different levels of discretization (n) and for: (a) Case A: Premixed flame; (b) Case B: Non-premixed flame.

As commented in section 4.3.2, the procedure considered on the domain decomposition technique would not be the most appropriate for elliptic problems. Nevertheless, the parabolic structure of some flows (as both selected benchmark problems), makes that these numerical difficulties could disappear. Furthermore, when fine discretizations are employed, the size's reduction of the system of discretized equations (due to the domain division) could avoid the degradation of segregated methods, decreasing in this sense the number of outer iterations in an iterative solution procedure.

To analyze this aspect, we have considered both selected benchmark flames with a single block discretization. Hereafter, the overall domains have been divided into 2, 4, 6 and 12 subdomains. The grid nodes distributions coincide to the single block case but including the overlapped zones. In figure 4.4, the influence of the number of subdomains to the number of outer iterations for different levels of refinement are plotted. The number of outer iterations nit^*, have been normalized by the number of outer iterations in the single block situation. The initial solutions for each level of refinement have been estimated with bi-quadratic Lagrangian interpolations from the previous mesh converged solutions.

As can be observed, the number of outer iterations in case A (figure 4.4.a) do not varies significantly ($\pm 30\%$) when different number of subdomains ($nsbd$) and different levels of refinement (n) are considered, increasing or decreasing but not with a defined tendency. In case B, the number of outer iterations always decreases with the employment of the domain decomposition method, obtaining in some cases a reduction of a 40%. When the last level of refinement is used ($n = 16$) the number of iterations remains almost constant.

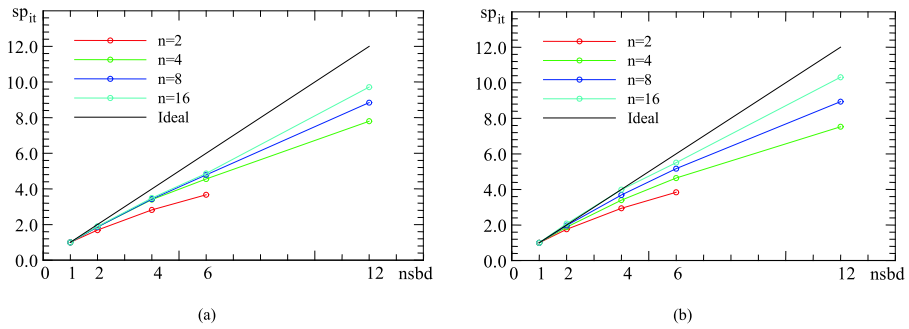

Figure 4.5: Parallel performance. Influence of the number of subdomains ($nsbd$) to the speed-up (sp_{it}) for: (a) Case A: Premixed flame; (b) Case B: Non-premixed flame.

Considering the flow structure of both flames, the premixed flame (case A) is the one which presents a more defined homogeneous parabolic flow. In this way, the expected results do not agree with the obtained ones. Considering that relaxation factors have been employed on their resolution (i.e. time-marching, linear systems solvers, update of some physical quantities such production/consumption rates, etc.), this fact could affect the global number of iterations, specially when multiblock discretization is used. Furthermore, the location of the interpolation boundaries (e.g. if coincides with the flame front) could also affect the iterative procedure.

Nevertheless, and as a main conclusion of this section, we can say that the number of outer iterations do not varies significantly, and the employment of the multiblock discretization do not adversely affect the iterative procedure.

4.5.2 Parallel performance

Once the domain has been divided in several subdomains (with a similar number of CV), each one can be assigned to different CPUs, distributing the work and getting faster with a converged solution. The amount of calculation work to be done for each processor has been chosen in a pre-processing task. Due to the introduction of overlapped zones where the information transfer among subdomains is realized, the total number of CV along y-direction (z, in the axialsymmetric case) corresponds to:

$$NY_{nsbd} = NY_1 + 4(nsbd - 1) \tag{4.19}$$

where NY_{nsbd}, is the total number of CV for $nsbd$ blocks, and NY_1 is the number of CV for the single block discretization.

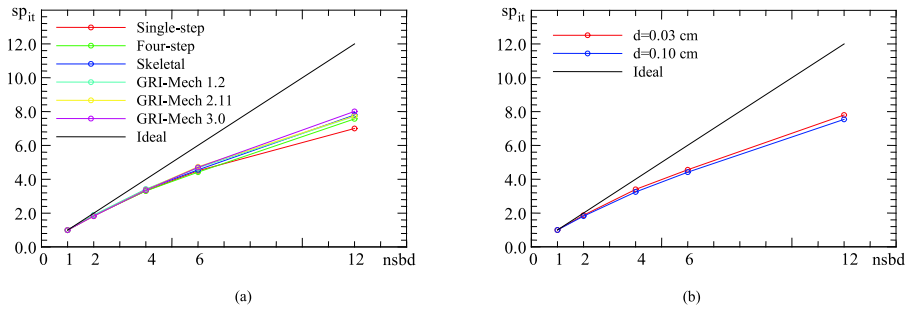

Figure 4.6: Parallel performance. Case A: Premixed flame. Influence of the number of subdomains ($nsbd$) to the speed-up (sp_{it}) for: (a) different chemical mechanisms; (b): two geometrical configurations.

The reduction of the computational time is expressed by means of speed-ups (sp_{it}). The speed-up considered, is defined as the computational time required in the single block discretization respect that required in the multiblock block discretization. Despite of the total computational time, the time required to make an outer iteration has been evaluated decoupling the influence of the number of outer iterations commented above.

In figure 4.5, computational savings due to the code's parallelization are shown. As can be seen, the higher level of discretization (n), the better parallel performance. This is basically due to the total number of CV employed. When NY_1 is big enough, the importance of the extra CVs introduced in the multiblock discretization due to the overlapped zones is reduced. Similar performance has been obtained for both flames. In case B (figure 4.5.b), slightly better speed-ups are obtained due to the higher number of CVs employed.

In Table 1, relevant computational aspects for single block versus 12 block discretization are given. As can be seen, for both flames the number of CVs increases for multiblock discretizations due to the definition of the overlapped zones. However, these increments decrease with the level of refinement. The speed-ups also improve as the level of refinement in terms of the grid parameter n becomes higher. When $n = 16$, speed-ups of 9.7 and 10.8 have been obtained for the premixed and non-premixed flames respectively.

It is important to point out the considerable weight of the chemical calculations, both on the evaluation of the mass production/consumption terms and on the resolution of the chemistry step in the operator-splitting procedure. As more complex is the kinetic mechanism, obviously this weight increases: skeletal (43%), GRI-Mech 1.2 (66%), GRI-Mech 2.11 (68%), GRI-Mech 3.0 (71%).

		Case A			Case B		
Meth.	$Grid(n)$	CV	$Cpu_{it}(s)$	Sp_{it}	CV	$Cpu_{it}(s)$	Sp_{it}
S	4	3584	1.96	1.0	11136	6.60	1.00
	8	14336	8.09	1.0	44544	26.89	1.00
	16	57344	35.7	1.0	178176	111.49	1.00
M12	4	4992	0.25	7.8	16240	0.84	7.86
	8	17152	0.84	8.8	54752	2.85	9.43
	16	62976	3.28	9.7	198592	10.29	10.8

Table 4.1: Computational features comparison. Single block vs Multiblock (12 blocks) discretization.

This aspect is specially important to point out the appropriateness of the proposed algorithm for loosely coupled computers. As the chemistry calculations are carried out locally for each control volume decoupled from the rest of the domain, they don't need to transfer information among the different processors during its computation. Furthermore, as more strong is the computational weight of the chemistry, lower is the computational weight of momentum, energy and convection-diffusion species mass fractions, and consequently the communication work to update the interpolation boundary conditions for the convection-diffusion discretized equations. In figure 4.6.a, speed-ups for the case A taking into account different chemical models are plotted. Higher speed-ups are obtained when the complexity of the chemical model is increased.

4.5.3 Verification of the numerical solutions

The appropriateness of the proposed algorithms would not be demonstrated without a proper verification of the numerical solutions obtained. Two verification studies have been carried out using the procedure described in section 4.3.3. The first study focuses on assuring that the use of the multiblock technique does not introduce additional uncertainty in the numerical solutions. The second study looks into the suitable numerical parameters that account for the discretization (grids and numerical schemes).

Global uncertainty estimates have been chosen for reporting in a compact manner the results of the verification process. Nevertheless, and as an example, local estimates obtained in the case A are shown in figure 4.7. They correspond to the analysis of the temperature field and to the level of refinement $n = 16$. Given are the non-dimensional contours $T^* = T/T_{in}$, the post-processing grid $n = 4$, the estimated order of accuracy $p(\mathbf{x})$ and the uncertainty due to discretization $GCI^*(\mathbf{x})$. The zones where it has not been possible to apply the post-processing procedure, non Richardson nodes, are

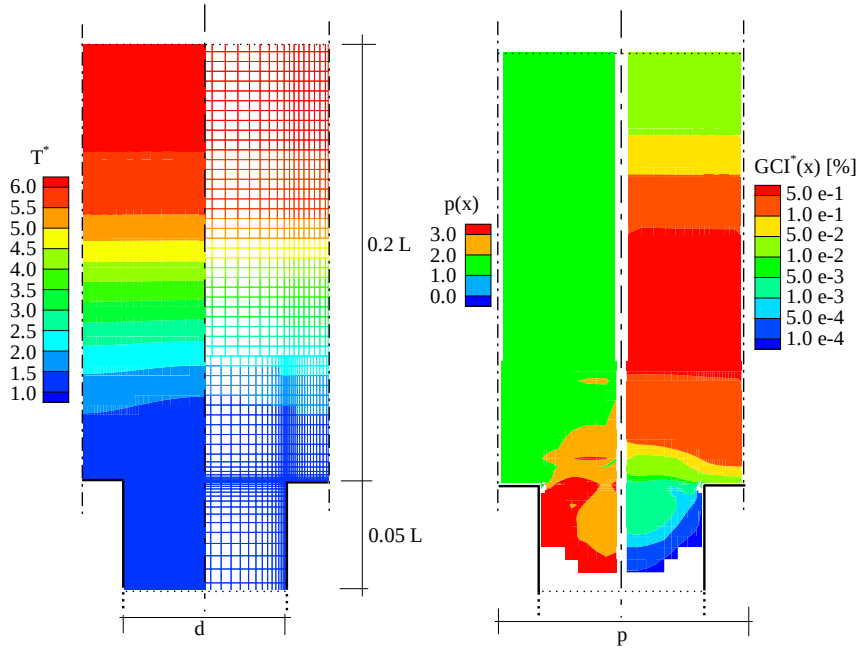

Figure 4.7: Uncertainty estimation studies on Case A: Premixed flame. Skeletal mechanism. Narrow flame (d=0.03 cm). Optimized Multiblock discretization (OM7, grid n=16). Left: Mesh and isocountours of non-dimensional temperature (T^*). Right: estimated order of accuracy, p($\mathbf{x}$), and non-dimensional Grid Convergence Index ,$GCI^*(\mathbf{x})$.

Meth.	$Grid(n)$	T_{max} [K]	sto^*	GCI^*[%]		
				V^*	T^*	Y_{CO_2}
S	4	2080.74	0.125	1.1	$7.4\text{x}10^{-1}$	$1.9\text{x}10^{-2}$
	8	2080.62	0.124	$2.7\text{x}10^{-1}$	$2.7\text{x}10^{-1}$	$6.6\text{x}10^{-3}$
	16	2080.59	0.123	$7.0\text{x}10^{-2}$	$7.0\text{x}10^{-2}$	$1.4\text{x}10^{-3}$
M12	4	2080.72	0.125	$9.3\text{x}10^{-1}$	$7.0\text{x}10^{-1}$	$2.1\text{x}10^{-2}$
	8	2080.59	0.124	$2.3\text{x}10^{-1}$	$3.7\text{x}10^{-1}$	$6.5\text{x}10^{-3}$
	16	2080.54	0.123	$1.2\text{x}10^{-1}$	$5.0\text{x}10^{-2}$	$3.0\text{x}10^{-3}$

Table 4.2: Accuracy of the numerical solutions. Single block vs Multiblock (12 blocks) comparison. Case A: Premixed flame. Skeletal mechanism. Narrow flame (d=0.03 cm).

blanked (see section 4.3.3 for details).

As shown, the local observed order of accuracy $p(\mathbf{x})$ has a mostly average value of 2, increasing this value near the burner walls. These results agree with the theoretical order of accuracy of the numerical schemes used (i.e. between 1 and 3 for the convective fluxes due to the use of SMART scheme, and 2 for diffusive fluxes due to the employment of Central differences).

$GCI^*(\mathbf{x})$ maps give in detail the local estimates of the uncertainty due to discretization. As it is shown, the higher computational uncertainties appears at the flame front. For the higher level of discretization, they do not exceed a 0.5% of the temperature's non-dimensional value. These kind of maps are very useful when analyzing the problem to be solved, giving criteria to the code user about how and where the grid has to be intensified so as to improve the quality of the numerical solution. As an example, we have observed that if the zones near the burner are discretized with an insufficient number of grid nodes, a phenomena of error transport occurs increasing notably the uncertainty in the flame front. This fact points out the importance of error estimation procedures.

In Table 4.2, summarized results are given for the premixed flame (case A). Single block and multiblock discretizations are compared. Estimates are given for the last three levels of refinement: $n = 4$, 8 and 16. Average values of the GCI^* for the non-dimensional temperature $T^* = T/T_{in}$, non-dimensional axial velocity $V^* = V/V_{in}$ and carbon dioxide mass fraction Y_{CO_2}, are shown. Estimates are given together with two global flame properties: the maximum temperature at the axis T_{max}, and the normalized stand-off distance sto^* (distance above the burner with the maximum heat release normalized by the computational length L).

The obtained results assess in a detailed manner the accuracy of the numerical

Meth.	$Grid(n)$	T_{max} $[K]$	H_f $[cm]$	$GCI^*[\%]$		
				V^*	T^*	Y_{CO_2}
S	4	2095.24	5.69	$6.0\text{x}10^{-1}$	$1.6\text{x}10^{-1}$	$2.5\text{x}10^{-3}$
	8	2096.87	5.48	$1.9\text{x}10^{-1}$	$3.3\text{x}10^{-2}$	$7.2\text{x}10^{-4}$
	16	2097.29	5.51	$7.6\text{x}10^{-2}$	$9.1\text{x}10^{-3}$	$1.9\text{x}10^{-4}$
M12	4	2095.24	5.69	$7.8\text{x}10^{-1}$	$1.6\text{x}10^{-1}$	$2.5\text{x}10^{-3}$
	8	2096.87	5.48	$1.5\text{x}10^{-1}$	$6.4\text{x}10^{-2}$	$1.3\text{x}10^{-3}$
	16	2097.28	5.51	$8.8\text{x}10^{-2}$	$1.4\text{x}10^{-2}$	$2.5\text{x}10^{-4}$

Table 4.3: Accuracy of the numerical solutions. Single block vs Multiblock (12 blocks) comparison Case B: Non-premixed flame. Skeletal mechanism.

solutions. Few discrepancies are observed in the maximum temperature and in the stand-off distance. Single and multiblock discretizations have a similar performance when the level of refinement n is increased. The uncertainty is reduced approximately by a factor of 4 for each level of refinement. Although some discrepancies appear on the GCI^*, they estimate in a similar manner the uncertainty due to discretization.

Similar results are obtained for the non-premixed flame (case B). In Table 4.3, the maximum temperature along the burner's axis T_{max}, and the flame height H_f, are given together with some illustrative uncertainty estimates. Irrelevant differences appear in the maximum temperature and flame height. Once again, the order of magnitude of GCI^* values assess the appropriateness of the multiblock discretizations.

4.5.4 Optimized discretizations

The domain decomposition method, besides offering a straight forward parallelization strategy, allows the employment of different mesh densities for the different resulting subdomains. This is specially interesting in our test cases, where the higher gradients are located in the flame fronts. Taking advantage of both attributes, computationally optimized discretizations are presented in this section.

The considered strategy focuses the attention on keeping the same level of refinement and the number of processors to solve the higher gradients regions, and on reducing the number of grid nodes in regions with smooth gradients. Consequently, these latter regions can be solved with less processors optimizing the computational resources. In figures 4.8 and 4.9, single block and optimized multiblock discretizations are shown. As can be seen, for the premixed flame (case A), the spatial distribution of the grid nodes is increased near the burner walls and at the flame front. On the other hand, for the non-premixed flame, the mesh is specially intensified at the entrance,

involving the higher gradients of methane and at the basis of the flame front (zone where fuel and oxidizer get in contact). These optimized discretizations have been selected with the aid of the verification process. Illustrative temperature contours for both discretizations are shown.

		Case A			Case B		
Meth.	$Grid(n)$	CV	Cpu_{it} $[s]$	Sp_{it}	CV	Cpu_{it} $[s]$	Sp_{it}
OM	4	2944	0.26	8.1	10888	0.82	8.08
	8	10496	1.00	9.5	38160	2.87	9.35
	16	39424	3.78	10.5	141856	10.99	10.1

Table 4.4: Parallel computational features. Optimized Multiblock discretization. Case A, 7 blocks. Case B, 8 blocks.

In table 4.4, the computational requirements and parallel performance for the optimized multiblock (OM) discretizations are summarized. The computational time savings when 12 processors are used are similar to those when less processors are employed with optimized multiblock (7 for the case A and 8 for the case B). For both flames, the employment of the parallel multiblock algorithms allows the reduction of approximately 10 times the CPU time respect the single block discretization when a level of refinement in terms of the grid parameter n is set to 16.

Another aspect that is interesting to point out is related to the RAM memory requirements. One of the properties of the employment of Newton-like methods, is the considerable amount of memory needs due to the Jacobian definition [2]. This is not the bottleneck in segregated methods, even though when complex kinetic mechanisms are considered. This property becomes more irrelevant when the proposed parallel multiblock algorithm is used. The assignment of the computational work to different processors allows the total memory requirements to be shared among them. In this way, for the finer mesh discretizations presented in this work, the memory requirements for each processor have not exceeded 150 Mb.

Tables 4.5 and 4.6, summarized post-processing results are given for both selected flames. As can be seen, the estimated uncertainty due to discretization of the numerical solutions have the same order of magnitude that those using single block or multiblock discretizations (see tables 4.2 and 4.3). Global flame values, practically do not differ.

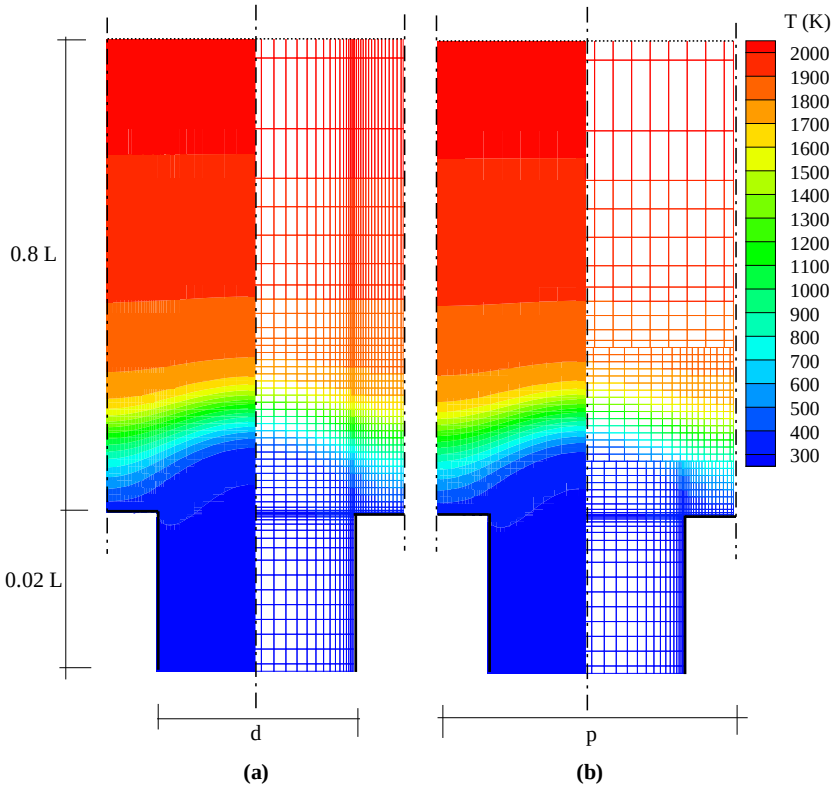

Figure 4.8: Case A: Premixed flame. Wide flame (d=0.10 cm). Skeletal mechanism. Level of refinement $n = 2$. Isotherms and computational grid. Left: Single block discretization (S). Right: Optimized Multiblock discretization (OM7).

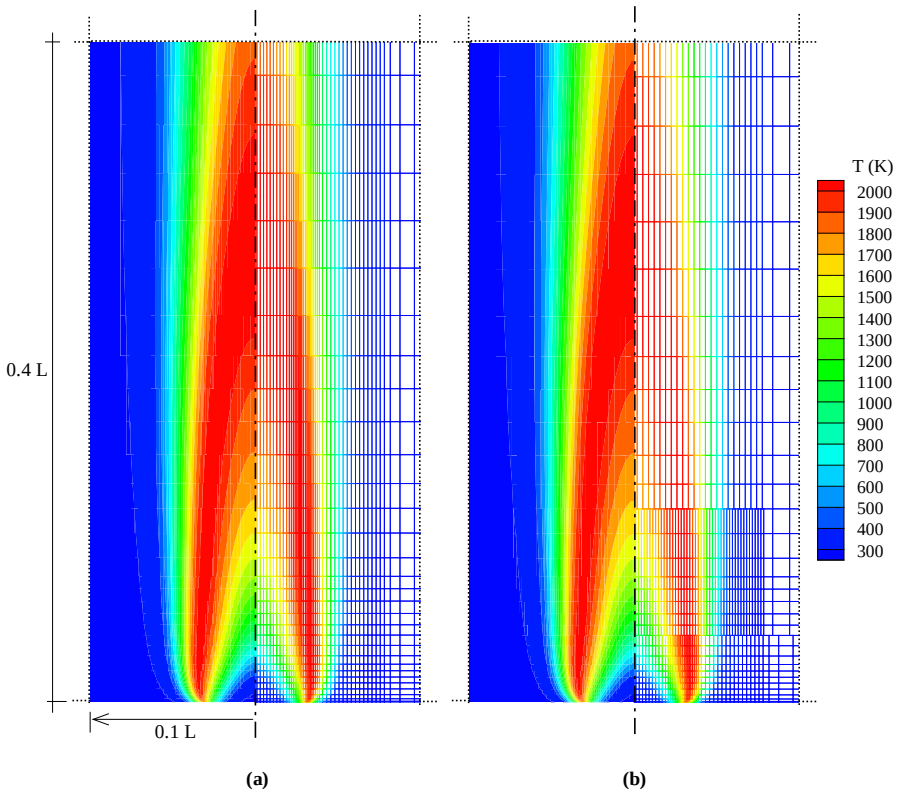

Figure 4.9: Case B: Non-premixed flame. Skeletal mechanism. Level of refinement $n = 2$. Isotherms and computational grid. Left: Single block discretization (S). Right: Optimized multiblock discretization (OM8).

Meth.	$Grid(n)$	T_{max} $[K]$	sto^*	$GCI^*[\%]$		
				V^*	T^*	Y_{CO_2}
OM7	4	2080.74	0.125	1.0	$6.7\text{x}10^{-1}$	$2.0\text{x}10^{-2}$
	8	2080.60	0.124	$3.0\text{x}10^{-1}$	$3.3\text{x}10^{-1}$	$5.6\text{x}10^{-3}$
	16	2080.59	0.123	$1.1\text{x}10^{-1}$	$8.0\text{x}10^{-2}$	$2.9\text{x}10^{-3}$

Table 4.5: Accuracy of the numerical solutions. Optimized Multiblock discretization (7 blocks). Case A: Premixed flame.Skeletal mechanism. Narrow flame (d=0.03 cm).

Meth.	$Grid(n)$	T_{max} $[K]$	H_f $[cm]$	$GCI^*[\%]$		
				V^*	T^*	Y_{CO_2}
OM8	4	2095.21	5.69	$9.5\text{x}10^{-1}$	$2.9\text{x}10^{-1}$	$4.9\text{x}10^{-3}$
	8	2097.08	5.48	$3.2\text{x}10^{-1}$	$7.1\text{x}10^{-2}$	$1.4\text{x}10^{-3}$
	16	2097.55	5.51	$9.2\text{x}10^{-2}$	$1.3\text{x}10^{-2}$	$3.2\text{x}10^{-4}$

Table 4.6: Accuracy of the numerical solutions. Optimized Multiblock discretization (8 blocks). Case B: Non-premixed flame. Skeletal mechanism.

4.5.5 Computational costs and uncertainty estimates for different chemical models

Finally, and in order to point out the numerical possibilities of the presented parallel algorithm, computational costs using optimized multiblock discretizations are given for both flames using different chemical models.

Table 4.7 summarizes the results obtained with the premixed flame problem (case A). Taking into account that in an average way 3000 outer iterations are needed to converge the iterative procedure, we would like to point out the acceptable CPU time consumed to obtain the solution considering 10.496 CVs ($n = 8$) and the GRI-Mech 3.0. As it is shown, with less of 10 hours, the code's users obtains a numerical solution with an acceptable averaged accuracy. For the same discretization, 40 minutes are sufficient to converge the simulation using the skeletal mechanism.

Table 4.8 presents the results obtained with the non-premixed flame problem (case B). Due to the bigger computational domain, wider special scales have to be treated (the size of the computational domain is approximately some thousand times the size of the flame front). This fact, obliges a considerable fine discretization specially at the flame's basis (near the bottom boundary), where higher methane mass fraction gradients are involved. Using the last version of GRI mechanisms and considering

Mechanism	$Grid(n)$	CV	Cpu_{it} $[s]$	GCI^*[%]		
				V^*	T^*	Y_{CO_2}
Single-step	4	2944	0.08	1.1	$3.0\text{x}10^{-1}$	$1.1\text{x}10^{-2}$
	8	10496	0.30	$1.1\text{x}10^{-1}$	$8.0\text{x}10^{-2}$	$1.9\text{x}10^{-3}$
	16	39424	1.21	$8.0\text{x}10^{-2}$	$3.7\text{x}10^{-2}$	$1.3\text{x}10^{-3}$
Four-step	4	2944	0.14	$8.6\text{x}10^{-1}$	$5.4\text{x}10^{-1}$	$9.6\text{x}10^{-3}$
	8	10496	0.49	$1.6\text{x}10^{-1}$	$1.4\text{x}10^{-1}$	$2.9\text{x}10^{-3}$
	16	39424	1.91	$6.7\text{x}10^{-2}$	$3.1\text{x}10^{-2}$	$3.8\text{x}10^{-4}$
Skeletal	4	2944	0.23	$9.3\text{x}10^{-1}$	$6.7\text{x}10^{-1}$	$2.0\text{x}10^{-2}$
	8	10496	0.80	$2.3\text{x}10^{-1}$	$2.9\text{x}10^{-1}$	$5.6\text{x}10^{-3}$
	16	39424	2.92	$1.2\text{x}10^{-1}$	$1.0\text{x}10^{-1}$	$2.9\text{x}10^{-3}$
GRI-Mech 1.2	4	2944	1.07	$8.0\text{x}10^{-1}$	$3.2\text{x}10^{-1}$	$3.6\text{x}10^{-3}$
	8	10496	3.64	$1.4\text{x}10^{-1}$	$7.0\text{x}10^{-2}$	$1.2\text{x}10^{-3}$
	16	39424	13.6	$4.5\text{x}10^{-2}$	$2.0\text{x}10^{-2}$	$1.4\text{x}10^{-4}$
GRI-Mech 2.11	4	2944	2.82	$8.0\text{x}10^{-1}$	$3.3\text{x}10^{-1}$	$3.5\text{x}10^{-3}$
	8	10496	9.46	$1.1\text{x}10^{-1}$	$7.0\text{x}10^{-2}$	$1.2\text{x}10^{-3}$
	16	39424	35.7	$4.0\text{x}10^{-2}$	$1.7\text{x}10^{-2}$	$2.2\text{x}10^{-4}$
GRI-Mech 3.0	4	2944	3.46	$7.2\text{x}10^{-1}$	$3.0\text{x}10^{-1}$	$5.2\text{x}10^{-3}$
	8	10496	11.5	$1.1\text{x}10^{-1}$	$1.4\text{x}10^{-1}$	$1.5\text{x}10^{-3}$
	16	39424	42.5	$3.6\text{x}10^{-2}$	$1.8\text{x}10^{-2}$	$5.7\text{x}10^{-4}$

Table 4.7: Computational costs and accuracy estimates. Optimized multiblock discretization (7 blocks). Case A: Premixed flame. Narrow flame (d=0.03 cm).

Mechanism	$Grid(n)$	CV	Cpu_{it} [s]	GCI^*[%]		
				V^*	T^*	Y_{CO_2}
Flame-Sheet	4	10888	0.148	1.1	$4.0\text{x}10^{-1}$	$8.7\text{x}10^{-3}$
	8	38160	0.520	$3.9\text{x}10^{-1}$	$7.7\text{x}10^{-2}$	$1.3\text{x}10^{-3}$
	16	141856	1.956	$6.5\text{x}10^{-2}$	$1.2\text{x}10^{-2}$	$2.1\text{x}10^{-4}$
Skeletal	4	10888	0.817	$9.5\text{x}10^{-1}$	$2.9\text{x}10^{-1}$	$4.9\text{x}10^{-3}$
	8	38160	2.875	$3.2\text{x}10^{-1}$	$7.0\text{x}10^{-2}$	$1.4\text{x}10^{-3}$
	16	141856	10.99	$9.2\text{x}10^{-1}$	$1.3\text{x}10^{-2}$	$3.2\text{x}10^{-4}$
GRI-Mech 1.2	4	10888	3.519	1.16	$3.4\text{x}10^{-1}$	$5.5\text{x}10^{-3}$
	8	38160	12.15	$2.6\text{x}10^{-1}$	$6.4\text{x}10^{-2}$	$1.8\text{x}10^{-3}$
	16	141856	46.40	$1.0\text{x}10^{-1}$	$1.6\text{x}10^{-2}$	$2.4\text{x}10^{-4}$
GRI-Mech 2.11	4	10888	9.158	1.16	$3.7\text{x}10^{-1}$	$5.9\text{x}10^{-3}$
	8	38160	31.83	$2.8\text{x}10^{-1}$	$6.4\text{x}10^{-2}$	$1.9\text{x}10^{-3}$
	16	141856	119.9	$1.0\text{x}10^{-1}$	$1.6\text{x}10^{-2}$	$2.4\text{x}10^{-4}$
GRI-Mech 3.0	4	10888	11.12	$9.5\text{x}10^{-1}$	$2.9\text{x}10^{-1}$	$5.0\text{x}10^{-3}$
	8	38160	38.57	$3.0\text{x}10^{-1}$	$6.7\text{x}10^{-2}$	$1.8\text{x}10^{-3}$
	16	141856	146.1	$9.9\text{x}10^{-2}$	$1.4\text{x}10^{-2}$	$2.5\text{x}10^{-4}$

Table 4.8: Computational costs and accuracy estimates. Optimized multiblock discretization (8 blocks). Case B: Confined co-flow non-premixed methane/air laminar flame.

38.160 CVs, 32 hours are needed to get with a converged solution. The GCI average values for the given variables shown the appropriate level of refinement. Nevertheless, considering a lower level of refinement ($n = 4$), approximately 10 hours are needed to achieve a converged solution with an acceptable accuracy.

The numerical results obtained for both flames, agree with the expected ones. Taking into account reference CPU costs for laminar flames given in the bibliography, the employment of the presented parallel algorithm represents a considerable improvement.

4.6 Conclusions

A parallel algorithm for the detailed multidimensional numerical simulation of laminar flames, able to work efficiently with loosely coupled computers, has been presented. The main characteristics of the algorithm have been explained pointing out the treatment of the stiffness of the governing equations, the domain decomposition method, the parallelization strategy, and the methodology employed for the verification of the obtained numerical results.

The main expected attributes of the proposed parallel algorithm have been successfully achieved. Speed-ups of approximately 10 with 12 CPUs have been obtained for the most significant situations. These savings are maintained with less resources (number of processors) when optimized locally refined multiblock discretizations are employed (7 and 8 processors for the premixed and non-premixed flames respectively). The computational costs for the resolution of the most complex chemical models have been reduced notably.

All the computations have been submitted to a verification process to estimate the accuracy of the numerical solutions. The appropriateness of the discretizations and the numerical schemes employed have been assessed. The computational effort of the presented results are directly related to its quality (uncertainty due to discretization).

This work presents an attractive option to improve the computational performance of existing segregate algorithms for solving laminar combustion problems, allowing the feasible resolution of such complex phenomena with detailed chemical models and with modest computational resources (loosely coupled parallel computers in PC clusters).

References

[1] L.M.T. Sommers and L.P.H. De Goey. A numerical study of a premixed flame on a slit burner. *Combustion Science and Technology*, 108:121–132, 1995.

[2] B.A. Bennett, C.S. McEnally, L.D. Pfefferle, and M.D. Smooke. Local rectangular refinement with application to axisymmetric laminar flames. *Combustion Theory and Modelling*, 2:221–258, 1998.

[3] M.D. Smooke, Y. Xu, R.M. Zurn, J.H. Frank, and M.B. Long. Computational and experimental study of OH and CH radicals in axisymmetric laminar diffusion flame. In *Proceedings of the Twenty-Fourth Symposium (International) on Combustion*, pages 813–821, 1992.

[4] R. Becker, M. Braack, and R. Rannacher. Numerical simulation of laminar flames at low mach number by adaptive finite elements. *Combustion Theory and Modelling*, 3:503–534, 1999.

[5] V.R. Katta and W.M. Roquemore. Simulation of dynamic methane jet diffusion flames using finite rate chemistry models. *AIAA Journal*, 36(11):2044–2054, 1998.

[6] M. Soria. *Parallel multigrid algorithms for computational fluid dynamics and heat transfer*. PhD thesis, Universitat Politècnica de Catalunya, 2000.

[7] R. Cònsul, C.D. Pérez-Segarra, and A. Oliva. Numerical studies on laminar premixed and diffusion flames. In *Proceedings of the 10th Conference on Numerical Methods in Thermal Problems*, pages 198–209, 1997.

[8] R.J. Kee, J.A. Miller, and T.H. Jefferson. Chemkin: a general-purpose, problem-independent, transient, fortran chemical kinetics code package. Technical report, Sandia National Laboratories, 1989.

[9] M.D. Smooke, R.E. Mitchell, and D.E. Keyes. Numerical solution of two-dimensional axisymmetric laminar diffusion flames. *Combustion Science and Technology*, 67:85–122, 1989.

[10] J.A. Miller and R.J. Kee. Chemical nonequilibrium effects in hydrogen-air laminar jet diffusion flames. *AIAA Journal*, 81(25):2534–2542, 1977.

[11] R.J. Kee and J.A. Miller. A split-operator, finite-difference solution for axissymmetric laminar-jet diffusion flames. *AIAA Journal*, 16(2):169–176, 1978.

[12] J.P. Jesse, R.F. Gansman, and W.A. Fiveland. Calculation of chemically reacting flows using finite kinetics. *Heat Transfer in Fire and Combustion Systems*, 250:43–53, 1993.

[13] J.B. Vos. Calculating turbulent reating flows using finite chemical kinetics. *AIAA Journal*, 25(10):1365–1372, 1986.

[14] P.J. Coelho and J.C.F. Pereira. Calculation of a confined axisymmetric laminar flame using grid refinement technique. *Combustion Science and Technology*, 92:243–264, 1993.

[15] R. Cònsul, C.D. Pérez-Segarra, J. Cadafalch, M. Soria, and A. Oliva. Numerical analysis of laminar flames using the domain decomposition method. In *Proceedings of the Fourth European Computational Fluid Dynamics Conference (ECCOMAS CFD)*, volume 1.2, pages 996–1001, 1998.

[16] L.M.T. Somers. *The simulation of flat flames with detailed and reduced chemical models*. PhD thesis, Technical University of Eindhoven, 1994.

[17] J. Cadafalch, A. Oliva, C.D. Pérez-Segarra, M. Costa, and J. Salom. Comparative study of conservative and nonconservative interpolation schemes for the domain decomposition method on laminar incompressible flows. *Numerical Heat Transfer, Part B*, 35(1):65–84, 1999.

[18] J. Cadafalch, C.D. Pérez-Segarra, R. Cònsul, and A. Oliva. Verification of finite volume computations on steady state fluid flow and heat transfer. *Journal of Fluids Engineering*, 124:11–21, 2002.

[19] P.J. Roache. Perspective: a method for uniform reporting of grid refinement studies. *Journal of Fluids Engineering*, 116:405–413, 1994.

[20] W.P. Jones and R.P. Lindstedt. Global reaction schemes for hydrocarbon combustion. *Combustion and Flame*, 73:233–249, 1988.

[21] R.E. Mitchell, Sarofim, and L.A. Clomburg. Experimental and numerical investigation of confined laminar diffusion flames. *Combustion and Flame*, 37:227–244, 1980.

[22] H.C. Lange and L.P.H. De Goey. Two-dimensional methane/air flames. *Combustion Science and Technology*, 92:423–427, 1993.

[23] B.A. Bennett, C.S. McEnally, L.D. Pfefferle, and M.D. Smooke. Computational and experimental study of axissymmetric coflow partially premixed methane/air flames. *Combustion and Flame*, 123:522–546, 2000.

[24] R.J. Kee, G. Dixon-Lewis, J. Warnatz, M.E. Coltrin, and J.A Miller. A fortran computer code package for the evaluation of gas-phase multi-component transport properties. Technical report, Sandia National Laboratories, 1986.

[25] C.T. Bowman, R.K. Hanson, Davidson, W.C. Gardiner, V.V. Lissianski, G.P. Smith, D.M. Golden, H. Wang, and M. Goldenberg. Gri-Mech 2.11, http://www.me.berkeley.edu/gri_mech/.

[26] G.P. Smith, D.M. Golden, M. Frenklach, N.W. Moriarty, B. Eiteneer, M. Goldenberg, C.T. Bowman, R.K. Hanson, S. Song, W.C. Gardiner, V.V. Lissianski, and Z. Qin. Gri-Mech 3.0, http://www.me.berkeley.edu/gri_mech/.

[27] P.H. Gaskell and A.K.C. Lau. Curvature-compensed convective transport: SMART, a new boundedness-preserving transport algorithm. *International Journal for Numerical Methods in Fluids*, 8:617–641, 1988.

[28] S.V. Patankar. *Numerical heat transfer and fluid flow.* Hemiosphere Publishing Corporation, 1980.

[29] B.R. Hutchinson and G.D.Raithby. A multigrid method based on the additive correction strategy. *Numerical Heat Transfer, Part B*, 9:511–537, 1986.

[30] O. Holm-Chistensen, I.P. Jones, N.S. Wilkes, B.A. Splawski, P.J. Stopford, B. Creemers, C.J.A. Pulles, and D.F. Fletcher. The solution of coupled flow and chemistry problems. *Progress in Computational Fluid Dynamics*, 1:43–49, 2001.

[31] P.H. Gaskell et al. Comparison of two solution strategies for use with higher-order discretization schemes in fluid flow simulation. *International Journal for Numerical Methods in Fluids*, 8:1203–1215, 1988.

[32] M. Soria, J. Cadafalch, R. Còsul, K. Claramunt, and A. Oliva. A parallel algorithm for the detailed numerical simulation of reactive flows. In *Proceedings of the 1999 Parallel Computational Fluid Dynamics Conference*, pages 389–396, 1999.

[33] J. Cadafalch, C.D. Pérez-Segarra, M. Sòria, and A. Oliva. Fully conservative multiblock method for the resolution of turbulent incompressible flows. In *Proceedings of the Fourth European Computational Fluid Dynamics Conference (ECCOMAS CFD)*, volume 1.2, pages 1234–1239, 1998.

[34] C.D. Pérez-Segarra, A. Oliva, M. Costa, and F. Escanes. Numerical experiments in turbulent natural and mixed convection in internal flows. *International Journal for Numerical Methods for Heat and Fluid Flow*, 5(1):13–33, 1995.

[35] C.S. McEnally and L.D. Pfefferle. Aromatic and linear hydrocarbon concentration measurements in a non-premixed flame. *Combustion Science and Technology*, 116–117:183–209, 1996.

Chapter 5

Numerical Analysis of Co-flow Methane/air Laminar Flames: Mathematical Modeling and Fundamental Studies

The goal of this chapter is to analyze, by means of detailed numerical simulations, fundamental aspects of co-flow partially premixed methane-air laminar flames, and the adequacy of several mathematical approaches employed on their modelization. The performance of different chemical mechanisms, radiation and mass transport models, are analyzed for five levels of premixing. Main flame properties are provided giving special emphasis to the analysis of pollutant formation. Results are compared with available experimental data, giving special emphasis to adjust experimental conditions by suitable boundary conditions. Finite volume technique over staggered grids is used to discretize governing equations. A parallel multiblock algorithm based on domain decomposition techniques running with loosely coupled computers has been used obtaining a competitive ratio between computational cost and resources. Numerical results presented in this paper, have been submitted to a verification process based on the generalized Richardson extrapolation and on the Grid Convergence Index (GCI).

5.1 Introduction

Deep knowledge of combustion phenomenon is of great scientific and technological interest due to its presence not only in nature but also in a wide range of industrial processes and equipment. Being the most important worldwide energy support provided by combustion of fossil fuels, the goal of developing more efficient and cleaner

systems or equipment is clearly justified. In the last decade, the importance of the reduction of pollutant emissions has increased considerably due to both environmental consciousness and to governmental policies, being one of the most important aspects to assure the competitiveness of combustion-related industries.

Traditionally, a high number of experimental studies based on trial-and-error analysis were needed to be done on the optimization of thermal equipment, where heat and mass transfer and fluid flow have a dominant role. In the last decades, in agreement with the development of computational capabilities, CFD simulations have become a worthful complement to experimental investigations, reducing in this sense production costs and time to market. However, the considerable complexity of combustion phenomena and the strong feedback between the flow and the chemistry, makes the task of development of accurate, computationally capable and robust numerical codes for combustion phenomena for industrial applications more difficult. This goal remains a promising challenge today and for the foreseeable future.

Although combustion nearly always takes place within a turbulence flow field to increase the mixing process and thereby enhance combustion [1], laminar flames are considered as an illustrative example of combustion phenomenon and their experimental and detailed numerical analysis is a basic ingredient on the modelization of turbulent combustion processes as well as for pollutant formation. Special attention has been given to co-flow non-premixed and partially premixed methane-air laminar flames. The wide application of these flames in house-hold and industrial heating systems due to both their intense combustion process and the relatively clean nature of natural gas (composed mainly by methane), has motivated extensive research on the experimental and numerical modelization of such flames.

First multidimensional simulations of co-flow methane-air flames were carried out by Mitchell et al [2], who analyzed non-premixed situation with two-dimensional governing equations assuming fast chemistry by means of the employment of a flame-sheet modelization. Numerical solutions were compared to experimental data. Detailed numerical simulations with complex transport and with detailed skeletal mechanisms for hydrogen-air flames appeared in the same decade [3][4]. However, these models neglected axial diffusion transport. Not was until the end of the eighties when Smooke et al [5] presented the first two-dimensional simulations of non-premixed co-flow methane-air flames with complex transport and detailed chemistry and with fully elliptic equations. The chemistry model considered 42 reactions and 15 species. Before this work, computational studies appeared in the literature restricted to one-dimensional configurations (i.e. burner-stabilized premixed flames and non-premixed counterflow flames) [6][7].

During the last decade, many authors focused their attention on these kind of flames and a considerable progress has been achieved. Together with the increase of the computational power and the accuracy of the experimental techniques, numerical

methods have been considerably improved [8][9][10]. Thus, both detailed experimental and numerical studies analyzing phenomenological properties of methane-air Bunsen flames have been appeared in the literature.

Experimental studies have provided measurements of temperature, major species, radicals, nitrogen oxides and soot. Mass spectrometry, Raman and LIF techniques have been employed to study co-flow flames under different geometric configurations, equivalence ratios, and pressure-conditions [8][11] [12][13].

Concerning to numerical studies, as computational power grows and numerical methods are improved, more detailed simulations have been carried out. The accuracy of the detailed mathematical models has been analyzed, comparing their results with those with simpler modelization and with experimental data. In these works, mainly C1 and C2 chemical mechanisms are employed and compared [14], molecular transport is modelized under different assumptions [15], soot formation is sometimes modeled [11], and radiation transfer, if considered, is evaluated with simplified models [10]. Usually, non-premixed or premixed flames are analyzed and just recently numerical simulations have also been performed on partially premixed flames for different equivalent ratios [12][16]. However, there is a lack in the literature of works where the relative importance of each phenomenological contribution could be analyzed.

The goal of the current chapter is to analyze the sensitivity of different modelization criteria based on the numerical simulation of partially premixed co-flow methane-air flames for a wide range of equivalence ratios.

Partially premixing is considered reproducing experimental and numerical studies of Bennet et al [16] for different equivalence ratios: from infinite (completely non-premixed) to 2.464 [16]. Both extremes are exhaustively studied. Special attention is given to reproduce experimental conditions by means of the selection of appropriate boundary conditions.

Different levels of chemical mechanism approaches are compared not only in the accuracy of the description of the thermal process and major species, but also in the pollutant species production. GRI-Mech release 3.0 is compared to previous releases (1.2 and 2.11), to a skeletal mechanism and to flame-sheet model. Mass molecular transport is also analyzed. Employing a mass averaged transport coefficients formulation, contribution of the Soret effect and the accuracy on the evaluation of species diffusivities are analyzed. The importance of radiant heat exchange has also been explored. Results considering the commonly employed optically-thin model are contrasted to results where radiation is neglected.

Model's comparison has been done both analyzing main flame characteristics (e.g. flame's height, temperatures, etc.) and local data (e.g. temperature and main species profiles). The chapter gives emphasis on the influence of the modelization criteria to NO_x formation.

To do so, numerical simulations have been performed using a parallel multiblock

algorithm running with loosely coupled computers. The governing equations have been discretized using the finite volume technique with fully implicit temporal differentiation, and cylindrical staggered grids. The discretized equations have been solved in a segregated manner, employing a pressure-based SIMPLE-like method to couple the velocity-pressure fields. The chemical terms are coupled by means of operator-splitting techniques. The domain decomposition technique is used to optimize the discretization and to parallelize the code, assigning one or several subdomains to different CPUs.

Numerical solutions are submitted to a verification process by means of a post-processing procedure [17], based on the Generalized Richardson extrapolation for h-refinement studies and on the Grid Convergence Index (GCI) proposed by Roache [18]. Estimates of the uncertainty due to discretization are evaluated in order to assess the accuracy of the numerical solutions, and in order to find the appropriate discretization parameters.

A *Beowulf cluster* composed by 48 standard PCs (AMD K7 CPU at 900 MHz and 512 Mbytes) with a conventional network, has been used to perform the numerical simulations. For an accurate enough discretization and for the most complex mechanism, converged solutions have been reached with less than 10 hours. The appropriate properties of the algorithm, and the relative low cost of PC clusters, make possible an exhaustive analysis of the flame with an excellent ratio between CPU time and resources.

5.2 Mathematical model

5.2.1 Governing equations

Assuming the mathematical formulation for Low-Mach number laminar flames exposed in section 2.4, the governing equations for a reactive gas (continuity, species, momentum, energy and state equation) can be written as follows [4]:

$$\frac{\partial \rho}{\partial t} + \nabla \cdot (\rho \vec{v}) = 0 \tag{5.1}$$

$$\frac{\partial (\rho Y_i)}{\partial t} + \nabla \cdot (\rho \vec{v} Y_i) = -\nabla \cdot \vec{j_i} + \dot{w}_i \tag{5.2}$$

$$\frac{\partial (\rho \vec{v})}{\partial t} + \nabla \cdot (\rho \vec{v} \vec{v}) = -\nabla p + \nabla \cdot \vec{\tau}^{\,T} + \rho \vec{g} \tag{5.3}$$

$$\frac{\partial (\rho h)}{\partial t} + \nabla \cdot (\rho \vec{v} h) = -\nabla \cdot \left(\vec{q}^{\,T} + \vec{q}^{\,R} \right) \tag{5.4}$$

[4] Even though the mathematical formulation has been presented in detail in chapter 2, a short review of the main aspects here considered have been included for clarity.

$$\rho = \frac{pM}{RT} \tag{5.5}$$

where t is time; ρ mass density; $\vec{v}$ average velocity of the mixture; $\vec{\tau}^{\,T}$ shear stress tensor; p pressure; $\vec{g}$ gravity; N total number of chemical species; h specific enthalpy of the mixture; $\dot{w}_i$ net rate of production of ith species; h_i specific enthalpy of ith species; M molecular weight of the mixture; $\vec{q}^{\,T}$ molecular heat flux; $\vec{q}^{\,R}$ radiant heat flux; Y_i mass fraction of ith species; $\vec{j_i}$ diffusion mass fluxes of ith species; and R gas universal constant.

The shear stress tensor is evaluated taking into account Stokes' law for Newtonian fluids, where μ is the mixture viscosity and $\vec{\delta}$ is the Kronecker Delta:

$$\vec{\tau}^{\,T} = \mu\left(\nabla\vec{v} + \nabla\vec{v}^{t}\right) - \frac{2}{3}\mu\nabla\cdot\vec{v}\vec{\delta} \tag{5.6}$$

Molecular heat flux considers Fourier's conduction and interdiffusional convection, where λ is the thermal conductivity of the mixture and T is the temperature:

$$\vec{q}^{\,T} = -\lambda\nabla T + \sum_{i=1}^{N} h_i\vec{j_i} \tag{5.7}$$

Enthalpy and temperature are related as,

$$h = \sum_{i=1}^{N} h_i Y_i = \sum_{i=1}^{N}\left(h_i^o + \int_{T^o}^{T} c_{p_i}dT\right)Y_i \tag{5.8}$$

where h_i^o is the standard heat of formation of ith species; c_{p_i} is the specific heat of ith species and T^o is the standard state temperature. Thermo-physical properties have been evaluated using the NASA thermodynamic data [19].

Mass fluxes of species are evaluated considering an equivalent Fickian diffusion process and thermal diffusion (Soret effect) [20]:

$$\vec{j_i} = -\rho\mathcal{D}_{im}\nabla Y_i - D_i^T\nabla\ln T \tag{5.9}$$

Pressure and forced diffusion contributions have been neglected. In equation 5.9, $\mathcal{D}_{im}$ and D_i^T are the multicomponent ordinary and thermal diffusion coefficients respectively.

5.2.2 Radiation model

Flame radiation is typically modeled using the assumption of optically thin transfer between the hot combustion gases and the cold surroundings. This assumption implies that each radiation point has an unimpeded isotropic view of the cold surroundings,

considered as a black body. The expected accuracy of this assumption has been shown to be quite reasonably [21], although according to [22] an over-prediction of both absorption in colder regions and emission in hotter regions is produced. The radiative heat loss term per unit of volume is expressed as:

$$\nabla \cdot \vec{q}^{\,R} = 4\sigma \left(T^4 - T_s^4\right) \sum_{i=1}^{N} \left(p_i \kappa_{P_i}\right) \tag{5.10}$$

where σ is Stefan-Boltzmann constant; T_b background temperature; p_i is the partial pressure of species i in atmospheres; κ_i is the Planck mean absorption coefficient for species i.

The summation term on the r.h.s of equation 5.10, accounts for the different radiating species present in hydrocarbon flames. The most important radiating species are CO_2, H_2O and, in less extension, CH_4 and CO.

Spectral absorption coefficient for each species is predicted using a narrow-band model, together with a combination of tabulated properties and theoretical approximations. From running RADCAL [23], Planck-mean absorption coefficients are obtained at different temperatures, which are fitted to polynomial expressions [21].

5.2.3 Chemical models

Three different levels of modelization have been considered for the treatment of the chemical reactions: i) full GRI-Mech mechanisms (releases 1.2, 2.11, 3.0) [19][24]; ii) skeletal mechanism [5], considering 15 species and 42 reactions; iii) irreversible single-step flame sheet model [2].

In the most general situation (finite rate chemistry), the evaluation of the net rate of production of each species, due to the N_r reactions, is obtained by summing up the individual contribution of each reaction:

$$\dot{w}_i = M_i \sum_{j=1}^{N_r} \left(\nu_{i,j}^{''} - \nu_{i,j}^{'}\right) \left[k_j^f \prod_{i=1}^{N} [X_i]^{\nu_{i,j}^{'}} - k_j^b \prod_{i=1}^{N} [X_i]^{\nu_{i,j}^{''}}\right] \tag{5.11}$$

Here, $[X_i]$ are the molar concentration, M_i the molecular weights of the species, $\nu_{i,j}^{'}$, $\nu_{i,j}^{''}$ the stoichiometric coefficients appearing as a reactant and as a product respectively for the ith species in the reaction j, and k_j^f, k_j^b the forward and backward rate constants.

5.2.4 Transport fluxes

Molecular fluxes of momentum $\vec{\tau}^{\,T}$, heat $\vec{q}^{\,T}$ and mass $\vec{j_i}$, have to be modeled requiring the introduction of transport coefficients. These coefficients are evaluated considering

a mixture-averaged formulation. Pure-species transport properties are evaluated using CHEMKIN's database.

For the mixture-averaged viscosity μ and thermal conductivity λ the semi-empirical formulas of Wilke (1950) and modified by Bird (1960) are used [20]. Mixture diffusion coefficients $\mathcal{D}_{im}$ that appear in equation 5.9 are calculated considering three possibilities:

- From *Stefan-Maxwell* equation and considering *trace-species* approximation [20]. Assuming that a given species see the rest moving with the same averaged velocity and when the mixture is composed by one majority species, the equivalent Fickian diffusion coefficient of one species into the mixture can be formulated as:
$$\mathcal{D}_{im} = \frac{1 - Y_i}{\sum_{\substack{j=1 \\ j \neq i}}^{N} X_j / \mathcal{D}_{ij}} \tag{5.12}$$
Here, $\mathcal{D}_{ij}$ are the binary diffusion coefficients.

- Consideration of a fixed Lewis number for each species, for instance: $Le_{CH_4} = 0.97$, $Le_{O_2} = 1.11$, $Le_{H_2} = 0.3$. Species $\mathcal{D}_{im}$ coefficients, are evaluated from their Lewis number value:
$$\mathcal{D}_{im} = \frac{k}{\rho Le_i c_{p_i}} \tag{5.13}$$
For major species, these fixed Lewis number are provided in the literature (see, for example [25]). For the fixed Lewis number not found in literature, they are obtained averaging the local Lewis values obtained from the numerical results performed with the previous approximation.

- Consideration of a unity Lewis number for all the species involved in the chemical model ($Le_i = 1.0$ $i = 1, 2, ...N$). This approximation is commonly used, for example, for the flamelet approach [26][27].

Thermal diffusion coefficients using calculated $\mathcal{D}_{im}$ values. This coefficient is related to the thermal diffusion ratio by:

$$D_i^T = \frac{\rho_i \mathcal{D}_{im}}{X_i} \Theta_i \tag{5.14}$$

where Θ_i is the thermal diffusion ratio of ith species and is given by:

$$\Theta_i = \sum_{j=1}^{N} \theta_{ij} X_i X_j \tag{5.15}$$

Here, θ_{ij} are the pairs of thermal diffusion ratios for light species into all other components of the mixture. These ratios are only given for chemical species with mass weights lower than $5 g/mol$.

5.3 Numerical Method

A brief review of the numerical methods is presented in this section. For more details see chapter 4. The governing equations have been discretized using the finite volume technique with fully implicit temporal differentiation for calculating steady or transitory compressible or incompressible flows, using rectangular or cylindrical staggered grids. Central differences have been employed for the evaluation of the diffusion terms, while third order schemes have been used for the evaluation of convection ones (SMART [28]). A SIMPLE-like algorithm has been considered in order to couple velocity-pressure fields. Discretized equations are solved in a segregated manner [29]. On the resolution of the linear equations system a multigrid solver has been employed [30].

On the resolution of species equations (eq. 5.2), and in order to overcome the stiffness of the governing equations, pseudo-time splitting technique is used. This technique splits each species equations into two steps: i) the convective-diffusion terms; ii) the chemical source terms [31]. The first step is solved in a segregated manner obtaining intermediate mass fractions (Y_i^*). The second step is solved in a coupled manner for all species and for each control volume using a Modified Damped Newton's method for stiff ordinary differential equations [25].

Energy equation (eq. 5.4) has been considered in terms of enthalpy transport. Usually, when this formulation is employed, a convection-diffusion equation for enthalpy transport is solved, and temperature is evaluated from enthalpy-temperature relationship (eq. 5.8) using, for example, a Newton's method [32]. Instead of following this procedure, a temperature convection-diffusion equation is considered, and the full enthalpy transport equation has been introduced in the source term by means of a deferred correction. In this way, the obtained temperature field satisfies the energy equation in terms of enthalpy (eq. 5.4). With this formulation, energy fluxes are directly evaluated with temperature and enthalpy nodal values by means of the employed numerical schemes and without any further numerical approach.

Domain decomposition method has been used as an strategy to reduce the number of grid nodes far from the flame fronts and as a parallelization technique. The whole domain is divided into several overlapped *subdomains* joined by the interpolation boundaries. The discretized governing equations are solved in each subdomain with the appropriate boundary conditions and the required grid (inner iteration). Once all blocks have been calculated, information of the interpolation boundaries is transferred among the different blocks in an explicit manner (outer iteration). If the parallel version of the code is used, this means that each CPU solve one (or a group) of subdomains and only one communication for each outer iteration is required.

Boundary conditions in the interpolation boundaries are calculated via procedures called *interpolation schemes*, which are responsible for the information transfer among subdomains [33]. For the Navier-Stokes equations, the entrance velocity is calculated

via local mass balances, and tangential velocity using local balances of the tangential momentum fluxes. This procedure has been proved to be suitable on laminar simply connected incompressible flows. For the scalar fields (Y_i and T) an asymptotically conservative scheme based on bi-quadratic Lagrangian interpolations is employed. This procedure has been used by the Group in previous works: in the simulation of incompressible flows [33], in the simulation of laminar flames [34] and in turbulent flows modeled with low-Reynolds number two-equation models [35]. When operator-splitting technique is used, the interpolated boundary conditions are considered for the intermediate species mass fractions (Y_i^*), while the species mass fractions (Y_i) are evaluated for each CV from the chemistry step.

5.4 Flame description

An axisymmetric, Bunsen-type, atmospheric-pressure, co-flowing partially premixed methane/air laminar flame has been analyzed. Two concentric tubes configurate the burner and a cylindrical chimney confines the flame. Methane mixed with sub-stoichiometric air is injected through the inner tube (primary inlet) while a stream of air injected through the outer tube (secondary inlet) surrounds it.

Many experimental and numerical studies have been carried out for these kind of flames in different physical configurations [2][5][9][36][10][37][38][11]. Our numerical studies have been performed considering the burner characteristics defined in [16]. Experimental apparatus and measurement techniques are extensively described in [13][11][37]. Hereafter, a briefly description is introduced.

5.4.1 Experimental set-up

Fuel mixed with primary air flows from an uncooled $r_i = 5.55$ mm inner radius brass tube with a wall thickness of $w_i = 0.8$ mm. Air is injected from the annular region between this tube and a concentric $r_o = 47.6$ mm inner radius brass cylinder. The outer tube thickness is of $w_o = 3.4$ mm. Fuel tube contains glass beads in order to smooth the flow, and their end is 110 mm from the lip to assure a fully developed velocity profile at the exit. A perforated brass plate, glass beads and finally a 1.5 mm cell-size ceramic honeycomb straighten the air flow. Inner tube extends 4 mm above the honeycomb surface to facilitate the access to the lowest flame regions. The cylindrical brass chimney that confines the flame and protects it from laboratory air movements has therefore a diameter of 102 mm.

Different levels of premixing of the primary inlet are considered from an equivalence ratio of $\Phi = \infty$ (non-premixed flame) to $\Phi = 2.464$. The lower limit was just before flashback began to affect the flame structure [37]. Equivalence ratios and mass flows are listed in table 5.1. Primary air is oxygen-enriched (25% O_2 by volume)

Φ	$\dot{m}_{CH_4}$ (g/min)	$\dot{m}_{air}$ (g/min)
Inner jet		
∞	0.2165031	0.0000000
12.320	0.2165031	0.2493036
6.160	0.2165031	0.4986071
4.107	0.2165031	0.7478500
2.464	0.2165031	1.2465180
Outer jet		
All	0.0000000	51.879520

Table 5.1: Flame parameters.

and secondary air is "regular" (20.9% O_2). A short explanation about experimental techniques and procedures used by the authors of these studies is given in order to have an order of magnitude of the uncertainties of the experimental results and to compare them with the numerical simulations performed in this chapter. Commercial high compressed-gas cylinders supply methane, and a mechanical compressor provides air. Flow rates are measured by rotameters. All experimental flow rates are estimated to be accurate to ±5%. Flame temperatures are measured with a 120 μm diameter type R (Pt-Pt/13%Rh) thermocouple-wire pairs. The uncoated thermocouple is stretched horizontally across the flame. These measurements have an absolute uncertainty of ±50 K, a relative uncertainty of ±10 K, and a spatial resolution of 0.3 mm [13][16]. Gas temperature measurements due to soot deposition-induced changes in the junction diameter and emissivity are about ±110 K at the flame location where the gas temperature is about 1550 K. Species concentrations are determined by extracting gas samples with a narrow-tipped quartz sample probe and analyzing them with mass spectrometry. Concentrations measurements of methane, acetylene, oxygen, water and carbon dioxide have absolute uncertainties of 30%. Measurements of formaldehyde and other higher hydrocarbons have relative uncertainties of 30% and absolute uncertainties up to a factor of three [37]. In order to calibrate species measurements, fuel and primary air mixtures are diluted with 1% of Argon in terms of the total volumetric flow rate of the fuel mixture [13].

5.4.2 Computational domain and boundary conditions

Even that, cylindrical brass chimney extends 250 to 370 mm above the honeycomb surface, a computational height of $L = 200\ mm$ has been considered according to numerical results presented in [16]. Computational domain is only defined in the

cylindrical chimney where the flame is confined ($z \geq 0$), methane and air flow within the inner and outer tubes have not been numerical simulated. See figure 5.1 for details.

Therefore, special attention have been paid for the inlet boundary conditions at $z = 0$ in order to relate their values with the known values at the bottom of the burner (section B in figure 5.1a). Species mass fractions are evaluated fixing the species mass flow rates and considering that no reaction occur inside the tube:

$$(\rho v_z Y_i)_B = \left(\rho v_z Y_i - \rho D_{im} \frac{\partial Y_i}{\partial z} - D_{im}^T \frac{\partial \ln T}{\partial z} \right)_{z=0} \tag{5.16}$$

For the energy equation, two possibilities have been considered and compared. The first one, and following a similar treatment, an enthalpy flux is evaluated at section B and assuming a temperature of $T_B = 298K$; then the temperature is estimated solving equation 5.17. The second possibility fixes inlet temperature of 298K at entrance of the computational domain ($z = 0$).

$$(\rho v_z h)_B = \left(\rho v_z h - \lambda \frac{\partial T}{\partial z} - \sum_{i=1}^{N} h_i \left(\rho D_{im} \frac{\partial Y_i}{\partial z} + D_{im}^T \frac{\partial \ln T}{\partial z} \right) \right)_{z=0} \tag{5.17}$$

Due to burner's configuration, radial component of the velocity has been neglected at the exit of both primary and secondary inlets. In order to take into account the considerable density gradients involved in the inlet region, because of the temperature and mass fractions gradients, axial velocity is calculated using the local density value and an assumed mass flow rate profile. A plug-flow profile has been considered at the secondary inlet, while for the primary one, a parabolic mass flow rate has been assumed.

The chimney has been assumed to be impermeable and chemically inert (material without any chemical activity), being the total flux of species normal to the wall equal to zero. A non-slip velocity boundary condition has been assumed. At the outlet of the burner, a pressure outflow boundary condition is imposed and a null gradient of the temperature and species is assumed.

The computational domain has been discretized using a cylindrical structured grid. Several zones with different grid nodes distributions are defined (figure 5.1b). The number of grid nodes is increased at the outlet of the inner tube where the gradients of methane are higher. As we move away from the bottom and from the flame front, the grid nodes density is progressively decreased by means of tanh-like functions. The parabolic structure of the flow suggested us to decompose the domain in eight subdomains in z-direction. The computational behavior of the parallel multiblock algorithm confirms it. The employment of the multiblock discretization, allows the definition of 3 macro zones characterized by having the same grid-nodes distribution in r-direction.

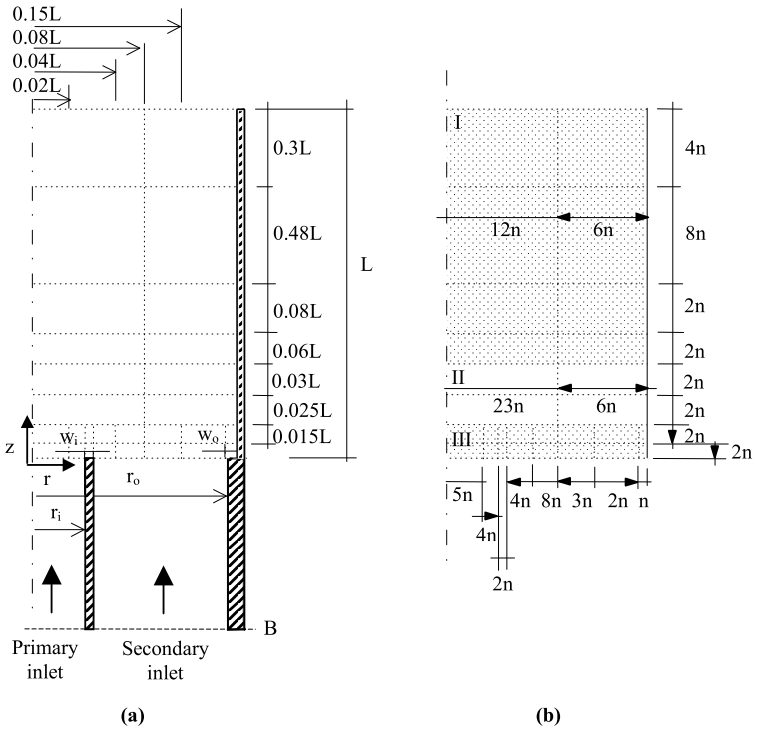

Figure 5.1: Confined co-flow methane/air laminar flame. (a) Burner idealized geometry and definition of the different zones for the non-equispaced cylindrical grid. (b) Definition of macro zones and their mesh nodes distribution.

The definition of these macro zones and the grid nodes distribution referred with the grid parameter n is shown in figure 5.1b. An h-refinement study is performed with five levels of refinement ($n = 1, 2, 4, 8$ and 16). For instance, for the finest discretization, 141.856 CV are employed.

5.5 Results

The influence of partially premixing in co-flow methane-air flames and the adequacy of different modelization criteria are presented. In these analysis, a highest level of modelization, hereafter referred as *reference model*, has been defined:

- GRI-Mech 3.0
- Detailed transport with diffusion coefficients calculated via equation 5.12 and with Soret effect
- Radiation included
- Special treatment of the boundary conditions by means of equation 5.17

Numerical results for the extreme premixing levels (i.e. $\Phi = \infty$ and $\Phi = 2.464$) have been submitted to a verification process based on a post-processing tool. This task not only has permitted to estimate the uncertainty due to the discretization for different levels of refinement, but also to select the appropriate grid nodes distribution. Obtaining an estimation for both premixing extremes, similar accuracy have been assumed for the intermediate levels of premixing.

Once verification studies are carried out, extreme premixing situations are deeply studied analyzing the consequences of the commented different modeling criteria: influence on the definition of boundary conditions, chemical approaches, molecular transport modelization and radiation. Finally, five levels of premixing are numerically simulated considering the reference model. Numerical results are compared to experimental data. Flame characteristics are analyzed and their most illustrative properties are described. Special emphasis is given to pollutant formation, CO and NO_x. The amount of pollutant produced is shown presenting axial and radial profiles, and evaluating emission indexes EI_x, defined as the fraction between the grams per second of pollutant species x and the kilograms per second of methane burned:

$$EI_x = 1000 \ \frac{g/s \ \ x}{g/s \ \ CH_4} \tag{5.18}$$

5.5.1 Verification of numerical solutions

A post-processing procedure [17], based on the generalized Richardson extrapolation for h-refinement studies and on the Grid Convergence Index (GCI) proposed by Roache [18], has been used in order to establish a criteria about the sensitivity of the simulation to the computational model parameters that account for the discretization: the mesh spacing and the order of accuracy. This tool estimates the order of accuracy of the numerical solution (observed order of accuracy p) and the error band where the grid independent solution is expected to be contained (uncertainty due to discretization GCI), also giving criteria about the credibility of these estimations.

The procedure processes three consecutive numerical solutions of the h-refinement studies. These solutions are interpolated at the post-processing grid, which in our case coincide with the coarsest mesh of the three numerical solutions considered. Thus, estimations are given for the numerical solutions obtained with the levels of

$\Phi = \infty$									
	$v_r^* = v_r/v_{in}$			$v_z^* = v_z/v_{in}$			$T^* = T/298$		
grid	Rn	p	GCI	Rn	p	GCI^*	Rn	p	GCI
$n_3/n_2/n_1$	[%]		[%]	[%]		[%]	[%]		[%]
1/2/4	81	2.0	$1.6\text{x}10^{-1}$	79	1.8	$1.2\text{x}10^{+0}$	74	1.6	$3.4\text{x}10^{-1}$
2/4/8	80	1.9	$4.6\text{x}10^{-2}$	91	1.8	$2.8\text{x}10^{-1}$	90	1.8	$6.0\text{x}10^{-2}$
4/8/16	87	1.9	$1.4\text{x}10^{-2}$	93	2.0	$4.6\text{x}10^{-2}$	90	2.1	$9.4\text{x}10^{-3}$
	Y_{CO}			Y_{NO}			Y_{NO_2}		
grid	Rn	p	GCI	Rn	p	GCI^*	Rn	p	GCI
$n_3/n_2/n_1$	[%]		[%]	[%]		[%]	[%]		[%]
1/2/4	68	1.5	$4.4\text{x}10^{-4}$	69	0.9	$9.2\text{x}10^{-5}$	77	2.3	$2.6\text{x}10^{-6}$
2/4/8	82	2.0	$1.0\text{x}10^{-4}$	96	1.5	$1.6\text{x}10^{-5}$	77	1.9	$1.2\text{x}10^{-6}$
4/8/16	92	1.9	$3.9\text{x}10^{-5}$	97	1.6	$6.0\text{x}10^{-6}$	75	1.6	$5.2\text{x}10^{-7}$
$\Phi = 2.464$									
	$v_r^* = v_r/v_{in}$			$v_z^* = v_z/v_{in}$			$T^* = T/298$		
grid	Rn	p	GCI	Rn	p	GCI	Rn	p	GCI
$n_3/n_2/n_1$	[%]		[%]	[%]		[%]	[%]		[%]
1/2/4	78	1.7	$3.5\text{x}10^{-1}$	80	1.7	$1.3\text{x}10^{+0}$	70	2.1	$1.6\text{x}10^{-1}$
2/4/8	65	2.0	$4.2\text{x}10^{-2}$	78	1.6	$3.7\text{x}10^{-1}$	70	2.1	$3.1\text{x}10^{-2}$
4/8/16	80	2.0	$1.1\text{x}10^{-2}$	82	2.1	$5.1\text{x}10^{-2}$	82	2.0	$7.7\text{x}10^{-3}$
	Y_{CO}			Y_{NO}			Y_{NO_2}		
grid	Rn	p	GCI	Rn	p	GCI	Rn	p	GCI
$n_3/n_2/n_1$	[%]		[%]	[%]		[%]	[%]		[%]
1/2/4	75	2.2	$4.7\text{x}10^{-4}$	42	1.7	$6.2\text{x}10^{-6}$	71	2.0	$1.4\text{x}10^{-6}$
2/4/8	74	1.3	$2.6\text{x}10^{-4}$	74	2.0	$1.7\text{x}10^{-6}$	69	1.2	$2.4\text{x}10^{-6}$
4/8/16	90	2.0	$2.8\text{x}10^{-5}$	80	2.2	$2.7\text{x}10^{-7}$	88	2.0	$2.9\text{x}10^{-7}$

Table 5.2: Verification studies. Post-processing results. (For table description see section 5.5.1.).

Φ	$Grid$ (n)	$Nodes$	$T_{max,C}$ $[K]$	Hf $[cm]$	EI_{CO} $[g/kg]$	EI_{NO} $[g/kg)$	EI_{NO_2} $[g/kg)$
∞	1	853	1888.80	5.82	0.41	3.01	0.48
	2	2652	1902.41	5.81	0.36	3.08	0.45
	4	10888	1908.37	5.86	0.33	3.18	0.45
	8	38160	1908.56	5.85	0.32	3.22	0.45
	16	141856	1908.51	5.84	0.32	3.24	0.45
2.464	1	853	2024.00	3.86	0.23	2.70	0.38
	2	2652	2030.28	4.01	0.23	2.68	0.37
	4	10888	2032.55	4.01	0.22	2.69	0.37
	8	38160	2033.59	3.98	0.22	2.70	0.37
	16	141856	2033.65	3.98	0.22	2.70	0.36

Table 5.3: Main flame features. h-refinement studies. (Φ: equivalence ratio; n: grid parameter; $T_{max,C}$: maximum temperature at the symmetry axis; Hf: flame height; EI_x: emission index).

refinement $n = 4$, 8 and 16. The zone limited by $0 \leq r \leq 1.59$ cm and $0 \leq z \leq 20$ cm, whicht is in fact the space region that enclose the flame, is analyzed.

Local estimators of the GCI and p are calculated at the grid nodes where its evaluation has been possible. These grid nodes are named Richardson nodes. Global values of GCI and p are calculated by means of a volumetric averaging. It is considered that an estimation is credible when the global observed order of accuracy p approaches the theoretical value, and when the number of Richardson nodes is high enough. See [33] for details.

Table 5.2 shows the post-processing results for the extreme cases of premixing, the non-premixed case with $\Phi = \infty$, and the maximum level of premixing case with $\Phi = 2.464$. The percentage of Richardson nodes, global observed order of accuracy p, and uncertainties due to discretization GCI are given for the non-dimensional velocity field, non-dimensional temperature and mass fractions of some representative components (specifically CO, NO and NO_2).

As can be seen, for all variables selected, the number of Richardson nodes are sufficiently large for the three estimations presented (i.e. in general bigger than 75%). The observed average order of accuracy agree with its theoretical value (i.e. from 1 to 3, as central differences for the diffusive terms and third-order SMART scheme for the convective terms are employed). From mesh to mesh, the number of Richardson nodes increase and GCI values reduce their value approximately by four as it is expected. These results made us belief that estimations are credible.

GCI values for the third level of refinement ($n = 4$), already reach an enough level of accuracy. For instance, non-dimensional temperature has an average uncertainty of $\pm 0.34\%$ (i.e. approximately $\pm 1K$ for its dimensional value). These estimations agree with the asymptotically behavior of mean flame properties printed in table 5.3.

Computational costs, in terms of CPU seconds per outer iteration, for the last three levels of refinements are 11.12, 38.57 and 146.1 respectively. Approximately 3000 outer iterations are needed to converge the numerical solutions with a low enough tolerance. According to these computational costs and the commented above uncertainty estimates, the third level of refinement ($n = 4$) has been considered the most appropriate to perform the numerical studies hereafter presented, both in terms of accuracy and computational time.

5.5.2 Boundary conditions analysis

The considerable complexity of the burner configuration below the flame bottom ($z = 0$), because of the presence of perforated brass plates, glass beads and ceramic honeycomb structures, makes difficult notably the task of simulate numerically the whole burner. In this sense, and as has been commented in section 5.4.2, only the region above the inner's tube exit has been simulated (i.e. $z > 0$), and suitable boundary conditions for the bottom edge have to be employed.

For species mass fractions, a total flux of species is usually defined, and species mass fractions at the boundaries are evaluated using equation 5.16. In preceding works [10] [16], fixed temperature values were considered. In front of the difficulty of selecting an appropriate value for the temperature, that should be obtained from the experimental data, measurement difficulties did not allow to provide such values, and therefore an ambient under-predicted temperature was considered. This fact introduces expected disagreements with experimental data, under-predicting the maximum flame temperature at the symmetry axis, and distinguishable differences in the flame's height.

In this chapter, the influence of the boundary conditions has been analyzed. Attention is given to the energy equation boundary condition. A similar treatment as that employed for species equations is followed. An enthalpy flux is defined and then temperature is evaluated from equation 5.17 (see section 5.4.2). This boundary condition implies that no heat flux is transferred through the inner tube between the primary and secondary fluxes.

In table 5.4, flame heights and maximum temperatures are printed for the extreme premixing levels. Notice that as it is expected, when temperature is fixed lower maximum temperatures are predicted. When the proposed boundary condition is considered, improved agreement to experimental measurements is obtained.

Figure 5.2 plots the temperature profile along the symmetry axis. There is a better agreement to experimental data when *reference model* is taken into account.

Φ	$Model$	$T_{max,C}$ $[K]$	Hf $[cm]$	T_{max} $[K]$	(r,z) $[cm]$
∞	Ref	1908 (1960)	5.9 (5.7)	2005	0.66, 0.66
	$Tfixed$	1885 (1960)	6.1 (5.7)	1968	0.61, 1.19
2.464	Ref	2033 (2090)	4.0 (3.8)	2083	0.57, 1.97
	$Tfixed$	2005 (2090)	4.2 (3.8)	2047	0.54, 2.42

Table 5.4: Main flame features comparison for different energy equation boundary conditions. *Reference model* vs. fixed temperature boundary condition. Experimental values in parenthesis. (Φ: equivalence ratio; $T_{max,C}$: maximum temperature at the symmetry axis; $T_{max}, (r,z)$: maximum flame temperature and its location).

Temperature profiles for both flames tend to move towards the right, increasing also the maximum temperature at the centerline.

With the suggested boundary condition, there is a certain improvement in the agreement to experimental measurements. However, and being such global parameters very sensitive to the chemistry model, to the transport modeling, and to other modeling criteria, in the next section their influences are going to be analyzed.

5.5.3 Mathematical formulation comparison

The extreme premixing situations ($\Phi = \infty$ and $\Phi = 2.464$) are analyzed. Summary of these studies is presented in table 5.5. The numerical solutions obtained with the *reference model* (defined previously at the beginning of section 5.5) are compared to those employing different mathematical approaches for: chemistry, transport or radiative heat exchange. Comments about the influence of each treatment are given in this section. Comparison is performed in such a way that *reference model* criteria are always applied except the mathematical aspect under analysis. Axial profiles for temperature, and mole fractions for CH_4, O_2, CO_2, H_2O, CO and OH are plotted from figures 5.3 to 5.9. If possible, comparison to experimental measurements is provided. NO_x mass fractions radial profiles are presented at three different axial positions (figures 5.10 and 5.11).

Chemical models

The objective of this section is to present numerical results employing GRI-Mech 3.0 and compare its predictions to previous releases and to the selected skeletal mechanism. Flame-sheet hypothesis, used as starting estimates, is also included giving idea

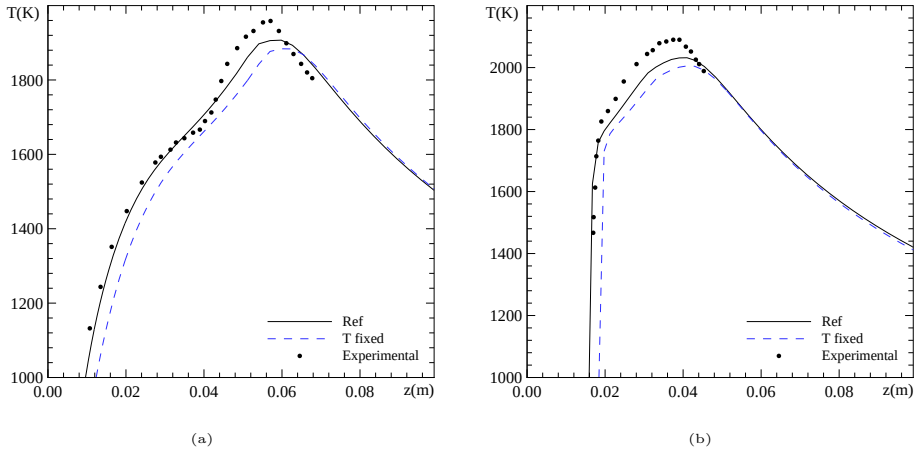

Figure 5.2: Temperature profiles along the symmetry axis. Energy equation boundary conditions comparison: *Reference model* vs fixed temperature boundary condition. (a) $\Phi = \infty$; (b) $\Phi = 2.464$.

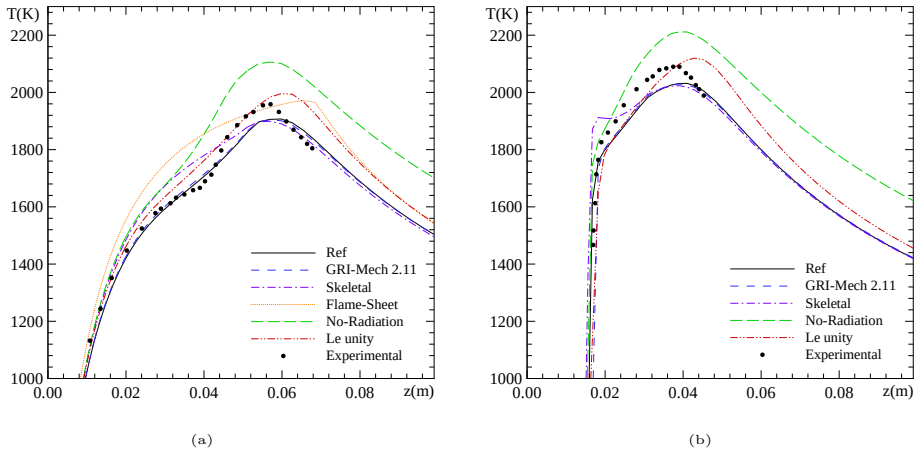

Figure 5.3: Mathematical formulation comparison. Temperature profiles along symmetry axis: (a) $\Phi = \infty$; (b) $\Phi = 2.464$.

$\Phi = \infty$								
Approach	*Model alternatives*	$T_{max,C}$ $[K]$	Hf $[cm]$	T_{max} $[K]$	(r,z) $[cm]$	EI_{CO} $[g/kg]$	EI_{NO} $[g/kg]$	EI_{NO_2} $[g/kg]$
Ref. model		1908	5.9	2005	0.66, 0.66	0.33	3.2	0.45
Chemistry	*GRI-Mech* 2.11	1904	5.7	2000	0.65, 0.78	0.35	1.6	0.21
	GRI-Mech 1.2	1905	5.7	2002	0.66, 0.59	0.37	−−	−−
	Skeletal	1900	5.6	2025	0.66, 0.66	0.66	−−	−−
	Flame-Sheet	1971	6.6	2244	0.64, 0.00	−−	−−	−−
Radiation	*No-Radiation*	2106	5.7	2106	0.00, 5.69	0.19	4.4	0.42
Transport	*No-Soret*	1910	5.9	2013	0.66, 0.66	0.32	3.2	0.41
	Lefixed	1891	5.9	2001	0.65, 0.78	0.33	3.2	0.46
	Leunity	1997	6.1	2042	0.67, 0.48	0.44	4.0	0.45

$\Phi = 2.464$								
Approach	*Model alternatives*	$T_{max,C}$ $[K]$	Hf $[cm]$	T_{max} $[K]$	(r,z) $[cm]$	EI_{CO} $[g/kg]$	EI_{NO} $[g/kg]$	EI_{NO_2} $[g/kg]$
Ref. model		2033	4.0	2083	0.57, 1.97	0.22	2.7	0.37
Chemistry	*GRI-Mech* 2.11	2029	3.9	2068	0.54, 2.12	0.24	2.0	0.23
	GRI-Mech 1.2	2030	3.9	2068	0.54, 2.12	0.26	−−	−−
	Skeletal	2024	3.9	2085	0.59, 0.84	0.46	−−	−−
Radiation	*No-Radiation*	2212	4.0	2211	0.00, 3.90	0.14	4.1	0.39
Transport	*No-Soret*	2033	4.0	2084	0.63, 1.26	0.22	2.8	0.35
	Lefixed	2016	4.0	2078	0.63, 1.34	0.22	2.7	0.36
	Leunity	2120	4.3	2139	0.63, 0.84	0.29	3.7	0.38

Table 5.5: Main flame characteristics. Mathematical formulation comparison. *Reference model* vs. chemistry, transport and radiation alternatives. (Φ: equivalence ratio; $T_{max,C}$: maximum temperature at the symmetry axis; $T_{max}, (r,z)$: maximum flame temperature and location; Hf: flame height; EI_x: emission index).

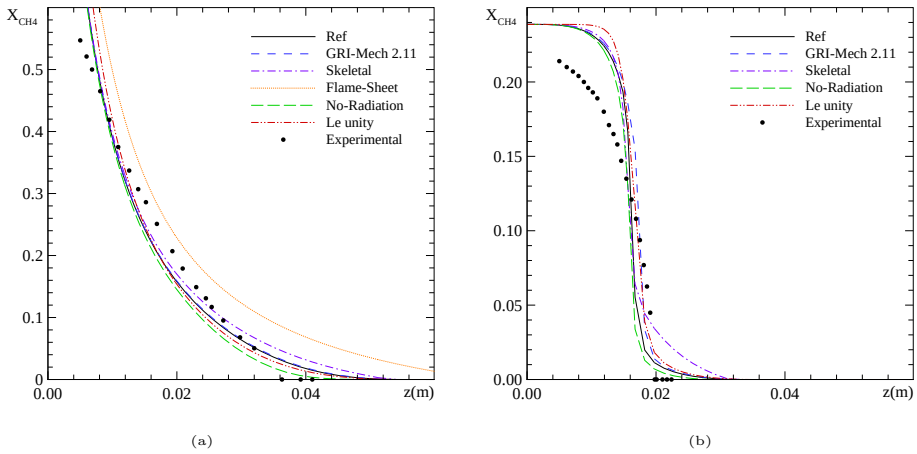

Figure 5.4: Mathematical formulation comparison. CH_4 mole fraction profiles along symmetry axis: (a) $\Phi = \infty$; (b) $\Phi = 2.464$.

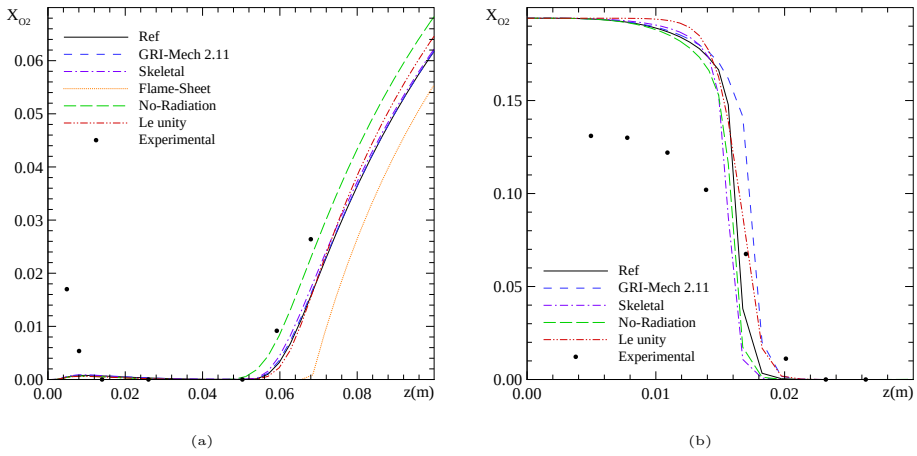

Figure 5.5: Mathematical formulation comparison. O_2 mole fraction profiles along symmetry axis: (a) $\Phi = \infty$; (b) $\Phi = 2.464$.

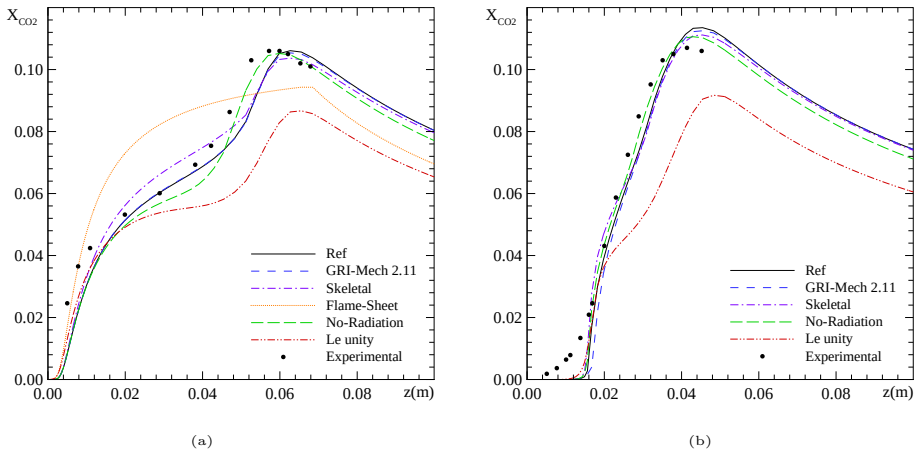

Figure 5.6: Mathematical formulation comparison. CO_2 mole fraction profiles along symmetry axis: (a) $\Phi = \infty$; (b) $\Phi = 2.464$.

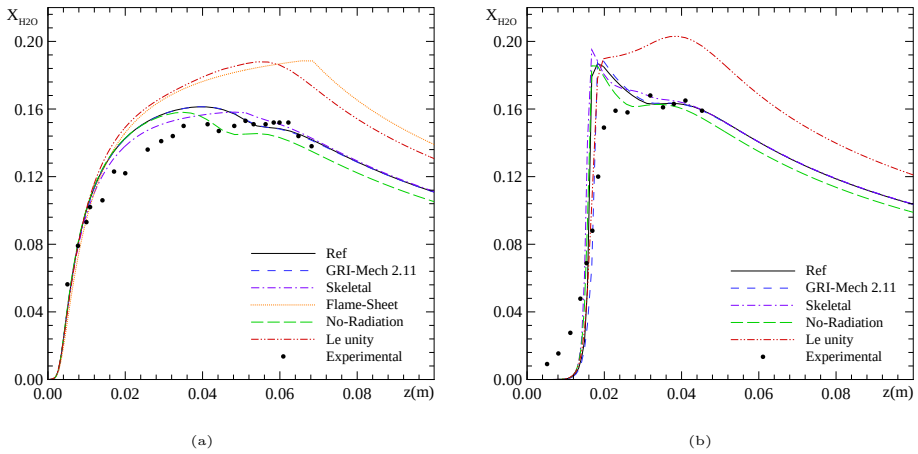

Figure 5.7: Mathematical formulation comparison. H_2O mole fraction profiles along symmetry axis: (a) $\Phi = \infty$; (b) $\Phi = 2.464$.

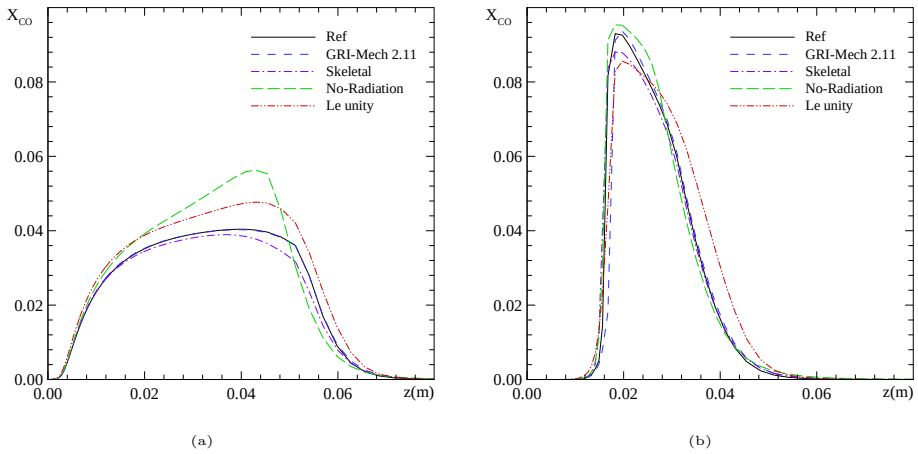

Figure 5.8: Mathematical formulation comparison. CO mole fraction profiles along symmetry axis: (a) $\Phi = \infty$; (b) $\Phi = 2.464$.

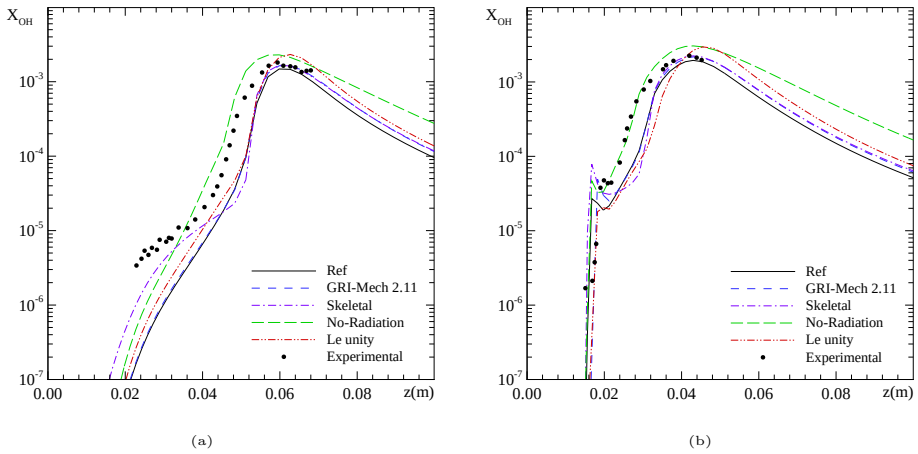

Figure 5.9: Mathematical formulation comparison. OH mole fraction profiles along symmetry axis: (a) $\Phi = \infty$; (b) $\Phi = 2.464$.

of its accuracy. Analysis is mainly focused on main flame properties and specially in pollutant formation. The latter aspect is restricted to GRI-Mech 3.0 and GRI-Mech 2.11 mechanisms, since the others do not include NO_x formation and no extra reactions have been added.

Very similar results have been obtained employing GRI-Mech 2.11 and 1.2, excepting obviously NO_x, not considered in version 1.2. In fact release 2.11 contains the same reactions defined in release 1.2 and just the reactions involved in the prediction of NO_x are added. This agreement suggests, as is usually done [39], the consideration of NO_x mechanisms in a post-processing procedure since they do not affect main flame characteristics (temperature and major species). Thus, in centerline and radial profiles, GRI-Mech 1.2 is not plotted due to its visual fitting with GRI-Mech 2.11 results.

In a general way, on the prediction of main flame features, there is a certain agreement for all mechanisms employed (without considering flame-sheet model). Differences lower than 0.5% are given for maximum temperature at the centerline, while flame heights differences are at least about 5.4%. These differences decrease when GRI-Mechs are employed, disagreements about 0.2% and 3.4% are obtained respectively in the most unfavorable situations.

Higher differences appear when emission indexes are evaluated. Skeletal mechanism clearly over-predicts CO formation (about 100%), while GRI-Mech 2.11 and 1.2 present disagreements of about 10%. Related to NO_x formation, GRI-Mech 3.0 predicts a higher production of these species. Specially, in non-premixed conditions higher differences are observed (about 50%).

The commented above results can be easily observed in the axial profiles presented. Slightly differences for temperature profiles and main species mole fractions can be seen for GRI-Mechs. Results obtained with these models adjust better to experimental measurements. For skeletal mechanism, although it predicts reasonably temperature and mole fractions profiles, relevant differences appear in the inner flame region.

Radial profiles of NO and NO_2 mole fractions (figures 5.10 and 5.11) emphasize the commented above disagreements between 3.0 and 2.11 GRI-Mech releases. As has been commented , version 2.11 under-predicts nitrogen oxides production. The differences obtained for these species, are the most important ones in the mathematical approaches comparison.

Radiation

Calculations without the consideration of radiative heat loss and considering an optically thin layer model for this quantity (see section 5.2.2), are compared in this section. Table 5.5 shows important disagreements for the maximum temperatures at the centerline with a difference of near 200K for $\Phi = \infty$ flame and about 180K for $\Phi = 2.464$ flame. These temperature over-predictions are nearly maintained along

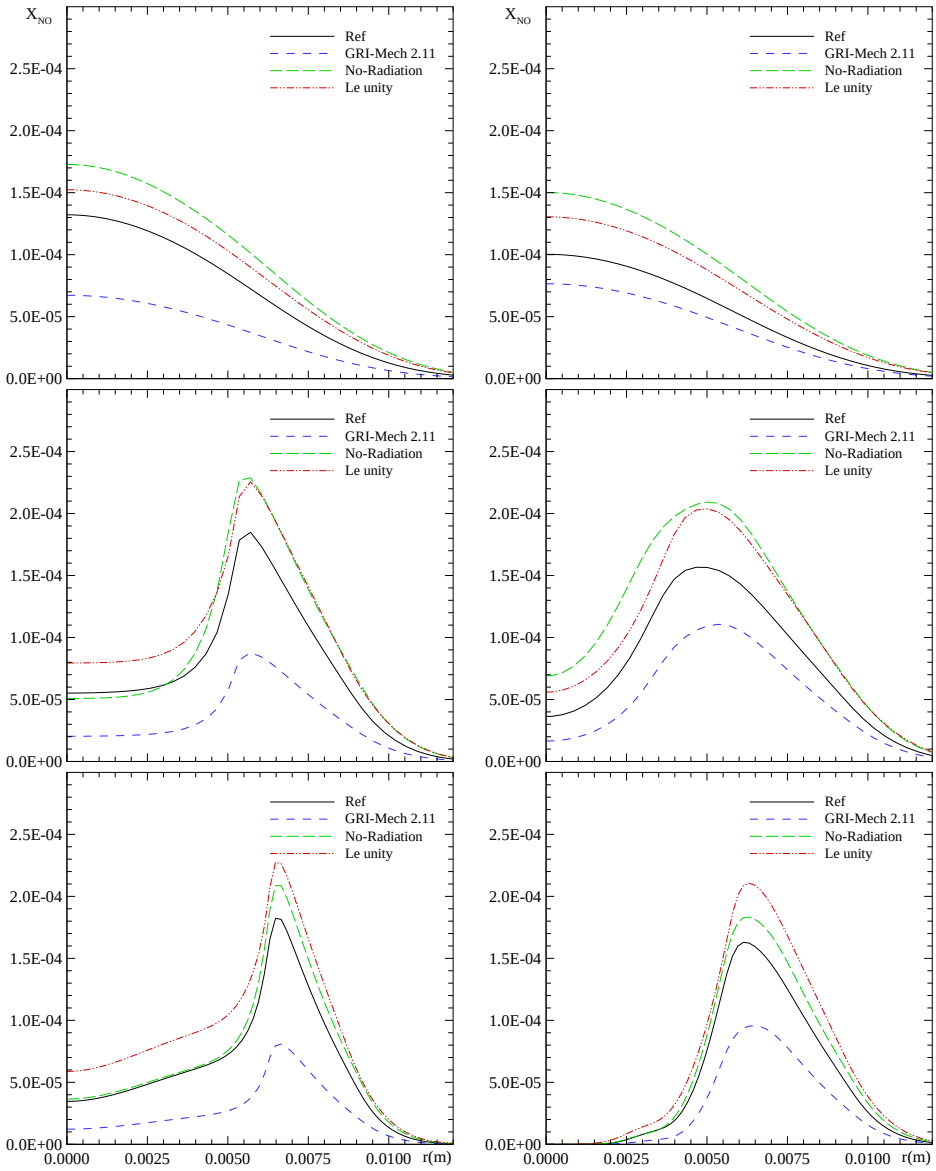

Figure 5.10: Mathematical formulation comparison. NO mole fraction radial profiles at different axial positions (bottom: 10 mm; middle: 25 mm; top: 100 mm) and for both extreme levels of premixing (left: $\Phi = \infty$; right: $\Phi = 2.464$).

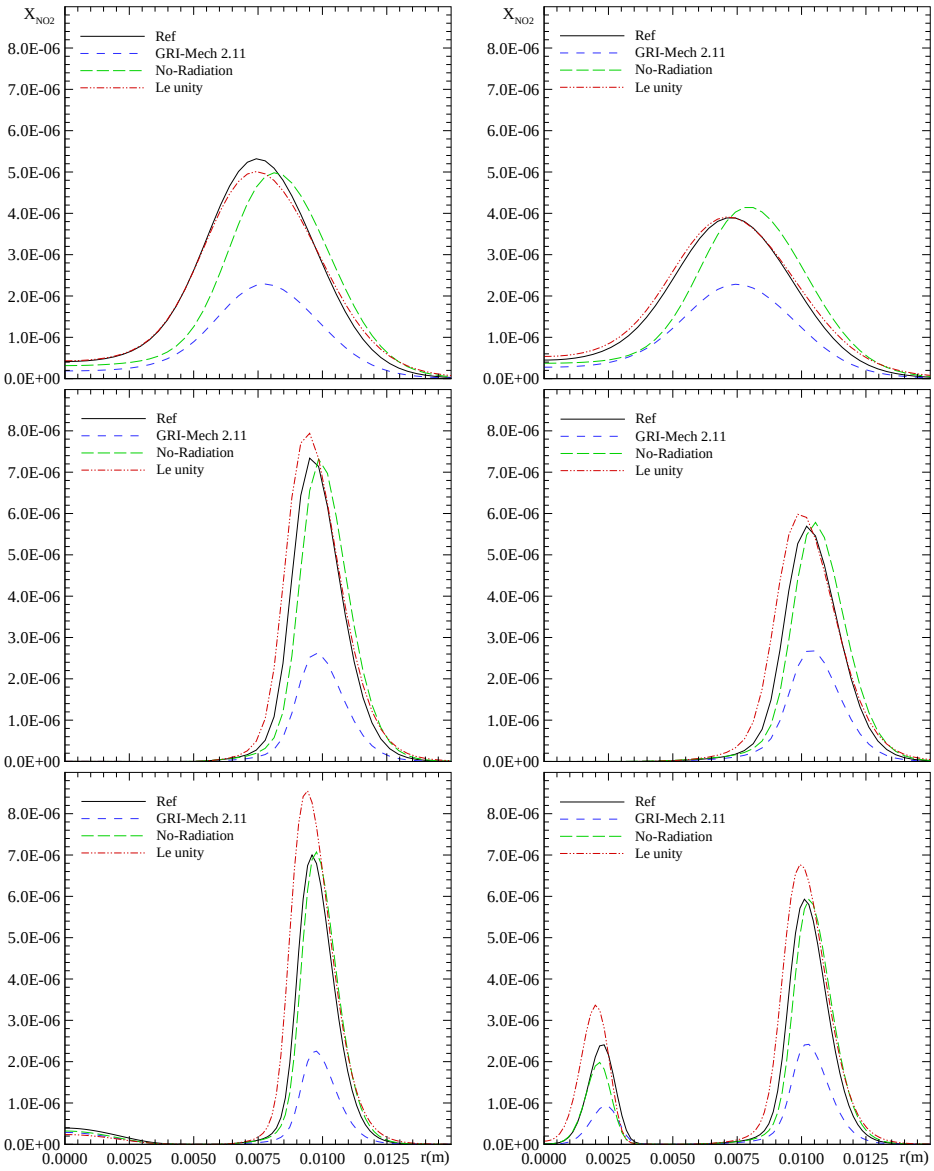

Figure 5.11: Mathematical formulation comparison. NO_2 mole fraction radial profiles at different axial positions (bottom: 10 mm; middle: 25 mm; top: 100 mm) and for both extreme levels of premixing (left: $\Phi = \infty$; right: $\Phi = 2.464$).

the centerline, except at the inner's tube exit, where both profiles concur (see figure 5.3).

The distributions of main species mole fractions have a similar trend. In fact, main differences between both modelizations appear when local radiative heat loss is important. At the inner's tube exit and for low enough temperatures, the influence of radiant heat source in energy equation is negligible. When this term increases in importance, local temperature is clearly affected, decreasing its magnitude notably. This temperature reduction obviously affects species concentrations, appearing the most important disagreements obtained in these studies.

Referring to nitrogen oxides, also important differences are predicted. In general, neglecting the radiative heat loss implies an over-prediction of NO formation with a factor of two, what is in concordance with the results of Barlow et al (2001) [21]. In fact, and being *thermal* NO_x one of the major contributions to NO_x formation, an increase of temperature consequently supposes and increase of NO_x due to the great temperature dependence of these mechanisms. As can be seen in figure 5.10, relevant disagreements appear at the top of the flame where *thermal* NO is mainly produced.

For NO_2 predictions, the level of the peak with and without the consideration of radiation model is similar, but a delay on this peak formation is revealed. Most NO_2 is formed at the flame front and it is basically attributed to a *prompt* production. NO_2 radial profile at the base of the flame ($z = 10\ mm$) for the maximum level of premixing considered in this chapter (i.e. $\Phi = 2.464$), shows the double flame structure characteristic of partially premixed flames. This can also be viewed in section 5.5.4 where isopleths for different equivalence ratios are presented.

Soret effect

Thermal diffusion ratios are only important for chemical species with mass weights lower than 5 g/mol, so for the methane combustion mechanisms considered in this chapter, only H and H_2 are taken into account. Main flame features printed in table 5.5 show that the contribution of thermal diffusion is not very important in these flames. Few differences appear if Soret effect is or is not considered. Axial and radial profiles for temperature and chemical species are not plotted for the simulation without considering Soret effect, since they visually coincide with the *reference model*.

Figure 5.12 shows the minor contribution of thermal diffusion in discretized species governing equations for H and H_2 in the non-premixed flame. As it is shown, main important contributions in species discretized equations are due to chemical reactions and ordinary diffusion fluxes.

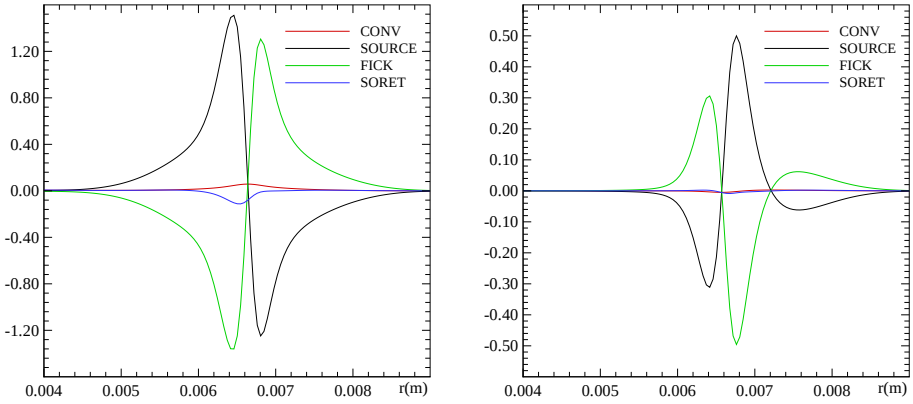

Figure 5.12: Mathematical formulation comparison. Thermal diffusion contribution in species governing equations ($\Phi = \infty$). Radial profile at $z = 10$ mm. SOURCE: production/consumption terms; FICK: ordinary diffusion terms; SORET: thermal diffusion terms; CONV: convective terms. (a) Hydrogen, H_2; (b) Hydrogen atom, H.

Species	*Le*	*Species*	*Le*	*Species*	*Le*
C	0.73	CH_3O	1.38 (1.30)	HNO	1.08
C_2H	1.31 (1.26)	CH_3OH	1.36	HO_2	1.08 (1.10)
C_2H_2	1.32 (1.28)	CH_4	0.97 (0.97)	$HOCN$	1.38
C_2H_3	1.33 (1.29)	CN	1.09	N	0.77
C_2H_4	1.35 (1.29)	CO	1.09 (1.10)	N_2	1.03 (1.00)
C_2H_5	1.47 (1.41)	CO_2	1.40 (1.39)	N_2O	1.39
C_2H_6	1.48 (1.42)	H	0.18 (0.18)	NH	0.66
C_3H_7	1.90 (1.84)	H_2	0.29 (0.30)	NH_2	0.67
C_3H_8	1.91 (1.84)	H_2CN	1.36	NH_3	0.94
CH	0.65 (0.64)	H_2O	0.91 (0.83)	NCO	1.37
CH_2	0.97 (0.95)	H_2O_2	1.09 (1.12)	NNH	1.10
$CH_2(S)$	0.95	$HCCO$	0.88 (0.86)	NO	1.09
CH_2CHO	1.57	$HCCOH$	1.56	NO_2	1.25
CH_2CO	1.56	HCN	1.34	O	0.69 (0.70)
CH_2O	1.36 (1.28)	$HCNN$	0.87	O_2	1.09 (1.11)
CH_2OH	1.35	$HCNO$	1.38	OH	0.71 (0.73)
CH_3	0.99 (1.00)	HCO	1.35 (1.27)		
CH_3CHO	1.57	$HNCO$	1.38		

Table 5.6: Species Lewis number. Averaged values obtained from detailed transport calculation in non-premixed conditions ($\Phi = \infty$). In parenthesis theoretical values [25].

Mass transport coefficients

Different mathematical approaches have been considered and compared on the evaluation of mass transport coefficients. The most detailed one using a mixture averaged formulation and corresponding to equation 5.12 is used as the reference approach.

Two simpler models using the definition of the Lewis number (eq. 5.13) are analyzed: the first one considers a fixed Lewis number for each one of the species, and the second model uses a constant unity Lewis number for all species.

First approach, use averaged Lewis numbers calculated from the numerical results obtained with the *reference model*. These values are reported in table 5.6. As can be seen, major species Lewis numbers agree with the values usually employed in the literature.

Excellent agreement for global and detailed flame properties is achieved, being the computational effort less intensive in comparison with the complete mixture averaged formulation. CPU time savings of about 25% are obtained. Profiles for this approach are also not plotted due to its fitting with the *reference model*.

When unity Lewis number is considered (second approach), considerable disagreements occur. The maximum temperature at the centerline and the flame height are over-predicted for both extreme levels of premixing. Species axial profiles present relevant deviations to experimental measurements. EI_{CO} is also over-predicted respect to the *reference model*. Differences about 33% for $\Phi = \infty$ and 30% for $\Phi = 2.464$ have been observed.

Even EI_{NO_2} do not varies significantly, EI_{NO} is also over-predicted with 25% for $\Phi = \infty$ and 39% for $\Phi = 2.464$. Radial profiles of NO show an over-prediction of this pollutant formation, while profiles of NO_2 are not so dissimilar.

5.5.4 Level of premixing. Equivalence ratio comparison

Five levels of premixing (see table 5.7) are compared, from a non-premixed flame with $\Phi = \infty$ to a level of premixing of $\Phi = 2.464$ just before flashback began to affect the flame structure [37]. *Reference model* exposed above has been considered for all numerical simulations. Extensive analysis of the main flame properties are given in detail by Bennet et al [16]. In this chapter, results for NO_x formation are pointed out.

Table 5.7 shows the main flame characteristics for all levels of partially premixing. Are pointed out the maximum flame temperature at the centerline, the flame height, and pollutant emission indexes. Experimental results, if available, are given in parenthesis [16].

As can be seen, as the partially premixing level increases, flame height decreases. The amount of oxygen introduced through the primary inlet reduces the axial distance that it has to overcome to diffuse into the flame and to create stoichiometric

Φ	$T_{max,C}$ $[K]$	Hf $[cm]$	T_{max} $[K]$	(r,z) $[mm]$	RHL $[W]$	HR $[W]$	EI_{CO} $[g/kg]$	EI_{NO} $[g/kg)$	EI_{NO_2} $[g/kg)$
∞	1908 (1960)	5.9 (5.7)	2005	$0.66, 0.66$	35.11	181.05	0.33	3.2	0.45
12.32	1933 (2000)	5.6 (5.2)	2009	$0.65, 0.72$	34.83	180.99	0.30	3.2	0.46
6.160	1956 (2020)	5.2 (4.9)	2017	$0.63, 0.97$	34.75	180.91	0.28	3.1	0.43
4.107	1980 (2040)	4.8 (4.5)	2031	$0.61, 1.41$	34.79	180.74	0.26	3.0	0.41
2.464	2033 (2090)	4.0 (3.8)	2083	$0.57, 1.97$	35.04	180.35	0.22	2.7	0.37

Table 5.7: Level of premixing analysis. Main flame characteristics. (Φ: equivalence ratio; $T_{max,C}$: maximum temperature at the symmetry axis; Hf: flame height; $T_{max}, (r,z)$: maximum flame temperature and location; RHL radiant heat loss; RH: heat release; EI_x: emission index).

conditions. Good agreement is observed with experimental results. In the most adversely situation $\Phi = 12.32$, an over-prediction respect to experimental measurements of about 7% is obtained.

Computational temperatures present also good agreement to experimental data. Maximum centerline temperatures disagree at least a 3.4% for all premixing cases. General trends observed in experimental studies are appropriately reproduced in the numerical results. Figure 5.13a shows the temperature profiles along the centerline for the different equivalence ratios. As can be seen, as equivalence ratio decreases, temperature increases, and profiles present sharper gradients. Considering experimental measurements accuracy described in section 5.4.1, acceptable agreements are obtained.

Isotherms for the extreme levels of premixing are plotted in figure 5.16a. Well-known temperature maps are obtained for the non-premixed situation, while for the flame with equivalence ratio $\Phi = 2.464$, the structure of non-premixed and premixed flames are mixed, forming what is known as a *double flame*. Outer flame region has clearly a non-premixed structure, while inner region defines a classical premixed shape. Streamlines given in figure 5.16b helps to understand one of the reasons for why higher temperatures are obtained with the partially premixed case. In the non-premixed situation, larger amount of fresh air (from the secondary inlet) enters inside the flame, decreasing in this sense temperature maps. On the other hand, and for the higher level of premixing, inner flame temperature has its well-known conical shape. Streamlines go parallel to the symmetry axis, changing its direction in a perpendicular manner when they arrive to the inner flame front. Another reason that accounts for the greater temperature prediction in highest premixing conditions, is the reduction of radiative heat loss (see table 5.7).

Major species centerline profiles are plotted in figures 5.13, 5.14 and 5.15. Sig-

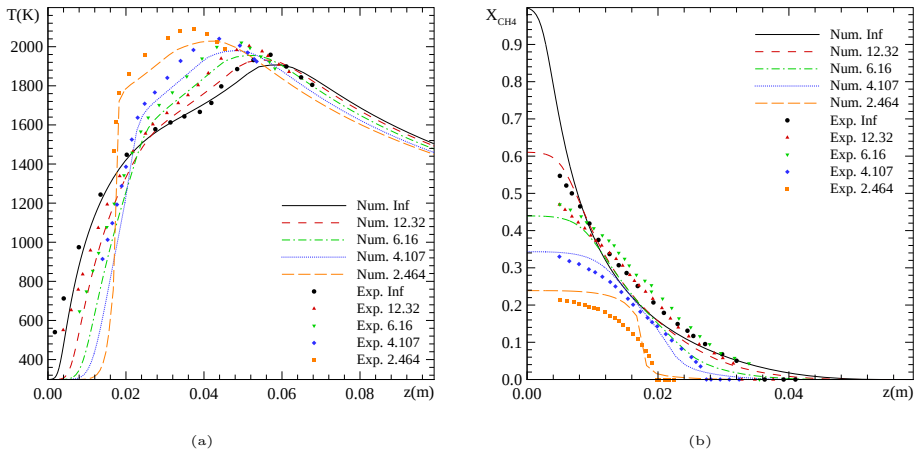

Figure 5.13: Level of premixing analysis. Profiles along symmetry axis: (a) Temperature; (b) CH_4 mole fraction.

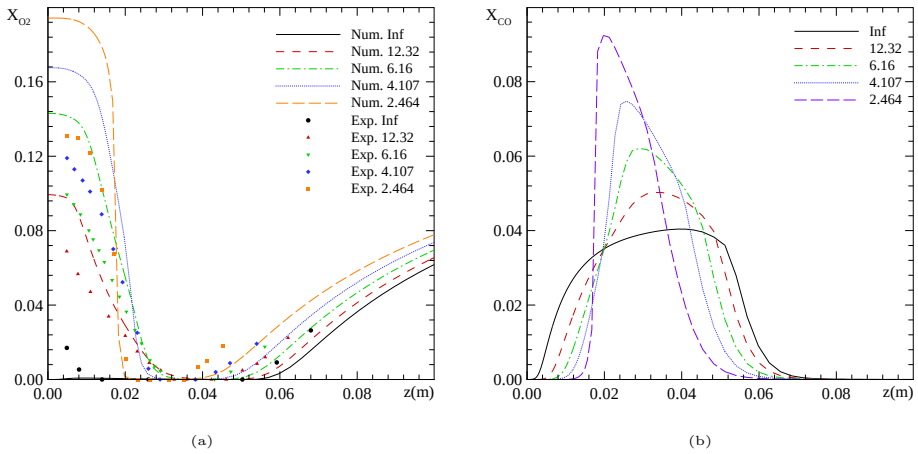

Figure 5.14: Level of premixing analysis. Mole fractions profiles along symmetry axis: (a) Oxygen, O_2; (b) Carbon Mon-oxide, CO.

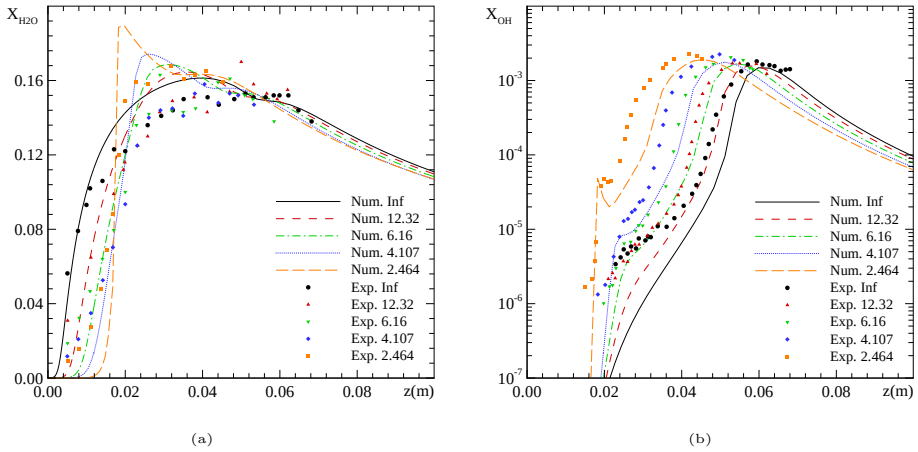

Figure 5.15: Level of premixing analysis. Mole fractions profiles along symmetry axis: (a) Water, H_2O; (b) Hydroxyl, OH.

nificant computational/experimental disagreements are obtained. Experimental difficulties to access to inner tube's exit, sharp concentration gradients, and the 30% absolute uncertainty of experimental measurements, relativizes the appropriateness of the mathematical model. Nevertheless, global trends of species mole fractions as the level of partially premixing increases are well predicted.

Results for the non-premixed flame show the well-known diffusion flame structure. Maximum CH_4 mole fractions are held at the axis, while O_2 and N_2 surrounds the flame. Combustion products are formed near the stoichiometric surface. Fuel decomposes forming H_2, CO and H_2O in the rich side of the flame front. CO oxidizes forming CO_2 mainly at the top of the flame. Isopleths for main products species are plotted in figure 5.17.

Reactants CH_4 and O_2, reach greater heights before they start to react as partially premixing increases. The higher injection velocities produce relatively flat profiles at the inner's tube exit. Sharper gradients are also predicted.

H_2O mole fractions given in figures 5.15 and 5.17 illustrate the double flame structure presented for $\phi = 2.464$. The presence of two marked peaks denotes two main zones of H_2O production. At the first flame front, with premixing features, the mole fraction peak increases with the level of premixing. H_2O measurements present a more aleatory behavior. Experimental calibration difficulties for H_2O mole fractions were given because of the low vapor pressure conditions [16]. However, both computational and experimental results coincide on the fact that major part of H_2O

is produced at the inner flame front, and on the observation of a inner peak for the higher premixing conditions.

Although CO mole fractions experimental measurements are not provided in [16], computational results are also given to show the premixing dependence of its production. As can be seen, for the non-premixed flame, CO production do not present a remarkable peak. It is progressively produced in the inner's flame region, and at the top of the flame, is partially consumed to produce CO_2. As the level of premixing increases, the CO peak becomes slender. O_2 injected through the primary inlet, does not reduce CO concentration, since CO is mainly oxidized by reactions involving OH radical. At the inner premixed flame front, a considerable amount of CO is produced. At the inner diffusion flame, carbon monoxide is progressively consumed. Similar trends are predicted for H_2 mole fractions. Both species isopleths are shown in figure 5.17.

OH mole fractions are also presented in figure 5.15. Although calibration difficulties due to the instability commented in the experimental measurements, the agreement to experimental data is observed. General trends coincide for both computational and experimental profiles. Again double flame structure for the highest levels of premixing is predicted by the presence of an inner peak. In this case the amount of OH formed in the inner flame is considerably lower than that produced in the outer one.

It is important to point out, that H_2O and OH experimental data were modified by a scale factor to agree experimental/computational values presented in [16]. Thus, for our purpose, absolute concentrations have to be put in doubt and only global trends should be taken into account.

Isopleths for OH concentrations as for hydrogen atom, ethane and propane are shown in figure 5.18. For $\Phi = 2.464$, the prediction of ethane and propane formation is considerable higher than for the non-premixed flame. This production takes places at the inner flame front. In fact, and as is recommended [40], for an accurate resolution of premixed rich methane/air flames, $C2$- and $C3$-chains initiated by methyl recombination should be considered.

One of the most relevant aspects in the analysis of co-flow methane/air flames are the studies of pollutant formation and its influence to equivalence ratio in partially premixed flames. In particular, experimental and numerical research on NO_x and CO emissions have motivated special attention [41][42]. Depending on the fuel type and on the working conditions, changes on NO_x production can have different trends. Actually, NO emissions can increase with increasing partially premixed due to the temperature increment (NO formation is a highly sensitive process) or due to higher presence of oxygen and radicals responsible for *prompt* NO formation at the flame fronts [41]. On the other hand, NO emission can decrease with increasing partially premixing due to the lowest residence time provoked by higher gas velocities at the

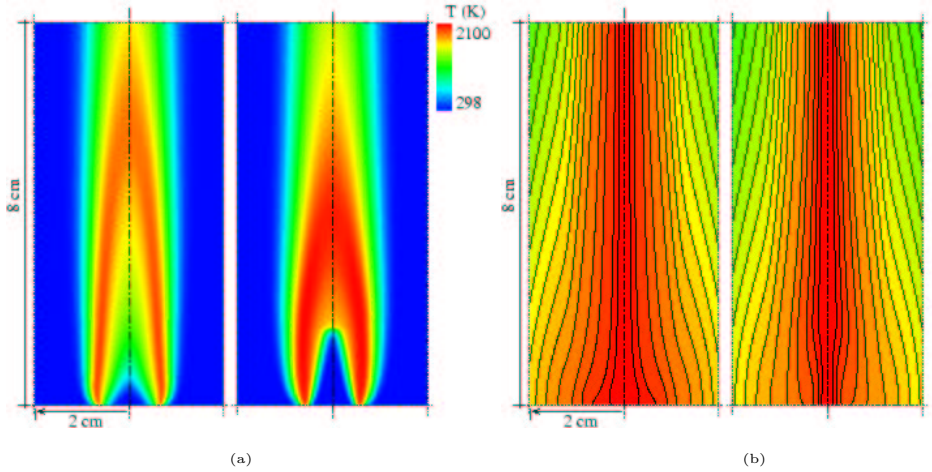

Figure 5.16: Level of premixing analysis: (a) Isotherms; (b) and Streamlines. (Left: $\Phi = \infty$; right: $\Phi = 2.464$).

burner exit. *Thermal NO* is a slow process in comparison to fluid mechanics, if the residence time is increased lower amount of NO can be produced.

Global trends of NO_x emission predicted by GRI-Mech 3.0 are given in table 5.7. As can be shown, similar amount of NO and NO_2 are predicted for equivalence ratios between $\Phi = 4.107$ and $\Phi = \infty$. When the premixing level increases, the higher production of thermal NO is balanced by a reduction of prompt NO [41]. Although the residence time reduces when the level of partial premixing increases, the higher temperatures achieved between inner and outer flames increases the amount of NO_x produced. For lower values of Φ, a reduction of NO_x is predicted. Similar trends were observed by Gore et al [41] in their experimental measurements. Gore et al suggested that these reduction could be associated to the reduction of prompt NO caused by intermediate hydrocarbon chemistry and contributions from the reverse prompt mechanism described by Takeno et al [43]. Isopleths for main species involved in the NO_x mechanism are plotted in figure 5.19. Qualitatively, higher NO_x emissions are observed for the non-premixed flame (left figures). As has been commented, prompt NO formed mainly at the stoichiometric surface can be highlighted for the non-premixed flame. NO_2 contours show the double flame structure for $\Phi = 2.464$. Figure 5.20 agree with the assumptions commented above. Lower peaks for NO_x are predicted at the outer flame surface as the level of partial premixing increases.

CO emission indexes are also given in table 5.7. Notice that CO emission are small in comparison with NO. Again, agreement with experimental data provided

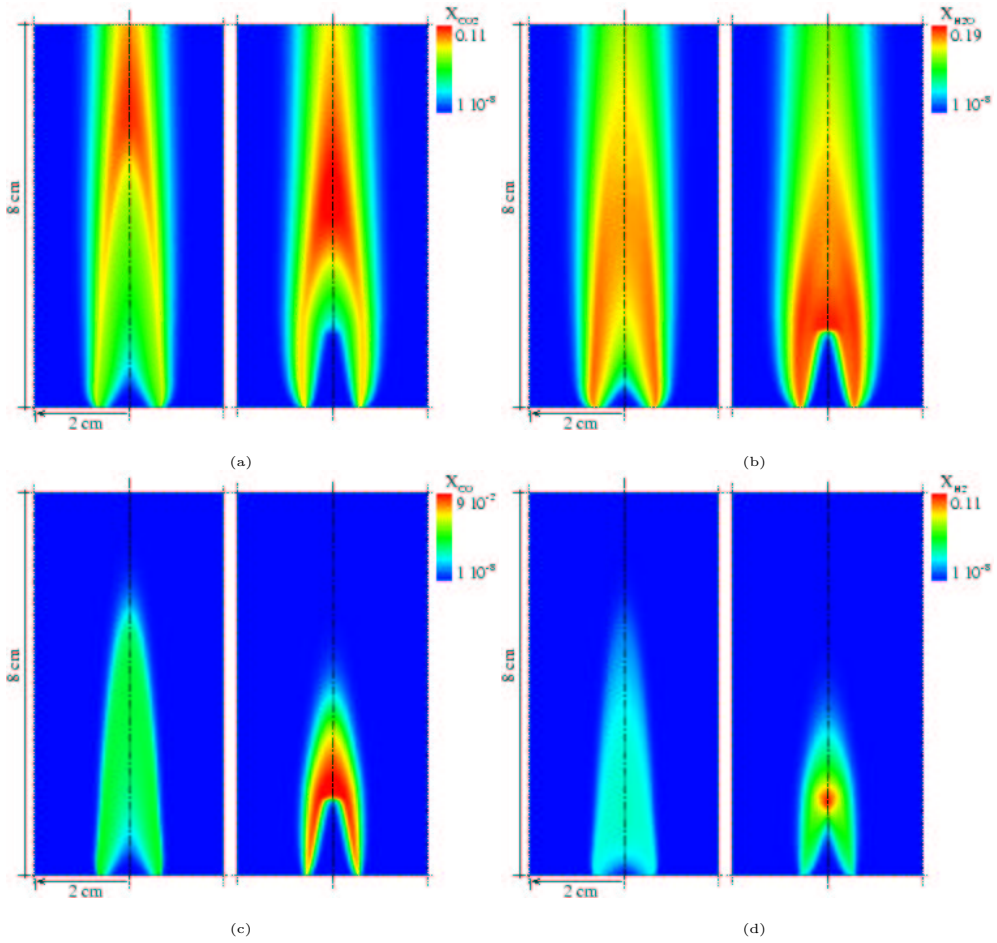

Figure 5.17: Level of premixing analysis. Main products mole fractions isopleths: (a) Carbon dioxide, CO_2; (b) water, H_2O; (c) Carbon monoxide, CO; (d) Hydrogen, H_2 . (Left: $\Phi = \infty$; right: $\Phi = 2.464$).

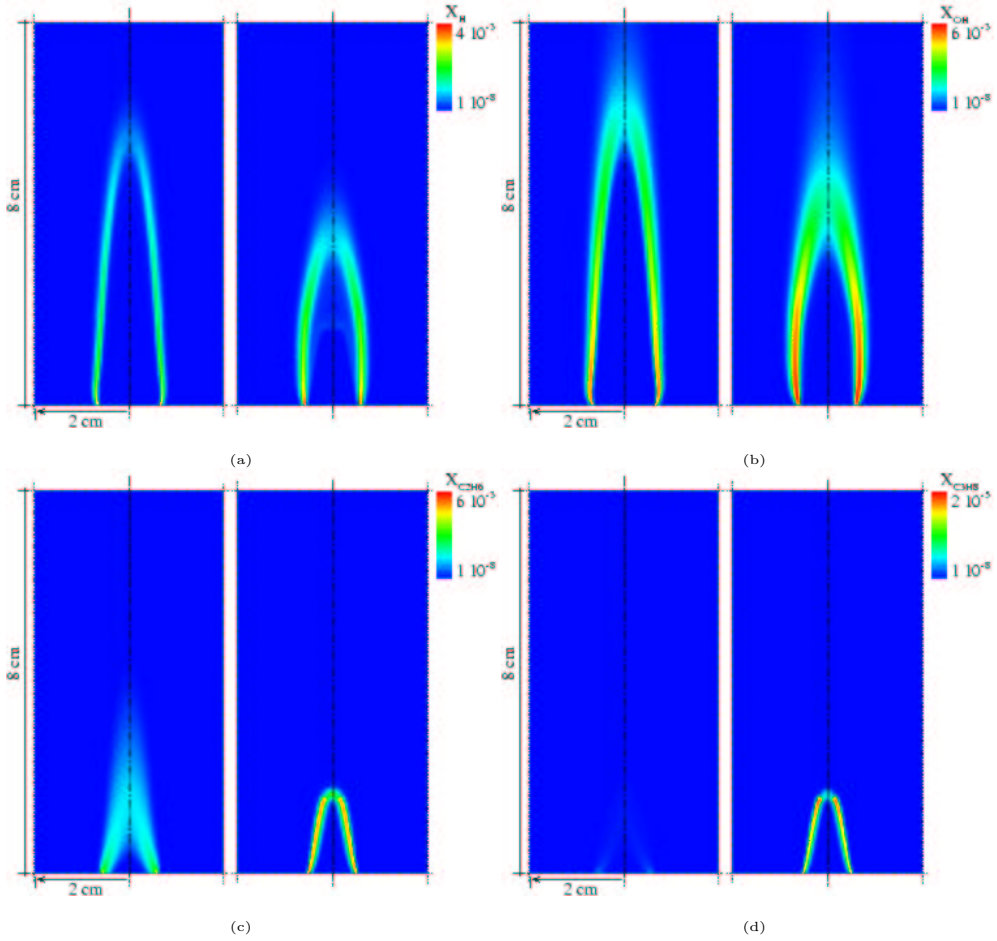

Figure 5.18: Level of premixing analysis. Intermediate species mole fractions isopleths: (a) Hydrogen atom, H; (b) Hydroxyl, OH; (c) Ethane, C_2H_6; (d) Propane, C_3H_8 . (Left: $\Phi = \infty$; right: $\Phi = 2.464$).

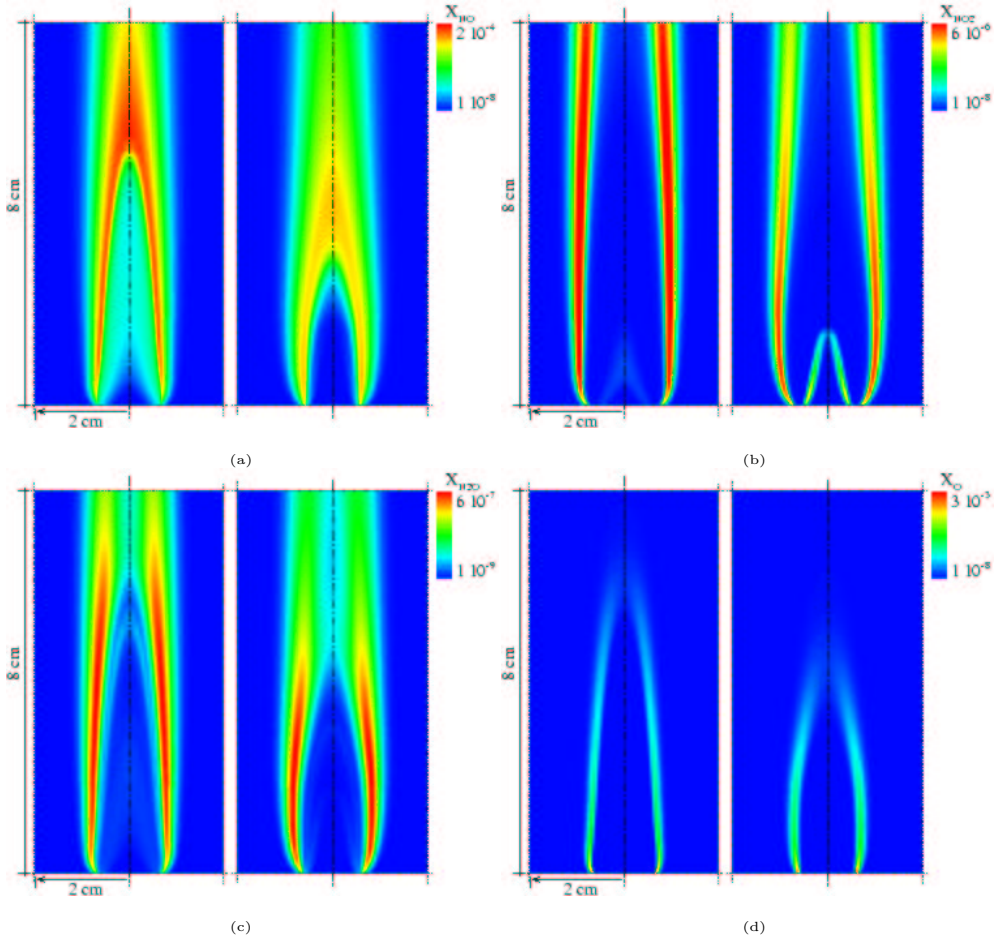

Figure 5.19: Level of premixing analysis. Main species involved in NO_x formation. Mole fractions isopleths for: (a) Nitrogen oxide, NO; (b) Nitrogen dioxide, NO_2 ; (c) N_2O; (d) oxygen atom, O . (Left: $\Phi = \infty$; right: $\Phi = 2.464$).

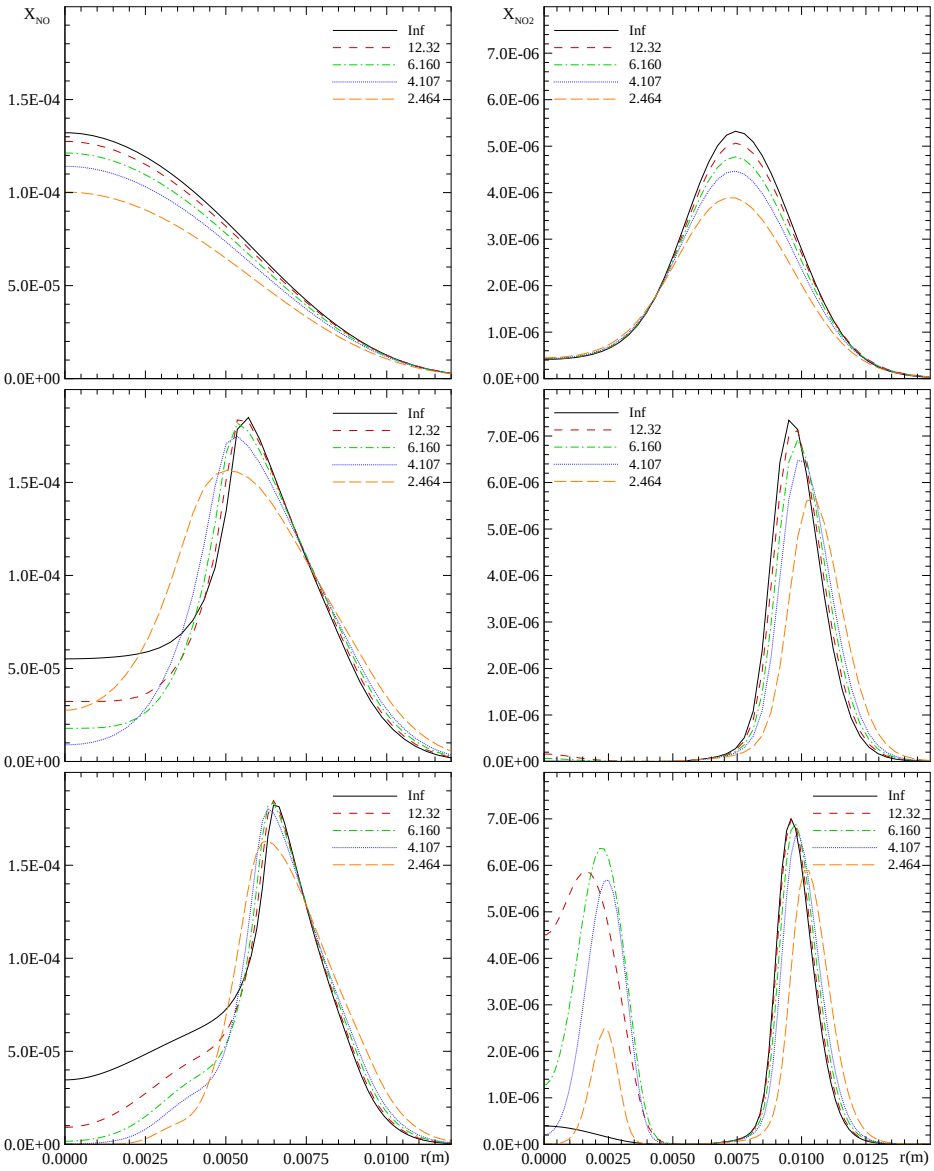

Figure 5.20: Level of premixing analysis. NO_x mole fractions radial profiles at different axial positions (bottom: 10 mm; middle: 25 mm; top: 100 mm). Left: NO, right: NO_2.

in [41] have been found. An increase of about 10% is predicted from $\Phi = 12.32$ to $\Phi = \infty$. These differences increase notably when the highest level of premixing is considered, reducing CO emission index to about 33%.

5.6 Conclusions

Detailed numerical simulations have been performed to analyze fundamental aspects of co-flow partially premixed methane-air laminar flames, and the adequacy of several mathematical approaches employed on their modelization. Available experimental data have been taken into account both on the analysis of the influence of partially premixing and on the mathematical approaches comparison.

Numerical results have been submitted to a verification process based on h-refinement studies, establishing criteria about the sensitivity of the simulation to the computational model parameters that account for the discretization. Post-processing results have provided uncertainty estimations and have been used as a valuable tool on the selection of the grid nodes distribution. A parallel multiblock algorithm running with loosely coupled computers has been employed to simulate the different cases. Accurate enough solutions employing the highest level of modelization (i.e. GRI-Mech 3.0, complex transport modeling and radiation included) have been obtained after approximately 10 hours on a *Beowulf cluster*.

Related to the mathematical formulation comparison, the proposed boundary condition for the energy equation have been proved to be suitable for adjusting flames height and the maximum flame temperatures at the centerline. Better agreement to experimental measurements have been obtained.

On the prediction of main flame features (i.e. flame height, maximum temperatures), there is a certain agreement for all mechanisms employed. However, significant disagreements have been obtained on the estimation of emission indices. While GRI-Mechs predicts a similar amount of CO formation, skeletal mechanism over-predicts it considerably. GRI-Mech 3.0 doubles the NO_x emission respect 2.11 release for the non-premixed flame, while for $\Phi = 2.464$ is 25% higher.

The consideration of radiant heat exchange have been shown to affect considerably flames temperature, and therefore it is important to be considered in pollutant formation studies.

On the transport modeling approaches analysis, the formulation considering non-unity Lewis numbers have been shown to be suitable both in terms of agreement with complex transport and in terms of computational savings. The employment of fixed Lewis numbers can suppose a 25% of CPU time reduction. For intermediate species which Lewis number was unknown, they have been obtained by calculating them from the detailed solutions and averaging their values for the whole domain. This procedure have been considered to be suitable, since predictions for major species

Lewis numbers coincide with those available in the literature. Thermal diffusion contributions in species diffusion fluxes do not affect considerably numerical results. Nevertheless, and due to the low computational cost that its consideration supposes, their omission is not recommended.

Effects of partial premixing level have been presented using the higher degree of modelization considered (*reference model*). Numerical results are presented for five levels of premixing, from $\Phi = 2.464$ to $\Phi = \infty$. Global flame features predicted coincide with both experimental and numerical results presented by other authors. However, better agreements to experimental data have been presented. Special emphasis has been given to NO_x and CO emission indexes. GRI-Mech 3.0 agree with global trends detected in previous experimental studies.

References

[1] N. Peters. *Turbulent combustion*. Cambridge University Press, 2000.

[2] R.E. Mitchell, Sarofim, and L.A. Clomburg. Experimental and numerical investigation of confined laminar diffusion flames. *Combustion and Flame*, 37:227–244, 1980.

[3] J.A. Miller and R.J. Kee. Chemical nonequilibrium effects in hydrogen-air laminar jet diffusion flames. *AIAA Journal*, 81(25):2534–2542, 1977.

[4] R.J. Kee and J.A. Miller. A split-operator, finite-difference solution for axissymmetric laminar-jet diffusion flames. *AIAA Journal*, 16(2):169–176, 1978.

[5] M.D. Smooke, R.E. Mitchell, and D.E. Keyes. Numerical solution of two-dimensional axisymmetric laminar diffusion flames. *Combustion Science and Technology*, 67:85–122, 1989.

[6] D.E. Keyes and M.D. Smooke. Flame sheet starting estimates for counterflow diffusion flame problems. *Combustion Science and Technology*, 73:267–288, 1987.

[7] G. Dixon-Lewis, T. David, P.H. Gaskell, S. Fukutani, H. Jinno, J.A. Miller, R.J. Kee, M.D. Smooke, N. Peters, E. Effelsberg, J. Warnatz, and F. Behrendt. Calculation of the structure and extinction limit of a methane-air counterflow diffusion flame in the forward stagnation region of a porous cylinder. In *Proceedings of the Twenty-Sixth Symposium (International) on Combustion*, pages 1893–1904, 1984.

[8] M.D. Smooke, Y. Xu, R.M. Zurn, J.H. Frank, and M.B. Long. Computational and experimental study of OH and CH radicals in axisymmetric laminar diffu-

sion flame. In *Proceedings of the Twenty-Fourth Symposium (International) on Combustion*, pages 813–821, 1992.

[9] P.J. Coelho and J.C.F. Pereira. Calculation of a confined axisymmetric laminar flame using grid refinement technique. *Combustion Science and Technology*, 92:243–264, 1993.

[10] B.A. Bennett, C.S. McEnally, L.D. Pfefferle, and M.D. Smooke. Local rectangular refinement with application to axisymmetric laminar flames. *Combustion Theory and Modelling*, 2:221–258, 1998.

[11] M.D. Smooke, C.S. McEnally, and L.D. Pfefferle. Computational and experimental study of soot formation in a coflow, laminar diffusion flame. *Combustion and Flame*, 117:117–139, 1999.

[12] Q.V. Nguyen, R.W. Dibble, C.D. Carter, G.J. Fiechtner, and R.S. Barlow. Raman-LIF measurements of temperature, major species, OH, and NO in a methane-air bunsen flame. *Combustion and Flame*, 105:499–510, 1996.

[13] C.S. McEnally and L.D. Pfefferle. Aromatic and linear hydrocarbon concentration measurements in a non-premixed flame. *Combustion Science and Technology*, 116–117:183–209, 1996.

[14] V.R. Katta and W.M. Roquemore. Simulation of dynamic methane jet diffusion flames using finite rate chemistry models. *AIAA Journal*, 36(11):2044–2054, 1998.

[15] V.R. Katta, L.P. Goss, and W.M. Roquemore. Effect of nonunity lewis number and finite-rate chemistry on the dynamics of a hydrogen-air jet diffusion flame. *Combustion and Flame*, 96:60–74, 1994.

[16] B.A. Bennett, C.S. McEnally, L.D. Pfefferle, and M.D. Smooke. Computational and experimental study of axissymmetric coflow partially premixed methane/air flames. *Combustion and Flame*, 123:522–546, 2000.

[17] J. Cadafalch, C.D. Pérez-Segarra, R. Cònsul, and A. Oliva. Verification of finite volume computations on steady state fluid flow and heat transfer. *Journal of Fluids Engineering*, 124:11–21, 2002.

[18] P.J. Roache. Perspective: a method for uniform reporting of grid refinement studies. *Journal of Fluids Engineering*, 116:405–413, 1994.

[19] G.P. Smith, D.M. Golden, M. Frenklach, N.W. Moriarty, B. Eiteneer, M. Goldenberg, C.T. Bowman, R.K. Hanson, S. Song, W.C. Gardiner, V.V. Lissianski, and Z. Qin. Gri-Mech 3.0, http://www.me.berkeley.edu/gri_mech/.

[20] R.B. Bird, E.E. Stewart, and E.N. Lightfoot. *Transport phenomena*. John Wiley and Sons Inc., 1960.

[21] R.S. Barlow, A.N. Karpetis, and J.Y. Frank, J.H. Chen. Scalar profiles and NO formation in laminar opposed-flow partially premixed methane/air flames. *Combustion and Flame*, 127:2102–2118, 2001.

[22] S. Mazumder and M.F. Modest. Advanced nongray radiation model coupled with a CFD code for large-scale fire and combustion applications. Technical report, National Sciencie Foundation, 2001.

[23] W.L. Grosshandler. RADCAL: A narrow-band model for radiation calculations in a combustion environment, NIST Technical Note 1402, 1993.

[24] C.T. Bowman, R.K. Hanson, Davidson, W.C. Gardiner, V.V. Lissianski, G.P. Smith, D.M. Golden, H. Wang, and M. Goldenberg. Gri-Mech 2.11, http://www.me.berkeley.edu/gri_mech/.

[25] L.M.T. Somers. *The simulation of flat flames with detailed and reduced chemical models*. PhD thesis, Technical University of Eindhoven, 1994.

[26] N. Peters. Laminar diffusion flamelet models in non-premixed turbulent combustion. *Progress in Energy and Combustion Science*, 10:319–339, 1984.

[27] N. Peters. Laminar flamelet concepts in turbulent combustion. In *Proceedings of the Twenty-First Symposium (International) on Combustion*, pages 1231–1250, 1986.

[28] P.H. Gaskell and A.K.C. Lau. Curvature-compensed convective transport: SMART, a new boundedness-preserving transport algorithm. *International Journal for Numerical Methods in Fluids*, 8:617–641, 1988.

[29] S.V. Patankar. *Numerical heat transfer and fluid flow*. Hemiosphere Publishing Corporation, 1980.

[30] B.R. Hutchinson and G.D.Raithby. A multigrid method based on the additive correction strategy. *Numerical Heat Transfer, Part B*, 9:511–537, 1986.

[31] J.B. Vos. Calculating turbulent reating flows using finite chemical kinetics. *AIAA Journal*, 25(10):1365–1372, 1986.

[32] O. Holm-Chistensen, I.P. Jones, N.S. Wilkes, B.A. Splawski, P.J. Stopford, B. Creemers, C.J.A. Pulles, and D.F. Fletcher. The solution of coupled flow and chemistry problems. *Progress in Computational Fluid Dynamics*, 1:43–49, 2001.

[33] J. Cadafalch, A. Oliva, C.D. Pérez-Segarra, M. Costa, and J. Salom. Comparative study of conservative and nonconservative interpolation schemes for the domain decomposition method on laminar incompressible flows. *Numerical Heat Transfer, Part B*, 35(1):65–84, 1999.

[34] R. Cònsul, C.D. Pérez-Segarra, J. Cadafalch, M. Soria, and A. Oliva. Numerical analysis of laminar flames using the domain decomposition method. In *Proceedings of the Fourth European Computational Fluid Dynamics Conference (ECCOMAS CFD)*, volume 1.2, pages 996–1001, 1998.

[35] J. Cadafalch, C.D. Pérez-Segarra, M. Sòria, and A. Oliva. Fully conservative multiblock method for the resolution of turbulent incompressible flows. In *Proceedings of the Fourth European Computational Fluid Dynamics Conference (ECCOMAS CFD)*, volume 1.2, pages 1234–1239, 1998.

[36] C.S. McEnally, Ü.Ö. Köylü, L.D. Pfefferle, and Rosner D.E. Soot volume fraction and temperature measurements in laminar nonpremixed flames using thermocouples. *Combustion and Flame*, 109:701–720, 1997.

[37] C.S. McEnally and L.D. Pfefferle. Experimental study of nonfuel hydrocarbon concentrations in coflowing partially premixed methane/air flames. *Combustion and Flame*, 118:619–632, 1999.

[38] B.A.V. Bennett, J. Fielding, R.J. Mauro, M.B. Long, and M.D. Smooke. A comparison of the structures of lean and rich axisymmetric laminar bunsen flames: application of local rectangular refinement solution-adaptive gridding. *Combustion Theory and Modelling*, 3:657–687, 1999.

[39] R.L.G.M. Eggels. *Modelling of Combustion Processes and NO Formation with Reduced Reaction Mechanisms*. PhD thesis, Technical University of Eindhoven, 1996.

[40] J. Warnatz, U. Maas, and Dibble R.W. *Combustion*. Springer-Berlag, 1996.

[41] J.P. Gore and N.J. Zhan. NO_x emission and major species concentrations in partially premixed laminar methane/air co-flow jet flames. *Combustion and Flame*, 105:414–427, 1996.

[42] C.P. Chou, J.Y. Chen, C.G Yam, and K.D. Marx. Numerical modeling of NO formation in laminar Bunsen flames - A flamelet approach. *Combustion and Flame*, 114:420–435, 1998.

[43] T. Takagi and Z. Xu. Numerical analysis of laminar diffusion flames-effects of preferential diffusion of heat and species. *Combustion and Flame*, 96:50–59, 1994.

Chapter 6

Concluding Remarks and Future Actions

This thesis presents the most relevant research work carried out on combustion modeling during the last years at CTTC (Centre Tecnològic de Transferència de Calor, *Heat and Mass Transfer Technological Center*). Being the first thesis in combustion topics developed in our Center, initially the research work was planned as more general as possible, and as a challenge for our Group on the initiation to this complex phenomena. Taking into account the know-how of our Group in numerical methods for heat and mass transfer, the first main objective planned was to look deeply into combustion fundamentals and to develop rigorous and efficient numerical multidimensional simulations of laminar flames. In fact, and due to the considerable difficulties inherent to combustion modeling that have had to be overcome, this first objective has supposed the major part of the research work developed in this thesis, limiting the analysis of the wide range of combustion problems to the detailed numerical simulation of laminar flames and the analysis of some of their fundamental aspects. Research on laminar flames was chosen because of their scientific and industrial interest. Detailed numerical simulations of laminar flames are being used for the design and optimization of industrial equipment (e.g. domestic gas burners), and for the understanding and modeling of more complex flows (e.g. turbulent flames) and pollutant formation. As a result of the research work carried out in this thesis, contributions to the detailed analysis of reactive flows, and specifically methane/air laminar flames, have been carried out.

The thesis is organized in four main chapters. In chapter 2, the mathematical fundamentals on heat and mass transfer are posed. The formulation described is limited to gaseous mixtures giving special emphasis to the derivation of the transport equations and to the modeling of molecular fluxes. Continuum mechanics and kinetic theory treatments have been compared in order to relate detailed molecular fluxes formulations available only for kinetic theory.

Chapter 3 introduces chemical kinetic fundamentals and summarizes the differ-

ent levels of chemical approaches employed on the modeling of combustion kinetics. Most detailed approaches are described pointing out methane combustion. Research accounting for methane combustion is primarily carried out due to its major concentration in natural gas, one of the most employed fuels in industrial applications. Main strategies to reduce the considerable complexity of combustion mechanisms and to consider them in problems of industrial interest are pointed out.

Main contributions of this thesis are given in chapters 4 and 5. Although, main conclusions of both works are included in the chapters itselves, they are hereafter highlighted. Chapter 4, summarizes most of the work done to develop a competitive an accurate numerical methodology for reactive flow analysis. A parallel algorithm for the detailed multidimensional numerical simulation of laminar flames, able to work efficiently with loosely coupled computers, is presented. The algorithm has been developed for a proper performance in this kind of parallel computers, taking advantage of the main attributes which present these so-called *Beowulf clusters*: considerable lower cost, being the computing power and RAM memory similar to parallel supercomputers. Implicit numerical difficulties in the simulation of reactive flows that imply a considerable computational cost, stiffness of the governing equations and the presence of high gradients in flame fronts, where a large number of grid points must be considered, have been overcome by means of the employment of pseudo-time splitting techniques [1] and the domain decomposition method [2][3][4]. The latter technique is also used to parallelize the code, assigning one or several subdomains to different CPUs [5]. The development of this algorithm has supposed that numerical results with a huge number of reactions and chemical species have been possible to be obtained with reasonable computational costs. Problems that were unexpected to be solved at the beginnings of the thesis, can be nowadays simulated [6] [7][8].

Chapter 4 also accounts for one of the most relevant topics in CFD simulations that has recently focused the attention of the scientific community, the verification of the numerical results. A post-processing procedure developed by the CTTC [9], based on the generalized Richardson extrapolation for h-refinement studies and on the Grid Convergence Index (GCI), has been used in order to establish a criteria about the sensitivity of the simulation to the computational model parameters that account for the discretization: the mesh spacing and the order of accuracy. Numerical solutions presented in this thesis have been submitted to the commented verification procedure. Discretizations with uncertainty estimates are chosen to perform parametric studies with an appropriate ratio between accuracy and computational cost.

The numerical infrastructure commented above has been employed to analyze fundamental aspects of partially premixed co-flow methane/air laminar flames. These studies, presented in chapter 5, are mainly focused on the adequacy of several mathematical approaches for the modeling of laminar flames (chemical mechanisms, molecular transport modeling, radiant heat exchange, boundary conditions, ...), and on the

influence of partially premixing to main flame attributes. Special attention has been given to pollutant emission, specifically carbon monoxide and nitrogen oxides formation. Experimental data available in the scientific literature have been compared to the numerical predictions. Main conclusions about the appropriateness of the mathematical approaches are described in detail in chapter's conclusions. Globally, and for the most detailed simulations, excellent agreement has been obtained with experimental measurements. Quantitative results and qualitative trends are shown.

Main objectives of the thesis have been considered to be accomplished. Combustion phenomena fundamentals have been introduced, a numerical infrastructure for the detailed numerical simulations of reactive flows have been developed, and methane/air laminar flames have been analyzed acquiring experience on their modeling and knowledge about their main characteristics. Nevertheless, and in order to improve the level of accuracy of the mathematical models considered in this thesis, work in progress and future actions are described in the next section.

Numerical experience in the modeling of combustion problems acquired throughout the development of this thesis, and the know-how on turbulence modeling of our Group, is expected to concur in the modeling of turbulent combustion problems. In the nearer future, special attention will be given to such complex phenomena. The strategies of our Group in this research area, in which the author have also been working during the development of this thesis, will be commented.

Future Actions

As future actions in **laminar flames**, and as a direct continuation of the research presented in this thesis, two main aspects are foreseen: improve the performance of the numerical methods and consider more detailed mathematical models.

Although they are not included in this work, one-dimensional numerical simulations of burner-stabilized premixed flames and non-premixed counterflow flames have also been analyzed. For these flames, a fully coupled method (i.e. Modified Damped Newton's method) has been employed on the solution of the resulting set of discretized equations. The main feature of this method is its better convergence ratio respect to segregated algorithms for good enough initial estimates. Improved ratios of convergence were obtained [3]. This fact, motivated us to employ the method for two-dimensional and even three-dimensional combustion problems. The Group has dedicated some effort to this purpose. However, numerical difficulties arisen, enabling the employment of this method in a robust way. Although many authors use this kind of techniques to solve combustion problems, numerical instabilities and difficulties of the method are recognized for the CFD community.

Related to mathematical modeling of laminar flames, multicomponent transport modeling is expected to be considered in future works. Mixture-averaged formulations

employed in this thesis will be compared to a more detailed evaluation. On the other hand, more accurate radiant exchange models are planned to be considered. In the last years, CTTC has been working on the resolution of Radiative Transfer Equation (RTE) with the *Discrete Ordinates Method (DOM)*. The resolution of RTE equation, has allowed a detailed evaluation of radiant heat exchange in participating media. Numerical studies have been mainly focused on the resolution of natural convection in three-dimensional enclosures [10]. Our purpose in a near future is to simulate combustion problems, where the influence of radiant heat exchange has been shown to have an important relevance, solving RTE equation. Considering in this way, effects of absorption and scattering of the medium, together with a more detailed evaluation of the influence of the surrounding walls. Partially premixed methane/air flames presented in chapter 5 are expected to be numerically simulated using DOM method.

On the other hand, simplified mathematical formulations to be used in problems of industrial interest are expected to be developed. Among these mathematical models, nowadays our Group is working in *flamelet* modeling. The laminar flamelet concept assumes fast chemistry (chemical time scales much shorter than convection-diffusion ones) and that combustion takes place in a thin layer in a one-dimensional manner perpendicular to the flame front. Assuming unity Lewis number for all species and considering the concepts of non-reacting variable (mixture fraction for non-premixed flames) and scalar dissipation rate, one dimensional flamelet equations can be derived. Given a chemical model, these equations can be solved in a pre-processing task and look-up tables are build. The main attribute of this kind of models is the considerable reduction of the computational costs of the numerical simulations, and also its application to the numerical simulation of turbulent flows hereafter commented.

In most industrial equipment, combustion nearly always takes place within a turbulence flow field to increase the mixing process and thereby enhance combustion. In **turbulent combustion**, the complex phenomena involved due to the structure of the flow and the presence of complex kinetic mechanisms, make the development of accurate mathematical models an extremely difficult task. Research on this area is one of the most attractive challenges of scientific community for the next decades. An accurate solution of laminar flows, as those presented in this thesis, are one of the most important ingredients to succeed with an appropriate modeling of turbulent flames. Furthermore, we do not have to forget inherent difficulties of non-reactive turbulent flows simulations. Basic research in this topic is also one of the most important areas of CFD community. In this way, turbulent combustion mixes two extremely complex phenomena, turbulence and chemistry, the strong feed-back between the flow field and chemical reactions, complicates even more the accurate modeling and numerical resolution of this phenomena and therefore its application to problems of industrial interest.

One of our objectives for the next years is the numerical simulation of turbulent flames. In fact, during the thesis some work has been developed in incompressible inert flows, and some experience in turbulence modeling have been acquired by the author [11] [12]. Although some preliminary results of turbulent non-premixed flames have also been recently obtained, we have decided not to include them in this thesis, waiting for improved analysis in a near future.

As we have commented above, one of the most important task before taking into account chemical reactions in a turbulent flow, is the modeling of inert turbulent problems. In this sense, CTTC has been given and still gives an especial attention to the mathematical formulation and numerical resolution of turbulent flows. Numerical simulations of turbulent flows, have their maximum level of accuracy when what is known as *Direct Numerical Simulation (DNS)* is considered. In these simulations, all temporal and spatial time scales are solved without the consideration of further empirical data. Navier-Stokes equations are solved over fine grids and considering extremely small time steps. However, nowadays numerical DNS simulations are restricted to few academic problems due to the huge computational cost that they involve. Recent research in CTTC, taking advantage of enhanced parallelization strategies, have allowed the resolution of turbulent flows in two-dimensional and three-dimensional enclosures (see for example [13]). DNS simulations are going to be used as benchmark solutions for the development and testing of mathematical models that with less computational resources could be able to model turbulent flows involved in problems of engineering interest.

Turbulence modeling is based on the employment of statistical treatments of the governing equations. In general, we can distinguish between two main modeling strategies: i) *Reynolds Averaged Navier-Stokes Simulations (RANS)*: based on the time averaging of Navier-Stokes equations; ii) and *Large Eddy Simulation (LES)*: where a volumetric average of the governing equations is done filtering the smallest scales of turbulence. Both methodologies deserve the interest of the CFD community. While RANS methods are the most employed for engineering purposes, LES techniques appear to bridge the gap between the most detailed DNS simulations and RANS models. During the last decade, CTTC has been given an special attention to RANS modeling. Low-Reynolds number two-equations models have been taken into account on the analysis of mixed and forced convection problems. In a short and mid terms, we have the intention to look deeper into these kind of modelizations. Non-linear eddy viscosity models in order to overcome isotropic considerations of standard two-equation models are being analyzed. In this sense, also *Algebraic Reynolds Stress Models (ARSM)* and *Differentially Reynolds Stress Models (DRSM)* will be studied. On the other hand, and in a mid-term, LES simulations are also planned to be taken into account.

Turbulent combustion modeling will be based on previous extensive works on non-

reactive flows. Advances in these previous studies will benefit directly the accuracy of combustion simulations. For detailed DNS simulations of turbulent flames, lower time steps are expected to be considered due to the smallest time-scales that appear in the kinetic mechanisms. Related to the own particularities of the modeling of turbulent reactive flows, two main aspects should be pointed out. The first accounts for the density fluctuations that characterizes reactive flows due to the high temperature and concentration gradients involved. When RANS methods are considered, *Favre-averaged* is recommended instead of *time-averaged* governing equations. The other aspect is the treatment of the chemical production/consumption terms. The mathematical formulation of these terms, involving species concentration products together with their exponential temperature dependence (i.e. Arrhenius Law), make difficult a statistical treatment. Most relevant work in turbulent combustion is done specially in the treatment of these rates.

The most common approach used on the modeling of turbulent combustion problems, specially for engineering purposes, are the *Eddy-Break-Up* models. These models are empirical formulations of the reaction rates considering fast chemistry by means of global reactions and assuming that chemical reactions are controlled by the mixing process defined by the turbulence time scale. Improved modelizations are statistical approaches that evaluate mean reaction rates integrating the chemical approach considered (i.e. from reduced to detailed mechanisms) by means of the definition of what is known as *Probability Density Functions (PDF)*. PDF functions can be assumed or calculated. Assumed PDF depends strongly on the flow field, and changes according to the problem of interest. Although the accuracy of assumed PDF functions is quiet limited, nowadays is probably the most employed approach used by the scientific community. A higher level of modeling appears when these PDF functions are evaluated. The most elegant way is the solution of a PDF-transport equation derived from species conservation equations. The considerable computational costs of these detailed simulations, reduces their application to basic research problems.

As future actions in this topic, Eddy-Break-Up models will be taken into account. In fact, they have already been employed on preliminary simulations of turbulent flames. Once experience on turbulent modeling has been acquired, statistical approaches are expected to be considered in a mid-term. These statistic approaches will be based on assumed PDFs and on the treatment of the chemical reactions considering the laminar *flamelet* concept. The flamelet concept in turbulent combustion views a turbulent flame as an ensemble of thin laminar locally one-dimensional structures embedded within the turbulent flow field.

References

[1] R. Cònsul, C.D. Pérez-Segarra, and A. Oliva. Numerical studies on laminar premixed and diffusion flames. In *Proceedings of the 10th Conference on Numerical Methods in Thermal Problems*, pages 198–209, 1997.

[2] J. Cadafalch, J. Salom, M. Costa, and A. Oliva. Domain decomposition as a method for the parallel computing of laminar incompressible flows. In *Proceedings of the Second European Congress on Computational Methods in Applied Sciences and Engineering (ECCOMAS)*, pages 845–851, 1996.

[3] R. Cònsul, C.D. Pérez-Segarra, J. Cadafalch, M. Soria, and A. Oliva. Numerical analysis of laminar flames using the domain decomposition method. In *Proceedings of the Fourth European Computational Fluid Dynamics Conference (ECCOMAS CFD)*, volume 1.2, pages 996–1001, 1998.

[4] J. Cadafalch, A. Oliva, C.D. Pérez-Segarra, M. Costa, and J. Salom. Comparative study of conservative and nonconservative interpolation schemes for the domain decomposition method on laminar incompressible flows. *Numerical Heat Transfer, Part B*, 35(1):65–84, 1999.

[5] M. Soria, J. Cadafalch, R. Cònsul, K. Claramunt, and A. Oliva. A parallel algorithm for the detailed numerical simulation of reactive flows. In *Proceedings of the 1999 Parallel Computational Fluid Dynamics Conference*, pages 389–396, 1999.

[6] R. Cònsul, K. Claramunt, C.D. Pérez-Segarra, and A. Oliva. Simulación numérica de procesos de difusión de espécies inertes y reactivas. In *Anales de Ingeniería Mecánica (Revista de la Asociación Española de Ingeniería Mecánica, Año 12)*, volume 3, pages 1697–1702, 2000.

[7] K. Claramunt, R. Cònsul, C.D. Pérez-Segarra, and A. Oliva. Analysis of some numerical treatments on the numerical simulation of reactive flows. In *Proceedings of the 8th International Conference on Numerical Combustion*, 2000.

[8] K. Claramunt, R. Cònsul, C.D. Pérez-Segarra, and A. Oliva. Analysis of some numerical treatments on the numerical simulation of laminar flames. In *Book of abstracts of the workshop on Computational Methods for Multidimensional Reactive Flows (COMREF 2000)*, 2000.

[9] J. Cadafalch, C.D. Pérez-Segarra, R. Cònsul, and A. Oliva. Verification of finite volume computations on steady state fluid flow and heat transfer. *Journal of Fluids Engineering*, 124:11–21, 2002.

[10] G. Colomer, M. Costa, R. Cònsul, and A. Oliva. Radiant exchange in domains with obstacles using the discrete ordinates method. In *Proceedings of the Third European Congress on Computational Methods in Applied Sciences and Engineering (ECCOMAS)*, pages 1–20, 2000.

[11] C.D. Pérez-Segarra, A. Oliva, and R. Cònsul. Analysis of some numerical aspects in the solution of the navier-stokes equations using non-orthogonal collocated finite-volume methods. In *Proceedings of the Second European Congress on Computational Methods in Applied Sciences and Engineering (ECCOMAS)*, pages 505–511, 1996.

[12] R. Cònsul, C.D. Pérez-Segarra, J. Cadafalch, and K. Claramunt. Numerical experiments on turbulent forced convection using low reynolds number two-equation models. In *Proceedings of the Third European Congress on Computational Methods in Applied Sciences and Engineering (ECCOMAS)*, pages 1–19, 2000.

[13] M. Soria, C.D. Pérez-Segarra, and A. Oliva. A direct parallel algorithm for the efficient solution of the pressure-correction equation of incompressible flow problems using loosely coupled computers. *Numerical Heat Transfer, Part B*, 41(2):117–138, 2002.

Apendix

Kinetic mechanisms

The kinetic mechanisms presented in this appendix are the product of the computational and experimental research sponsored by the Gas Research Institute and carried out at the University of California at Berkeley, Standford University, The University of Texas at Austion and SRI International.

GRI-Mech is one of the most optimised detailed chemical reaction mechanism capable of the best representation of natural gas flames and ignition. GRI-Mech is basically a list of elementary reactions together with their rate constants, obtained after comprehensive studies, and tested for different combustion problems.

Nowadays, GRI-Mech offers its last release, GRI-Mech 3.0. In this thesis, previous realeses have been also used, specifically GRI-Mech 2.11 that is no longer provided. In this appendices both releases are listed.

Further information about GRI-Mech and its applications is given at www.berkeley.edu/gri-mech.

GRI-Mech v. 2.11

No.	Reaction	A	β	E_a
1.	$2O + M \Leftrightarrow O_2 + M^a$	$1.200e+17$	-1.00	$0.000e+00$
2.	$O + H + M \Leftrightarrow OH + M^b$	$5.000e+17$	-1.00	$0.000e+00$
3.	$O + H_2 \Leftrightarrow H + OH$	$5.000e+04$	2.67	$6.290e+03$
4.	$O + HO_2 \Leftrightarrow O_2 + OH$	$2.000e+13$	0.00	$0.000e+00$
5.	$O + H_2O_2 \Leftrightarrow OH + HO_2$	$9.630e+06$	2.00	$4.000e+03$
6.	$O + CH \Leftrightarrow CO + H$	$5.700e+13$	0.00	$0.000e+00$
7.	$O + CH_2 \Leftrightarrow H + HCO$	$8.000e+13$	0.00	$0.000e+00$
8.	$O + CH_2(S) \Leftrightarrow H_2 + CO$	$1.500e+13$	0.00	$0.000e+00$
9.	$O + CH_2(S) \Leftrightarrow H + HCO$	$1.500e+13$	0.00	$0.000e+00$
10.	$O + CH_3 \Leftrightarrow H + CH_2O$	$8.430e+13$	0.00	$0.000e+00$
11.	$O + CH_4 \Leftrightarrow OH + CH_3$	$1.020e+09$	1.50	$8.600e+03$
12.	$O + CO + M \Leftrightarrow CO_2 + M^c$	$6.020e+14$	0.00	$3.000e+03$
13.	$O + HCO \Leftrightarrow CO + OH$	$3.000e+13$	0.00	$0.000e+00$
14.	$O + HCO \Leftrightarrow CO_2 + H$	$3.000e+13$	0.00	$0.000e+00$
15.	$O + CH_2O \Leftrightarrow OH + HCO$	$3.900e+13$	0.00	$3.540e+03$

continued on next page

continued from previous page

16.	$O + CH_2OH \Leftrightarrow OH + CH_2O$	$1.000e+13$	0.00	$0.000e+00$
17.	$O + CH_3O \Leftrightarrow OH + CH_2O$	$1.000e+13$	0.00	$0.000e+00$
18.	$O + CH_3OH \Leftrightarrow OH + CH_2OH$	$3.880e+05$	2.50	$3.100e+03$
19.	$O + CH_3OH \Leftrightarrow OH + CH_3O$	$1.300e+05$	2.50	$5.000e+03$
20.	$O + C_2H \Leftrightarrow CO + CH$	$5.000e+13$	0.00	$0.000e+00$
21.	$O + C_2H_2 \Leftrightarrow H + HCCO$	$1.020e+07$	2.00	$1.900e+03$
22.	$O + C_2H_2 \Leftrightarrow OH + C_2H$	$4.600e+19$	-1.41	$2.895e+04$
23.	$O + C_2H_2 \Leftrightarrow CO + CH_2$	$1.020e+07$	2.00	$1.900e+03$
24.	$O + C_2H_3 \Leftrightarrow H + CH_2CO$	$3.000e+13$	0.00	$0.000e+00$
25.	$O + C_2H_4 \Leftrightarrow HCO + CH_3$	$1.920e+07$	1.83	$2.200e+02$
26.	$O + C_2H_5 \Leftrightarrow CH_3 + CH_2O$	$1.320e+14$	0.00	$0.000e+00$
27.	$O + C_2H_6 \Leftrightarrow OH + C_2H_5$	$8.980e+07$	1.92	$5.690e+03$
28.	$O + HCCO \Leftrightarrow 2CO + H$	$1.000e+14$	0.00	$0.000e+00$
29.	$O + CH_2CO \Leftrightarrow OH + HCCO$	$1.000e+13$	0.00	$8.000e+03$
30.	$O + CH_2CO \Leftrightarrow CO_2 + CH_2$	$1.750e+12$	0.00	$1.350e+03$
31.	$O_2 + CO \Leftrightarrow O + CO_2$	$2.500e+12$	0.00	$4.780e+04$
32.	$O_2 + CH_2O \Leftrightarrow HO_2 + HCO$	$1.000e+14$	0.00	$4.000e+04$
33.	$O_2 + H + M \Leftrightarrow HO_2 + M^d$	$2.800e+18$	-0.86	$0.000e+00$
34.	$2O_2 + H \Leftrightarrow O_2 + HO_2$	$3.000e+20$	-1.72	$0.000e+00$
35.	$O_2 + H_2O + H \Leftrightarrow H_2O + HO_2$	$9.380e+18$	-0.76	$0.000e+00$
36.	$O_2 + H + N_2 \Leftrightarrow HO_2 + N_2$	$3.750e+20$	-1.72	$0.000e+00$
37.	$O_2 + AR + H \Leftrightarrow AR + HO_2$	$7.000e+17$	-0.80	$0.000e+00$
38.	$O_2 + H \Leftrightarrow O + OH$	$8.300e+13$	0.00	$1.441e+04$
39.	$2H + M \Leftrightarrow H_2 + M^e$	$1.000e+18$	-1.00	$0.000e+00$
40.	$H_2 + 2H \Leftrightarrow 2H_2$	$9.000e+16$	-0.60	$0.000e+00$
41.	$H_2O + 2H \Leftrightarrow H_2 + H_2O$	$6.000e+19$	-1.25	$0.000e+00$
42.	$CO_2 + 2H \Leftrightarrow H_2 + CO_2$	$5.500e+20$	-2.00	$0.000e+00$
43.	$H + OH + M \Leftrightarrow H_2O + M^f$	$2.200e+22$	-2.00	$0.000e+00$
44.	$H + HO_2 \Leftrightarrow O + H_2O$	$3.970e+12$	0.00	$6.710e+02$
45.	$H + HO_2 \Leftrightarrow O_2 + H_2$	$2.800e+13$	0.00	$1.068e+03$
46.	$H + HO_2 \Leftrightarrow 2OH$	$1.340e+14$	0.00	$6.350e+02$
47.	$H + H_2O_2 \Leftrightarrow H_2 + HO_2$	$1.210e+07$	2.00	$5.200e+03$
48.	$H + H_2O_2 \Leftrightarrow H_2O + OH$	$1.000e+13$	0.00	$3.600e+03$
49.	$H + CH \Leftrightarrow H_2 + C$	$1.100e+14$	0.00	$0.000e+00$
50.	$H + CH_2(+M) \Leftrightarrow CH_3(+M^b)$	$2.500e+16$	-0.80	$0.000e+00$
	Low Pressure Limit :	$3.200e+27$	-3.14	$1.230e+03$
	Troe Centering :			
	$c1 : 6.800e-01$; $c2 : 7.800e+01$			
	$c2 : 1.995e+03$; $c3 : 5.590e+03$			
51.	$H + CH_2(S) \Leftrightarrow H_2 + CH$	$3.000e+13$	0.00	$0.000e+00$
52.	$H + CH_3(+M) \Leftrightarrow CH_4(+M^b)$	$1.270e+16$	-0.63	$3.830e+02$
	Low Pressure Limit :	$2.477e+33$	-4.76	$2.440e+03$
	Troe Centering :			
	$c1 : 7.830e-01$; $c2 : 7.400e+01$			
	$c2 : 2.941e+03$; $c3 : 6.964e+03$			
53.	$CH_4 + H \Leftrightarrow H_2 + CH_3$	$6.600e+08$	1.62	$1.084e+04$
54.	$H + HCO(+M) \Leftrightarrow CH_2O(+M^b)$	$1.090e+12$	0.48	$-2.600e+02$
	Low Pressure Limit :	$1.350e+24$	-2.57	$1.425e+03$
	Troe Centering :			
	$c1 : 7.824e-01$; $c2 : 2.710e+02$			
	$c2 : 2.755e+03$; $c3 : 6.570e+03$			
55.	$H + HCO \Leftrightarrow H_2 + CO$	$7.340e+13$	0.00	$0.000e+00$
56.	$H + CH_2O(+M) \Leftrightarrow CH_2OH(+M^g)$	$5.400e+11$	0.45	$3.600e+03$
	Low Pressure Limit :	$1.270e+32$	-4.82	$6.530e+03$
	Troe Centering :			
	$c1 : 7.187e-01$; $c2 : 1.030e+02$			
	$c2 : 1.291e+03$; $c3 : 4.160e+03$			
57.	$H + CH_2O(+M) \Leftrightarrow CH_3O(+M^g)$	$5.400e+11$	0.45	$2.600e+03$

continued on next page

continued from previous page

	$Low\ Pressure\ Limit:$	$2.200e+30$	-4.80	$5.560e+03$
	$Troe\ Centering:$			
	$c1: 7.580e-01;\ c2: 9.400e+01$			
	$c2: 1.555e+03;\ c3: 4.200e+03$			
58.	$H + CH_2O \Leftrightarrow H_2 + HCO$	$2.300e+10$	1.05	$3.275e+03$
59.	$H + CH_2OH(+M) \Leftrightarrow CH_3OH(+M^g)$	$1.800e+13$	0.00	$0.000e+00$
	$Low\ Pressure\ Limit:$	$3.000e+31$	-4.80	$3.300e+03$
	$Troe\ Centering:$			
	$c1: 7.679e-01;\ c2: 3.380e+02$			
	$c2: 1.812e+03;\ c3: 5.081e+03$			
60.	$H + CH_2OH \Leftrightarrow H_2 + CH_2O$	$2.000e+13$	0.00	$0.000e+00$
61.	$H + CH_2OH \Leftrightarrow OH + CH_3$	$1.200e+13$	0.00	$0.000e+00$
62.	$H + CH_2OH \Leftrightarrow H_2O + CH_2(S)$	$6.000e+12$	0.00	$0.000e+00$
63.	$H + CH_3O(+M) \Leftrightarrow CH_3OH(+M^g)$	$5.000e+13$	0.00	$0.000e+00$
	$Low\ Pressure\ Limit:$	$8.600e+28$	-4.00	$3.025e+03$
	$Troe\ Centering:$			
	$c1: 8.902e-01;\ c2: 1.440e+02$			
	$c2: 2.838e+03;\ c3: 4.557e+04$			
64.	$H + CH_3O \Leftrightarrow H + CH_2OH$	$3.400e+06$	1.60	$0.000e+00$
65.	$H + CH_3O \Leftrightarrow H_2 + CH_2O$	$2.000e+13$	0.00	$0.000e+00$
66.	$H + CH_3O \Leftrightarrow OH + CH_3$	$3.200e+13$	0.00	$0.000e+00$
67.	$H + CH_3O \Leftrightarrow H_2O + CH_2(S)$	$1.600e+13$	0.00	$0.000e+00$
68.	$H + CH_3OH \Leftrightarrow H_2 + CH_2OH$	$1.700e+07$	2.10	$4.870e+03$
69.	$H + CH_3OH \Leftrightarrow H_2 + CH_3O$	$4.200e+06$	2.10	$4.870e+03$
70.	$H + C_2H(+M) \Leftrightarrow C_2H_2(+M^b)$	$1.000e+17$	-1.00	$0.000e+00$
	$Low\ Pressure\ Limit:$	$3.750e+33$	-4.80	$1.900e+03$
	$Troe\ Centering:$			
	$c1: 6.464e-01;\ c2: 1.320e+02$			
	$c2: 1.315e+03;\ c3: 5.566e+03$			
71.	$H + C_2H_2(+M) \Leftrightarrow C_2H_3(+M^b)$	$5.600e+12$	0.00	$2.400e+03$
	$Low\ Pressure\ Limit:$	$3.800e+40$	-7.27	$7.220e+03$
	$Troe\ Centering:$			
	$c1: 7.507e-01;\ c2: 9.850e+01$			
	$c2: 1.302e+03;\ c3: 4.167e+03$			
72.	$H + C_2H_3(+M) \Leftrightarrow C_2H_4(+M^b)$	$6.080e+12$	0.27	$2.800e+02$
	$Low\ Pressure\ Limit:$	$1.400e+30$	-3.86	$3.320e+03$
	$Troe\ Centering:$			
	$c1: 7.820e-01;\ c2: 2.075e+02$			
	$c2: 2.663e+03;\ c3: 6.095e+03$			
73.	$H + C_2H_3 \Leftrightarrow H_2 + C_2H_2$	$3.000e+13$	0.00	$0.000e+00$
74.	$H + C_2H_4(+M) \Leftrightarrow C_2H_5(+M^b)$	$1.080e+12$	0.45	$1.820e+03$
	$Low\ Pressure\ Limit:$	$1.200e+42$	-7.62	$6.970e+03$
	$Troe\ Centering:$			
	$c1: 9.753e-01;\ c2: 2.100e+02$			
	$c2: 9.840e+02;\ c3: 4.374e+03$			
75.	$H + C_2H_4 \Leftrightarrow H_2 + C_2H_3$	$1.325e+06$	2.53	$1.224e+04$
76.	$H + C_2H_5(+M) \Leftrightarrow C_2H_6(+M^b)$	$5.210e+17$	-0.99	$1.580e+03$
	$Low\ Pressure\ Limit:$	$1.990e+41$	-7.08	$6.685e+03$
	$Troe\ Centering:$			
	$c1: 8.422e-01;\ c2: 1.250e+02$			
	$c2: 2.219e+03;\ c3: 6.882e+03$			
77.	$H + C_2H_5 \Leftrightarrow H_2 + C_2H_4$	$2.000e+12$	0.00	$0.000e+00$
78.	$C_2H_6 + H \Leftrightarrow H_2 + C_2H_5$	$1.150e+08$	1.90	$7.530e+03$
79.	$H + HCCO \Leftrightarrow CO + CH_2(S)$	$1.000e+14$	0.00	$0.000e+00$
80.	$H + CH_2CO \Leftrightarrow H_2 + HCCO$	$5.000e+13$	0.00	$8.000e+03$
81.	$H + CH_2CO \Leftrightarrow CO + CH_3$	$1.130e+13$	0.00	$3.428e+03$
82.	$H + HCCOH \Leftrightarrow H + CH_2CO$	$1.000e+13$	0.00	$0.000e+00$
83.	$H_2 + CO(+M) \Leftrightarrow CH_2O(+M^b)$	$4.300e+07$	1.50	$7.960e+04$

continued on next page

continued from previous page

	$Low\ Pressure\ Limit:$	$5.070e+27$	-3.42	$8.435e+04$
	$Troe\ Centering:$			
	$c1: 9.320e-01;\ c2: 1.970e+02$			
	$c2: 1.540e+03;\ c3: 1.030e+04$			
84.	$H_2 + OH \Leftrightarrow H_2O + H$	$2.160e+08$	1.51	$3.430e+03$
85.	$2OH(+M) \Leftrightarrow H_2O_2(+M^b)$	$7.400e+13$	-0.37	$0.000e+00$
	$Low\ Pressure\ Limit:$	$2.300e+18$	-0.90	$-1.700e+03$
	$Troe\ Centering:$			
	$c1: 7.346e-01;\ c2: 9.400e+01$			
	$c2: 1.756e+03;\ c3: 5.182e+03$			
86.	$2OH \Leftrightarrow O + H_2O$	$3.570e+04$	2.40	$-2.110e+03$
87.	$OH + HO_2 \Leftrightarrow O_2 + H_2O$	$2.900e+13$	0.00	$-5.000e+02$
88.	$OH + H_2O_2 \Leftrightarrow H_2O + HO_2$	$1.750e+12$	0.00	$3.200e+02$
89.	$OH + H_2O_2 \Leftrightarrow H_2O + HO_2$	$5.800e+14$	0.00	$9.560e+03$
90.	$OH + C \Leftrightarrow CO + H$	$5.000e+13$	0.00	$0.000e+00$
91.	$OH + CH \Leftrightarrow H + HCO$	$3.000e+13$	0.00	$0.000e+00$
92.	$OH + CH_2 \Leftrightarrow H + CH_2O$	$2.000e+13$	0.00	$0.000e+00$
93.	$OH + CH_2 \Leftrightarrow H_2O + CH$	$1.130e+07$	2.00	$3.000e+03$
94.	$OH + CH_2(S) \Leftrightarrow H + CH_2O$	$3.000e+13$	0.00	$0.000e+00$
95.	$OH + CH_3(+M) \Leftrightarrow CH_3OH(+M^g)$	$6.300e+13$	0.00	$0.000e+00$
	$Low\ Pressure\ Limit:$	$2.700e+38$	-6.30	$3.100e+03$
	$Troe\ Centering:$			
	$c1: 2.105e-01;\ c2: 8.350e+01$			
	$c2: 5.398e+03;\ c3: 8.370e+03$			
96.	$OH + CH_3 \Leftrightarrow H_2O + CH_2$	$5.600e+07$	1.60	$5.420e+03$
97.	$OH + CH_3 \Leftrightarrow H_2O + CH_2(S)$	$2.501e+13$	0.00	$0.000e+00$
98.	$CH_4 + OH \Leftrightarrow H_2O + CH_3$	$1.000e+08$	1.60	$3.120e+03$
99.	$CO + OH \Leftrightarrow CO_2 + H$	$4.760e+07$	1.23	$7.000e+01$
100.	$OH + HCO \Leftrightarrow H_2O + CO$	$5.000e+13$	0.00	$0.000e+00$
101.	$OH + CH_2O \Leftrightarrow H_2O + HCO$	$3.430e+09$	1.18	$-4.470e+02$
102.	$OH + CH_2OH \Leftrightarrow H_2O + CH_2O$	$5.000e+12$	0.00	$0.000e+00$
103.	$OH + CH_3O \Leftrightarrow H_2O + CH_2O$	$5.000e+12$	0.00	$0.000e+00$
104.	$OH + CH_3OH \Leftrightarrow H_2O + CH_2OH$	$1.440e+06$	2.00	$-8.400e+02$
105.	$OH + CH_3OH \Leftrightarrow H_2O + CH_3O$	$6.300e+06$	2.00	$1.500e+03$
106.	$OH + C_2H \Leftrightarrow H + HCCO$	$2.000e+13$	0.00	$0.000e+00$
107.	$OH + C_2H_2 \Leftrightarrow H + CH_2CO$	$2.180e-04$	4.50	$-1.000e+03$
108.	$OH + C_2H_2 \Leftrightarrow H + HCCOH$	$5.040e+05$	2.30	$1.350e+04$
109.	$OH + C_2H_2 \Leftrightarrow H_2O + C_2H$	$3.370e+07$	2.00	$1.400e+04$
110.	$OH + C_2H_2 \Leftrightarrow CO + CH_3$	$4.830e-04$	4.00	$-2.000e+03$
111.	$OH + C_2H_3 \Leftrightarrow H_2O + C_2H_2$	$5.000e+12$	0.00	$0.000e+00$
112.	$OH + C_2H_4 \Leftrightarrow H_2O + C_2H_3$	$3.600e+06$	2.00	$2.500e+03$
113.	$C_2H_6 + OH \Leftrightarrow H_2O + C_2H_5$	$3.540e+06$	2.12	$8.700e+02$
114.	$OH + CH_2CO \Leftrightarrow H_2O + HCCO$	$7.500e+12$	0.00	$2.000e+03$
115.	$2HO_2 \Leftrightarrow O_2 + H_2O_2$	$1.300e+11$	0.00	$-1.630e+03$
116.	$2HO_2 \Leftrightarrow O_2 + H_2O_2$	$4.200e+14$	0.00	$1.200e+04$
117.	$HO_2 + CH_2 \Leftrightarrow OH + CH_2O$	$2.000e+13$	0.00	$0.000e+00$
118.	$HO_2 + CH_3 \Leftrightarrow O_2 + CH_4$	$1.000e+12$	0.00	$0.000e+00$
119.	$HO_2 + CH_3 \Leftrightarrow OH + CH_3O$	$2.000e+13$	0.00	$0.000e+00$
120.	$CO + HO_2 \Leftrightarrow CO_2 + OH$	$1.500e+14$	0.00	$2.360e+04$
121.	$HO_2 + CH_2O \Leftrightarrow H_2O_2 + HCO$	$1.000e+12$	0.00	$8.000e+03$
122.	$O_2 + C \Leftrightarrow O + CO$	$5.800e+13$	0.00	$5.760e+02$
123.	$CH_2 + C \Leftrightarrow H + C_2H$	$5.000e+13$	0.00	$0.000e+00$
124.	$CH_3 + C \Leftrightarrow H + C_2H_2$	$5.000e+13$	0.00	$0.000e+00$
125.	$O_2 + CH \Leftrightarrow O + HCO$	$3.300e+13$	0.00	$0.000e+00$
126.	$H_2 + CH \Leftrightarrow H + CH_2$	$1.107e+08$	1.79	$1.670e+03$
127.	$H_2O + CH \Leftrightarrow H + CH_2O$	$1.713e+13$	0.00	$-7.550e+02$
128.	$CH + CH_2 \Leftrightarrow H + C_2H_2$	$4.000e+13$	0.00	$0.000e+00$
129.	$CH + CH_3 \Leftrightarrow H + C_2H_3$	$3.000e+13$	0.00	$0.000e+00$

continued on next page

continued from previous page

130.	$CH_4 + CH \Leftrightarrow H + C_2H_4$	$6.000e+13$	0.00	$0.000e+00$
131.	$CO + CH(+M) \Leftrightarrow HCCO(+M^b)$	$5.000e+13$	0.00	$0.000e+00$
	$Low\ Pressure\ Limit:$	$2.690e+28$	-3.74	$1.936e+03$
	$Troe\ Centering:$			
	$c1: 5.757e-01;\ c2: 2.370e+02$			
	$c2: 1.652e+03;\ c3: 5.069e+03$			
132.	$CO_2 + CH \Leftrightarrow CO + HCO$	$3.400e+12$	0.00	$6.900e+02$
133.	$CH + CH_2O \Leftrightarrow H + CH_2CO$	$9.460e+13$	0.00	$-5.150e+02$
134.	$CH + HCCO \Leftrightarrow CO + C_2H_2$	$5.000e+13$	0.00	$0.000e+00$
135.	$O_2 + CH_2 \Leftrightarrow OH + HCO$	$1.320e+13$	0.00	$1.500e+03$
136.	$H_2 + CH_2 \Leftrightarrow H + CH_3$	$5.000e+05$	2.00	$7.230e+03$
137.	$2CH_2 \Leftrightarrow H_2 + C_2H_2$	$3.200e+13$	0.00	$0.000e+00$
138.	$CH_2 + CH_3 \Leftrightarrow H + C_2H_4$	$4.000e+13$	0.00	$0.000e+00$
139.	$CH_4 + CH_2 \Leftrightarrow 2CH_3$	$2.460e+06$	2.00	$8.270e+03$
140.	$CO + CH_2(+M) \Leftrightarrow CH_2CO(+M^b)$	$8.100e+11$	0.50	$4.510e+03$
	$Low\ Pressure\ Limit:$	$2.690e+33$	-5.11	$7.095e+03$
	$Troe\ Centering:$			
	$c1: 5.907e-01;\ c2: 2.750e+02$			
	$c2: 1.226e+03;\ c3: 5.185e+03$			
141.	$CH_2 + HCCO \Leftrightarrow CO + C_2H_3$	$3.000e+13$	0.00	$0.000e+00$
142.	$CH_2(S) + N_2 \Leftrightarrow CH_2 + N_2$	$1.500e+13$	0.00	$6.000e+02$
143.	$AR + CH_2(S) \Leftrightarrow AR + CH_2$	$9.000e+12$	0.00	$6.000e+02$
144.	$O_2 + CH_2(S) \Leftrightarrow CO + H + OH$	$2.800e+13$	0.00	$0.000e+00$
145.	$O_2 + CH_2(S) \Leftrightarrow H_2O + CO$	$1.200e+13$	0.00	$0.000e+00$
146.	$H_2 + CH_2(S) \Leftrightarrow H + CH_3$	$7.000e+13$	0.00	$0.000e+00$
147.	$H_2O + CH_2(S)(+M) \Leftrightarrow CH_3OH(+M^g)$	$2.000e+13$	0.00	$0.000e+00$
	$Low\ Pressure\ Limit:$	$2.700e+38$	-6.30	$3.100e+03$
	$Troe\ Centering:$			
	$c1: 1.507e-01;\ c2: 1.340e+02$			
	$c2: 2.383e+03;\ c3: 7.265e+03$			
148.	$H_2O + CH_2(S) \Leftrightarrow H_2O + CH_2$	$3.000e+13$	0.00	$0.000e+00$
149.	$CH_2(S) + CH_3 \Leftrightarrow H + C_2H_4$	$1.200e+13$	0.00	$-5.700e+02$
150.	$CH_4 + CH_2(S) \Leftrightarrow 2CH_3$	$1.600e+13$	0.00	$-5.700e+02$
151.	$CO + CH_2(S) \Leftrightarrow CO + CH_2$	$9.000e+12$	0.00	$0.000e+00$
152.	$CO_2 + CH_2(S) \Leftrightarrow CO_2 + CH_2$	$7.000e+12$	0.00	$0.000e+00$
153.	$CO_2 + CH_2(S) \Leftrightarrow CO + CH_2O$	$1.400e+13$	0.00	$0.000e+00$
154.	$C_2H_6 + CH_2(S) \Leftrightarrow CH_3 + C_2H_5$	$4.000e+13$	0.00	$-5.500e+02$
155.	$O_2 + CH_3 \Leftrightarrow O + CH_3O$	$2.675e+13$	0.00	$2.880e+04$
156.	$O_2 + CH_3 \Leftrightarrow OH + CH_2O$	$3.600e+10$	0.00	$8.940e+03$
157.	$H_2O_2 + CH_3 \Leftrightarrow CH_4 + HO_2$	$2.450e+04$	2.47	$5.180e+03$
158.	$2CH_3(+M) \Leftrightarrow C_2H_6(+M^b)$	$2.120e+16$	-0.97	$6.200e+02$
	$Low\ Pressure\ Limit:$	$1.770e+50$	-9.67	$6.220e+03$
	$Troe\ Centering:$			
	$c1: 5.325e-01;\ c2: 1.510e+02$			
	$c2: 1.038e+03;\ c3: 4.970e+03$			
159.	$2CH_3 \Leftrightarrow H + C_2H_5$	$4.990e+12$	0.10	$1.060e+04$
160.	$HCO + CH_3 \Leftrightarrow CH_4 + CO$	$2.648e+13$	0.00	$0.000e+00$
161.	$CH_3 + CH_2O \Leftrightarrow CH_4 + HCO$	$3.320e+03$	2.81	$5.860e+03$
162.	$CH_3 + CH_3OH \Leftrightarrow CH_4 + CH_2OH$	$3.000e+07$	1.50	$9.940e+03$
163.	$CH_3 + CH_3OH \Leftrightarrow CH_4 + CH_3O$	$1.000e+07$	1.50	$9.940e+03$
164.	$CH_3 + C_2H_4 \Leftrightarrow CH_4 + C_2H_3$	$2.270e+05$	2.00	$9.200e+03$
165.	$C_2H_6 + CH_3 \Leftrightarrow CH_4 + C_2H_5$	$6.140e+06$	1.74	$1.045e+04$
166.	$H_2O + HCO \Leftrightarrow H_2O + CO + H$	$2.244e+18$	-1.00	$1.700e+04$
167.	$HCO + M \Leftrightarrow CO + H + M^h$	$1.870e+17$	-1.00	$1.700e+04$
168.	$O_2 + HCO \Leftrightarrow CO + HO_2$	$7.600e+12$	0.00	$4.000e+02$
169.	$O_2 + CH_2OH \Leftrightarrow HO_2 + CH_2O$	$1.800e+13$	0.00	$9.000e+02$
170.	$O_2 + CH_3O \Leftrightarrow HO_2 + CH_2O$	$4.280e-13$	7.60	$-3.530e+03$
171.	$O_2 + C_2H \Leftrightarrow CO + HCO$	$5.000e+13$	0.00	$1.500e+03$

continued on next page

continued from previous page

172.	$H_2 + C_2H \Leftrightarrow H + C_2H_2$	$4.070e+05$	2.40	$2.000e+02$
173.	$O_2 + C_2H_3 \Leftrightarrow HCO + CH_2O$	$3.980e+12$	0.00	$-2.400e+02$
174.	$C_2H_4(+M) \Leftrightarrow H_2 + C_2H_2(+M^b)$	$8.000e+12$	0.44	$8.877e+04$
	$Low\ Pressure\ Limit:$	$7.000e+50$	-9.31	$9.986e+04$
	$Troe\ Centering:$			
	$c1: 7.345e-01;\ c2: 1.800e+02$			
	$c2: 1.035e+03;\ c3: 5.417e+03$			
175.	$O_2 + C_2H_5 \Leftrightarrow HO_2 + C_2H_4$	$8.400e+11$	0.00	$3.875e+03$
176.	$O_2 + HCCO \Leftrightarrow 2CO + OH$	$1.600e+12$	0.00	$8.540e+02$
177.	$2HCCO \Leftrightarrow 2CO + C_2H_2$	$1.000e+13$	0.00	$0.000e+00$
178.	$N + NO \Leftrightarrow O + N_2$	$3.500e+13$	0.00	$3.300e+02$
179.	$O_2 + N \Leftrightarrow O + NO$	$2.650e+12$	0.00	$6.400e+03$
180.	$OH + N \Leftrightarrow H + NO$	$7.333e+13$	0.00	$1.120e+03$
181.	$O + N_2O \Leftrightarrow O_2 + N_2$	$1.400e+12$	0.00	$1.081e+04$
182.	$O + N_2O \Leftrightarrow 2NO$	$2.900e+13$	0.00	$2.315e+04$
183.	$H + N_2O \Leftrightarrow OH + N_2$	$4.400e+14$	0.00	$1.888e+04$
184.	$OH + N_2O \Leftrightarrow HO_2 + N_2$	$2.000e+12$	0.00	$2.106e+04$
185.	$N_2O(+M) \Leftrightarrow O + N_2(+M^b)$	$1.300e+11$	0.00	$5.962e+04$
	$Low\ Pressure\ Limit:$	$6.200e+14$	0.00	$5.610e+04$
186.	$HO_2 + NO \Leftrightarrow OH + NO_2$	$2.110e+12$	0.00	$-4.800e+02$
187.	$O + NO + M \Leftrightarrow NO_2 + M^b$	$1.060e+20$	-1.41	$0.000e+00$
188.	$O + NO_2 \Leftrightarrow O_2 + NO$	$3.900e+12$	0.00	$-2.400e+02$
189.	$H + NO_2 \Leftrightarrow OH + NO$	$1.320e+14$	0.00	$3.600e+02$
190.	$O + NH \Leftrightarrow H + NO$	$5.000e+13$	0.00	$0.000e+00$
191.	$H + NH \Leftrightarrow H_2 + N$	$3.200e+13$	0.00	$3.300e+02$
192.	$OH + NH \Leftrightarrow H + HNO$	$2.000e+13$	0.00	$0.000e+00$
193.	$OH + NH \Leftrightarrow H_2O + N$	$2.000e+09$	1.20	$0.000e+00$
194.	$O_2 + NH \Leftrightarrow O + HNO$	$4.610e+05$	2.00	$6.500e+03$
195.	$O_2 + NH \Leftrightarrow OH + NO$	$1.280e+06$	1.50	$1.000e+02$
196.	$N + NH \Leftrightarrow H + N_2$	$1.500e+13$	0.00	$0.000e+00$
197.	$H_2O + NH \Leftrightarrow H_2 + HNO$	$2.000e+13$	0.00	$1.385e+04$
198.	$NO + NH \Leftrightarrow OH + N_2$	$2.160e+13$	-0.23	$0.000e+00$
199.	$NO + NH \Leftrightarrow H + N_2O$	$4.160e+14$	-0.45	$0.000e+00$
200.	$O + NH_2 \Leftrightarrow OH + NH$	$7.000e+12$	0.00	$0.000e+00$
201.	$O + NH_2 \Leftrightarrow H + HNO$	$4.600e+13$	0.00	$0.000e+00$
202.	$H + NH_2 \Leftrightarrow H_2 + NH$	$4.000e+13$	0.00	$3.650e+03$
203.	$OH + NH_2 \Leftrightarrow H_2O + NH$	$9.000e+07$	1.50	$-4.600e+02$
204.	$NNH \Leftrightarrow H + N_2$	$3.300e+08$	0.00	$0.000e+00$
205.	$NNH + M \Leftrightarrow H + N_2 + M^b$	$1.300e+14$	-0.11	$4.980e+03$
206.	$O_2 + NNH \Leftrightarrow HO_2 + N_2$	$5.000e+12$	0.00	$0.000e+00$
207.	$O + NNH \Leftrightarrow OH + N_2$	$2.500e+13$	0.00	$0.000e+00$
208.	$O + NNH \Leftrightarrow NO + NH$	$7.000e+13$	0.00	$0.000e+00$
209.	$H + NNH \Leftrightarrow H_2 + N_2$	$5.000e+13$	0.00	$0.000e+00$
210.	$OH + NNH \Leftrightarrow H_2O + N_2$	$2.000e+13$	0.00	$0.000e+00$
211.	$CH_3 + NNH \Leftrightarrow CH_4 + N_2$	$2.500e+13$	0.00	$0.000e+00$
212.	$H + NO + M \Leftrightarrow HNO + M^b$	$8.950e+19$	-1.32	$7.400e+02$
213.	$O + HNO \Leftrightarrow OH + NO$	$2.500e+13$	0.00	$0.000e+00$
214.	$H + HNO \Leftrightarrow H_2 + NO$	$4.500e+11$	0.72	$6.600e+02$
215.	$OH + HNO \Leftrightarrow H_2O + NO$	$1.300e+07$	1.90	$-9.500e+02$
216.	$O_2 + HNO \Leftrightarrow HO_2 + NO$	$1.000e+13$	0.00	$1.300e+04$
217.	$O + CN \Leftrightarrow CO + N$	$7.700e+13$	0.00	$0.000e+00$
218.	$OH + CN \Leftrightarrow H + NCO$	$4.000e+13$	0.00	$0.000e+00$
219.	$H_2O + CN \Leftrightarrow OH + HCN$	$8.000e+12$	0.00	$7.460e+03$
220.	$O_2 + CN \Leftrightarrow O + NCO$	$6.140e+12$	0.00	$-4.400e+02$
221.	$H_2 + CN \Leftrightarrow H + HCN$	$2.100e+13$	0.00	$4.710e+03$
222.	$O + NCO \Leftrightarrow CO + NO$	$2.350e+13$	0.00	$0.000e+00$
223.	$H + NCO \Leftrightarrow CO + NH$	$5.400e+13$	0.00	$0.000e+00$
224.	$OH + NCO \Leftrightarrow CO + H + NO$	$2.500e+12$	0.00	$0.000e+00$

continued on next page

continued from previous page

225.	$N + NCO \Leftrightarrow CO + N_2$	$2.000e+13$	0.00	$0.000e+00$
226.	$O_2 + NCO \Leftrightarrow CO_2 + NO$	$2.000e+12$	0.00	$2.000e+04$
227.	$NCO + M \Leftrightarrow CO + N + M^b$	$8.800e+16$	-0.50	$4.800e+04$
228.	$NO + NCO \Leftrightarrow CO + N_2O$	$2.850e+17$	-1.52	$7.400e+02$
229.	$NO + NCO \Leftrightarrow CO_2 + N_2$	$5.700e+18$	-2.00	$8.000e+02$
230.	$HCN + M \Leftrightarrow H + CN + M^b$	$1.040e+29$	-3.30	$1.266e+05$
231.	$O + HCN \Leftrightarrow H + NCO$	$1.107e+04$	2.64	$4.980e+03$
232.	$O + HCN \Leftrightarrow CO + NH$	$2.767e+03$	2.64	$4.980e+03$
233.	$O + HCN \Leftrightarrow OH + CN$	$2.134e+09$	1.58	$2.660e+04$
234.	$OH + HCN \Leftrightarrow H + HOCN$	$1.100e+06$	2.03	$1.337e+04$
235.	$OH + HCN \Leftrightarrow H + HNCO$	$4.400e+03$	2.26	$6.400e+03$
236.	$OH + HCN \Leftrightarrow CO + NH_2$	$1.600e+02$	2.56	$9.000e+03$
237.	$H + HCN + M \Leftrightarrow H_2CN + M^b$	$1.400e+26$	-3.40	$1.900e+03$
238.	$N + H_2CN \Leftrightarrow CH_2 + N_2$	$6.000e+13$	0.00	$4.000e+02$
239.	$C + N_2 \Leftrightarrow N + CN$	$6.300e+13$	0.00	$4.602e+04$
240.	$CH + N_2 \Leftrightarrow N + HCN$	$2.857e+08$	1.10	$2.040e+04$
241.	$CH + N_2(+M) \Leftrightarrow HCNN(+M^b)$	$3.100e+12$	0.15	$0.000e+00$
	$Low\,Pressure\,Limit:$	$1.300e+25$	-3.16	$7.400e+02$
	$Troe\,Centering:$			
	$c1: 6.670e-01;\ c2: 2.350e+02$			
	$c2: 2.117e+03;\ c3: 4.536e+03$			
242.	$CH_2 + N_2 \Leftrightarrow NH + HCN$	$1.000e+13$	0.00	$7.400e+04$
243.	$CH_2(S) + N_2 \Leftrightarrow NH + HCN$	$1.000e+11$	0.00	$6.500e+04$
244.	$C + NO \Leftrightarrow O + CN$	$1.900e+13$	0.00	$0.000e+00$
245.	$C + NO \Leftrightarrow CO + N$	$2.900e+13$	0.00	$0.000e+00$
246.	$CH + NO \Leftrightarrow O + HCN$	$5.000e+13$	0.00	$0.000e+00$
247.	$CH + NO \Leftrightarrow H + NCO$	$2.000e+13$	0.00	$0.000e+00$
248.	$CH + NO \Leftrightarrow HCO + N$	$3.000e+13$	0.00	$0.000e+00$
249.	$CH_2 + NO \Leftrightarrow H + HNCO$	$3.100e+17$	-1.38	$1.270e+03$
250.	$CH_2 + NO \Leftrightarrow OH + HCN$	$2.900e+14$	-0.69	$7.600e+02$
251.	$CH_2 + NO \Leftrightarrow H + HCNO$	$3.800e+13$	-0.36	$5.800e+02$
252.	$CH_2(S) + NO \Leftrightarrow H + HNCO$	$3.100e+17$	-1.38	$1.270e+03$
253.	$CH_2(S) + NO \Leftrightarrow OH + HCN$	$2.900e+14$	-0.69	$7.600e+02$
254.	$CH_2(S) + NO \Leftrightarrow H + HCNO$	$3.800e+13$	-0.36	$5.800e+02$
255.	$CH_3 + NO \Leftrightarrow H_2O + HCN$	$9.600e+13$	0.00	$2.880e+04$
256.	$CH_3 + NO \Leftrightarrow OH + H_2CN$	$1.000e+12$	0.00	$2.175e+04$
257.	$O + HCNN \Leftrightarrow CO + H + N_2$	$2.200e+13$	0.00	$0.000e+00$
258.	$O + HCNN \Leftrightarrow NO + HCN$	$2.000e+12$	0.00	$0.000e+00$
259.	$O_2 + HCNN \Leftrightarrow O + HCO + N_2$	$1.200e+13$	0.00	$0.000e+00$
260.	$OH + HCNN \Leftrightarrow H + HCO + N_2$	$1.200e+13$	0.00	$0.000e+00$
261.	$H + HCNN \Leftrightarrow CH_2 + N_2$	$1.000e+14$	0.00	$0.000e+00$
262.	$O + HNCO \Leftrightarrow CO_2 + NH$	$9.800e+07$	1.41	$8.500e+03$
263.	$O + HNCO \Leftrightarrow CO + HNO$	$1.500e+08$	1.57	$4.400e+04$
264.	$O + HNCO \Leftrightarrow OH + NCO$	$2.200e+06$	2.11	$1.140e+04$
265.	$H + HNCO \Leftrightarrow CO + NH_2$	$2.250e+07$	1.70	$3.800e+03$
266.	$H + HNCO \Leftrightarrow H_2 + NCO$	$1.050e+05$	2.50	$1.330e+04$
267.	$OH + HNCO \Leftrightarrow H_2O + NCO$	$4.650e+12$	0.00	$6.850e+03$
268.	$OH + HNCO \Leftrightarrow CO_2 + NH_2$	$1.550e+12$	0.00	$6.850e+03$
269.	$HNCO + M \Leftrightarrow CO + NH + M^b$	$1.180e+16$	0.00	$8.472e+04$
270.	$H + HCNO \Leftrightarrow H + HNCO$	$2.100e+15$	-0.69	$2.850e+03$
271.	$H + HCNO \Leftrightarrow OH + HCN$	$2.700e+11$	0.18	$2.120e+03$
272.	$H + HCNO \Leftrightarrow CO + NH_2$	$1.700e+14$	-0.75	$2.890e+03$
273.	$H + HOCN \Leftrightarrow H + HNCO$	$2.000e+07$	2.00	$2.000e+03$
274.	$HCCO + NO \Leftrightarrow CO + HCNO$	$2.350e+13$	0.00	$0.000e+00$
275.	$CH_3 + N \Leftrightarrow H + H_2CN$	$6.100e+14$	-0.31	$2.900e+02$
276.	$CH_3 + N \Leftrightarrow H_2 + HCN$	$3.700e+12$	0.15	$-9.000e+01$
277.	$H + NH_3 \Leftrightarrow H_2 + NH_2$	$5.400e+05$	2.40	$9.915e+03$
278.	$OH + NH_3 \Leftrightarrow H_2O + NH_2$	$5.000e+07$	1.60	$9.550e+02$

continued on next page

continued from previous page

279.	$O + NH_3 \Leftrightarrow OH + NH_2$	$9.400e+06$	1.94	$6.460e+03$

Third Body efficiencies:

M^a $H_2 : 2.4;\ H_2O : 15.4;\ CH_4 : 2.0;\ CO : 1.8;\ CO_2 : 3.6;\ C_2H_6 : 3.0;\ AR : 0.8$

M^b $H_2 : 2.0;\ H_2O : 6.0;\ CH_4 : 2.0;\ CO : 1.5;\ CO_2 : 2.0;\ C_2H_6 : 3.0;\ AR : 0.7$

M^c $O_2 : 6.0;\ H_2 : 2.0;\ H_2O : 6.0;\ CH_4 : 2.0;\ CO : 1.5;\ CO_2 : 3.5;\ C_2H_6 : 3.0;\ AR : 0.5$

M^d $O_2 : 0.0;\ H_2O : 0.0;\ CO : 0.8;\ CO_2 : 1.5;\ C_2H_6 : 1.5;\ AR : 0.0;\ N_2 : 0.0$

M^e $H_2 : 0.0;\ H_2O : 0.0;\ CH_4 : 2.0;\ CO_2 : 0.0;\ C_2H_6 : 3.0;\ AR : 0.6;$

M^f $H_2 : 0.7;\ H_2O : 3.6;\ CH_4 : 2.0;\ C_2H_6 : 3.0;\ AR : 0.4;$

M^g $H_2 : 2.0;\ H_2O : 6.0;\ CH_4 : 2.0;\ CO : 1.5;\ CO_2 : 2.0;\ C_2H_6 : 3.0$

M^h $H_2 : 2.0;\ H_2O : 0.0;\ CH_4 : 2.0;\ CO : 1.5;\ CO_2 : 2.0;\ C_2H_6 : 3.0$

GRI-Mech v. 3.0

No.	Reaction	A	β	E_a
1.	$2O + M \Leftrightarrow O_2 + M^a$	$1.200e+17$	-1.00	$0.000e+00$
2.	$O + H + M \Leftrightarrow OH + M^b$	$5.000e+17$	-1.00	$0.000e+00$
3.	$O + H_2 \Leftrightarrow H + OH$	$3.870e+04$	2.70	$6.260e+03$
4.	$O + HO_2 \Leftrightarrow O_2 + OH$	$2.000e+13$	0.00	$0.000e+00$
5.	$O + H_2O_2 \Leftrightarrow OH + HO_2$	$9.630e+06$	2.00	$4.000e+03$
6.	$O + CH \Leftrightarrow CO + H$	$5.700e+13$	0.00	$0.000e+00$
7.	$O + CH_2 \Leftrightarrow H + HCO$	$8.000e+13$	0.00	$0.000e+00$
8.	$O + CH_2(S) \Leftrightarrow H_2 + CO$	$1.500e+13$	0.00	$0.000e+00$
9.	$O + CH_2(S) \Leftrightarrow H + HCO$	$1.500e+13$	0.00	$0.000e+00$
10.	$O + CH_3 \Leftrightarrow H + CH_2O$	$5.060e+13$	0.00	$0.000e+00$
11.	$O + CH_4 \Leftrightarrow OH + CH_3$	$1.020e+09$	1.50	$8.600e+03$
12.	$O + CO(+M) \Leftrightarrow CO_2(+M^c)$	$1.800e+10$	0.00	$2.385e+03$
	$Low\ Pressure\ Limit:$	$6.020e+14$	0.00	$3.000e+03$
13.	$O + HCO \Leftrightarrow CO + OH$	$3.000e+13$	0.00	$0.000e+00$
14.	$O + HCO \Leftrightarrow CO_2 + H$	$3.000e+13$	0.00	$0.000e+00$
15.	$O + CH_2O \Leftrightarrow OH + HCO$	$3.900e+13$	0.00	$3.540e+03$
16.	$O + CH_2OH \Leftrightarrow OH + CH_2O$	$1.000e+13$	0.00	$0.000e+00$
17.	$O + CH_3O \Leftrightarrow OH + CH_2O$	$1.000e+13$	0.00	$0.000e+00$
18.	$O + CH_3OH \Leftrightarrow OH + CH_2OH$	$3.880e+05$	2.50	$3.100e+03$
19.	$O + CH_3OH \Leftrightarrow OH + CH_3O$	$1.300e+05$	2.50	$5.000e+03$
20.	$O + C_2H \Leftrightarrow CO + CH$	$5.000e+13$	0.00	$0.000e+00$
21.	$O + C_2H_2 \Leftrightarrow H + HCCO$	$1.350e+07$	2.00	$1.900e+03$
22.	$O + C_2H_2 \Leftrightarrow OH + C_2H$	$4.600e+19$	-1.41	$2.895e+04$
23.	$O + C_2H_2 \Leftrightarrow CO + CH_2$	$6.940e+06$	2.00	$1.900e+03$
24.	$O + C_2H_3 \Leftrightarrow H + CH_2CO$	$3.000e+13$	0.00	$0.000e+00$
25.	$O + C_2H_4 \Leftrightarrow HCO + CH_3$	$1.250e+07$	1.83	$2.200e+02$
26.	$O + C_2H_5 \Leftrightarrow CH_3 + CH_2O$	$2.240e+13$	0.00	$0.000e+00$
27.	$O + C_2H_6 \Leftrightarrow OH + C_2H_5$	$8.980e+07$	1.92	$5.690e+03$
28.	$O + HCCO \Leftrightarrow 2CO + H$	$1.000e+14$	0.00	$0.000e+00$
29.	$O + CH_2CO \Leftrightarrow OH + HCCO$	$1.000e+13$	0.00	$8.000e+03$
30.	$O + CH_2CO \Leftrightarrow CO_2 + CH_2$	$1.750e+12$	0.00	$1.350e+03$
31.	$O_2 + CO \Leftrightarrow O + CO_2$	$2.500e+12$	0.00	$4.780e+04$
32.	$O_2 + CH_2O \Leftrightarrow HO_2 + HCO$	$1.000e+14$	0.00	$4.000e+04$
33.	$O_2 + H + M \Leftrightarrow HO_2 + M^d$	$2.800e+18$	-0.86	$0.000e+00$
34.	$2O_2 + H \Leftrightarrow O_2 + HO_2$	$2.080e+19$	-1.24	$0.000e+00$
35.	$O_2 + H_2O + H \Leftrightarrow H_2O + HO_2$	$1.126e+19$	-0.76	$0.000e+00$
36.	$O_2 + H + N_2 \Leftrightarrow HO_2 + N_2$	$2.600e+19$	-1.24	$0.000e+00$
37.	$O_2 + AR + H \Leftrightarrow AR + HO_2$	$7.000e+17$	-0.80	$0.000e+00$
38.	$O_2 + H \Leftrightarrow O + OH$	$2.650e+16$	-0.67	$1.704e+04$
39.	$2H + M \Leftrightarrow H_2 + M^e$	$1.000e+18$	-1.00	$0.000e+00$
40.	$H_2 + 2H \Leftrightarrow 2H_2$	$9.000e+16$	-0.60	$0.000e+00$
41.	$H_2O + 2H \Leftrightarrow H_2 + H_2O$	$6.000e+19$	-1.25	$0.000e+00$
42.	$CO_2 + 2H \Leftrightarrow H_2 + CO_2$	$5.500e+20$	-2.00	$0.000e+00$
43.	$H + OH + M \Leftrightarrow H_2O + M^f$	$2.200e+22$	-2.00	$0.000e+00$
44.	$H + HO_2 \Leftrightarrow O + H_2O$	$3.970e+12$	0.00	$6.710e+02$
45.	$H + HO_2 \Leftrightarrow O_2 + H_2$	$4.480e+13$	0.00	$1.068e+03$
46.	$H + HO_2 \Leftrightarrow 2OH$	$8.400e+13$	0.00	$6.350e+02$
47.	$H + H_2O_2 \Leftrightarrow H_2 + HO_2$	$1.210e+07$	2.00	$5.200e+03$
48.	$H + H_2O_2 \Leftrightarrow H_2O + OH$	$1.000e+13$	0.00	$3.600e+03$
49.	$H + CH \Leftrightarrow H_2 + C$	$1.650e+14$	0.00	$0.000e+00$
50.	$H + CH_2(+M) \Leftrightarrow CH_3(+M^b)$	$6.000e+14$	0.00	$0.000e+00$

continued on next page

continued from previous page

	$Low\ Pressure\ Limit:$	$1.040e+26$	-2.76	$1.600e+03$
	$Troe\ Centering:$			
	$c1: 5.620e-01;\ c2: 9.100e+01$			
	$c2: 5.836e+03;\ c3: 8.552e+03$			
51.	$H + CH_2(S) \Leftrightarrow H_2 + CH$	$3.000e+13$	0.00	$0.000e+00$
52.	$H + CH_3(+M) \Leftrightarrow CH_4(+M^g)$	$1.390e+16$	-0.53	$5.360e+02$
	$Low\ Pressure\ Limit:$	$2.620e+33$	-4.76	$2.440e+03$
	$Troe\ Centering:$			
	$c1: 7.830e-01;\ c2: 7.400e+01$			
	$c2: 2.941e+03;\ c3: 6.964e+03$			
53.	$CH_4 + H \Leftrightarrow H_2 + CH_3$	$6.600e+08$	1.62	$1.084e+04$
54.	$H + HCO(+M) \Leftrightarrow CH_2O(+M^b)$	$1.090e+12$	0.48	$-2.600e+02$
	$Low\ Pressure\ Limit:$	$2.470e+24$	-2.57	$4.250e+02$
	$Troe\ Centering:$			
	$c1: 7.824e-01;\ c2: 2.710e+02$			
	$c2: 2.755e+03;\ c3: 6.570e+03$			
55.	$H + HCO \Leftrightarrow H_2 + CO$	$7.340e+13$	0.00	$0.000e+00$
56.	$H + CH_2O(+M) \Leftrightarrow CH_2OH(+M^h)$	$5.400e+11$	0.45	$3.600e+03$
	$Low\ Pressure\ Limit:$	$1.270e+32$	-4.82	$6.530e+03$
	$Troe\ Centering:$			
	$c1: 7.187e-01;\ c2: 1.030e+02$			
	$c2: 1.291e+03;\ c3: 4.160e+03$			
57.	$H + CH_2O(+M) \Leftrightarrow CH_3O(+M^h)$	$5.400e+11$	0.45	$2.600e+03$
	$Low\ Pressure\ Limit:$	$2.200e+30$	-4.80	$5.560e+03$
	$Troe\ Centering:$			
	$c1: 7.580e-01;\ c2: 9.400e+01$			
	$c2: 1.555e+03;\ c3: 4.200e+03$			
58.	$H + CH_2O \Leftrightarrow H_2 + HCO$	$5.740e+07$	1.90	$2.742e+03$
59.	$H + CH_2OH(+M) \Leftrightarrow CH_3OH(+M^h)$	$1.055e+12$	0.50	$8.600e+01$
	$Low\ Pressure\ Limit:$	$4.360e+31$	-4.65	$5.080e+03$
	$Troe\ Centering:$			
	$c1: 6.000e-01;\ c2: 1.000e+02$			
	$c2: 9.000e+04;\ c3: 1.000e+04$			
60.	$H + CH_2OH \Leftrightarrow H_2 + CH_2O$	$2.000e+13$	0.00	$0.000e+00$
61.	$H + CH_2OH \Leftrightarrow OH + CH_3$	$1.650e+11$	0.65	$-2.840e+02$
62.	$H + CH_2OH \Leftrightarrow H_2O + CH_2(S)$	$3.280e+13$	-0.09	$6.100e+02$
63.	$H + CH_3O(+M) \Leftrightarrow CH_3OH(+M^h)$	$2.430e+12$	0.52	$5.000e+01$
	$Low\ Pressure\ Limit:$	$4.660e+41$	-7.44	$1.408e+04$
	$Troe\ Centering:$			
	$c1: 7.000e-01;\ c2: 1.000e+02$			
	$c2: 9.000e+04;\ c3: 1.000e+04$			
64.	$H + CH_3O \Leftrightarrow H + CH_2OH$	$4.150e+07$	1.63	$1.924e+03$
65.	$H + CH_3O \Leftrightarrow H_2 + CH_2O$	$2.000e+13$	0.00	$0.000e+00$
66.	$H + CH_3O \Leftrightarrow OH + CH_3$	$1.500e+12$	0.50	$-1.100e+02$
67.	$H + CH_3O \Leftrightarrow H_2O + CH_2(S)$	$2.620e+14$	-0.23	$1.070e+03$
68.	$H + CH_3OH \Leftrightarrow H_2 + CH_2OH$	$1.700e+07$	2.10	$4.870e+03$
69.	$H + CH_3OH \Leftrightarrow H_2 + CH_3O$	$4.200e+06$	2.10	$4.870e+03$
70.	$H + C_2H(+M) \Leftrightarrow C_2H_2(+M^b)$	$1.000e+17$	-1.00	$0.000e+00$
	$Low\ Pressure\ Limit:$	$3.750e+33$	-4.80	$1.900e+03$
	$Troe\ Centering:$			
	$c1: 6.464e-01;\ c2: 1.320e+02$			
	$c2: 1.315e+03;\ c3: 5.566e+03$			
71.	$H + C_2H_2(+M) \Leftrightarrow C_2H_3(+M^b)$	$5.600e+12$	0.00	$2.400e+03$
	$Low\ Pressure\ Limit:$	$3.800e+40$	-7.27	$7.220e+03$
	$Troe\ Centering:$			
	$c1: 7.507e-01;\ c2: 9.850e+01$			
	$c2: 1.302e+03;\ c3: 4.167e+03$			
72.	$H + C_2H_3(+M) \Leftrightarrow C_2H_4(+M^b)$	$6.080e+12$	0.27	$2.800e+02$

continued on next page

continued from previous page

	$Low\ Pressure\ Limit:$	$1.400e+30$	-3.86	$3.320e+03$
	$Troe\ Centering:$			
	$c1: 7.820e-01;\ c2: 2.075e+02$			
	$c2: 2.663e+03;\ c3: 6.095e+03$			
73.	$H+C_2H_3 \Leftrightarrow H_2+C_2H_2$	$3.000e+13$	0.00	$0.000e+00$
74.	$H+C_2H_4(+M) \Leftrightarrow C_2H_5(+M^b)$	$5.400e+11$	0.45	$1.820e+03$
	$Low\ Pressure\ Limit:$	$6.000e+41$	-7.62	$6.970e+03$
	$Troe\ Centering:$			
	$c1: 9.753e-01;\ c2: 2.100e+02$			
	$c2: 9.840e+02;\ c3: 4.374e+03$			
75.	$H+C_2H_4 \Leftrightarrow H_2+C_2H_3$	$1.325e+06$	2.53	$1.224e+04$
76.	$H+C_2H_5(+M) \Leftrightarrow C_2H_6(+M^b)$	$5.210e+17$	-0.99	$1.580e+03$
	$Low\ Pressure\ Limit:$	$1.990e+41$	-7.08	$6.685e+03$
	$Troe\ Centering:$			
	$c1: 8.422e-01;\ c2: 1.250e+02$			
	$c2: 2.219e+03;\ c3: 6.882e+03$			
77.	$H+C_2H_5 \Leftrightarrow H_2+C_2H_4$	$2.000e+12$	0.00	$0.000e+00$
78.	$C_2H_6+H \Leftrightarrow H_2+C_2H_5$	$1.150e+08$	1.90	$7.530e+03$
79.	$H+HCCO \Leftrightarrow CO+CH_2(S)$	$1.000e+14$	0.00	$0.000e+00$
80.	$H+CH_2CO \Leftrightarrow H_2+HCCO$	$5.000e+13$	0.00	$8.000e+03$
81.	$H+CH_2CO \Leftrightarrow CO+CH_3$	$1.130e+13$	0.00	$3.428e+03$
82.	$H+HCCOH \Leftrightarrow H+CH_2CO$	$1.000e+13$	0.00	$0.000e+00$
83.	$H_2+CO(+M) \Leftrightarrow CH_2O(+M^b)$	$4.300e+07$	1.50	$7.960e+04$
	$Low\ Pressure\ Limit:$	$5.070e+27$	-3.42	$8.435e+04$
	$Troe\ Centering:$			
	$c1: 9.320e-01;\ c2: 1.970e+02$			
	$c2: 1.540e+03;\ c3: 1.030e+04$			
84.	$H_2+OH \Leftrightarrow H_2O+H$	$2.160e+08$	1.51	$3.430e+03$
85.	$2OH(+M) \Leftrightarrow H_2O_2(+M^b)$	$7.400e+13$	-0.37	$0.000e+00$
	$Low\ Pressure\ Limit:$	$2.300e+18$	-0.90	$-1.700e+03$
	$Troe\ Centering:$			
	$c1: 7.346e-01;\ c2: 9.400e+01$			
	$c2: 1.756e+03;\ c3: 5.182e+03$			
86.	$2OH \Leftrightarrow O+H_2O$	$3.570e+04$	2.40	$-2.110e+03$
87.	$OH+HO_2 \Leftrightarrow O_2+H_2O$	$1.450e+13$	0.00	$-5.000e+02$
88.	$OH+H_2O_2 \Leftrightarrow H_2O+HO_2$	$2.000e+12$	0.00	$4.270e+02$
89.	$OH+H_2O_2 \Leftrightarrow H_2O+HO_2$	$1.700e+18$	0.00	$2.941e+04$
90.	$OH+C \Leftrightarrow CO+H$	$5.000e+13$	0.00	$0.000e+00$
91.	$OH+CH \Leftrightarrow H+HCO$	$3.000e+13$	0.00	$0.000e+00$
92.	$OH+CH_2 \Leftrightarrow H+CH_2O$	$2.000e+13$	0.00	$0.000e+00$
93.	$OH+CH_2 \Leftrightarrow H_2O+CH$	$1.130e+07$	2.00	$3.000e+03$
94.	$OH+CH_2(S) \Leftrightarrow H+CH_2O$	$3.000e+13$	0.00	$0.000e+00$
95.	$OH+CH_3(+M) \Leftrightarrow CH_3OH(+M^h)$	$2.790e+18$	-1.43	$1.330e+03$
	$Low\ Pressure\ Limit:$	$4.000e+36$	-5.92	$3.140e+03$
	$Troe\ Centering:$			
	$c1: 4.120e-01;\ c2: 1.950e+02$			
	$c2: 5.900e+03;\ c3: 6.394e+03$			
96.	$OH+CH_3 \Leftrightarrow H_2O+CH_2$	$5.600e+07$	1.60	$5.420e+03$
97.	$OH+CH_3 \Leftrightarrow H_2O+CH_2(S)$	$6.440e+17$	-1.34	$1.417e+03$
98.	$CH_4+OH \Leftrightarrow H_2O+CH_3$	$1.000e+08$	1.60	$3.120e+03$
99.	$CO+OH \Leftrightarrow CO_2+H$	$4.760e+07$	1.23	$7.000e+01$
100.	$OH+HCO \Leftrightarrow H_2O+CO$	$5.000e+13$	0.00	$0.000e+00$
101.	$OH+CH_2O \Leftrightarrow H_2O+HCO$	$3.430e+09$	1.18	$-4.470e+02$
102.	$OH+CH_2OH \Leftrightarrow H_2O+CH_2O$	$5.000e+12$	0.00	$0.000e+00$
103.	$OH+CH_3O \Leftrightarrow H_2O+CH_2O$	$5.000e+12$	0.00	$0.000e+00$
104.	$OH+CH_3OH \Leftrightarrow H_2O+CH_2OH$	$1.440e+06$	2.00	$-8.400e+02$
105.	$OH+CH_3OH \Leftrightarrow H_2O+CH_3O$	$6.300e+06$	2.00	$1.500e+03$
106.	$OH+C_2H \Leftrightarrow H+HCCO$	$2.000e+13$	0.00	$0.000e+00$

continued on next page

continued from previous page

107.	$OH + C_2H_2 \Leftrightarrow H + CH_2CO$	$2.180e-04$	4.50	$-1.000e+03$
108.	$OH + C_2H_2 \Leftrightarrow H + HCCOH$	$5.040e+05$	2.30	$1.350e+04$
109.	$OH + C_2H_2 \Leftrightarrow H_2O + C_2H$	$3.370e+07$	2.00	$1.400e+04$
110.	$OH + C_2H_2 \Leftrightarrow CO + CH_3$	$4.830e-04$	4.00	$-2.000e+03$
111.	$OH + C_2H_3 \Leftrightarrow H_2O + C_2H_2$	$5.000e+12$	0.00	$0.000e+00$
112.	$OH + C_2H_4 \Leftrightarrow H_2O + C_2H_3$	$3.600e+06$	2.00	$2.500e+03$
113.	$C_2H_6 + OH \Leftrightarrow H_2O + C_2H_5$	$3.540e+06$	2.12	$8.700e+02$
114.	$OH + CH_2CO \Leftrightarrow H_2O + HCCO$	$7.500e+12$	0.00	$2.000e+03$
115.	$2HO_2 \Leftrightarrow O_2 + H_2O_2$	$1.300e+11$	0.00	$-1.630e+03$
116.	$2HO_2 \Leftrightarrow O_2 + H_2O_2$	$4.200e+14$	0.00	$1.200e+04$
117.	$HO_2 + CH_2 \Leftrightarrow OH + CH_2O$	$2.000e+13$	0.00	$0.000e+00$
118.	$HO_2 + CH_3 \Leftrightarrow O_2 + CH_4$	$1.000e+12$	0.00	$0.000e+00$
119.	$HO_2 + CH_3 \Leftrightarrow OH + CH_3O$	$3.780e+13$	0.00	$0.000e+00$
120.	$CO + HO_2 \Leftrightarrow CO_2 + OH$	$1.500e+14$	0.00	$2.360e+04$
121.	$HO_2 + CH_2O \Leftrightarrow H_2O_2 + HCO$	$5.600e+06$	2.00	$1.200e+04$
122.	$O_2 + C \Leftrightarrow O + CO$	$5.800e+13$	0.00	$5.760e+02$
123.	$CH_2 + C \Leftrightarrow H + C_2H$	$5.000e+13$	0.00	$0.000e+00$
124.	$CH_3 + C \Leftrightarrow H + C_2H_2$	$5.000e+13$	0.00	$0.000e+00$
125.	$O_2 + CH \Leftrightarrow O + HCO$	$6.710e+13$	0.00	$0.000e+00$
126.	$H_2 + CH \Leftrightarrow H + CH_2$	$1.080e+14$	0.00	$3.110e+03$
127.	$H_2O + CH \Leftrightarrow H + CH_2O$	$5.710e+12$	0.00	$-7.550e+02$
128.	$CH + CH_2 \Leftrightarrow H + C_2H_2$	$4.000e+13$	0.00	$0.000e+00$
129.	$CH + CH_3 \Leftrightarrow H + C_2H_3$	$3.000e+13$	0.00	$0.000e+00$
130.	$CH_4 + CH \Leftrightarrow H + C_2H_4$	$6.000e+13$	0.00	$0.000e+00$
131.	$CO + CH(+M) \Leftrightarrow HCCO(+M^b)$	$5.000e+13$	0.00	$0.000e+00$
	Low Pressure Limit :	$2.690e+28$	-3.74	$1.936e+03$
	Troe Centering :			
	$c1 : 5.757e-01$; $c2 : 2.370e+02$			
	$c2 : 1.652e+03$; $c3 : 5.069e+03$			
132.	$CO_2 + CH \Leftrightarrow CO + HCO$	$1.900e+14$	0.00	$1.579e+04$
133.	$CH + CH_2O \Leftrightarrow H + CH_2CO$	$9.460e+13$	0.00	$-5.150e+02$
134.	$CH + HCCO \Leftrightarrow CO + C_2H_2$	$5.000e+13$	0.00	$0.000e+00$
135.	$O_2 + CH_2 \Rightarrow CO + H + OH$	$5.000e+12$	0.00	$1.500e+03$
136.	$H_2 + CH_2 \Leftrightarrow H + CH_3$	$5.000e+05$	2.00	$7.230e+03$
137.	$2CH_2 \Leftrightarrow H_2 + C_2H_2$	$1.600e+15$	0.00	$1.194e+04$
138.	$CH_2 + CH_3 \Leftrightarrow H + C_2H_4$	$4.000e+13$	0.00	$0.000e+00$
139.	$CH_4 + CH_2 \Leftrightarrow 2CH_3$	$2.460e+06$	2.00	$8.270e+03$
140.	$CO + CH_2(+M) \Leftrightarrow CH_2CO(+M^b)$	$8.100e+11$	0.50	$4.510e+03$
	Low Pressure Limit :	$2.690e+33$	-5.11	$7.095e+03$
	Troe Centering :			
	$c1 : 5.907e-01$; $c2 : 2.750e+02$			
	$c2 : 1.226e+03$; $c3 : 5.185e+03$			
141.	$CH_2 + HCCO \Leftrightarrow CO + C_2H_3$	$3.000e+13$	0.00	$0.000e+00$
142.	$CH_2(S) + N_2 \Leftrightarrow CH_2 + N_2$	$1.500e+13$	0.00	$6.000e+02$
143.	$AR + CH_2(S) \Leftrightarrow AR + CH_2$	$9.000e+12$	0.00	$6.000e+02$
144.	$O_2 + CH_2(S) \Leftrightarrow CO + H + OH$	$2.800e+13$	0.00	$0.000e+00$
145.	$O_2 + CH_2(S) \Leftrightarrow H_2O + CO$	$1.200e+13$	0.00	$0.000e+00$
146.	$H_2 + CH_2(S) \Leftrightarrow H + CH_3$	$7.000e+13$	0.00	$0.000e+00$
147.	$H_2O + CH_2(S)(+M) \Leftrightarrow CH_3OH(+M^h)$	$4.820e+17$	-1.16	$1.145e+03$
	Low Pressure Limit :	$1.880e+38$	-6.36	$5.040e+03$
	Troe Centering :			
	$c1 : 6.027e-01$; $c2 : 2.080e+02$			
	$c2 : 3.922e+03$; $c3 : 1.018e+04$			
148.	$H_2O + CH_2(S) \Leftrightarrow H_2O + CH_2$	$3.000e+13$	0.00	$0.000e+00$
149.	$CH_2(S) + CH_3 \Leftrightarrow H + C_2H_4$	$1.200e+13$	0.00	$-5.700e+02$
150.	$CH_4 + CH_2(S) \Leftrightarrow 2CH_3$	$1.600e+13$	0.00	$-5.700e+02$
151.	$CO + CH_2(S) \Leftrightarrow CO + CH_2$	$9.000e+12$	0.00	$0.000e+00$
152.	$CO_2 + CH_2(S) \Leftrightarrow CO_2 + CH_2$	$7.000e+12$	0.00	$0.000e+00$

continued on next page

continued from previous page

153.	$CO_2 + CH_2(S) \Leftrightarrow CO + CH_2O$	$1.400e+13$	0.00	$0.000e+00$
154.	$C_2H_6 + CH_2(S) \Leftrightarrow CH_3 + C_2H_5$	$4.000e+13$	0.00	$-5.500e+02$
155.	$O_2 + CH_3 \Leftrightarrow O + CH_3O$	$3.560e+13$	0.00	$3.048e+04$
156.	$O_2 + CH_3 \Leftrightarrow OH + CH_2O$	$2.310e+12$	0.00	$2.032e+04$
157.	$H_2O_2 + CH_3 \Leftrightarrow CH_4 + HO_2$	$2.450e+04$	2.47	$5.180e+03$
158.	$2CH_3(+M) \Leftrightarrow C_2H_6(+M^b)$	$6.770e+16$	-1.18	$6.540e+02$
	$Low\ Pressure\ Limit:$	$3.400e+41$	-7.03	$2.762e+03$
	$Troe\ Centering:$			
	$c1: 6.190e-01;\ c2: 7.320e+01$			
	$c2: 1.180e+03;\ c3: 9.999e+03$			
159.	$2CH_3 \Leftrightarrow H + C_2H_5$	$6.840e+12$	0.10	$1.060e+04$
160.	$HCO + CH_3 \Leftrightarrow CH_4 + CO$	$2.648e+13$	0.00	$0.000e+00$
161.	$CH_3 + CH_2O \Leftrightarrow CH_4 + HCO$	$3.320e+03$	2.81	$5.860e+03$
162.	$CH_3 + CH_3OH \Leftrightarrow CH_4 + CH_2OH$	$3.000e+07$	1.50	$9.940e+03$
163.	$CH_3 + CH_3OH \Leftrightarrow CH_4 + CH_3O$	$1.000e+07$	1.50	$9.940e+03$
164.	$CH_3 + C_2H_4 \Leftrightarrow CH_4 + C_2H_3$	$2.270e+05$	2.00	$9.200e+03$
165.	$C_2H_6 + CH_3 \Leftrightarrow CH_4 + C_2H_5$	$6.140e+06$	1.74	$1.045e+04$
166.	$H_2O + HCO \Leftrightarrow H_2O + CO + H$	$1.500e+18$	-1.00	$1.700e+04$
167.	$HCO + M \Leftrightarrow CO + H + M^i$	$1.870e+17$	-1.00	$1.700e+04$
168.	$O_2 + HCO \Leftrightarrow CO + HO_2$	$1.345e+13$	0.00	$4.000e+02$
169.	$O_2 + CH_2OH \Leftrightarrow HO_2 + CH_2O$	$1.800e+13$	0.00	$9.000e+02$
170.	$O_2 + CH_3O \Leftrightarrow HO_2 + CH_2O$	$4.280e-13$	7.60	$-3.530e+03$
171.	$O_2 + C_2H \Leftrightarrow CO + HCO$	$1.000e+13$	0.00	$-7.550e+02$
172.	$H_2 + C_2H \Leftrightarrow H + C_2H_2$	$5.680e+10$	0.90	$1.993e+03$
173.	$O_2 + C_2H_3 \Leftrightarrow HCO + CH_2O$	$4.580e+16$	-1.39	$1.015e+03$
174.	$C_2H_4(+M) \Leftrightarrow H_2 + C_2H_2(+M^b)$	$8.000e+12$	0.44	$8.677e+04$
	$Low\ Pressure\ Limit:$	$1.580e+51$	-9.30	$9.780e+04$
	$Troe\ Centering:$			
	$c1: 7.345e-01;\ c2: 1.800e+02$			
	$c2: 1.035e+03;\ c3: 5.417e+03$			
175.	$O_2 + C_2H_5 \Leftrightarrow HO_2 + C_2H_4$	$8.400e+11$	0.00	$3.875e+03$
176.	$O_2 + HCCO \Leftrightarrow 2CO + OH$	$3.200e+12$	0.00	$8.540e+02$
177.	$2HCCO \Leftrightarrow 2CO + C_2H_2$	$1.000e+13$	0.00	$0.000e+00$
178.	$N + NO \Leftrightarrow O + N_2$	$2.700e+13$	0.00	$3.550e+02$
179.	$O_2 + N \Leftrightarrow O + NO$	$9.000e+09$	1.00	$6.500e+03$
180.	$OH + N \Leftrightarrow H + NO$	$3.360e+13$	0.00	$3.850e+02$
181.	$O + N_2O \Leftrightarrow O_2 + N_2$	$1.400e+12$	0.00	$1.081e+04$
182.	$O + N_2O \Leftrightarrow 2NO$	$2.900e+13$	0.00	$2.315e+04$
183.	$H + N_2O \Leftrightarrow OH + N_2$	$3.870e+14$	0.00	$1.888e+04$
184.	$OH + N_2O \Leftrightarrow HO_2 + N_2$	$2.000e+12$	0.00	$2.106e+04$
185.	$N_2O(+M) \Leftrightarrow O + N_2(+M^j)$	$7.910e+10$	0.00	$5.602e+04$
	$Low\ Pressure\ Limit:$	$6.370e+14$	0.00	$5.664e+04$
186.	$HO_2 + NO \Leftrightarrow OH + NO_2$	$2.110e+12$	0.00	$-4.800e+02$
187.	$O + NO + M \Leftrightarrow NO_2 + M^b$	$1.060e+20$	-1.41	$0.000e+00$
188.	$O + NO_2 \Leftrightarrow O_2 + NO$	$3.900e+12$	0.00	$-2.400e+02$
189.	$H + NO_2 \Leftrightarrow OH + NO$	$1.320e+14$	0.00	$3.600e+02$
190.	$O + NH \Leftrightarrow H + NO$	$4.000e+13$	0.00	$0.000e+00$
191.	$H + NH \Leftrightarrow H_2 + N$	$3.200e+13$	0.00	$3.300e+02$
192.	$OH + NH \Leftrightarrow H + HNO$	$2.000e+13$	0.00	$0.000e+00$
193.	$OH + NH \Leftrightarrow H_2O + N$	$2.000e+09$	1.20	$0.000e+00$
194.	$O_2 + NH \Leftrightarrow O + HNO$	$4.610e+05$	2.00	$6.500e+03$
195.	$O_2 + NH \Leftrightarrow OH + NO$	$1.280e+06$	1.50	$1.000e+02$
196.	$N + NH \Leftrightarrow H + N_2$	$1.500e+13$	0.00	$0.000e+00$
197.	$H_2O + NH \Leftrightarrow H_2 + HNO$	$2.000e+13$	0.00	$1.385e+04$
198.	$NO + NH \Leftrightarrow OH + N_2$	$2.160e+13$	-0.23	$0.000e+00$
199.	$NO + NH \Leftrightarrow H + N_2O$	$3.650e+14$	-0.45	$0.000e+00$
200.	$O + NH_2 \Leftrightarrow OH + NH$	$3.000e+12$	0.00	$0.000e+00$
201.	$O + NH_2 \Leftrightarrow H + HNO$	$3.900e+13$	0.00	$0.000e+00$

continued on next page

continued from previous page

202.	$H + NH_2 \Leftrightarrow H_2 + NH$	$4.000e+13$	0.00	$3.650e+03$
203.	$OH + NH_2 \Leftrightarrow H_2O + NH$	$9.000e+07$	1.50	$-4.600e+02$
204.	$NNH \Leftrightarrow H + N_2$	$3.300e+08$	0.00	$0.000e+00$
205.	$NNH + M \Leftrightarrow H + N_2 + M^b$	$1.300e+14$	-0.11	$4.980e+03$
206.	$O_2 + NNH \Leftrightarrow HO_2 + N_2$	$5.000e+12$	0.00	$0.000e+00$
207.	$O + NNH \Leftrightarrow OH + N_2$	$2.500e+13$	0.00	$0.000e+00$
208.	$O + NNH \Leftrightarrow NO + NH$	$7.000e+13$	0.00	$0.000e+00$
209.	$H + NNH \Leftrightarrow H_2 + N_2$	$5.000e+13$	0.00	$0.000e+00$
210.	$OH + NNH \Leftrightarrow H_2O + N_2$	$2.000e+13$	0.00	$0.000e+00$
211.	$CH_3 + NNH \Leftrightarrow CH_4 + N_2$	$2.500e+13$	0.00	$0.000e+00$
212.	$H + NO + M \Leftrightarrow HNO + M^b$	$4.480e+19$	-1.32	$7.400e+02$
213.	$O + HNO \Leftrightarrow OH + NO$	$2.500e+13$	0.00	$0.000e+00$
214.	$H + HNO \Leftrightarrow H_2 + NO$	$9.000e+11$	0.72	$6.600e+02$
215.	$OH + HNO \Leftrightarrow H_2O + NO$	$1.300e+07$	1.90	$-9.500e+02$
216.	$O_2 + HNO \Leftrightarrow HO_2 + NO$	$1.000e+13$	0.00	$1.300e+04$
217.	$O + CN \Leftrightarrow CO + N$	$7.700e+13$	0.00	$0.000e+00$
218.	$OH + CN \Leftrightarrow H + NCO$	$4.000e+13$	0.00	$0.000e+00$
219.	$H_2O + CN \Leftrightarrow OH + HCN$	$8.000e+12$	0.00	$7.460e+03$
220.	$O_2 + CN \Leftrightarrow O + NCO$	$6.140e+12$	0.00	$-4.400e+02$
221.	$H_2 + CN \Leftrightarrow H + HCN$	$2.950e+05$	2.45	$2.240e+03$
222.	$O + NCO \Leftrightarrow CO + NO$	$2.350e+13$	0.00	$0.000e+00$
223.	$H + NCO \Leftrightarrow CO + NH$	$5.400e+13$	0.00	$0.000e+00$
224.	$OH + NCO \Leftrightarrow CO + H + NO$	$2.500e+12$	0.00	$0.000e+00$
225.	$N + NCO \Leftrightarrow CO + N_2$	$2.000e+13$	0.00	$0.000e+00$
226.	$O_2 + NCO \Leftrightarrow CO_2 + NO$	$2.000e+12$	0.00	$2.000e+04$
227.	$NCO + M \Leftrightarrow CO + N + M^b$	$3.100e+14$	0.00	$5.405e+04$
228.	$NO + NCO \Leftrightarrow CO + N_2O$	$1.900e+17$	-1.52	$7.400e+02$
229.	$NO + NCO \Leftrightarrow CO_2 + N_2$	$3.800e+18$	-2.00	$8.000e+02$
230.	$HCN + M \Leftrightarrow H + CN + M^b$	$1.040e+29$	-3.30	$1.266e+05$
231.	$O + HCN \Leftrightarrow H + NCO$	$2.030e+04$	2.64	$4.980e+03$
232.	$O + HCN \Leftrightarrow CO + NH$	$5.070e+03$	2.64	$4.980e+03$
233.	$O + HCN \Leftrightarrow OH + CN$	$3.910e+09$	1.58	$2.660e+04$
234.	$OH + HCN \Leftrightarrow H + HOCN$	$1.100e+06$	2.03	$1.337e+04$
235.	$OH + HCN \Leftrightarrow H + HNCO$	$4.400e+03$	2.26	$6.400e+03$
236.	$OH + HCN \Leftrightarrow CO + NH_2$	$1.600e+02$	2.56	$9.000e+03$
237.	$H + HCN(+M) \Leftrightarrow H_2CN(+M^b)$	$3.300e+13$	0.00	$0.000e+00$
	$Low\ Pressure\ Limit:$	$1.400e+26$	-3.40	$1.900e+03$
238.	$N + H_2CN \Leftrightarrow CH_2 + N_2$	$6.000e+13$	0.00	$4.000e+02$
239.	$C + N_2 \Leftrightarrow N + CN$	$6.300e+13$	0.00	$4.602e+04$
240.	$CH + N_2 \Leftrightarrow N + HCN$	$3.120e+09$	0.88	$2.013e+04$
241.	$CH + N_2(+M) \Leftrightarrow HCNN(+M^h)$	$3.100e+12$	0.15	$0.000e+00$
	$Low\ Pressure\ Limit:$	$1.300e+25$	-3.16	$7.400e+02$
	$Troe\ Centering:$			
	$c1: 6.670e-01;\ c2: 2.350e+02$			
	$c2: 2.117e+03;\ c3: 4.536e+03$			
242.	$CH_2 + N_2 \Leftrightarrow NH + HCN$	$1.000e+13$	0.00	$7.400e+04$
243.	$CH_2(S) + N_2 \Leftrightarrow NH + HCN$	$1.000e+11$	0.00	$6.500e+04$
244.	$C + NO \Leftrightarrow O + CN$	$1.900e+13$	0.00	$0.000e+00$
245.	$C + NO \Leftrightarrow CO + N$	$2.900e+13$	0.00	$0.000e+00$
246.	$CH + NO \Leftrightarrow O + HCN$	$4.100e+13$	0.00	$0.000e+00$
247.	$CH + NO \Leftrightarrow H + NCO$	$1.620e+13$	0.00	$0.000e+00$
248.	$CH + NO \Leftrightarrow HCO + N$	$2.460e+13$	0.00	$0.000e+00$
249.	$CH_2 + NO \Leftrightarrow H + HNCO$	$3.100e+17$	-1.38	$1.270e+03$
250.	$CH_2 + NO \Leftrightarrow OH + HCN$	$2.900e+14$	-0.69	$7.600e+02$
251.	$CH_2 + NO \Leftrightarrow H + HCNO$	$3.800e+13$	-0.36	$5.800e+02$
252.	$CH_2(S) + NO \Leftrightarrow H + HNCO$	$3.100e+17$	-1.38	$1.270e+03$
253.	$CH_2(S) + NO \Leftrightarrow OH + HCN$	$2.900e+14$	-0.69	$7.600e+02$
254.	$CH_2(S) + NO \Leftrightarrow H + HCNO$	$3.800e+13$	-0.36	$5.800e+02$

continued on next page

continued from previous page

255.	$CH_3 + NO \Leftrightarrow H_2O + HCN$	$9.600e+13$	0.00	$2.880e+04$
256.	$CH_3 + NO \Leftrightarrow OH + H_2CN$	$1.000e+12$	0.00	$2.175e+04$
257.	$O + HCNN \Leftrightarrow CO + H + N_2$	$2.200e+13$	0.00	$0.000e+00$
258.	$O + HCNN \Leftrightarrow NO + HCN$	$2.000e+12$	0.00	$0.000e+00$
259.	$O_2 + HCNN \Leftrightarrow O + HCO + N_2$	$1.200e+13$	0.00	$0.000e+00$
260.	$OH + HCNN \Leftrightarrow H + HCO + N_2$	$1.200e+13$	0.00	$0.000e+00$
261.	$H + HCNN \Leftrightarrow CH_2 + N_2$	$1.000e+14$	0.00	$0.000e+00$
262.	$O + HNCO \Leftrightarrow CO_2 + NH$	$9.800e+07$	1.41	$8.500e+03$
263.	$O + HNCO \Leftrightarrow CO + HNO$	$1.500e+08$	1.57	$4.400e+04$
264.	$O + HNCO \Leftrightarrow OH + NCO$	$2.200e+06$	2.11	$1.140e+04$
265.	$H + HNCO \Leftrightarrow CO + NH_2$	$2.250e+07$	1.70	$3.800e+03$
266.	$H + HNCO \Leftrightarrow H_2 + NCO$	$1.050e+05$	2.50	$1.330e+04$
267.	$OH + HNCO \Leftrightarrow H_2O + NCO$	$3.300e+07$	1.50	$3.600e+03$
268.	$OH + HNCO \Leftrightarrow CO_2 + NH_2$	$3.300e+06$	1.50	$3.600e+03$
269.	$HNCO + M \Leftrightarrow CO + NH + M^b$	$1.180e+16$	0.00	$8.472e+04$
270.	$H + HCNO \Leftrightarrow H + HNCO$	$2.100e+15$	-0.69	$2.850e+03$
271.	$H + HCNO \Leftrightarrow OH + HCN$	$2.700e+11$	0.18	$2.120e+03$
272.	$H + HCNO \Leftrightarrow CO + NH_2$	$1.700e+14$	-0.75	$2.890e+03$
273.	$H + HOCN \Leftrightarrow H + HNCO$	$2.000e+07$	2.00	$2.000e+03$
274.	$HCCO + NO \Leftrightarrow CO + HCNO$	$9.000e+12$	0.00	$0.000e+00$
275.	$CH_3 + N \Leftrightarrow H + H_2CN$	$6.100e+14$	-0.31	$2.900e+02$
276.	$CH_3 + N \Leftrightarrow H_2 + HCN$	$3.700e+12$	0.15	$-9.000e+01$
277.	$H + NH_3 \Leftrightarrow H_2 + NH_2$	$5.400e+05$	2.40	$9.915e+03$
278.	$OH + NH_3 \Leftrightarrow H_2O + NH_2$	$5.000e+07$	1.60	$9.550e+02$
279.	$O + NH_3 \Leftrightarrow OH + NH_2$	$9.400e+06$	1.94	$6.460e+03$
280.	$CO_2 + NH \Leftrightarrow CO + HNO$	$1.000e+13$	0.00	$1.435e+04$
281.	$NO_2 + CN \Leftrightarrow NO + NCO$	$6.160e+15$	-0.75	$3.450e+02$
282.	$NO_2 + NCO \Leftrightarrow CO_2 + N_2O$	$3.250e+12$	0.00	$-7.050e+02$
283.	$CO_2 + N \Leftrightarrow CO + NO$	$3.000e+12$	0.00	$1.130e+04$
284.	$O + CH_3 \Rightarrow H_2 + CO + H$	$3.370e+13$	0.00	$0.000e+00$
285.	$O + C_2H_4 \Leftrightarrow H + CH_2CHO$	$6.700e+06$	1.83	$2.200e+02$
286.	$O + C_2H_5 \Leftrightarrow H + CH_3CHO$	$1.096e+14$	0.00	$0.000e+00$
287.	$OH + HO_2 \Leftrightarrow O_2 + H_2O$	$5.000e+15$	0.00	$1.733e+04$
288.	$OH + CH_3 \Rightarrow H_2 + CH_2O$	$8.000e+09$	0.50	$-1.755e+03$
289.	$H_2 + CH(+M) \Leftrightarrow CH_3(+M^b)$	$1.970e+12$	0.43	$-3.700e+02$
	Low Pressure Limit :	$4.820e+25$	-2.80	$5.900e+02$
	Troe Centering :			
	$c1 : 5.780e-01$; $c2 : 1.220e+02$			
	$c2 : 2.535e+03$; $c3 : 9.365e+03$			
290.	$O_2 + CH_2 \Rightarrow CO_2 + 2H$	$5.800e+12$	0.00	$1.500e+03$
291.	$O_2 + CH_2 \Leftrightarrow O + CH_2O$	$2.400e+12$	0.00	$1.500e+03$
292.	$2CH_2 \Rightarrow 2H + C_2H_2$	$2.000e+14$	0.00	$1.099e+04$
293.	$H_2O + CH_2(S) \Rightarrow H_2 + CH_2O$	$6.820e+10$	0.25	$-9.350e+02$
294.	$O_2 + C_2H_3 \Leftrightarrow O + CH_2CHO$	$3.030e+11$	0.29	$1.100e+01$
295.	$O_2 + C_2H_3 \Leftrightarrow HO_2 + C_2H_2$	$1.337e+06$	1.61	$-3.840e+02$
296.	$O + CH_3CHO \Leftrightarrow OH + CH_2CHO$	$2.920e+12$	0.00	$1.808e+03$
297.	$O + CH_3CHO \Rightarrow CO + OH + CH_3$	$2.920e+12$	0.00	$1.808e+03$
298.	$O_2 + CH_3CHO \Rightarrow CO + HO_2 + CH_3$	$3.010e+13$	0.00	$3.915e+04$
299.	$H + CH_3CHO \Leftrightarrow H_2 + CH_2CHO$	$2.050e+09$	1.16	$2.405e+03$
300.	$H + CH_3CHO \Rightarrow H_2 + CO + CH_3$	$2.050e+09$	1.16	$2.405e+03$
301.	$OH + CH_3CHO \Rightarrow H_2O + CO + CH_3$	$2.343e+10$	0.73	$-1.113e+03$
302.	$HO_2 + CH_3CHO \Rightarrow CO + H_2O_2 + CH_3$	$3.010e+12$	0.00	$1.192e+04$
303.	$CH_3 + CH_3CHO \Rightarrow CH_4 + CO + CH_3$	$2.720e+06$	1.77	$5.920e+03$
304.	$H + CH_2CO(+M) \Leftrightarrow CH_2CHO(+M^b)$	$4.865e+11$	0.42	$-1.755e+03$
	Low Pressure Limit :	$1.012e+42$	-7.63	$3.854e+03$
	Troe Centering :			
	$c1 : 4.650e-01$; $c2 : 2.010e+02$			
	$c2 : 1.773e+03$; $c3 : 5.333e+03$			

continued on next page

continued from previous page

305.	$O + CH_2CHO \Rightarrow CO_2 + H + CH_2$	$1.500e+14$	0.00	$0.000e+00$
306.	$O_2 + CH_2CHO \Rightarrow CO + OH + CH_2O$	$1.810e+10$	0.00	$0.000e+00$
307.	$O_2 + CH_2CHO \Rightarrow OH + 2HCO$	$2.350e+10$	0.00	$0.000e+00$
308.	$H + CH_2CHO \Leftrightarrow HCO + CH_3$	$2.200e+13$	0.00	$0.000e+00$
309.	$H + CH_2CHO \Leftrightarrow H_2 + CH_2CO$	$1.100e+13$	0.00	$0.000e+00$
310.	$OH + CH_2CHO \Leftrightarrow H_2O + CH_2CO$	$1.200e+13$	0.00	$0.000e+00$
311.	$OH + CH_2CHO \Leftrightarrow HCO + CH_2OH$	$3.010e+13$	0.00	$0.000e+00$
312.	$CH_3 + C_2H_5(+M) \Leftrightarrow C_3H_8(+M^b)$	$9.430e+12$	0.00	$0.000e+00$
	$Low\ Pressure\ Limit:$	$2.710e+74$	-16.82	$1.306e+04$
	$Troe\ Centering:$			
	$c1: 1.527e-01;\ c2: 2.910e+02$			
	$c2: 2.742e+03;\ c3: 7.748e+03$			
313.	$O + C_3H_8 \Leftrightarrow OH + C_3H_7$	$1.930e+05$	2.68	$3.716e+03$
314.	$H + C_3H_8 \Leftrightarrow H_2 + C_3H_7$	$1.320e+06$	2.54	$6.756e+03$
315.	$OH + C_3H_8 \Leftrightarrow H_2O + C_3H_7$	$3.160e+07$	1.80	$9.340e+02$
316.	$H_2O_2 + C_3H_7 \Leftrightarrow HO_2 + C_3H_8$	$3.780e+02$	2.72	$1.500e+03$
317.	$CH_3 + C_3H_8 \Leftrightarrow CH_4 + C_3H_7$	$9.030e-01$	3.65	$7.154e+03$
318.	$CH_3 + C_2H_4(+M) \Leftrightarrow C_3H_7(+M^b)$	$2.550e+06$	1.60	$5.700e+03$
	$Low\ Pressure\ Limit:$	$3.000e+63$	-14.60	$1.817e+04$
	$Troe\ Centering:$			
	$c1: 1.894e-01;\ c2: 2.770e+02$			
	$c2: 8.748e+03;\ c3: 7.891e+03$			
319.	$O + C_3H_7 \Leftrightarrow CH_2O + C_2H_5$	$9.640e+13$	0.00	$0.000e+00$
320.	$H + C_3H_7(+M) \Leftrightarrow C_3H_8(+M^b)$	$3.613e+13$	0.00	$0.000e+00$
	$Low\ Pressure\ Limit:$	$4.420e+61$	-13.54	$1.136e+04$
	$Troe\ Centering:$			
	$c1: 3.150e-01;\ c2: 3.690e+02$			
	$c2: 3.285e+03;\ c3: 6.667e+03$			
321.	$H + C_3H_7 \Leftrightarrow CH_3 + C_2H_5$	$4.060e+06$	2.19	$8.900e+02$
322.	$OH + C_3H_7 \Leftrightarrow CH_2OH + C_2H_5$	$2.410e+13$	0.00	$0.000e+00$
323.	$HO_2 + C_3H_7 \Leftrightarrow O_2 + C_3H_8$	$2.550e+10$	0.26	$-9.430e+02$
324.	$HO_2 + C_3H_7 \Rightarrow OH + CH_2O + C_2H_5$	$2.410e+13$	0.00	$0.000e+00$
325.	$CH_3 + C_3H_7 \Leftrightarrow 2C_2H_5$	$1.927e+13$	-0.32	$0.000e+00$

Third Body efficiencies:

M^a	$H_2: 2.4;\ H_2O: 15.4;\ CH_4: 2.0;\ CO: 1.8;\ CO_2: 3.6;\ C_2H_6: 3.0;\ AR: 0.8$
M^b	$H_2: 2.0;\ H_2O: 6.0;\ CH_4: 2.0;\ CO: 1.5;\ CO_2: 2.0;\ C_2H_6: 3.0;\ AR: 0.7$
M^c	$O_2: 6.0;\ H_2: 2.0;\ H_2O: 6.0;\ CH_4: 2.0;\ CO: 1.5;\ CO_2: 3.5;\ C_2H_6: 3.0;\ AR: 0.5$
M^d	$O_2: 0.0;\ H_2O: 0.0;\ CO: 0.8;\ CO_2: 1.5;\ C_2H_6: 1.5;\ AR: 0.0;\ N_2: 0.0$
M^e	$H_2: 0.0;\ H_2O: 0.0;\ CH_4: 2.0;\ CO_2: 0.0;\ C_2H_6: 3.0;\ AR: 0.6$
M^f	$H_2: 0.7;\ H_2O: 3.6;\ CH_4: 2.0;\ C_2H_6: 3.0;\ AR: 0.4$
M^g	$H_2: 2.0;\ H_2O: 6.0;\ CH_4: 3.0;\ CO: 1.5;\ CO_2: 2.0;\ C_2H_6: 3.0;\ AR: 0.7$
M^h	$H_2: 2.0;\ H_2O: 6.0;\ CH_4: 2.0;\ CO: 1.5;\ CO_2: 2.0;\ C_2H_6: 3.0$
M^i	$H_2: 2.0;\ H_2O: 0.0;\ CH_4: 2.0;\ CO: 1.5;\ CO_2: 2.0;\ C_2H_6: 3.0$
M^j	$H_2: 2.0;\ H_2O: 6.0;\ CH_4: 2.0;\ CO: 1.5;\ CO_2: 2.0;\ C_2H_6: 3.0;\ AR: 0.6$